Geological and petrological study of Oligocene to Miocene volcanic rocks from the Toyama basin, the SW Japan arc: Temporal change of arc volcanism during Cenozoic back-arc spreading in the Japan Sea

西南日本弧富山堆積盆に分布する漸新世～中新世火山岩類の
地質学的および岩石学的研究：
日本海拡大期の沈み込み帯火山活動の時間変遷

Doctoral Program in Environmental Science and Technology,
Graduate School of Science and Technology, Niigata University
Raiki YAMADA (F19N004A)
新潟大学大学院自然科学研究科環境科学専攻　山田来樹

(Supervisor: Associate Professor Toshiro TAKAHASHI)
指導教員：高橋俊郎准教授

This page is intentionally left blank

English abstract

The present study aims to investigate the role of igneous activity associated with back-arc spreading in modern plate tectonics, which is considered to have started in 1.0 Ga. In this study, the author focuses on the Japan Sea opening, which is a typical back arc spreading, and conduct geological and petrological studies of volcanic rocks distributed in the Toyama Basin of the southwest Japan arc during the Japan Sea opening (Oligocene to Miocene) in order to clarify the time evolution of subduction zone volcanism and its role during the spreading.

Strata related to the Japan Sea opening distributed in the Toyama Basin are subdivided into the Nanto Group (Johana and Nirehara Formations) and the Yatsuo Group (Iwaine Formation, Iozen Formation, and the other eight formations). Lithofacies formed on land (e.g., lava, pyroclastic flow deposit and debris flow deposit) and in shallow marine (e.g., inner bay and shallow water deposits) to deep marine environment (e.g., turbidite) were found from the strata. Zircon U-Pb ages of 22.8 ± 0.2 Ma, 23.6 ± 0.3 Ma, 17.1 ± 0.4 Ma, and 16.8 ± 0.2 Ma were obtained from the Johana, Nirehara, Iwaine and Iozen Formations. The following geotectonic history of the Toyama basin is considered, based on the lithology and the ages of each formation. The Toyama Basin was formed by deposition of non-marine to shallow marine strata and rhyolitic pyroclastic flows at about 23 Ma, followed by andesitic volcanism (non-marine to shallow marine) at 18–17 Ma and dacite to rhyolitic volcanism (non-marine to shallow marine) at 17–16 Ma. The sedimentary environment is considered to have changed to deep marine by around 15 Ma.

Among the strata that have been geologically examined above, the

volcanic rocks collected from the Johana, Iwaine and Iozen Formations in the Nanto area were examined for their petrogenesis. Based on petrography, the volcanic rocks of each formation are classified into one type for the Johana Formation (Jh-Pyr), three types for the Iwaine Formation (Iw-OlPx, Iw-Amp and Iw-Px) and one type for the Iozen Formation (Io-Aph). Based on the major and trace element compositions, Sr-Nd isotopes, and zircon trace element compositions, the following petrogenesis of the volcanic rocks is considered. Although Jh-Pyr and Io-Aph have different K_2O contents, they show similar trace element trends. The involvement of crustal melting to produce those rhyolitic magma was inferred from enriched light rare earth elements (LREE), Nb–Ta depletion, steeply positive trend in La–La/Yb diagram, low Cr and Ni concentrations, enriched Sr–Nd isotope, and enriched zircon trace element composition. Iw-OlPx has a maximum Mg# of 65, suggesting that it was formed by the partial melting of mantle hydrous with slab-derived fluids. Iw-Amp is characterized by, for instance, high Sr/Y ratio and considered as results of partial melting of mantle metasomatized by adakite melt. Iw-Px can be explained by differentiation of basaltic magma, based on the trend of compositional variation diagrams, however it is thought to assimilate the crust because of its highly enriched Sr-Nd isotopic composition. The mantle wedge is thought to have been relatively hot during the Japan Sea opening, when such geochemically various volcanic rocks were formed. It is estimated that the old and cold Pacific Plate was subducting into the southwest Japan arc at that time. Therefore, an event that maintains the mantle wedge in a high-temperature state, such as upwelling of the asthenospheric mantle into the mantle wedge, is necessary to generate large-scale andesitic volcanism.

Because rhyolitic magmatism of the Johana and Iozen Formations

accompanies basaltic to andesitic volcanism, the basaltic to andesitic volcanism is considered to have played a role as heat source. Jh-Pyr and Io-Aph have more enriched whole-rock Sr-Nd isotope and zircon Hf isotope than the Hida belt, suggesting that old continental crust such as the North and South China Craton involved the genesis of the rhyolites. Trace element compositions of rhyolites from the Johana and Iozen Formations are similar to those of the upper crust. Rhyolites distributed in the rift zone of the subduction zone also show similar trends. This indicates that felsic magmatism related to rifting in the subduction zone, such as back-arc spreading, contributes to recycling of crustal materials in the continental crust that the new upper crust is generated by crustal melting.

日本語要旨

1.0 Ga に始まったと考えられている現在のプレートテクトニクスの中でも、背弧拡大に伴う火成活動はその原因やプレートテクトニクスでの役割に関して、未だ多くの未解明な点がある。本研究では背弧拡大の典型例の一つとされている日本海拡大に注目し、背弧拡大中の沈み込み帯火山活動の時間変遷とその役割を明らかにするため、西南日本弧富山堆積盆に分布する日本海拡大期（漸新世～中新世）火山岩類の地質学的および岩石学的研究を行った。

富山堆積盆に分布する日本海拡大期層は下位より、南砺層群（城端層，楡原層）と八尾層群（岩稲層，医王山層，他 8 層）に区分される。これらの地層から陸上環境を示す岩相（溶岩、火砕流堆積物、河川成堆積物など）や浅海環境（内湾堆積物、浅海成堆積物など）～深海環境（タービダイトなど）を示す岩相が見出された。城端層、楡原層、岩稲層、医王山層からは 22.8 ± 0.2 Ma、23.6 ± 0.3 Ma、17.1 ± 0.4 Ma、16.8 ± 0.2 Ma のジルコン U–Pb 年代を得た。各層の岩相と年代値から、以下の地質学的変遷が考えられる。富山堆積盆は約 23 Ma に陸成層～浅海成層および流紋岩質火砕流の堆積によって形成が開始し、18–17 Ma の安山岩質火山活動（陸上～浅海）と 17–16 Ma のデイサイト～流紋岩質火山活動（陸上～浅海）を経て、15 Ma 頃までに堆積環境が深海へと変化した。

上記の地質学的検討がなされた地層のうち、南砺地域の城端層、岩稲層、医王山層から採取した火山岩類について、その岩石成因を検討した。岩石記載に基づくと、各層の火山岩類は城端層が 1 タイプ（Jh-Pyr）、岩稲層が 3 タイプ（Iw-OlPx、Iw-Amp、Iw-Px）、医王山層（Io-Aph）が 1 タイプに分類される、全岩主要・微量元素組成、全岩 Sr–Nd 同位体比組成、ジルコン微量元素組成から、以下のような成因が考えられた。Jh-Pyr と Io-Aph は異なる K_2O 量などをもつが、微量元素の傾向などは類似している。両層の流紋岩はともに、肥沃的な

LREE，Nb・Ta の負異常、低い Cr・Ni 量、肥沃的な Sr-Nd 同位体比組成、肥沃的なジルコン微量元素組成を示し、これは地殻の溶融によって流紋岩が形成されたことを示唆する。lw-OlPx は最大 Mg#が 65 に達する高マグネシア安山岩で、スラブ由来の流体で汚染されたマントルの部分溶融によって形成されたと考えられる。一方、lw-Amp はその特徴的な微量化学組成（例えば高 Sr/Y 比）から、スラブ由来のアダカイトメルトに汚染されたマントルの部分溶融で形成されたと考えられる。lw-Px は、その主成分元素組成などの特徴は玄武岩マグマからの結晶分化作用で説明できるものの、Sr–Nd 同位体比組成は非常に肥沃的であることから，結晶分化作用と同時に地殻の同化作用が生じていた可能性が示唆される。このような多様な火山岩が形成された日本海拡大期のマントルは高温であったと考えられるが、当時の西南日本弧には古く冷たい太平洋プレートが沈み込んでいたと推定されている。よって、大規模な安山岩質の火山活動を発生させるためにはアセノスフェリックマントルのマントルウェッジへの湧昇のようなマントルウェッジを高温状態にする現象が必要である。

城端層と医王山層の流紋岩類は玄武岩～安山岩質火山活動を伴うことから、それらが熱源となり地殻が部分溶融を起こしたと考えられる。これら流紋岩類は基盤岩の飛騨帯よりも肥沃的な Sr–Nd 同位体比組成、ジルコン Hf 同位体比組成を持つことから、さらに古い大陸地殻（南北中国地塊？）を起源とする可能性がある。また、流紋岩類の微量元素組成は上部地殻平均化学組成に類似し、沈み込み帯にあるリフト帯で活動する流紋岩と同様の化学的特徴を示す。このことは、背弧拡大のような沈み込み帯におけるリフティングに伴う珪長質火成活動が、地殻の部分溶融によって引き起こされる上部地殻の生成という地殻内での物質循環に寄与していることを示している。

Table of contents

List of figures and tables

Figures and tables are shown in the last part of each chapter.

Preface

My Ph.D. research might have started in 2003, when I was a 3rd class student of elementary school. In a weekend, my father and mother took me and my younger sister to a science museum in Niigata City of Niigata Prefecture, Japan. In the museum, there are many kinds of scientific exhibitions including geography, physics, chemistry, biology and engineering for kids. I really got interested in geoscience, especially astronomy, and my parents bought a book on astronomy to me in the museum shop. I used to read it repeatedly until night and thought to become an astronomer. However, one event completely changed my life. In October 23, 2004, when I was still an elementary school student, a huge earthquake called “2004 Chuetsu earthquake” attacked my place, Niigata Prefecture. I felt really scared but got interested in earthquakes and the solid earth. After entering junior high school, I knew that a mountain behind my house is a Quaternary volcano and visited an active volcano, Kusatsu-Shirane volcano, in Gunma Prefecture with my family. I understood that our earth is alive and dynamic, and this travel made me fix the way of my life. After graduation from high school, I entered the Department of Earth Sciences, Faculty of Science, University of Toyama to learn many areas of earth sciences and fixed majoring geology and petrology. Since master’s course, I have joined the Graduate School of Science and Technology, Niigata University, to further learn geology, petrology and geochemistry, belonging to Toshiro-sensei’s laboratory. Because my interest in petrology and geochemistry increased more and more in master’s course, I decided to become a Ph.D. to continue learning about the earth.

My research goal is understanding temporal evolution of

magmatism on the earth and relationships with tectonics (e.g., stagnant lid tectonics and plate tectonics). I believe that my research contributes understanding differentiation of solid planets. To reveal relationships between back-arc spreading and growth of the arc crust, I wrote down my Ph.D. thesis as one goal of my research interests.

In chapter 1 and 2 of this thesis, magmatism on the earth, Cenozoic back-arc spreading, and geological background of the study area are reviewed, and purpose of my Ph.D. research is explained. In chapter 3, 4, and 5 geology of the study area is described. In chapter 5, 6 and 7, I show geochronological and geochemical methods and data obtained in this study. In chapter 8, I discuss the petrogenesis of rhyolites erupted during the Japan Sea opening, one of the Cenozoic back-arc formations. My geochemical results and discussions further give implications for tectonics of the Japan Sea opening and growth of arc crust during back-arc spreading. In chapter 9 and 10, my thesis is summarized, and future plans of this study are shown. Figures and tables are shown in the last part of each chapter.

1. Introduction

In this chapter, magmatism through the earth's history is overviewed to explain purpose and target of Ph.D. research. The author consider that back-arc spreading is a significant key to understand temporal change of magmatism related to plate tectonics. In this thesis, Cenozoic rhyolites related to the Japan Sea opening, one of the classical examples of back-arc formations, is targeted to reveal the relationships between magmatism related to back-arc spreading and growth of arc crust.

1.1. Temporal evolution of magmatism on the earth

The earth, one of the solid planets in the solar system, has been geochemically differentiating since its birth at ~ 4.56 Ga as a dry planet without atmosphere and ocean (**Figure 1.1**). The magma ocean which was formed by collision of meteorites had been covering the surface and solidified at 4.53 Ga only 30 million years after the birth of the earth (Maruyama and Ebisuzaki, 2017). During differentiation and solidification of the magma ocean, volatiles (e.g., O, H, C, and S) and metals (e.g., Na, K, U, Th, Fe, Al, Ca, Mg, Si, and Ni) moved and were differentiated to form the primary atmosphere, the mantle, and the core (Putirka et al., 2021; **Figure 1.1**). Stagnant lid tectonics had controlled differentiation of the earth from 4.53 Ga to 4.37 Ga (Solomatov and Zharkov, 1990; Moresi and Solomatov, 1995; Solomatov, 1995; Solomatov and Moresi, 1996; Maruyama and Ebisuzaki, 2017). After ABEL (advent of bio-elements) bombardment from 4.37 Ga to 4.20 Ga, plate tectonics is thought to have initiated at 4.20 Ga (Maruyama and Ebisuzaki, 2017). Therefore, magmatism related to plate tectonics had differentiated the earth for 4.2 billion

years.

Plate tectonics and related magmatism have temporally changed the styles, and they can be classified into four stages (Sawada et al., 2018a, b): (1) 4.2–3.2 Ga, (2) 3.2–1.8 Ga, (3) 1.8–1.0 Ga, and (4) 1.0–0 Ga. (1) Oceanic plates initiated subduction to form small continents during 4.2–3.2 Ga. Since the small continents were subducted and recycled into the mantle, old continental crust has not been preserved. (2) Large sized continents (600 km square) were formed due to collision of small continents during 3.2–1.8 Ga. The large continents were sometimes torn apart because of rifting or back-arc spreading. Accordingly, the margins of the continental crust were replaced with the young crust (Sawada et al., 2016, 2018a, b). (3) Larger continents (several thousand km square) than that of stage 2 were formed due to collision of the continents during 1.8-1.0 Ga. Since the mantle was still 100 °C hotter than present (Komiya, 2004; Herzberg et al., 2010), the oceanic plates would have been composed of small oceanic plates. In this stage, the volume of the continental crust reached 1.5 times of present. (4) The modern style plate tectonics is thought to have initiated ~ 1.0 Ga (Sawada et al., 2018a, b), evidenced from existence of blue schist suggesting ultra-high-pressure metamorphism (Stern, 2005) and compilation of dT/dP (Brown and Johnson, 2018). Small oceanic plates and oceanic arc have been reducing in this stage. From the above, information on the history of the earth after 4.2 Ga is thought to be preserved in the continental crust.

In the modern style plate tectonics after 1.0 Ga, magmatism on the earth occurs in three tectonic settings as sketched in **Figure 1.2**: mid-ocean ridges, hot spots, and subduction zones. Since the continental crust has been formed in subduction zones (Tamura et al., 2016; Sawada et al., 2018a, b), the continental crust generated in

subduction zones provides a very significant key to reveal mechanism of the continental growth.

1.2. Overview on back-arc spreading

Back-arc spreading is one of the crucial phenomena in subduction zone to understand the growth and development and mantle dynamics (Sdrolias and Müller, 2006). As continents have grown in subduction zones through the earth's history (Tamura et al., 2016; Sawada et al., 2018a, b), back-arc spreading is also considered to have provided complementary information on tectono-thermal evolution of active continental margins (Wolfram et al., 2019).

Sdrolias and Müller (2006) defined back-arc spreading as extension at convergent plate margins where rifting and seafloor spreading develops on the overriding plate (**Figure 1.3**). Mechanisms of back-arc spreading is still under debated and can be classified into the following three types (Heuret and Lallemand, 2005; Nakakuki and Mura, 2013): (1) overriding plate motion away from the trench (Uyeda and Kanamori, 1979; Scholz and Campos, 1995; Nakakuki and Mura, 2013), (2) slab rollback driven by mantle flow pressure or asthenosphere injection (Tatsumi et al., 1990; Ricard et al. 1991; Doglioni, 1993; Flower et al., 2001), and (3) rollback of the gravitationally unstable slab (Elsasser, 1971; Molnar and Atwater, 1978; Garfunkel et al., 1986). On the other hand, it is known that active magmatism (especially basaltic to andesitic magmatism) occurs while back-arc basins opens and that hot state in the mantle wedge cause the active magmatism (Taylor and Martinez, 2003; Pearce and Stern, 2006; Wiens et al., 2006). However, it has been not extensively discussed relationships between magmatism associated with back-arc spreading and growth of arc crust. Because back-arc spreading has occurred since Archean (Sawada et al.,

2018a, b), it is very important to understand the relationships between magmatism related to back-arc spreading and growth of arc crust.

In late Cenozoic era, many back-arc basins were formed especially in the western Pacific as shown in **Figure 1.4**. Cenozoic back-arc formations are thought to be suitable to reveal the relationships, because young back-arc basins well preserve the geological records.

1.3. Japan Sea opening

The Japan Sea opening is one of the classical examples of back-arc basin formations in the western Pacific that started during the Oligocene to Miocene (Jolivet et al., 1994). The Japan Sea, separating the Eurasian continent and the Japan arc, opened rapidly during 21–15 Ma (Kano, 2018; Nakajima, 2018) because of (1) asthenospheric mantle injection into the mantle wedge (Tatsumi et al., 1989; Okamura et al., 1998; Zadeh et al., 2013; Shuto et al., 2006, 2015), (2) rollback of the Pacific and Philippine Sea plates (Martin, 2011), (3) collision between the Indian subcontinent and the Eurasian continent (Kimura and Tamaki, 1986; Jolivet et al., 1994; Ren et al., 2002; Horne et al., 2017), and/or (4) oblique subduction of the Pacific plate (Yin, 2010). The model of asthenospheric mantle injection is an idea that volcanic arc is torn apart toward the trench to form the back-arc basin due to asthenospheric mantle upwelling into the mantle wedge (Tatsumi et al., 1989). This model focuses on temporal change of chemical composition of igneous rocks, and many petrologists and geochemists support this idea. The rollback of the Pacific and Philippine Sea plates causes tension stress to tear apart the Japan arc from the continent (Martin, 2011). The model of collision between the Indian subcontinent and the Eurasian continent can be classified into two ideas: (1) deformation and strike-slip in the eastern Asia due to the collision (Kimura and Tamaki, 1986; Jolivet et al., 1994; Horne

et al., 2017) and (2) convection pattern changes under the eastern Asia due to the collision (Ren et al., 2002). The oblique subduction model of the Pacific plate is an idea that the oblique subduction caused strike-slip in the eastern Asia (Yin, 2010).

The models on spreading pattern of the Japan Sea also can be classified into three models: (1) double-door model (Otofuji et al., 1985), (2) pull-apart basin model (Lallemand and Jolivet, 1986; Soma and Maruyama, 1989; Yanai et al., 2010), and two-step spreading model (Hayashida et al., 1991). (1) The double-door model is based on paleomagnetism and an idea that the NE and SW Japan arcs rotated anticlockwise and clockwise, respectively, around 15 Ma (Otofuji et al., 1985). Hoshi et al. (2015) and Hoshi (2018) compared paleomagnetic data and concluded that the rotation occurred not around 15 Ma but in 18–16 Ma. There are two ideas in the pull-apart basin model: (1) Strike-slip of the NE and SW Japan arcs (Lallemand and Jolivet, 1986) and (2) parallel spreading of many micro-blocks to the continent (Soma and Maruyama, 1989; Yanai et al., 2010). The two-step spreading model is an idea that parallel spreading of the Japan arc (20–16 Ma) was followed by double-door opening (16–14 Ma; Hayashida et al., 1991).

The Japan Sea opening can be divided into four stages (Kano, 2018; Nakajima, 2018; Yamada and Takahashi, 2021): Stage I (44–28 Ma), Stage II (28–23 Ma), Stage III (23–18 Ma), and Stage IV (18–15.3 or 13.5 Ma). In the early stage of the Japan Sea opening, rifting initiated and progressed slowly during the Stage I (Kano et al., 2007a; Kano, 2018; Nakajima, 2018). During this period, in the SW Japan arc, large-scale felsic magmatism resulted in calderas (Imaoka et al., 2011), in contrast to the emplacement of Sr–Nd isotopically depleted basalts in the NE Japan arc (Shuto et al., 2015). During 28–23 Ma (Stage II), regional uplift caused by the upwelling of asthenospheric

mantle into the mantle wedge formed unconformities in the entire Japan arc (Kano et al., 2007a; Kano, 2018). Subsidence by rifting parallel to the continent margins (Hayashida et al., 1991) repeated, with minor volcanic activity in the eastern Japan Sea at 23 Ma (Kano, 2018), and unconformities are found between 19 and17 Ma (Stage III; Kano et al., 2007a). Subsequently, the Japan arc was separated rapidly from the continent during ~18–15.3 Ma interval, with clockwise and anticlockwise rotation of the SW and NE Japan arc, respectively. In the NE Japan arc, rifting continued until 13.5 Ma (Stage IV; Kano, 2018; Nakajima, 2018). Most of volcanic rocks related to the Japan Sea opening were formed during this period.

Mafic to felsic active volcanism occurred widely in the sedimentary basins during the Japan Sea opening, as shown in **Figure 1.5a**. Temporal changes in the Sr–Nd isotopic composition of basalts to andesites in the NE Japan arc suggest that the upwelling of the asthenospheric mantle into the mantle wedge during the Japan Sea opening generated geochemically distinct basaltic to andesitic magma (e.g., Shuto et al., 2015). In contrast, in the SW Japan arc, Kimura et al. (2003, 2005) revealed a temporal change in volcanism during and after the Japan Sea opening, based primarily on basalt and andesite geochronology and geochemistry. However, despite voluminous distribution of rhyolites equivalent to basalts and andesites in the Japan arc (**Figure 1.5a**), their petrogenesis has not been discussed extensively.

1.4. Objectives and purpose of the Ph.D. research

In addition to basalts and andesites, it has been revealed that large volumes of felsic volcanic rocks (dacite to rhyolite) were erupted during Cenozoic back-arc formations in the western Pacific (e.g., Gill et al., 1984; Taylor, 1995). However, geochemical and tectonic impact

of felsic volcanism to arc crust during back-arc spreading has not been discussed in detail. Thus, two main issues on felsic volcanism related to back-arc spreading to be solved are as follows: (1) How large volumes of rhyolitic magma are generated during back-arc spreading? (2) Do large volumes of felsic magmatism during back-arc spreading contribute to the growth or destruction of the arc crust?

The Toyama basin in the Hokuriku region of SW Japan is one of the sedimentary basins in the back-arc province of the Japan arc, with a large volume of two rhyolites that formed during in the early and main stages of the Japan Sea opening (**Figure 1.5b**). Ishida et al. (1998) and Ayalew and Ishiwatari (2011) reported the geochemistry of rhyolite formed during the early stage of the opening from the Toyama basin and concluded that it is a rift-type rhyolite. However, the magmatic processes of rhyolitic magma and the reasons for the large volume of felsic magmatism during the main stage of the opening have been seldom discussed in detail. Additionally, reliable ages of rhyolites in the Toyama basin have not been reported.

On this basis, the author examined zircon U–Pb ages, zircon geochemistry (trace element and Lu–Hf isotope), and whole-rock geochemistry (major and trace elements, and Sr–Nd isotopes) of the latest Oligocene to middle Miocene rhyolites in the Toyama basin, including accompanying andesites, and revealed the petrogenesis. Combining the zircon and whole-rock geochemistry of these rhyolites, the author further discusses the implications for tectonic discrimination of rhyolites and development of arc crust during back-arc spreading.

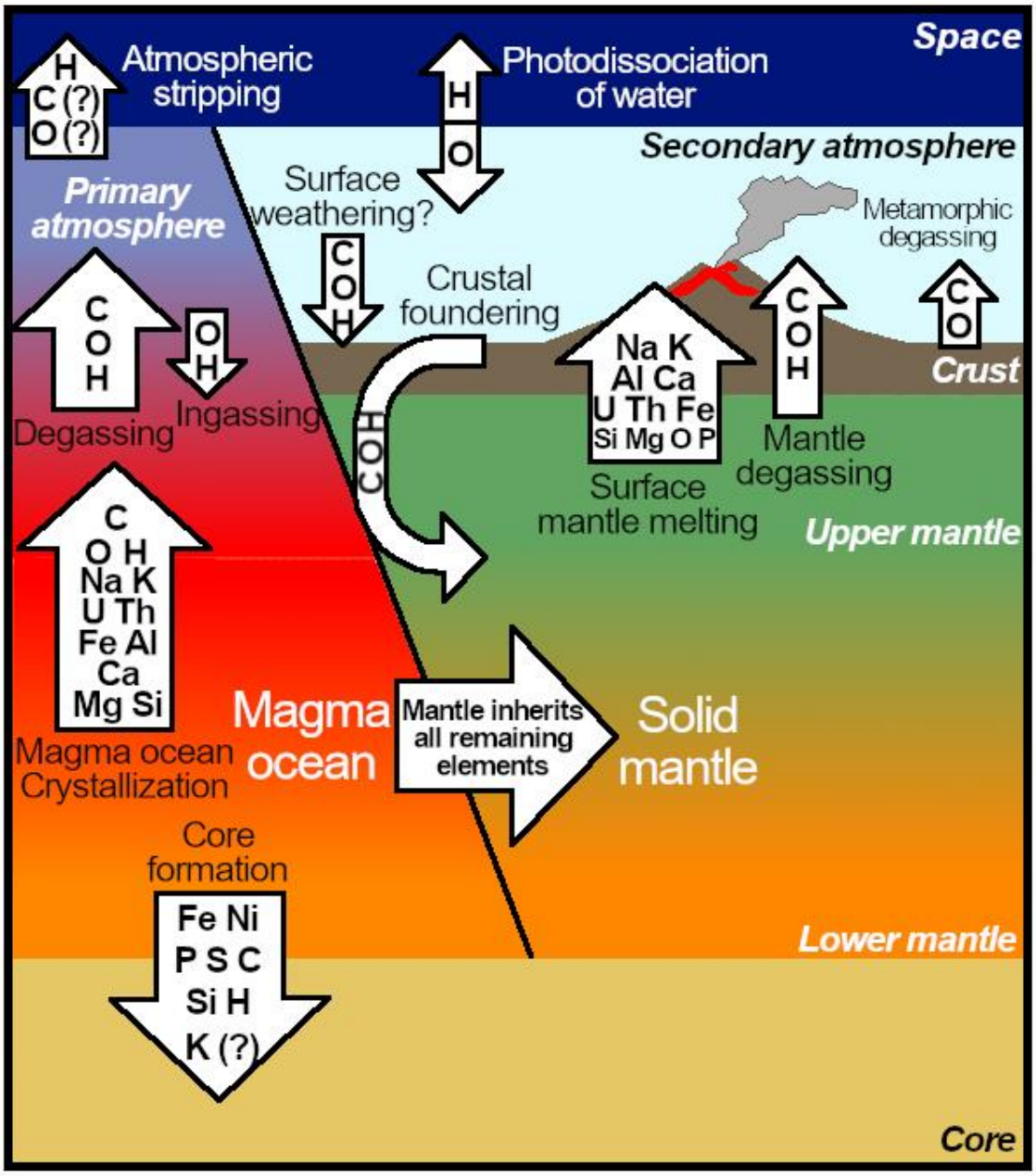

Figure1.1 Schematic sketch showing differentiation processes of the earth (modified after Putirka et al., 2021).

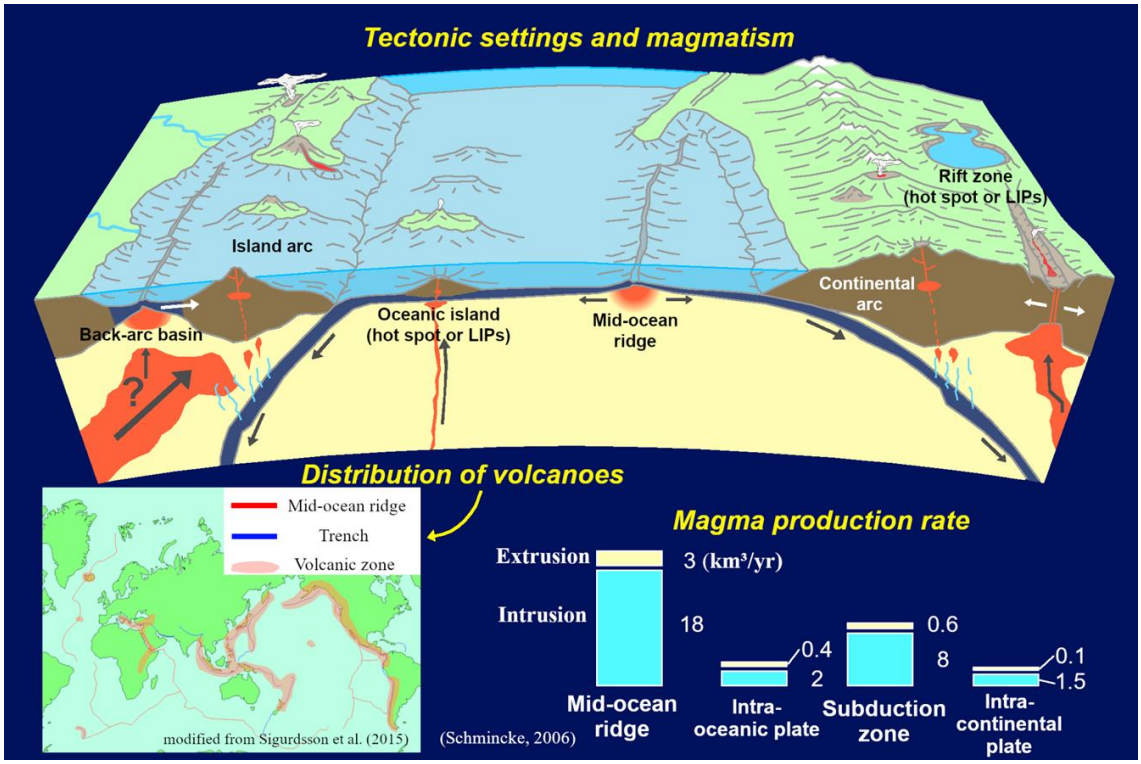

Figure 1.2 Schematic models of magmatism related to the modern plate tectonics, distribution of Quaternary volcanoes (modified from Sigurdsson et al., 2015), and magma production rate of each tectonic setting (Schmincke, 2004).

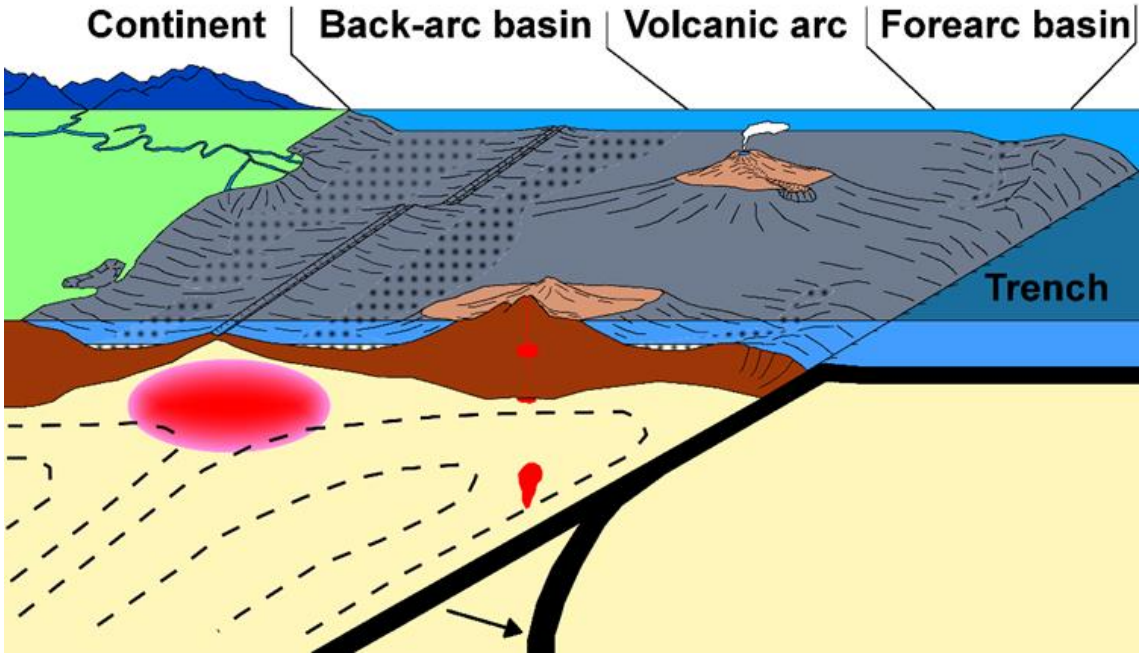

Figure 1.3 Schematic sketch on definition of back-arc basin.

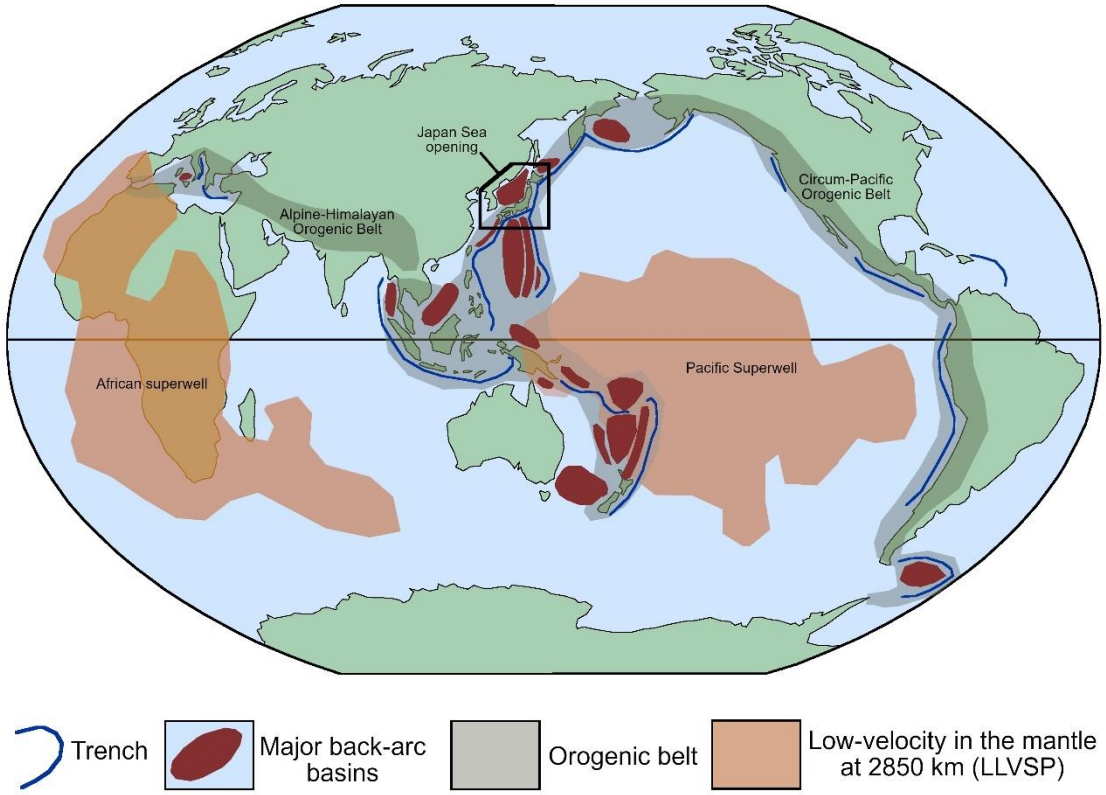

Figure 1.4 Distribution of major Cenozoic back-arc basins, with low-velocity in the mantle at 2850 km (LLVSP) and orogenic belts (modified from Potter and Szatmari, 2015).

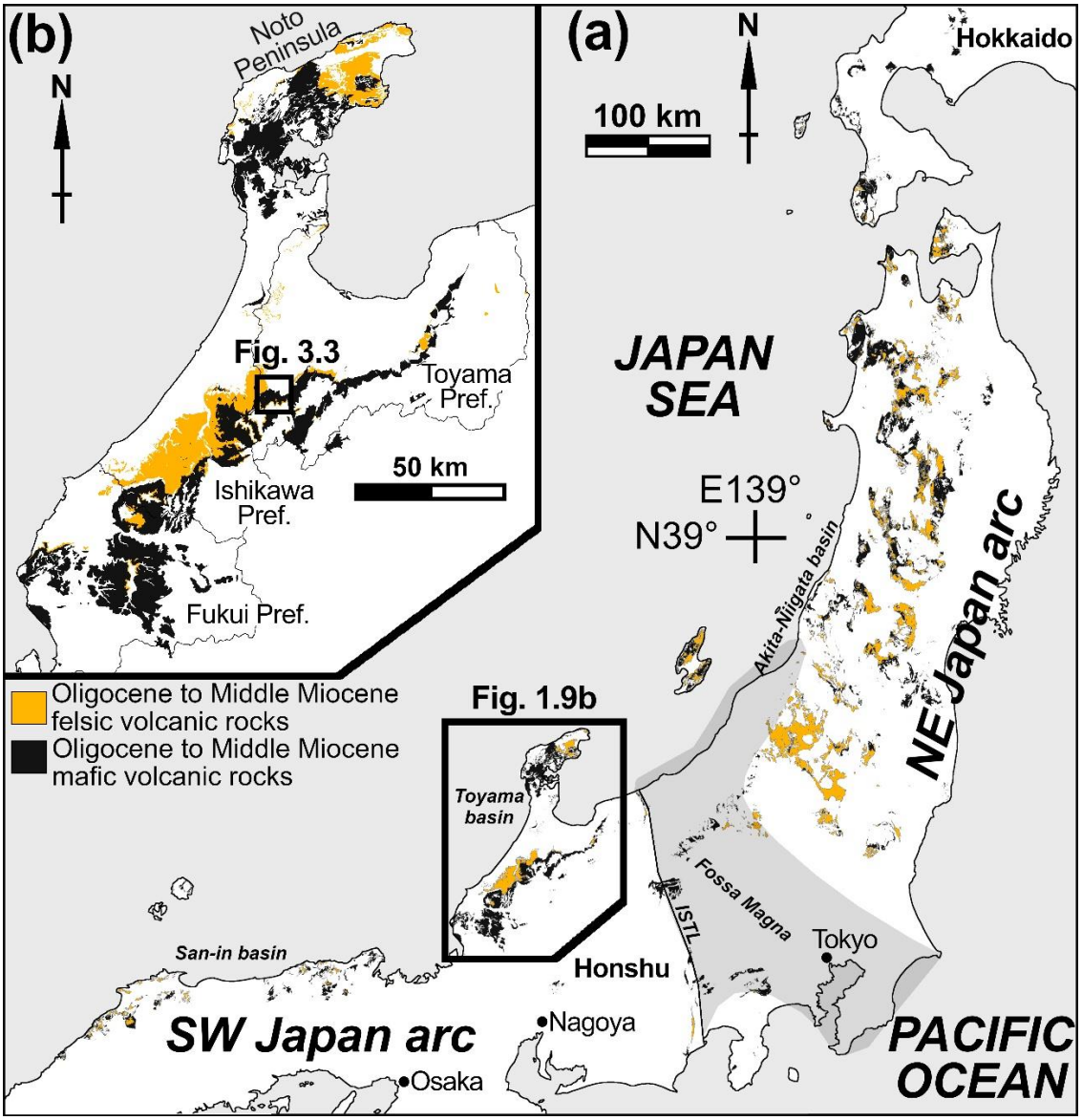

Figure 1.5 Distribution of Oligoce;pne to Middle Miocene volcanic rocks in the Japan arc (modified from Geological Survey of Japan, 2022). (a) Main part of the Japan arc. (b) Hokuriku region. ISTL, Itoigawa–Shizuoka Tectonic Line.

2. Geological background

In this chapter, temporal change of Cenozoic magmatism in the Hokuriku region, where the Toyama basin is located, is overviewed, and geological setting of the Toyama basin is explained in detail. Distribution, stratigraphic subdivision, lithostratigraphy of the Cenozoic strata, and temporal change of Cenozoic volcanism are shown in **Figure 2.1**, **2.2**, **2.3**, and **2.4** respectively.

Extensive magmatism occurred during this event in the Japan Sea and the circum-Japan Sea province, including the Hokuriku region where volcanism was initiated with basalts and andesites (Konosuyama Formation) in the Noto peninsula in the early Oligocene (ca. 33 Ma?). In the Early Miocene, andesitic volcanism (Kamiwazumi and Matsunagi Formations) followed the deposition of late Oligocene dacitic pyroclastic flows (Goroku Formation). Rhyolitic pyroclastic rocks including moonstone rhyolites were deposited widely as pyroclastic flows in the Hokuriku region from ca. 23–22 Ma. The moonstone rhyolites are alkalic in composition, suggesting a continental-arc rift origin. From ca. 21–17 Ma, basaltic to andesitic volcanic rocks (Iwaine and Ito-o formations and Besshodake andesites) of various geochemical compositions (tholeiitic and calc-alkalic basalts to andesites, adakite, and high-Mg andesite) were effused widely in the Hokuriku region. This basaltic to andesitic volcanism was followed from ca. 17–16 Ma by active dacitic to rhyolitic volcanism (Iozen and Fukuhira formations) with geochemical compositions indicating a continental-arc to island-arc origin. This rhyolitic volcanic episode, and minor basalts and andesites from 16 Ma, mark the end of the magmatism related to the opening of the Japan Sea, coinciding with the termination of the clockwise rotation

of southwest Japan. Previous petrological and geochemical studies suggest that magmatism related to the opening of the Japan Sea in the Hokuriku region was caused by upwelling of the asthenosphere into the mantle wedge below the margin of the eastern Eurasian continent.

2.1. Temporal change of Cenozoic magmatism in the Hokuriku region

2.1.1. Stage I (44–28 Ma)

The oldest igneous rocks in the Hokuriku region related to the Japan Sea opening are the Konosuyama Formation and the Shinobu Diorite (**Figure 2.1**) in the Noto peninsula (**Figure 2.3, 2.4**). They are considered to have been formed during ~ 33–26 Ma (Yamada and Takahashi, 2021). Since Paleocene to Eocene volcanic rocks were reported from the Noto peninsula by Tsukamoto (1988), there is a possibility that volcanic rocks formed during the early stage of the Tamagawa stage (44–30 Ma) are distributed in the Noto peninsula. In the early Oligocene when the Konosuyama Formation was deposited, the entire Japan arc was lifted up to form unconformity (Kano et al., 1991; Kano et al., 2007a). This lifting up continued until the latest Oligocene (Kano et al., 1991; Kano et al., 2007a).

The Konosuyama Formation is composed of geochemically various basalts and andesites which are not erupted in the Quaternary Japan arc, and researchers have especially focused and examined high magnesian andesite with basalts and andesites (Uematsu et al., 1995; López and Ishiwatari, 2002; Sato et al., 2013). Phenocrysts in these basalts and andesites have high Mg#, and most of the volcanic rocks show depleted Sr and Nd isotopic composition plotted from midocean ridge basalt (MORB) to the mantle array (Uematsu et al., 1995; Sato et al., 2013). From the above, the original magma is

considered to have been generated by partial melting of the hot mantle wedge due to the asthenosphere upwelling and subducting oceanic crust (Sato et al., 2013). Since such volcanism occurred also in the NE Japan arc (Shuto, 2009; Sato et al., 2013, 2014; Shuto et al., 2015), it is considered that continental arc type volcanism took place also in the Hokuriku region. Felsic volcanism in the SW Japan arc (Imaoka et al., 2011) is not found in the Hokuriku region, but felsic volcanic rocks is included in the report of K–Ar age by Tsukamoto (1988). The felsic volcanism which occurred in the SW Japan arc is also considered to have caused by the asthenosphere upwelling into the mantle wedge (Imaoka et al., 2011).

2.1.2.Stage II (28–23 Ma)

After the deposition of the Konosuyama Formation, dacitic pyroclastic flow deposits and lava flow were emplaced in the Noto peninsula during 25–23.5 Ma to form the Goroku Formation (Yoshikawa et al., 2002; Momma et al., 2016; **Figure 2.1**). As petrological and geochemical studies for the Goroku Formation have not been conducted, the genesis of the dacitic magma and relationships with other magmatism have not been revealed. The oceanic crust was initiated to be formed in the Japan Sea at ~ 24 Ma (Kaneoka et a., 1992, 1996).

2.1.3.Stage III to IV (23–15.3 Ma)

In the Noto peninsula, basaltic to andesitic volcanism occurred to form the Matsunagi and Kamiwazumi Formations during 23–20 Ma (**Figure 2.1, 2.2, 2.3**). It is known that aphyric andesite containing bronzite in andesites of the Matsunagi and Kamiwazumi Formations (Hoshina, 1984), however, the petrogenesis of the andesites is not revealed because of lack of petrological and geochemical data. Shimazu et al. (1993) exhibited whole-rock chemical compositions of volcanic rocks from the Kamiwazumi and Anamizu Formations

(Konosuyama Formation?) and conducted that the andesites are derived from the lithospheric mantle below the continental crust because of its enriched Sr and Nd isotopic compositions. Recently, Okamura et al. (2016) showed whole-rock geochemical compositions of volcanic rocks from the Matsunagi and Kamiwazumi Formations and the Besshodake Andesites to compare with Miocene volcanic rocks from the norther part of Fossa Magna. Miocene HMA containing bronzite has been reported also from the Choshi area of Chiba Prefecture, forearc region (Hanyu et al., 2006). Existence of HMA in both of back-arc (Noto peninsula) and forearc sides (Choshi area) is a very interesting issue to understand mantle dynamics during the Japan Sea opening.

While, so called “moonstone rhyolites”, which is rhyolitic welded tuff containing alkali feldspar, were erupted widely from the Toyama to Fukui Prefectures during 23–22 Ma (**Figure 2.4**). The moonstone rhyolites were deposited on land, and it is considered to have been erupted in the rift zone formed during formation of unconformity during Oligocene (Nakajima et al., 2019), deposition of conglomerate (Johana and Nirehara Formations; **Figure 2.1, 2.2**). These rhyolites have alkali-rich compositions and are characterized by chemical compositions similar to within plate type rhyolites (Ishida et al., 1998; Ayalew and Ishiwatari, 2011). Ishida et al. (1998), Ishiwatari and Tsujimori (2001), and Ayalew and Ishiwatari (2011) reported whole-rock chemical compositions from some areas in the Hokuriku region and found that there is spatial variation of chemical compositions. Especially, the Mt. Wasso moonstone rhyolite (**Figure 2.1, 2.2**) have chemical compositions the most similar to within plate type rhyolites in the moonstone rhyolites, and the other moonstone rhyolites are characterized by lower Zr concentration (Ishiwatari and Tsujimori, 2001). These moonstone rhyolites are interpreted as results of

magmatism related to rifting in the continental margin during the early stage of the Japan Sea opening (Ishida et al., 1998; Ishiwatari and Tsujimori, 2001; Ayalew and Ishiwatari, 2011). However, the heat source and the petrogenesis of the moonstone rhyolites are still unsolved issues due to lack of mafic volcanic rocks such as basalts.

The andesitic magmatism forming the Matsunagi and Kamiwazumi Formations continued until 21 Ma in the Noto peninsula, while the Horyuzan Formation (**Figure 2.1, 2.2**) was deposited by eruption of dacitic pyroclastic flow during 19.5–18 Ma (Yoshikawa et al., 2002). Andesites correlated to the Iwaine Formation were erupted and deposited to form the Besshodake Andesites in the northwest and southern part of the Noto peninsula during the stage IV (**Figure 2.1**). The Hegurajima and Nanatsujima volcanic rocks (**Figure 2.1**) might have been formed in stage III and IV, respectively (Yamada and Takahashi, 2021). While, the moonstone rhyolites terminated to be erupted around 22 Ma, and basaltic to andesitic magmatism initiated at ~ 21 Ma after magmatic hiatus of ~ 1 Ma. The SW Japan arc including the Hokuriku region rotated clockwise in 18–16 Ma of the stage IV (Otofuji et al., 1985; Hoshi et al., 2015; Hoshi, 2018), and the Japan Sea opened rapidly. The formative ages of the Ito-o and Iwaine Formations are considered as 21–18 Ma (Kano et al., 2007b; Yabe, 2008) and 17.5–17.2 Ma (Nakajima et al., 2019). This means that there is a spatial variation of basaltic to andesitic magmatism during the stage III to IV. The reason is still unknown: there are two possibilities to explain. (1) The volcanic activity changed laterally from Fukui Prefecture to the Toyama basin. (2) The lower part of the Ito-o Formation lacks in the Toyama basin due to unconformity (Miura and Azuma, 1974; Miura, 1979). To solve this issue, it is necessary to compare the detailed stratigraphy and geochronology in the Hokuriku region (Yamada and Takahashi, 2021).

Sato (1989) reported aphyric andesite containing bronzite from the Hegurajima and Nanatsujima islands and discussed the aphyric andesite was generated by magma mixing between primitive basaltic magma and dacitic magma. Katsuragi and Ishiwatari (2001, 2002), and Yamazaki and Ishiwatari (2007) reported basalt to dacite from the Ito-o Formation and found geochemically various volcanic rocks such as high K basalt, high and low Ni basalts, and adakitic andesite to dacite. Tomioka et al. (2000) examined whole-rock major and trace element compositions and Sr isotope of the Arashimadake cauldron, which is one of the early Miocene plutonic rocks related to the Ito-o Formation. According to them, it is considered that the basaltic to andesitic magma which formed the Arashimadake cauldron was generated by magma mixing between alkali-rich arc basalt and tholeiitic basalt similar to MORB, assimilated with paragneiss of the basement rocks. Ishiwatari and Ohama (1997) reported high Al basalt and shoshonitic basalt from dikes in the Ito-o, Wagatani, and Iwaine Formations and found that degree of assimilation changes larger from east to west. There is a possibility that this variation of the assimilate degree is related to age variation of the Ito-o and Iwaine Formations.

The most examined volcanic rocks related to the Japan Sea opening in the Hokuriku region is the Iwaine Formation (17.5–17.2 Ma). The geochemical features and the petrogenesis of the andesites from the Iwaine Formation (**Figure 2.1, 2.2**) have been examined and discussed by Ishiwatari and Ohama (1997), Takahashi and Shuto (1999), Tsuchihashi and Ishiwatari (2006), Ishiwatari et al. (2007), Watanabe et al. (2020). The most examined andesite by many researchers (Takahashi and Shuto, 1999; Tsuchihashi and Ishiwatari, 2006; Ishiwatari et al., 2007; Sato et al., 2013; Watanabe et al., 2020) is adakitic andesite. Especially, it is very interesting that only amphibole andesites from the lower part of the Iwaine Formation have

adakitic chemical compositions (Takahashi and Shuto, 1999; Yamada and Yamada, 2018). Other than adakitic andesites, geochemically various basalts to andesites such as high Mg andesite (HMA), calc-alkalic andesite, tholeiitic andesite were reported by Takahashi and Shuto (1999). This chemical variation is considered that hot state of the mantle wedge due to asthenosphere upwelling caused partial melting and assimilation of generated basaltic to andesitic magma with the continental crust (Ishiwatari and Ohama, 1997; Takahashi and Shuto, 1999; Sato et al., 2013).

After 17 Ma, volcanism terminated in the Noto peninsula, whereas large scaled felsic volcanism represented by the Iozen Formation (**Figure 2.1, 2.2**) occurred in the Toyama Prefecture, the Kaga district of Ishikawa Prefecture and Fukui Prefecture (Yamada and Takahashi, 2021). Rhyolites from the Iozen Formation is the most examined rhyolites in these rhyolites. However, it is cannot said that the petrogenesis of the rhyolites has not been revealed. Morishita et al. (2006) examined dark-colored silica veins in the Iozen Formation and concluded that the veins resulted from cracking of host rocks and input of SiO_2. Ayalew and Ishiwatari (2011) found that the rhyolites from the Iozen Formation is similar to arc type rhyolites. While, the Fukuhira Formation was deposited by andesitic to dacitic volcanism in the eastern part of Toyama Prefecture, and the Nanamagari Formation was formed with basalts (Kurokabe Basalts) in the Kanazawa area of Ishikawa Prefecture. Watanabe and Takahashi (2019) reported whole-rock geochemistry of basalts and andesites from the Fukuhira Formation and found that they have enriched Sr–Nd isotopic composition like rhyolites of the Iozen Formation. The basalts from the Kurokabe Basalts show low K composition, and its chemical compositions are similar to volcanic rocks from the Quaternary volcanic front of the NE Japan arc (Sakayori et al., 1997).

While felsic volcanism to form the Iozen and Fukuhira Formations took place, subsidence in the Hokuriku basin (especially in and around the Toyama basin) initiated. The depth of the subsidence reached ~ 2000 m (Hayakawa and Takemura, 1987; Itoh et al., 1997). Due to this subsidence and rifting, shallow marine deposits sedimented in mangrove forest (e.g., Kurosedani Formation; Yamanoi and Tsuda, 1986) and mudstone deposited in deep marine (e.g., Higashibessho Formation) were formed in the Hokuriku basin (Yamada and Takahashi, 2021). Magmatism continued also during the subsidence (e.g., Awagura Formation, Kunimi Formation, Kurokabe Balsalts). However, volcanism related to the Japan Sea opening in the Hokuriku region terminated rapidly at ~ 16 Ma when the Iozen and Fukuhira Formation stopped to be formed (Yamada and Takahashi, 2021).

2.2. Geological setting in the Toyama basin

2.2.1. Geological outline of the Toyama basin

The Cenozoic strata in the Toyama basin can be subdivided into the Johana Formation (newly defined), the Nirehara Formation, the Yatsuo Group, the Tonami Group, the Kurehayama Gravel Bed including alluvium and terrace deposits. They are distributed in the mountain, hilly and plane areas, unconformably covering the Paleozoic to Mesozoic basement rocks. The basement rocks are distributed in the mountain area and comprise of the Hida Belt (the Hida Metamorphic Rocks, the Unazuki Metamorphic Rocks and the Hida Granites; Takahashi et al., 2010), the Tetori Group (sensu lato; Sano, 2015) and the Futomiyama Group (Sudo, 1979b). The metamorphic rocks of the Hida Belt are composed mainly of sedimentary and plutonic origin gneisses, amphibolite and sedimentary origin schists. The Hida Granites consists of the pre-

Jurassic plutons (the Hida Older Granites) composed of granite mylonite and non-deformed granitoids and the Jurassic plutons (the Hida Younger Granites) composed of non-deformed to weakly deformed granitoids (Takahashi et al., 2010; Yamada et al., 2021). The Tetori Group is the Middle Jurassic to Lower Cretaceous stratum composed of clastic rocks (Sano, 2015). It is composed of conglomerate, sandstone and mudstone, with abundant fossils of plants and mollusks. The Futomiyama Group can be correlated to the Upper Cretaceous based on zircon U–Pb age (Kaneko et al., 2019), and it is composed mainly of rhyolites. Since these basement rocks are contained in the Cenozoic strata as gravels, it is considered that they were exposed on the surface as provenances during the Japan Sea opening.

The Johana and Nirehara Formations are the upper Oligocene to lower Miocene stratum composed mainly of conglomerate and sandstone, and they are distributed narrowly from the eastern part to the western part of the Toyama basin. The distributions and strikes are consistent with the upper Yatsuo Group. However, the dips (30–50°N) are slightly oblique with those of the Yatsuo Group, suggesting unconformity between them. The Yatsuo Group is the lower to middle Miocene stratum and can be distinguished into three major lithostratigraphic units (andesites, felsic volcanic rocks and alternation of sandstone and mudstone, massive mudstone). The Yatsuo Group is distributed thickly (the maximum thickness is ~ 3000 m) and widely from the eastern to western parts of the Toyama basin. It strikes NE–SW in the eastern part of the Toyama basin, whereas it strikes E–W (the dips are 10–30°N) in the central to western part of the Toyama basin. The Tonami Group is the middle Miocene to lower Pleistocene stratum composed mainly of sandstone (Nakajima et al., 2019), and it is distributed in hilly area of the Toyama basin, unconformably

covering the Yatsuo Group. The Kurehayama Gravel Bed and the equivalent beds are distributed in the hilly and plane areas of the Toyama basin, forming fluvial terrace and alluvial fans.

The stratigraphic subdivision in the Yatsuo area, known as type locality of the Cenozoic strata in the Hokuriku region, related to the Japan Sea opening has been reported many researchers (Imamura 1936; Nakaseko, 1953, 1954; Tsuda, 1953, 1955; Sakamoto and Nozawa, 1960; Hayakawa, 1983; Hayakawa and Takemura, 1987; Yamada and Yamada, 2018; Nakajima et al., 2019) since Makiyama (1930) firstly explained. In addition, based on the stratigraphic subdivision in and around the Yatsuo area, the stratigraphic subdivisions in the Toyama basin and the Hokuriku region have been summarized by Imamura (1937), Fujita and Nakagawa (1948), Ikebe (1949), Ikebe and Nakaseko (1955), Matsuomoto and Ikebe (1958), Sakamoto et al. (1959), Kaseno et al. (1961), Sakamoto (1966), Yamashita et al. (1988), Kaseno and Shimokawa (1989), Fujii et al. (1992a, b), and Yamada and Yamada (2018). Recently, Nakajima et al. (2019) reexamined chronostratigraphy and biostratigraphy in the Yatsuo area and revised the stratigraphic subdivision. In this study, I describe the Cenozoic stratigraphy in the Toyama basin, following the subdivision by Nakajima et al. (2019). Based on Ganzawa (1983), Yanagisawa (1999a), Kaneko (2001), and Nakajima et al. (2019), the Cenozoic strata in the Toyama basin can be classified into the Tori (Johana Formation in this study), Nirehara, Iwaine, Iozen, Kurosedani, Fukuhira, Sunagozaka, Doyama, Higashibessho, and Omine Formations, in stratigraphically ascending order (Yamada and Takahashi, 2021; **Figure 2.2**).

2.2.2. Stage III (23–18 Ma)

The Tori Formation is distributed narrowly in the western part of the Toyama basin and composed mainly of conglomerate, arkose coarse

sandstone and rhyolitic welded tuff (**Figure 2.1, 2.2**). This rhyolitic welded tuff contains “moonstone” and has been known as “moonstone rhyolite” since Imamura (1932) firstly reported. The rhyolitic welded tuff comprises several flow units of pyroclastic flow deposits, showing reddish brown color (Yamasaki and Miyajima, 1970; Sudo, 1979b; Ganzawa, 1983; this study; **Figure 2.5b**). K–Ar ages of 25–24 Ma (Uyeda and Aoki, 1970), zircon fission track (FT) ages of 25.0–22.2 Ma (Ganzawa, 1983; Nakajima et al., 1983), and a zircon U–Pb age of 22.5 ± 0.5 Ma (Ota et al., 2019) have been reported from the welded tuff.

The Nirehara Formation is distributed narrowly from the eastern part to the central part of the Toyama basin (**Figure 2.1, 2.2**) and composed mainly of conglomerate and arkose sandstone (Hayakawa and Takemura, 1987; Kashiwagi, 2012; Nakajima et al., 2019; **Figure 2.5a**).

2.2.3. Stage IV (18–15.3 Ma)

The Iwaine Formation is distributed widely from the eastern part of Toyama Prefecture to the Kaga district of Ishikawa Prefecture, and equivalent formation is distributed also in Fukui Prefecture (**Figure 2.1, 2.2**). Equivalent formations in Toyama Prefecture are distributed as the Ganzo Formation in the eastern part of Toyama Prefecture (Itoh, 1985; Takeuchi et al., 2017) and the Naratoge Formation in a boundary area between Toyama and Gifu Prefectures (Nozawa et al., 1981). The Iwaine Formation is composed mainly of two-pyroxene andesites and andesitic pyroclastic rocks with clastic rocks (Matsumoto and Ikebe, 1958; Takahashi and Shuto, 1999; Yamada and Yamada, 2018; **Figure 2.5c**). In some areas, the lower part of the Iwaine Formation is characterized by amphibole andesites (Sakamoto and Nozawa, 1960; Ganzawa, 1983; Yamada and Yamada, 2018). Lavas with clinker are observed in many areas (Takahashi and Shuto,

1999; Kaneko, 2001; Yamada and Yamada, 2018), while pillow lava and hyaloclastite were found by Ganzawa (1983) and Fujii et al. (1992b). K–Ar ages of 18.9–13.6 Ma (Shibata, 1973; Japan National Oil Corporation, 1985; Shinmura et al., 1994; Kaneko, 2001; Shinmura and Arakawa, 2008), a zircon FT age of 17.2 ± 0.9 Ma (Itoh and Watanabe, 2006), and zircon U–Pb age of 17.6 ± 0.3 Ma (Nakajima et al., 2019) have been reported. K–Ar ages showing young ages are considered due to alteration (Shibata, 1973). Nakajima et al. (2019) presumed the formation age of the Iwaine Formation as ~ 17.5–17.2 Ma, based on radiometric ages and paleomagnetism.

The Iozen Formation is distributed from the central part of Toyama Prefecture to the Kaga district of Ishikawa Prefecture, and the equivalent formations are distributed thickly in the Kaga district (**Figure 2.1, 2.2**). The Iozen Formation is composed mainly of rhyolites and rhyolitic pyroclastic rocks, and rhyolitic lava and pyroclastic flow deposits were observed by many researchers (Inoue et al., 1964; Matsuo and Nakanishi, 1967; Ganzawa, 1983; Fujii et al., 1992b; this study; **Figure 2.5d**). Structure like pillow lava emplaced on the sea floor was found (Inoue et al., 1964), whereas, rhyolites and welded tuff showing reddish brown color due to high-temperature oxidation in subaerial environment were observed (Matsuo and Nakanishi, 1967; Kaseno, 1993; this study). K–Ar ages of 14.3–14.1 Ma (Shibata, 1973; Kaneko, 2001) considered as not reliable ages due to alteration and zircon FT ages of 17.2–15.0 Ma (Ganzawa, 1983; Itoh and Watanabe, 2005) have been reported from the Iozen Formation in Toyama Prefecture. The Sasagawa Formation equivalent to the Iozen Formation is composed of mudstone and rhyolites. Rhyolites are composed mainly of pumiceous tuff breccia, while massive lava is also found (Takeuchi et al., 2017). Zircon U–Pb

ages of 16.3–16.2 Ma (Itoh et al., 2016; Takeuchi et al., 2017) and zircon FT ages of 18.2–14.0 Ma (Itoh, 1985; Itoh et al., 2016; Takeuchi et al., 2017) have been reported from the Sasagawa Formation.

The Kurosedani Formation is distributed in the central part of Toyama Prefecture and composed mainly of conglomerate and alternating beds of sandstone and mudstone (Tsuda, 1953, 1955; Sakamoto and Nozawa, 1960; Hayakawa and Takemura, 1987; Kaneko, 2001; Nakajima et al., 2019; **Figure 2.2**). The Kurosedani Formation is very famous as a fossiliferous formation containing various fossils, and the molluscan fauna is called the Yatsuo fauna (or the Kurosedani fauna; Oyama, 1950; Tsuda, 1960; Kaseno, 1964). The Yamadanaka Tuff Bed of the uppermost part of the Kurosedani Formation is thick tuff key bed (16.6 ± 0.2 Ma; zircon U–Pb age; Nakajima et al., 2019), and it can be observed widely in the Toyama basin (Hayakawa and Takemura, 1987; Nakajima et al., 2019).

The Fukuhira Formation is a heterotopic formation with the Kurosedani Formation, which is distributed in the eastern part of Toyama Prefecture (**Figure 2.1, 2.2**). It is composed mainly of andesitic to dacitic pyroclastic rocks, with lava and clastic rocks including basalts (Kaneko, 2001; **Figure 2.5f**). Lavas with clinker, volcanic bomb and pisolite can be observed, whereas hyaloclastite is also observed (Kaneko, 2001). Therefore, this formation is considered to have been deposited in both of subaerial and subaqueous environments (Kaneko, 2001). K–Ar ages of 15.34–12.19 Ma (Yamada et al., 1998; Kaneko, 2001), zircon FT ages of 14.3–12.2 Ma (Itoh and Watanabe, 2006; Takeuchi et al., 2017), and a zircon U–Pb age of 15.9 ± 0.2 Ma (Takeuchi et al., 2017) have been reported from the Fukuhira Formation. Although Takeuchi et al. (2017) discussed that the Fukuhira Formation was formed from 16 Ma to 12 Ma, based on these radiometric ages, K–Ar ages and zircon FT ages

are much younger than a zircon U–Pb age and not consistent with the depositional age of the upper Higashibessho Formation.

The Higashibessho Formation is distributed from the eastern to the central parts of Toyama Prefecture and composed mainly of massive mudstone (Tsuda, 1953, 1955; Sakamoto and Nozawa, 1960; Hayakawa and Takemura, 1987; Nakajima et al., 2019; **Figure 2.1, 2.2, 2.5f**). The Sunagozaka, Doyama and Omine Formations are distributed narrowly in the western part of Toyama Prefecture, and they are heterotopic with the Kurosedani and Higashibessho Formations (**Figure 2.2**). These three formations are composed of volcaniclastic sandstone and mudstone, and tuff beds are frequently intercalated (Inoue et al., 1964; Yanagisawa, 1999a; **Figure 2.5e**).

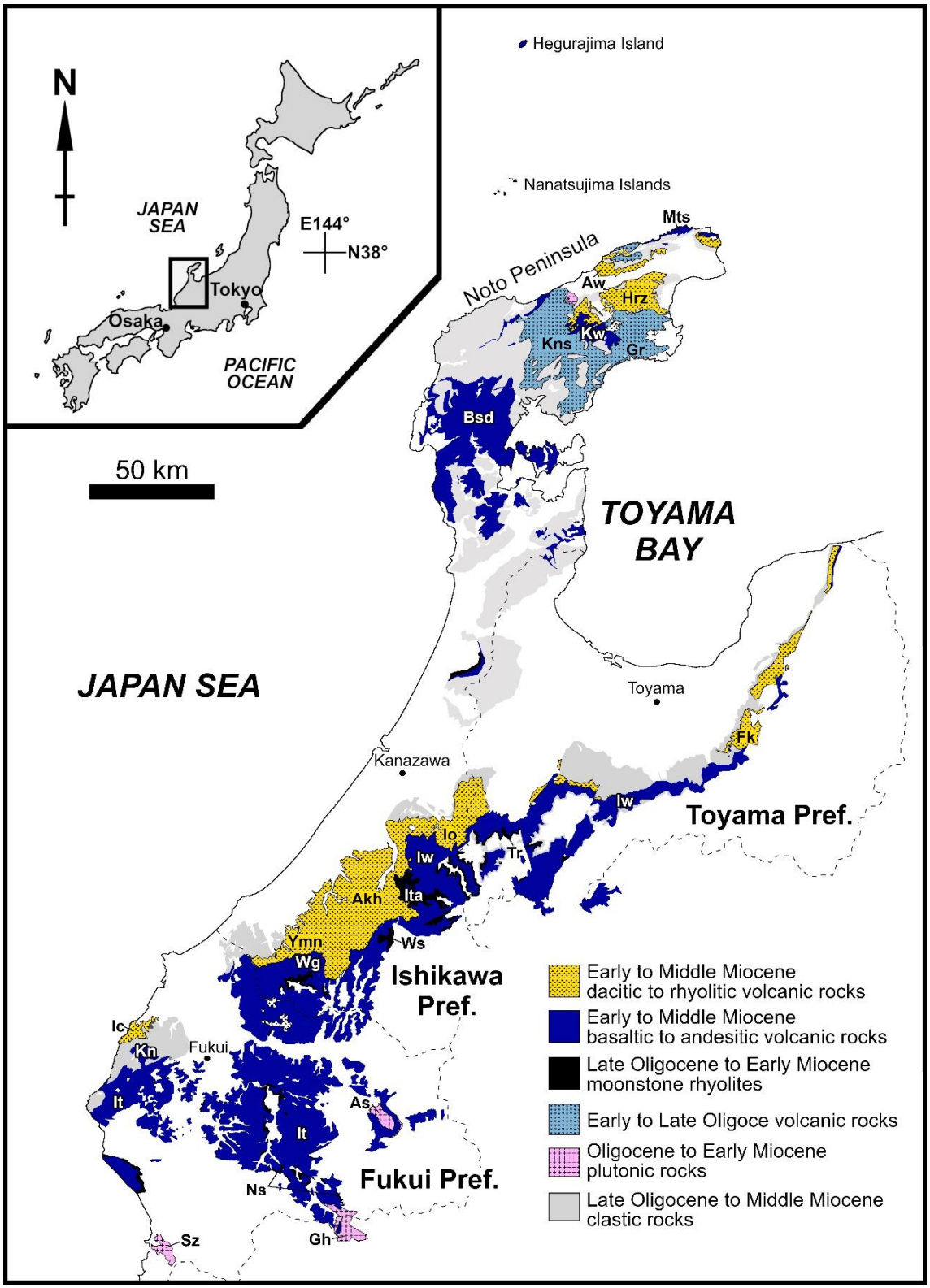

Figure 2.1 Index map showing the distributions of Oligocene to Miocene igneous rocks formed during and immediately after the opening of the Japan Sea in the Hokuriku region (modified after

Yamada and Takahashi, 2021). The map is modified from the 1:200,000 geological map of the northern Noto Peninsula (Ozaki, 2010), the 1:100,000 geological map of Fukui Prefecture (Fukui Prefecture, 2010), and the seamless geological map V2 (Geological Society of Japan, 2022). Abbreviations: Akh (Akahotani Fm.), As (Arashimadake Diorite), Aw (Awagura Fm.), Bsd (Besshodake Andesite), Fk (Fukuhira Fm.), Gh (Gouno-hakusan Granodiorite), Gr (Goroku Fm.), Hrz (Horyuzan Fm.), Ic (Ichinose Rhyolite), Io (Iozen Fm.), It (Ito-o Fm.), Ita (Itao Fm.), Iw (Iwaine Fm.), Kn (Kunimidake Volcanic Rocks), Kns (Konosuyama Fm.), Kw (Kamiwazumi Fm.), Mts (Matsunagi Fm.), Ns (Nishitani Fm.), Sz (Suizu Granodiorite), Tr (Tori Fm.), Wg (Wagatani Fm.), Ws (Mt. Wasso Moonstone Rhyolite), Ymn (Yamanaka Fm.), and Pref. (Prefecture).

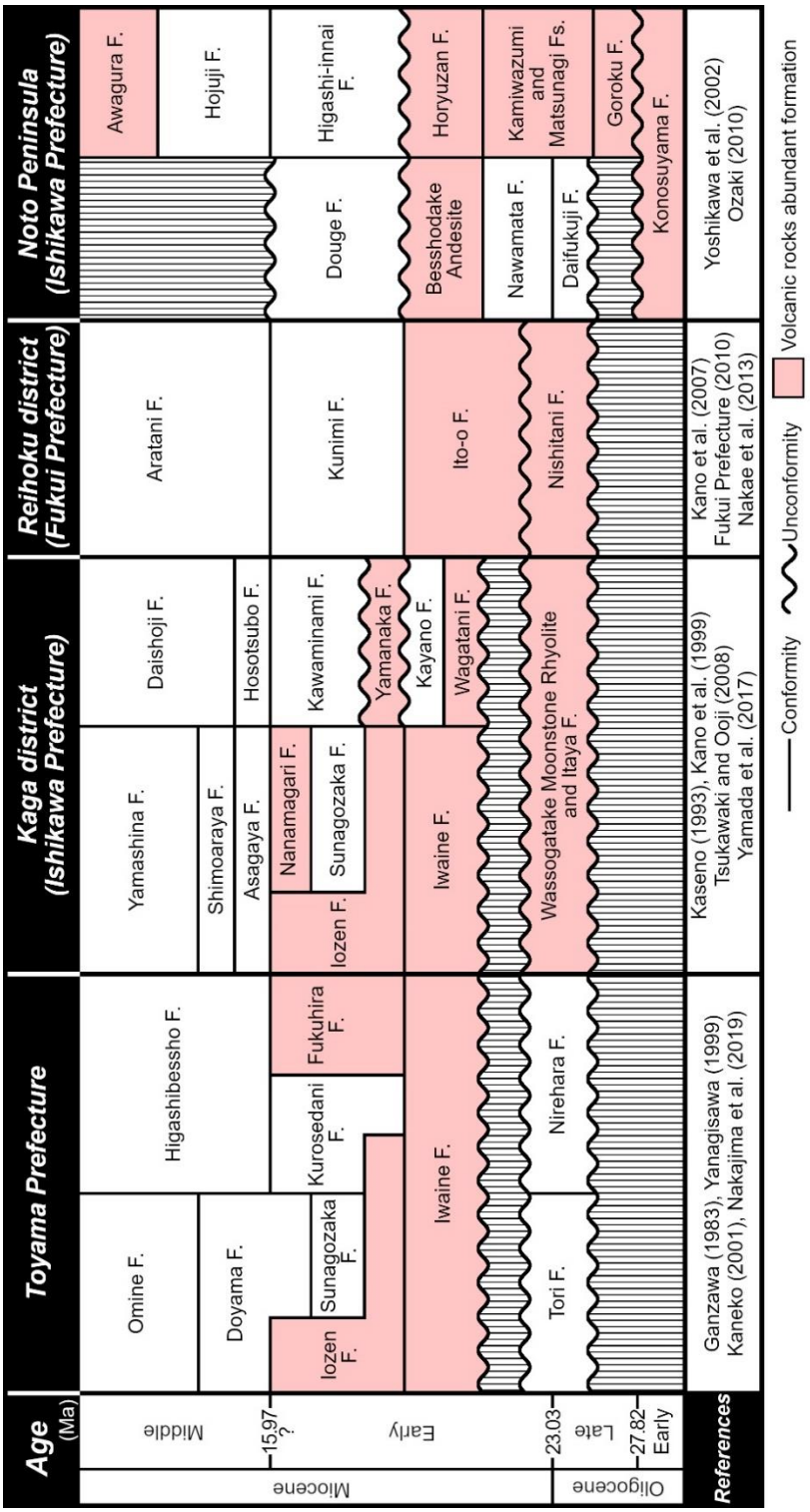

Figure 2.2 Regional comparison of the Oligocene to Middle Miocene stratigraphic classification in the Hokuriku region (modified after Yamada and Takahashi, 2021). Abbreviations: F. (Formation), Fs. (formations).

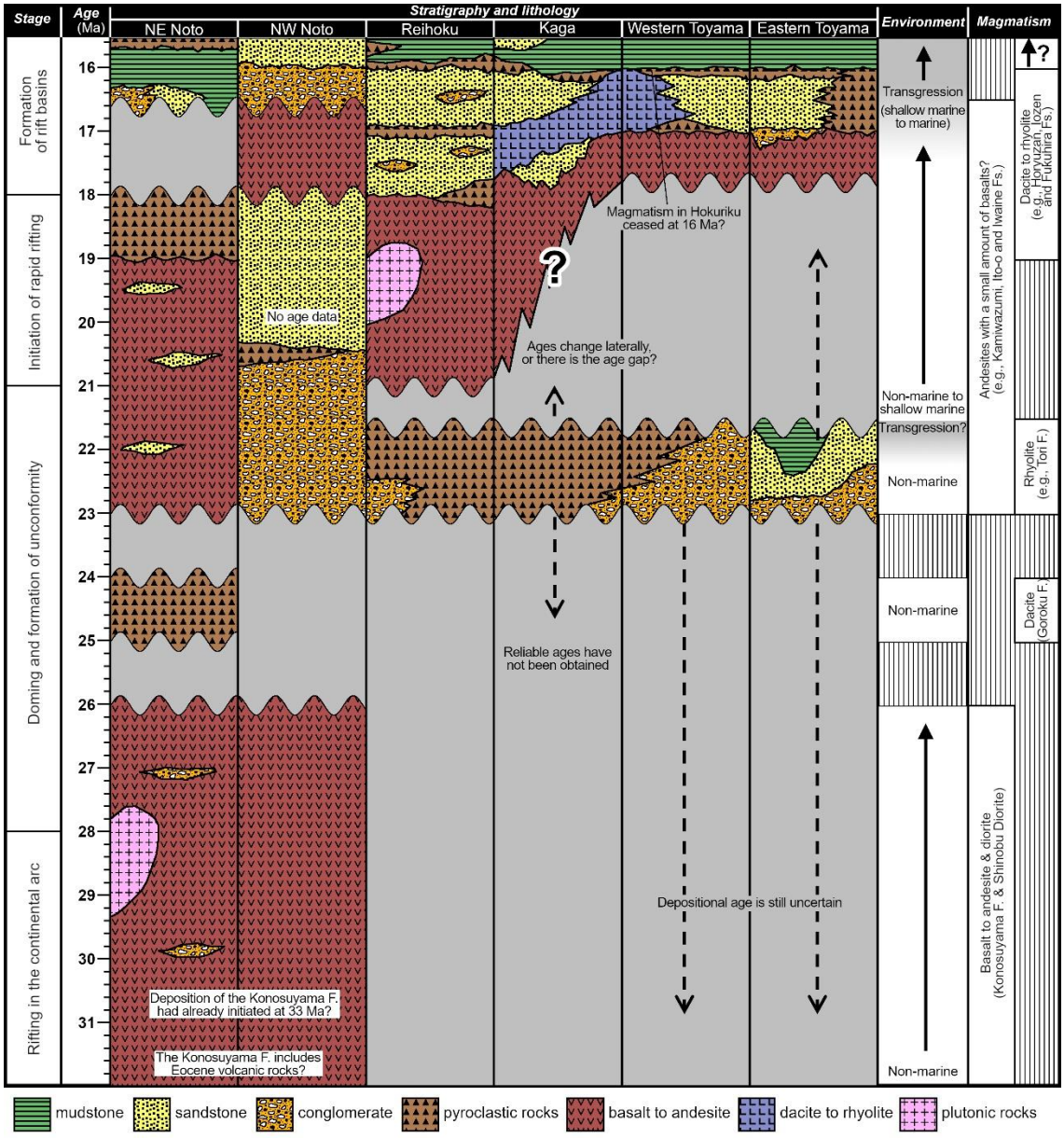

Figure 2.3 Comparison of lithological characteristics between major areas, showing the temporal change in volcanism related to the Japan Sea opening in the Hokuriku region (modified after Yamada and Takahashi, 2021). Stratigraphy and lithology are after Bito et al. (1980), Fukui Prefecture (2010), Ganzawa (1983), Ishida et al. (1998), Kaneko (2001), Kano et al. (1999, 2002, 2007b), Kaseno (1993), Kobayashi et al. (2005), Nakagawa and Tahara (1991), Nakajima et al. (2019), Ozaki (2010), Sakamoto et al. (1959), Sakamoto (1966), Sudo (1979a, b), Tsukawaki and Ooji (2008), Umeda (1997), Yamada

et al. (2017), Yanagisawa (1999a) and Yoshikawa et al. (2002). Abbreviations: F. (Formation), Fs. (formations).

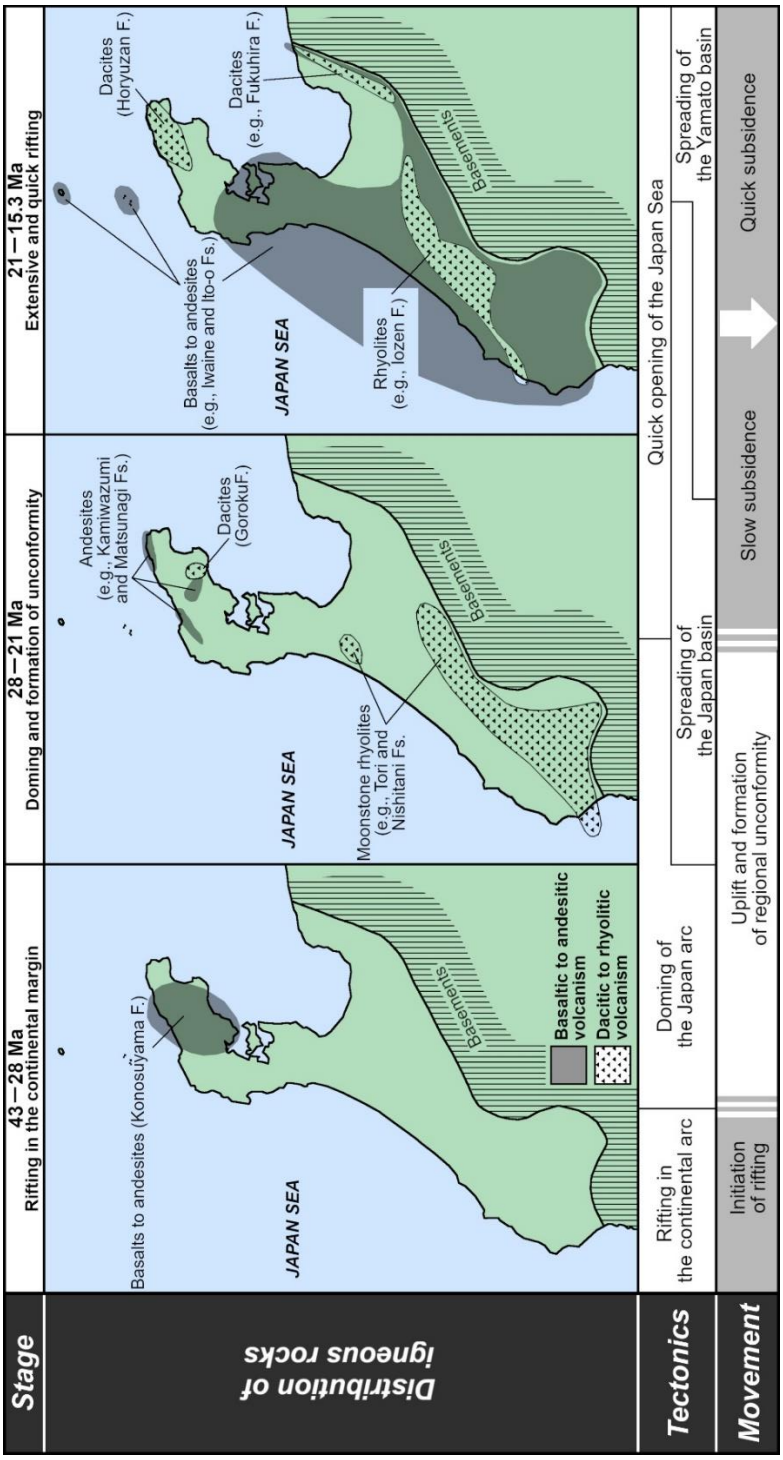

Figure 2.4 Schematic illustration of the spatial change in volcanism related to the Japan Sea opening in the Hokuriku region (modified after Yamada and Takahashi, 2021). Tectonic interpretations are after Kano (2018) and Nakajima (2018). Abbreviations: F. (Formation), Fs. (formations).

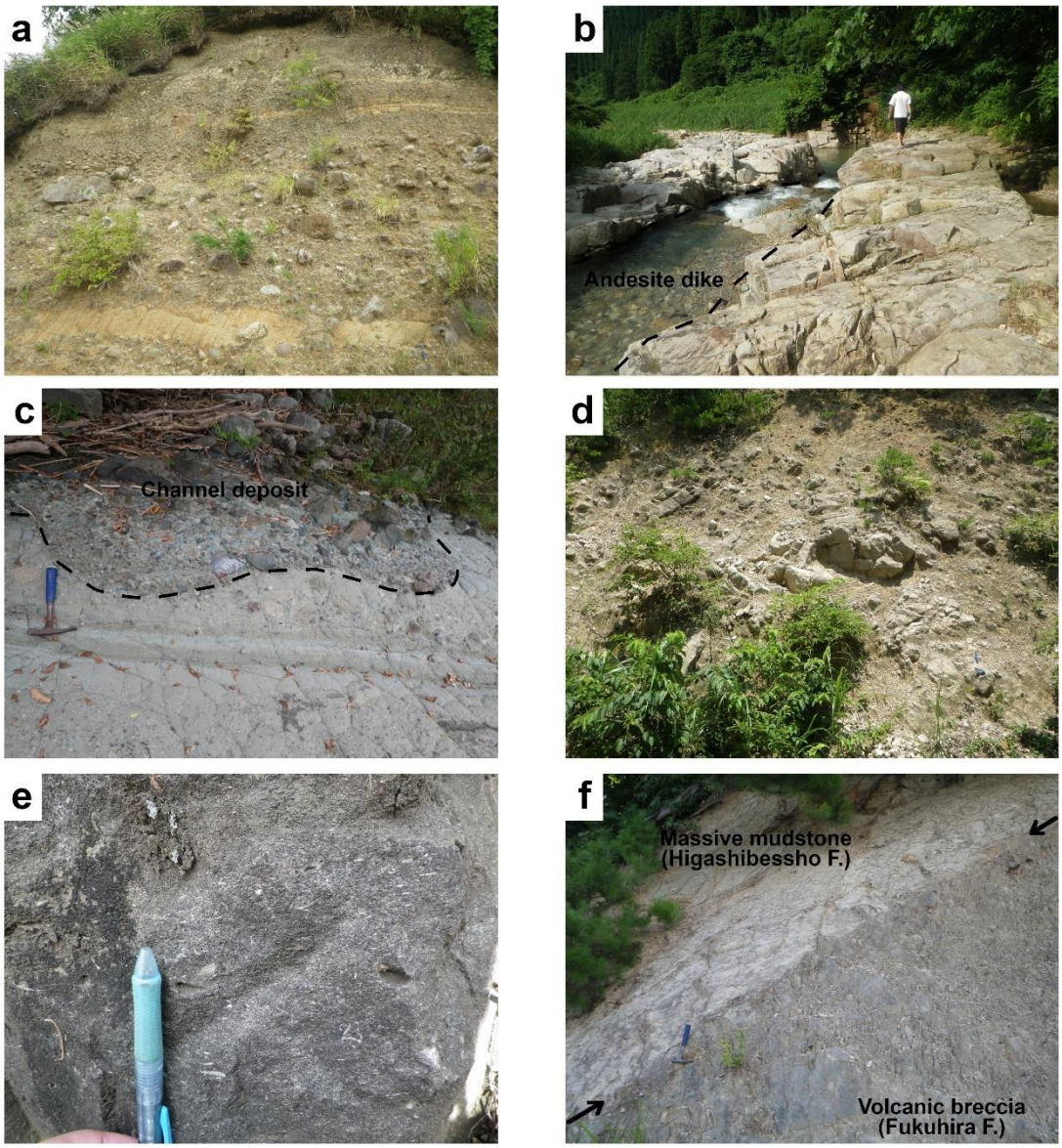

Figure 2.5 Field occurrences of the Oligocene to Middle Miocene strata in Toyama basin. (a) alternation of conglomerate and sandstone of the Nirehara Formation in the Kamiichi area of eastern Toyama basin. (b) densely welded tuff, intruded by an andesite dike, of the Usunaka Moonstone Rhyolite Member, the Johana (Tori) Formation, in the Johana area of western Toyama basin. (c) andesitic volcaniclastic rocks showing channel structure of the Iwaine Formation in the Yatsuo area of central Toyama basin. (d) rhyolitic block lava of the Iozen Formation in the Iozen area of western Toyama

basin. (e) fossiliferous massive sandstone, including fragments of fossils, of the Sunagozaka Formation in the Iozen area of western Toyama basin. (f) a formation boundery between the Fukuhira and Higashibessho formations in the Uozu area of eastern Toyama basin.

3. Geology of the Toyama basin

In this chapter, detailed geology of the study area (entire area of the Toyama basin) is explained. The Cenozoic strata in the study area consists of the Nanto (the Johana and Nirehara Formations) and Yatsuo Groups (the Iwaine, Ganzo, Iozen, Sasagawa, Kurosedani, Fukuhira, Sunagozaka, Doyama, Higashibessho and Omine Formations) in stratigraphic ascending order. The Johana and Nirehara Formations are composed mainly of conglomerate and sandstone with rhyolitic welded tuff. The Iwaine and Ganzo Formations are composed mainly of andesites. The Iozen and Sasagawa Formations is composed mainly of rhyolites and clastic rocks. The Kurosedani Formation is composed mainly of irregular alternation of conglomerate, sandstone, and mudstone. The Fukuhira Formation is composed mainly of andesites to dacites with clastic rocks. The Sunagozaka and Doyama Formations are composed mainly of sandstone with pyroclastic rocks. The Higashibeesho and Omine Formations are composed mainly of massive mudstone.

Index map showing the distribution of Late Oligocene to Miocene strata in the Hokuriku region is shown **Figure 3.1**. In **Figure 3.2** to **Figure 3.5**, stratigraphic subdivisions of Oligocene to Middle Miocene strata in the Toyama basin are reviewed and summarized. The geological map of the Late Oligocene to Middle Miocene strata in the Toyama basin is shown in **Figure 3.6**. An index map showing the study area is shown in **Figure 3.7**. Stratigraphic subdivision and summarized lithology are shown in **Figure 3.8**. Columnar sections and photographs of typical outcrops are shown in **Figure 3.9** and **3.10**, respectively. The author studied petrology and geochemistry for Late Oligocene to Middle Miocene volcanic rocks from the Nanto area,

where the typical lithostratigraphy of the volcanic rocks can be observed. Hence, figures on detailed geology of the Nanto area are shown **Figure 3.11** to **Figure 3.15**. The geological map and stratigraphic subdivisions are shown in **Figure 3.11** and **3.12**, respectively. The route map and columnar sections in the Nanto area are shown in **Figure 3.13** and **3.14**, respectively. In the last (**Figure 3.15**), field occurrences in the Nanto area are shown.

3.1. Basement rocks

3.1.1.Hida Belt

To compare geochemistry of the target Cenozoic volcanic rocks of this study to the Hida belt, metamorphic and plutonic rock samples were collected and examined by Yamada et al. (2021), Yamada et al. (unpublished data). The Hida belt consists of the Hida metamorphic rocks, the Unazuki metamorphic rocks, and the Hida granites (Takahashi et al., 2010). The Hida metamorphic rocks are composed of shelf sediment-derived paragneisses and marbles with amphibolites and orthogneisses that were formed mainly by low P/T metamorphism in 250–235 Ma, and the metamorphic grade reached from amphibolite to granulite facies (Sohma and Kunugiza, 1993; Takahashi et al., 2018; Wallis et al., 2020; Yamada et al., unpublished data). The Unazuki metamorphic rocks were also metamorphosed by medium *P*/*T* conditions around 250 Ma, and their protoliths were late Paleozoic sediments, limestone, and acidic volcanic rocks (Hiroi, 1978, 1983; Horie et al., 2018). Previous studies considered that those metamorphic rocks of the Hida belt were formed during the collision between the North and South China blocks (e.g., Sohma and Kunugiza, 1993; Takahashi et al., 2018; Wallis et al., 2020). The Hida granites consist of the pre-Jurassic plutons and the Jurassic plutons (Yamada et al., 2021). Takahashi et al. (2018) and Yamada et al. (2021) discussed that the pre-Jurassic and Jurassic plutons were

formed in 250–235 Ma and 200–180 Ma, respectively, and inferred that the magmatism prior to main metamorphism of the Hida belt (250–235 Ma) occurred at 330 Ma, 274 Ma, 266 Ma, 255 Ma, and 240 Ma. Cho et al. (2021a) examined zircon Hf isotope of paragneiss, orthogneiss and Jurassic granitoid from the Hida belt and concluded that the Hida belt is derived from the North China craton. However, Yamada et al. (unpublished data) considered that the origin of the Hida belt is the Songnen block of the Central Asian Orogenic Belt (CAOB) in the NE China, based on zircon geochronology and geochemistry.

3.1.2.Tetori and Futomiyama Groups

The Middle Jurassic to Lower Cretaceous Tetori Group is composed of clastic rocks (Sano, 2015). Conglomerate, sandstone, mudstone containing molluscan and plant fossils were observed in this study.

The Cretaceous Futomiyama Group (Sudo, 1979b) is composed mainly of rhyolitic tuff breccia, rhyolitic tuff, rhyolitic lava and rhyolitic intrusive rocks (Sudo, 1979b; Ganzawa, 1983; Kaneko et al., 2019). Kaneko et al. (2019) reported zircon U–Pb ages of 70.2–66.7 Ma from the type locality and concluded that the Futomiyama Group was emplaced during Maastrichtian of the Late Cretaceous. The Futomiyama Group of the type locality consists of breccia and tuff breccia (the thickness is ~ 150 m), rhyolitic lava (the thickness is ~ 200 m), tuff breccia, tuff and welded tuff (the thickness is ~ 400 m), and rhyolitic lava (the thickness is ~ 200 m) in stratigraphically ascending order (Sudo, 1979b). The total thickness is up to ~ 1000 m. In this study, rhyolitic pyroclastic rocks and rhyolitic lava were observed in the study area.

3.2. Nanto Group

The Nanto Group was newly defied and named in this study. The Yatuo Group consists of the Johana and Nirehara Formations (**Figure 3.8**). The type locality is located in the Nanto area, Toyama Prefecture, and the typical lithostratigraphy can be observed along the Yamada-gawa basin.

3.2.1.Johana Formation

Name and definition: The Johana Formation is a newly defined formation. Ganzawa (1983) termed this formation “the Tori Formation”, however, the terminology of “Tori” was firstly used for the conglomerate member in this formation (Sudo, 1979a and b). “Tori” is given to both of formation and member in Ganzawa (1983). Double use of unit name is not recommended in the International Stratigraphic Guide (Murphy and Salvador, 1999), therefore, “Johohana” is proposed as formation name in this study. The Johana Formation is defined as formation which is composed mainly of conglomerate, arkose sandstone, and moonstone rhyolite and unconformably covers the Futomiyama Group (**Figure 3.8**). The stratum distributed between the Kazura fault (Fujii et al., 1992b) and Saikawa river in Kanazawa City of Ishikawa Prefecture is regarded as the Johana Formation.

Type locality: The type locality is along the Yamada-gawa and Futatsuya-gawa basins in Nanto City, Toyama Prefecture.

Distribution and thickness: The Johana Formation is distributed narrowly between the Kazura fault and Saikawa river in Kanazawa City, Ishikawa Prefecture (**Figure 3.6**). The maximum thickness is ~400 m (Sudo, 1979b).

Stratigraphic relationship: The Johana Formation unconformably covers the Futomiyama Group, the basement, and it is in the stratigraphically same horizon with the Nirehara Formation (**Figure**

3.8 and **3.9**).

Lithology: The Johana Formation is composed mainly of conglomerate, arkose sandstone and rhyolitic welded tuff. Clastic rocks are abundant in the lower part (Tori Conglomerate Member), meanwhile rhyolitic welded tuff is abundant in the upper part (Usunaka Moonstone Rhyolite Member). The lower and upper members are interfingering with each other. The Tori Conglomerate Member is composed mainly of irregular alternation of conglomerate and sandstone, and the lateral continuity of beds is poor. The Conglomerate is composed of imbricated pebble and cobble of orthoquartzite, rhyolite, granitoid, gneiss, chert, sandstone, and mudstone (**Figure 3.15a**). The sandstone and matrix of conglomerate are composed of reddish brown-colored fine to coarse sandstone, with cross laminae and abundant grains of feldspar and quartz. The Usunaka Moonstone Rhyolite Member is composed mainly of reddish brown-colored weakly to densely rhyolitic welded tuff showing columnar joints (**Figure 3.15b**). The welded tuff contains abundant mineral grains of moonstone (alkali feldspar) and quartz. These lithological characteristics suggest that the Johana Formation was deposited in non-marine environment such as fan delta.

Fossil: Fossils have not been found.

Age: K–Ar of 25–24 Ma (Ueda and Aoki, 1970) and zircon fission-track (FT) ages of 25.0–22.2 Ma (Ganzawa, 1983; Nakajima et al., 1983) have been reported. Recently, Ota et al. (2019) reported zircon U–Pb age of 22.4 Ma. In this study, the ^{238}U–^{206}Pb weighted average age of 22.8 ± 0.2 Ma was obtained.

3.2.2.Nirehara Formation

Name and definition: The Nirehara Formation was defined and named by Tsuda and Chiji (1950). The Nirehara Formation is defined as a formation which is composed mainly of conglomerate, arkose

sandstone and unconformably covers the basement rocks. This formation is distributed between the eastern part of the Toyama basin and the Soyama dome (Sakamoto, 1966). Since rhyolitic welded tuff called “Usunaka rhyolite” in the Shirakimine area is included in the Nirehara Formation, following the definition of this study, the rhyolite is defined as the Sakaue Rhyolite Member of the Nirehara Formation in this study.

Type locality: Riverbank of the Jinzu-gawa river in Nirehara, Toyama City, Toyama Prefecture (Nakajima et al., 2019).

Distribution and thickness: The Nirehara Formation is distributed narrowly between Mt. Takamineyama in Kamiichi Town, Toyama Prefecture and Ohasegawa river in Toyama City, Toyama Prefecture (**Figure 3.6**) and has 400 m of thickness in the maximum (Sakamoto et al., 1959; Sakamoto, 1966). In the central part of the Toyama basin, this formation is exposed thinly (the maximum thickness is approximately 200 m) surrounding the Iwaine Formation due to structure of the Soyama dome.

Stratigraphic relationship: The Nirehara Formation unconformably covers the Hida belt, the Tetori Group and the Futomiyama Group (**Figure 3.8** and **3.9**). This formation had been considered as the stratigraphically upper formation than the Johana Formation by Yamashita et al. (1988), Fujii et al. (1992b), Yamada and Yamada (2018) and Nakajima et al. (2019). However, lithology of both of the Johana and Nirehara Formations are similar to each other (both are composed mainly of conglomerate, arkose sandstone). In addition, there is no gap of their geological structure, and there is no unconformity between the Johana and Nirehara Formations. In the Shirakimine area, the Nirehara Formation includes so called “moonstone rhyolite” as the Sakaue Rhyolite Member (Nozawa et al., 1981), indicating the lithology is the same as the Johana Formation.

Based on these lithological and structural features, the Nirehara Formation is considered to be in the same stratigraphic horizon as the Johana Formation (**Figure 3.8** and **3.9**).

Lithology: The Nirehara Formation is composed mainly of conglomerate, arkose sandstone and mudstone, including rhyolitic welded tuff. Basically, conglomerate, containing gravels of granitoids, rhyolites, chert and gneiss (Imozu Conglomerate Member), occupies the lower part of the formation (**Figure 3.10a**), and arkose sandstone and mudstone (Ashiu Sandstone Member and Myogashima Alteration Member) cover the Imozu Conglomerate Member. In the eastern part of the Toyama basin, breccia of talus deposits is observed (Nomura et al., 1978). Rhyolitic welded tuff (Sakaue Rhyolite Member) is distributed in the Soyama dome (Sakamoto, 1966) of the Shirakimine area, and its lithology is similar to the Usunaka Moonstone Rhyolite Member of the Johana Formation (Moonstone (hecatolite) is also contained).

Fossil: Except for small trace fossils (Kashiwagi, 2012; Nakajima et al., 2019) and not well-preserved plant fossils (*Metasequoia* sp. and *Quercus* sp.; Fujii et al., 1992b), many researchers have reported fragments of plant fossils. Nevertheless, Matsumoto and Ikebe (1958) reported molluscan and plant fossils, the localities are not shown.

Age: Ota et al. (2018) reported of zircon U–Pb age of 36.9 ± 2.6 Ma as the youngest zircon grain from the Imozu Conglomerate Member. From the Ashiu Sandstone Member, Nakajima et al. (2019) reported zircon ^{238}U–^{206}Pb weighted mean age of 68.6 ± 0.7 Ma and zircon fission track age of 69.0 ± 2.9 Ma. Since Kaneko et al. (2019) reported zircon U–Pb ages of ~ 70 Ma from the Futomiyama Group, these ages are considered to be derived from the basement rocks. In this study, zircon ^{238}U–^{206}Pb age of 23.6 ± 0.3 Ma is obtained from a rhyolite gravel in the Nirehara Formation distributed in the eastern part of the

Toyama basin. Accordingly, the Nirehara Formation is considered to have been deposited in Late Oligocene to Early Miocene.

3.3. Yatsuo Group

The Yatsuo Group was defied and named by Makiyama (1930). The Yatuo Group consists of the Iwaine, Iozen, Kurosedani, and Higashibessho Formations (Nakajima et al., 2019). In this study, the Ganzo, Sasagawa, Fukuhira, Sunagozaka, Doyama and Omine Formations are included in the Yatsuo Group (**Figure 3.8**). The type locality is located in the Yatsuo area, Toyama Prefecture, and the typical lithostratigraphy can be observed along the Jinzu-gawa basin (Makiyama, 1930).

3.3.1.Iwaine Formation

Name and definition: The Iwaine Formation was defied and named by Imamura (1937). The Iwaine Formation is defined as a formation which is composed mainly of andesitic lava and pyroclastic rocks and unconformably covers the Nirehara and Johana and the basement rocks.

Type locality: River bank of the Jinzu-gawa river in Iwaine, Toyama City, Toyama Prefecture (Nakajima et al., 2019).

Distribution and thickness: The Iwaine Formation is distributed from the eastern part to the western part of Toyama Prefecture (**Figure 3.6**), and it thickly exposures on mountains of the Soyama dome (Sakamoto, 1966), surrounding the basement rocks. The thickness is ~1000 m (maximum 1500 m) in the western part to the central part of Toyama prefecture, whereas it becomes ~200 m in the eastern part of Toyama Prefecture.

Stratigraphic relationship: The Iwaine Formation unconformably covers the Johana and Nirehara Formations (**Figure 3.8** and **3.12**).

Lithology: The Iwaine Formation is composed mainly of andesitic

lava, andesitic pyroclastic rocks, and clastic rocks. Olivine two-pyroxene andesite and amphibole andesite occupy the lower part of the Formation, and two-pyroxene andesite and clastic rocks overlie them (**Figure 3.12**). These andesites are totally and weakly altered, therefore, they show greenish brown and white color. Lava flows consists of massive lava and block lava showing dark brown color, and columnar and platy joints are partly observed. Clastic rocks just under lava flows rarely exhibit reddish brown color due to high temperature oxidation (**Figure 3.15c**). Clastic rocks are composed of irregular alternating beds of conglomerate, sandstone, and mudstone, rarely showing channel structure (**Figure 3.10c**). Clasts are composed of andesites derived from the Iwaine Formation. Amphibole andesitic pyroclastic rocks in the lower part of the formation are composed of massive lapilli tuff and partly welded. These lithological characteristics suggest that the Iwaine Formation was deposited in non-marine environment.

Fossil: Fossils have not been found in the study area. Plant and molluscan fossils were reported from the Yatsuo area, Toyama Prefecture, by Sakamoto and Nozawa (1960) and Yamada and Yamada (2018).

Age: K–Ar and zircon FT ages have been reported by Shibata (1973; K–Ar age; 13.6 ± 0.7, 15.9 ± 0.9, 16.0 ± 0.9 Ma), Japan National Oil Corporation (1985; K–Ar age; 15.8 ± 1.1, 18.9 ± 0.9 Ma), Kaneko (2001; K–Ar age; 16.3 ± 0.9, 16.5 ± 0.9 Ma), Itoh and Watanabe (2006; FT age; 17.2 ± 0.9 Ma), and Shinmura and Arakawa (2008; 17.3 ± 1.0 Ma). Recently, Nakajima et al. (2019) reported the weighted average of ^{238}U–^{206}Pb ages of 17.6 ± 0.3 Ma from zircons in the welded tuff of the Iwaine Formation in the Kubusugawa basin. In this study, the ^{238}U–^{206}Pb weighted average age of 17.1 ± 0.4 Ma was obtained.

3.3.2. Ganzo Formation

Name and definition: The Ganzo Formation was defined and named by Ichimura (1935). The Ganzo Formation is defined as a formation which is composed of andesitic lava and pyroclastic rocks and covers the basement rocks through the Kurobishiyama fault (Takeuchi et al., 2017).

Type locality: River floor of the Sasagawa river in Ganzo of Asahi Town of the eastern Toyama basin (Fujii, 1959).

Distribution and thickness: The Ganzo Formation is distributed only in the mountain area of Asahi Town (**Figure 3.6**), and its thickness is up to 300 m in the maximum (Takeuchi et al., 2017).

Stratigraphic relationship: The Ganzo Formation covers the basement rocks through the Kurobishiyama fault (Takeuchi et al., 2017; **Figure 3.8**). This formation is heterotopic to the Iwaine Formation.

Lithology: The Ganzo Formation is composed mainly of andesitic lava and andesitic pyroclastic rocks and clastic rocks. Andesitic massive lava flow can be observed in the type locality, and block lava flow are distributed in other areas.

Fossil: Fossils have not been reported from this formation.

Age: Radiometric ages have not been reported from the Gano Formation. Based on the stratigraphic relationships with the Sasagawa and Iwaine Formations, the Ganzo Formation is considered to have been formed in Early Miocene.

3.3.3. Iozen Formation

Name and definition: The Iozen Formation was defined and named by Fujita and Nakagawa (1948). The Iozen Formation is defined as a formation which is composed mainly of rhyolitic lava and pyroclastic rocks and conformably covers the Iwaine Formation.

Type locality: Mt. Iozen on the boundary between Nanto City, Toyama Prefecture, and Kanazawa City, Ishikawa Prefecture (Nakajima et al., 2019).

Distribution and thickness: The thickness is the maximum (>1000 m) around Mt. Iozen on the boundary between Toyama and Ishikawa Prefectures (**Figure 3.6** and **3.11**). In the central and eastern parts of Toyama, the thickness becomes ~400 m.

Stratigraphic relationship: The Iozen Formation conformably covers the Iwaine Formation.

Lithology: The Iozen Formation is composed mainly of rhyolitic lava, rhyolitic pyroclastic rocks, and clastic rocks. Rhyolitic lava and pyroclastic rocks exhibit variegated color (white, black, pale green, pale pink, and reddish brown). Rhyolitic lavas are observed as massive lava in the summit area of Mt. Iozen, whereas block lava is distributed in the foot area of Mt. Iozen (**Figure 3.10d**). Rhyolitic pyroclastic rocks are composed mainly of massive pumiceous lapilli tuff. Irregularly alternating beds of conglomerate, sandstone, and mudstone whose clasts are composed of rhyolites are intercalated in some stratigraphically horizons (**Figure 3.14**). Dome structure develops around Mt. Iozen, pyroclastic rocks and clastic rocks dip toward the foot area of Mt. Iozen (e.g., Ikebe, 1949; Ganzawa, 1983). These lithological characteristics suggest that the Iozen Formation was deposited in non-marine environment.

Fossil: Matsuo and Nakanishi (1967) found plant fossils from interbedded mudstone.

Age: Zircon FT ages of 16.5–15.0 Ma have been reported from the Nanto area by Ganzawa (1983) and Itoh et al. (2000). Shibata (1973) reported K–Ar ages of 14.3–14.1 Ma from the Yamada-gawa basin of the Yatsuo area, however, the ages are thought to be young due to alteration (Shibata, 1973). In addition, a zircon FT age of 17.2 ± 0.6

Ma and a zircon U–Pb age 16 ± 4 Ma were obtained from the Yamada-gawa basin by Itoh and Watanabe (2005) and Nakama et al. (2010), respectively. In this study, the ^{238}U–^{206}Pb weighted average age of 16.8 ± 0.2 Ma was obtained.

3.3.4.Kurosedani Formation

Name and definition: The Kurosedani Formation was defined and named by Tsuda and Chiji (1950). The Kurosedani Formation is defined as a formation which is composed mainly of conglomerate and alternation of sandstone and mudstone.

Type locality: An area between Kakehata and Do in Toyama City, Toyama Prefecture.

Distribution and thickness: The Kurosedani Formation is distributed between the right bank of Shogawa river in the Tonami area and the Oiwagawa basin in the eastern Toyama Prefecture (**Figure 3.6**). The maximum thickness is up to 900 m in the Yatsuo area (Hayakawa and Takemura, 1987; Nakajima et al., 2019), and the thickness become thin toward the eastern part of Toyama Prefecture.

Stratigraphic relationship: Generally, the Kurosedani Formation conformably covers the Iwaine Formation (**Figure 3.8** and **3.9**), but it partly and unconformably covers the Iwaine Formation with basal conglomerate (Nozawa and Sakamoto, 1960; Sakamoto and Nozawa, 1960; Yamada and Yamada, 2018). The Kurosedani Formation is heterotopic or interfingering with the Iozen, Fukuhira, Sunagozaka and lower part of the Doyama Formations (**Figure 3.8** and **3.9**).

Lithology: The Kurosedani Formation is composed of irregular alternating beds of conglomerate, sandstone and mudstone. The lithology varies largely and laterally. In the type locality and the eastern part of Toyama Prefecture, the lower part of the Kurosedani Formation is composed mainly of conglomerate containing andesite gravels, and alternating beds of sandstone and mudstone become

abundant upward, indicating finning-upward (Nozawa and Sakamoto, 1960; Sakamoto and Nozawa, 1960; Hayakawa and Takemura, 1987; Kaneko, 2001; Yamada and Yamada, 2018; this study). Westward from the type locality, sandstone and mudstone become abundant rather than conglomerate (Hayakawa and Takemura, 1987; Nakajima et al., 2019). The Yamadanaka Tuff composed of massive or well-bedded pumiceous tuff is observed widely in the Toyama basin (Nakajima et al., 2019).

Fossil: The Kurosedani Formation is very famous, because lots of fossils have been reported from this formation. The fauna (Kurosedani fauna; Tsuda, 1960; Kaseno, 1964) is termed “the Yatstuo-Kadonosawa fauna (Chinzei, 1986; Ogasawara et al., 1990; Ogasawara et al., 2008)” together with the Kadonosawa fauna of the NE Japan arc. Makiyama (1930) and Imamura (1931) reported fossils as pioneering reports, and Tsuda (1953, 1959) and many researchers have been reported fossils of mollusks, vertebrates, plankton and plants. Nakajima et al. (2019) showed the detailed list of literature on fossils from this formation in the type locality. Imamura et al. (1951), Nozawa and Sakamoto (1960), Sumi and Nozawa (1973), and Kaneko (2001) reported fossils from the eastern part of the Toyama basin.

Age: Hayakawa (1983), Nakajima and Mizushima (1984), Nakajima et al. (2019) reported zircon fission track ages of 16.4–15.0 Ma, and Nakajima et al. (2019) reported a zircon ^{238}U–^{206}Pb weighted mean age of 16.6 ± 0.2 Ma from the Yamadanaka Tuff. Hayakawa and Danhara (1986) reported a zircon fission track age of 16.8 ± 0.9 Ma from tuff in the upper part of the formation. Yamada et al. (1998) and Kaneko (2001) reported K–Ar ages of 14.8–13.92 Ma from andesitic lava and dyke in the Kurosedani Formation.

3.3.5.Sasagawa Formation

Name and definition: The Sasagawa Formation was defined and named by Ichimura (1935). Takeuchi et al. (2017) subdivided this formation into two formations: the Sasagawa and Hanyu Formations. Nevertheless, lithology and distribution of both are similar and consistent with each other. Accordingly, the Sasagawa and Hanyu Formations by Takeuchi et al. (2017) are unified and regarded as one formation (Sasagawa Formation) in this study. The Sasagawa Formation is defined as a formation which conformably covers the Ganzo Formation and is composed mainly of sandstone, mudstone and rhyolitic lava.

Type locality: River bank and floor of Sasagawa river in Sasagawa, Asahi Town, Toyama Prefecture (Itoh, 1985).

Distribution and thickness: The Sasagawa Formation is distributed in hill and mountain area between Asahi Town and Nyuzen Town (**Figure 3.8**), and the maximum thickness is up to 550 m (Takeuchi et al., 2017).

Stratigraphic relationship: Since there is no outcrop that the Sasagawa Formation covers the lower Ganzo Formation (**Figure 3.8**), the stratigraphic relationship between the Sasagawa and Ganzo Formations is still unknown (Takeuchi et al., 2017). However, the geological structure of both is consistent with each other, suggesting that the Sasagawa Formation conformably covers the Ganzo Formation (Takeuchi et al., 2017). The Sasagawa Formation is heterotopic with the Fukuhira Formation.

Lithology: The Sasagawa Formation is composed mainly of massive mudstone to sandstone and rhyolite. Massive sandstone and mudstone are abundant in the northern and southern part of the distribution (Takeuchi et al., 2017). Rhyolite contains quartz phenocryst and shows the occurrence as massive to block lava flow

in and around the type locality. In other areas, rhyolites are composed mainly of pumiceous lapilli tuff (Takeuchi et al., 2017).

Fossil: Trace fossils, wood fossil including *Teredinidae* sp. (Takeuchi et al., 2017) and microfossils (Itoh, 1985) have been reported from the Sasagawa Formation.

Age: Zircon fission track ages of 18.2–14.0 Ma (Itoh, 1985; Itoh et al., 2016; Takeuchi et al., 2017) and zircon U–Pb ages of 16.3–16.2 Ma (Itoh et al., 2016; Takeuchi et al., 2017) have been reported from several outcrops of the formation.

3.3.6.Fukuhira Formation

Name and definition: The Fukuhira Formation was defined and named by Imamura et al. (1951). The Fukuhira Formation is defined as a heterotopic formation with the Kurosedani Formation, composed mainly of andesitic to dacitic lava, pyroclastic rocks and clastic rocks. The Kurosedani Formation in this study includes the Tsubono Formation by Takeuchi et al. (2017).

Type locality: River bank of Fusegawa river in Fukuhira, Kurobe City, Toyama Prefecture (Kaneko, 2001).

Distribution and thickness: The Fukuhira Formation is distributed between Shiroishigawa basin and Kurobegawa basin in the eastern part of the Toyama basin (Kaneko, 2001; Takeuchi et al., 2017; **Figure 3.6**). The maximum thickness is considered to be up to ~ 600 m, on the basis of Kaneko (2001), and the thickness becomes thin toward the Kurobegawa basin.

Stratigraphic relationship: The Fukuhira Formation conformably covers the Iwaine Formation and unconformably covers the Iozen Formation (Sumi and Nozawa (1973) considered it as the Iwaine Formation) and the basement rocks. It is heterotopic and interfingering with the Kurosedani Formation. (**Figure 3.8** and **3.9)**

Lithology: The Fukuhira Formation is composed mainly of andesitic

to dacitic lava, dyke, pyroclastic rocks and epiclastic rocks (**Figure 3.10f**). The lithology of this formation varies largely and complicatedly, and hence Kaneko (2001) subdivided the formation into ten members. Lava with clinker, volcanic bomb, pisolite, welded tuff can be observed, whereas, hyaloclastite and peperite are also intercalated. Sandstone and mudstone are composed of volcanic-origin grains.

Fossil: Imamura et al. (1951), Wadatsumi et al. (1955), Nozawa and Sakamoto (1960), Sumi and Nozawa (1973), and Kaneko (2001) reported a lot of molluscan fossils and some microfossils.

Age: K–Ar ages of 15.34–12.19 Ma were reported from andesitic lavas and dykes by Yamada et al. (1998) and Kaneko (2001). Itoh and Watanabe (2006) reported a zircon fission track age of 14.3 ± 0.7 Ma from pumice tuff sample. Recently, Takeuchi et al. (2017) reported a zircon fission track age of 12.2 ± 1.0 Ma and a zircon ^{238}U–^{206}Pb weighted mean age of 15.9 ± 0.2 Ma from a dacitic lava sample.

3.3.7.Sunagozaka Formation

Name and definition: The Sunagozaka Formation was defied and named by Fujita and Nakagawa (1948). The Sunagozaka Formation is defined as a heterotopic formation with the Iozen Formation, composed mainly of sandstone and mudstone and conformably covers the Iozen Formation.

Type locality: Sunagozaka-machi, Kanazawa City, Ishikawa Prefecture (Ichihara et al., 1950).

Distribution and thickness: The Sunagozaka Formation is distributed from the northern and western foot part of the Iozen area, surrounding Mt. Iozen (**Figure 3.6** and **3.11**). The thickness is approximately 100 m.

Stratigraphic relationship: The sunagozaka Formation is considered to be a heterotopic formation with the Iozen Formation, because rhyolitic tuff beds is frequently intercalated, and the lower

part of the Doyama Formation can be correlated to the Iozen Formation (Inoue et al., 1964; **Figure 3.8**, **3.12** and **3.14**). This formation can be correlated to the Kurosedani Formation in the Yatsuo area, Toyama Prefecture.

Lithology: The Sunagozaka Formation is composed mainly of alternating beds of sandstone and mudstone (**Figure 3.10e**). Both of sandstone and mudstone are compacted densely, and cross laminae are common in sandstone. Clasts of pumice, obsidian, and rhyolite are contained in sandstone. Rhyolitic tuff beds are intercalated in many stratigraphic horizons. Detailed lithostratigraphy and geological structure have been studied by Sugimoto (1979, 1981, 1988, 1996, 1999), Sugimoto et al. (1980), and Sugimoto and Sakaguchi (1984). These lithological characteristics suggest that the Sunagozaka Formation was deposited in shallow marine and inner bay environment.

Fossil: Ichihara et al. (1950), Inoue et al. (1964), Matsumoto and Nakanishi (1967), Sasaki and Ogasawara (1986), and Sugimoto (1988) found many fossils of mollusks, plants, foot print of mammals, microfossils. Chiji (1961; *Nodosaria longiscata* zonule) and Tanaka et al. (2004; *Pseudoaurila okumurai-Cornucoquimba saitoi* association) reported microfossils including foraminifera. In this study, fossil shards of mollusks were found.

Age: Radiometric ages have not been reported from the Sunagozaka Formation. This formation is considered to have been deposited from early to middle Miocene, based on stratigraphic relationships with other formations.

3.3.8.Doyama Formation

Name and definition: The Doyama Formation was defined and named by Fujita and Nakagawa (1948). This formation is distributed only in the northern foot area of Mt. Iozen.

Type locality: Doyama, Nanto City, Toyama Prefecture (Ichihara et al., 1950).

Distribution and thickness: The Doyama Formation has similar distribution to the Sunagozaka and Omine Formations, surrounding Mt. Iozen in the northern foot area of Mt. Iozen (**Figure 3.6** and **3.11**). The thickness is up to approximately 150 m.

Stratigraphic relationship: The Doyama Formation conformably cover the Sunagozaka Formation (**Figure 3.8**, **3.12** and **3.14**). There is a possibility that the Doyama Formation is a heterotopic formation with the Iozen Formation, because the Doyama Formation contains abundant clasts of rhyolite derived from the Iozen Formation. The lower part of the Doyama Formation is considered to be correlated to the uppermost part of the Iozen Formation and the Yamadanaka tuff bed of the Kurosedani Formation in the Yatsuo area (Inoue et al., 1964). Therefore, the lower part and the middle to upper part of the Doyama Formation can be correlated to the Kurosedani and Higashibessho Formations in the Yatsuo area, Toyama Prefecture, respectively.

Lithology: The Doyama Formation consists of the lower part (conglomerate) and the middle to upper part (sandstone and mudstone). It has been considered that the lower part is composed of lapilli tuff and volcanic breccia containing angular to subangular rhyolitic pumice, tuff, sandstone, mudstone (Sugimoto and Toyoshima, 1984; Yanagisawa, 1999a). However, cross bedded conglomerate containing rhyolitic pumice and no pyroclastic rocks were found from the lowest part in this study. The middle part is composed of cross bedded mudstone and sandstone, meanwhile the upper part comprises cross bedded sandstone and conglomerate containing abundant clasts of rhyolite. Clasts of rhyolite from the Doyama Formation seem similar to rhyolite from the Iozen Formation. These

lithological characteristics suggest that the Doyama Formation was deposited in shallow marine and inner bay environment.

Fossil: Ichihara et al. (1950) and Inoue et al. (1964) found mollusk fossils and microfossils from the Doyama Formation. Chiji (1961; *Nodosaria longiscata* zonule) and Yanagisawa (1999a; *Denticulopsis lauta* zone) reported foraminifera and diatom fossils from this formation.

Age: Radiometric ages have not been reported from the Doyama Formation. Nevertheless, Yanagisawa (1999a) reported the first occurrence of *Cavitatus lanceolatus* (D41.5). The Doyama Formation is considered to have been deposited from early to middle Miocene, based on the stratigraphy and biostratigraphy of diatom.

3.3.9.Higashibessho Formation

Name and definition: The Higashibessho Formation was defined and named by Fujita and Nakagawa (1948). The Higashibessho Formation is defined as a formation composed mainly of massive mudstone conformably covering the Kurosedani and Fukuhira Formations. The Higashibessho Formation in this study includes the Shakusenji Formation by Takeuchi et al. (2017).

Type locality: Higashibessho, Tonami City, Toyama Prefecture (Nakajima et al., 2019).

Distribution and thickness: The Higashibessho Formation is distributed continuously between the right bank of Shogawa river and the left bank of Jinzugawa river (**Figure 3.6**), with the maximum thickness of 600 m (Nakajima et al., 2019). The Distribution of the Higashibessho Formation becomes not continuous in the eastern part of the Toyama basin due to erosion by the Otogawa Formation of the Tonami Group (Nozawa and Sakamoto, 1960), with the thickness of ~ 200 m (Kaneko, 2001).

Stratigraphic relationship: The Higashibessho Formation

conformably covers the Kurosedani and Fukuhira Formations (**Figure 3.8**, **3.9**, **3.12** and **3.14**). The Higashibessho Formation is heterotopic with the upper part of the Doyama Formation and the Omine Formation.

Lithology: The Higashibessho Formation is composed mainly of massive mudstone and fine-grained sandstone, partly showing laminae like shale (**Figure 3.10f**).

Fossil: Although reported number of fossils are less than the Kurosedani Formation, Morishita (1950), Tsuda (1953), Shimizu et al. (2000), Amano et al. (2004) and other researchers have reported molluscan fossils. In addition, many researchers have reported microfossils (Nakajima et al. (2019) showed the literatures). From the eastern part of the Toyama basin, Chiji (1961), Sumi and Nozawa (1973), and Kaneko (2001) reported foraminifera, molluscan, plant fossils.

Age: Itoh and Watanabe (2006) reported a zircon fission track age of 13.7 ± 0.9 Ma from the uppermost part of the formation. However, they considered that this age is much younger compared to biostratigraphy.

3.3.10. Omine Formation

Name and definition: The Omine Formation was defied and named by Fujita and Nakagawa (1948). The Omine Formation is defined as a formation composed of massive mudstone and conformably covers the Doyama Formation.

Type locality: Mt. Omine-yama near Doyama, Nanto City, Toyama Prefecture (Ichihara et al., 1950).

Distribution and thickness: The Omine Formation has similar distribution to the Sunagozaka and Doyama Formations, surrounding Mt. Iozen in the northern foot area of Mt. Iozen (**Figure 3.6** and **3.11**). The thickness is up to approximately 150 m (Ichihara et al., 1950;

Yanagisawa, 1999a).

Stratigraphic relationship: The Omine Formation conformably covers the Doyama Formation (**Figure 3.8**, **3.9**, **3.12** and **3.14**). This formation is in conformity with the upper Kurahara Formation, lithology between the formations gradually changes (Ichihara et al., 1950; Inoue et al., 1964; Yanagisawa, 1999a). The Omine Formation can be correlated to the Higashibessho Formation in the Yatsuo area, Toyama Prefecture.

Lithology: The Doyama Formation is composed of gray-colored massive mudstone (**Figure 3.15f**). Thin tuff beds and nodule are contained in this formation (Ichihara et al., 1950; Inoue et al., 1964). These lithological characteristics suggest that the Omine Formation was deposited in deep marine environment.

Fossil: Ichihara et al. (1950) found many molluscan fossils from the Omine Formation, however, Inoue et al. (1964) pointed out that some horizons containing fossils by Ichihara et al. (1950) should be included in the upper Kurahara Formation. Chiji (1961; *Bolivina marginata adelaidana* zonule) and Inoue et al. (1964) reported foraminifera fossils, and Itoh (1986; *Denticulopsis lauta* zone) reported diatom fossils from the Omine Formation.

Age: Radiometric ages have not been reported from the Imone Formation. Nevertheless, Yanagisawa (1999a) reported the first (D42) and last occurrences (D43) of *Denticulopsis okunoi*. The Omine Formation is considered to have been deposited from 15.6 to 15.3 Ma, based on the stratigraphic relationships with other formations and the biostratigraphy of diatom.

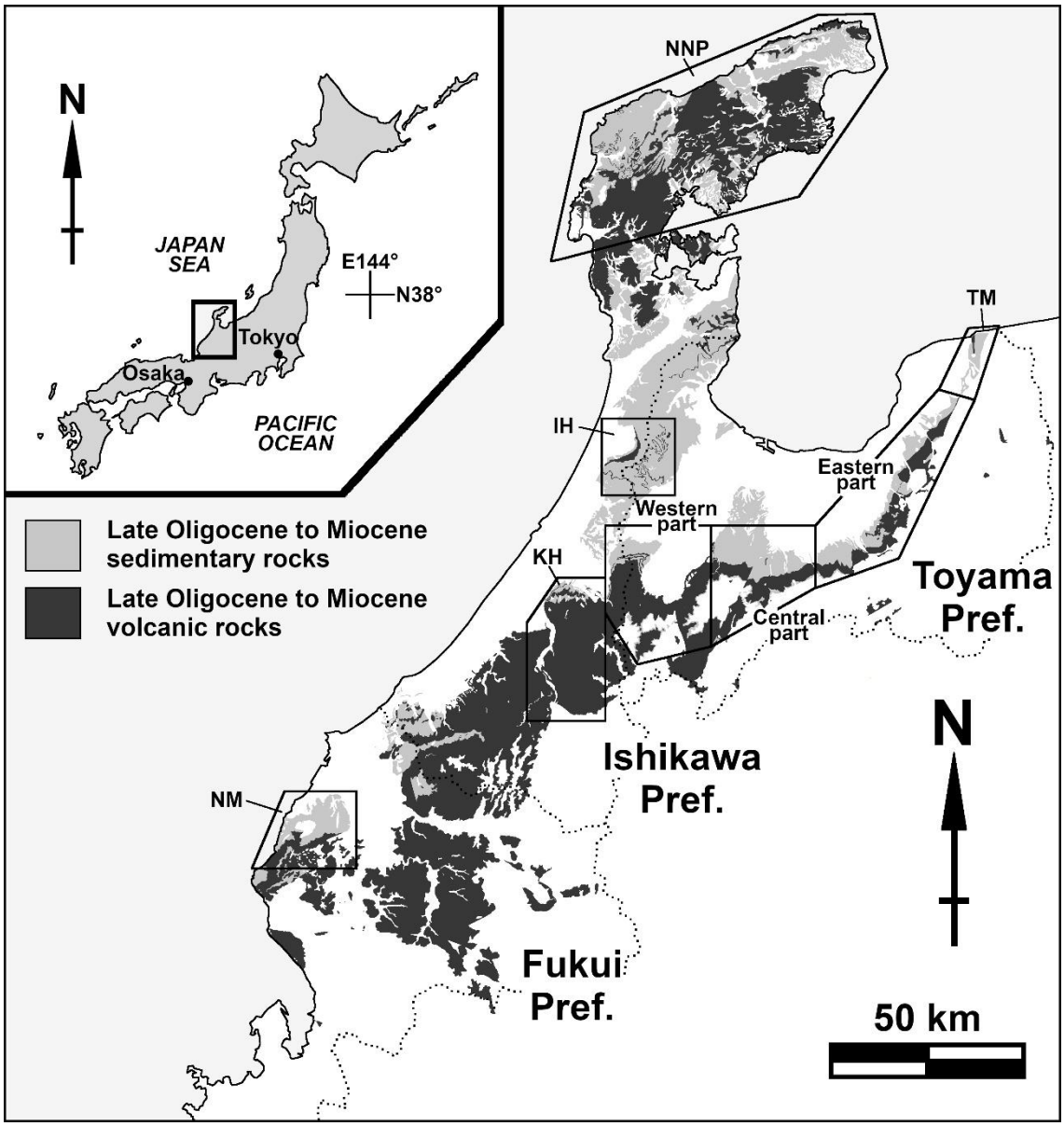

Figure 3.1 Index map showing the distribution of Late Oligocene to Miocene strata in the Hokuriku region (modified from Geological Survey of Japan, 2022). A review on the stratigraphy of the eastern, central and western parts of Toyama Prefecture is carried out in this study. TM: Tomari area, NNP: Northern part of Noto Peninsula, IH: Isurugi-Hodatsu area, KH: Kanazawa-Hakusan area, NM: Niu Mountains area. Pref.: prefecture.

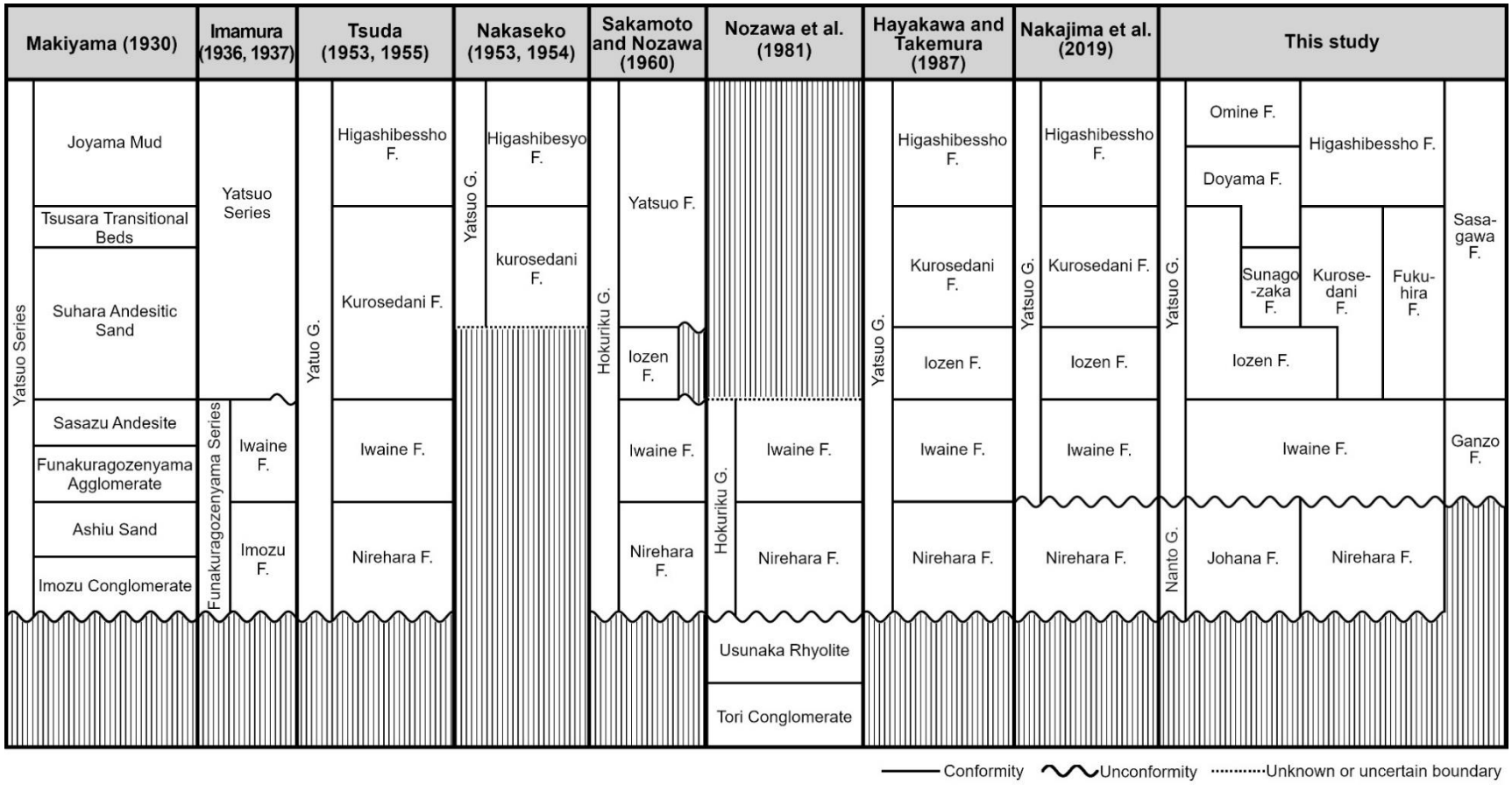
Makiyama (1930)
Imamura (1936, 1937)
Tsuda (1953, 1955)
Nakaseko (1953, 1954)
Sakamoto and Nozawa (1960)
Nozawa et al. (1981)
Hayakawa and Takemura (1987)
Nakajima et al. (2019)
This study
Yatsuo Series
Joyama Mud
Tsusara Transitional Beds
Suhara Andesitic Sand
Sasazu Andesite
Funakuragozenyama Agglomerate
Ashiu Sand
Imozu Conglomerate
Yatsuo Series
Funakuragozenyama Series
Iwaine F.
Imozu F.
Yatuo G.
Higashibessho F.
Kurosedani F.
Iwaine F.
Nirehara F.
Yatsuo G.
Higashibesyo F.
kurosedani F.
Hokuriku G.
Yatsuo F.
Iozen F.
Iwaine F.
Nirehara F.
Hokuriku G.
Iwaine F.
Nirehara F.
Usunaka Rhyolite
Tori Conglomerate
Yatsuo G.
Higashibessho F.
Kurosedani F.
Iozen F.
Iwaine F.
Nirehara F.
Yatsuo G.
Higashibessho F.
Kurosedani F.
Iozen F.
Iwaine F.
Nirehara F.
Yatsuo G.
Omine F.
Doyama F.
Higashibessho F.
Sunago-zaka F.
Kurose-dani F.
Fuku-hira F.
Iozen F.
Sasa-gawa F.
Iwaine F.
Ganzo F.
Nanto G.
Johana F.
Nirehara F.
Conformity
Unconformity
Unknown or uncertain boundary

Figure 3.2 Comparison of main stratigraphic subdivisions of Oligocene to Middle Miocene strata in the central part of Toyama Prefecture (See Figure 3.1 for the details of each location). G.: Group, F.: Formation.

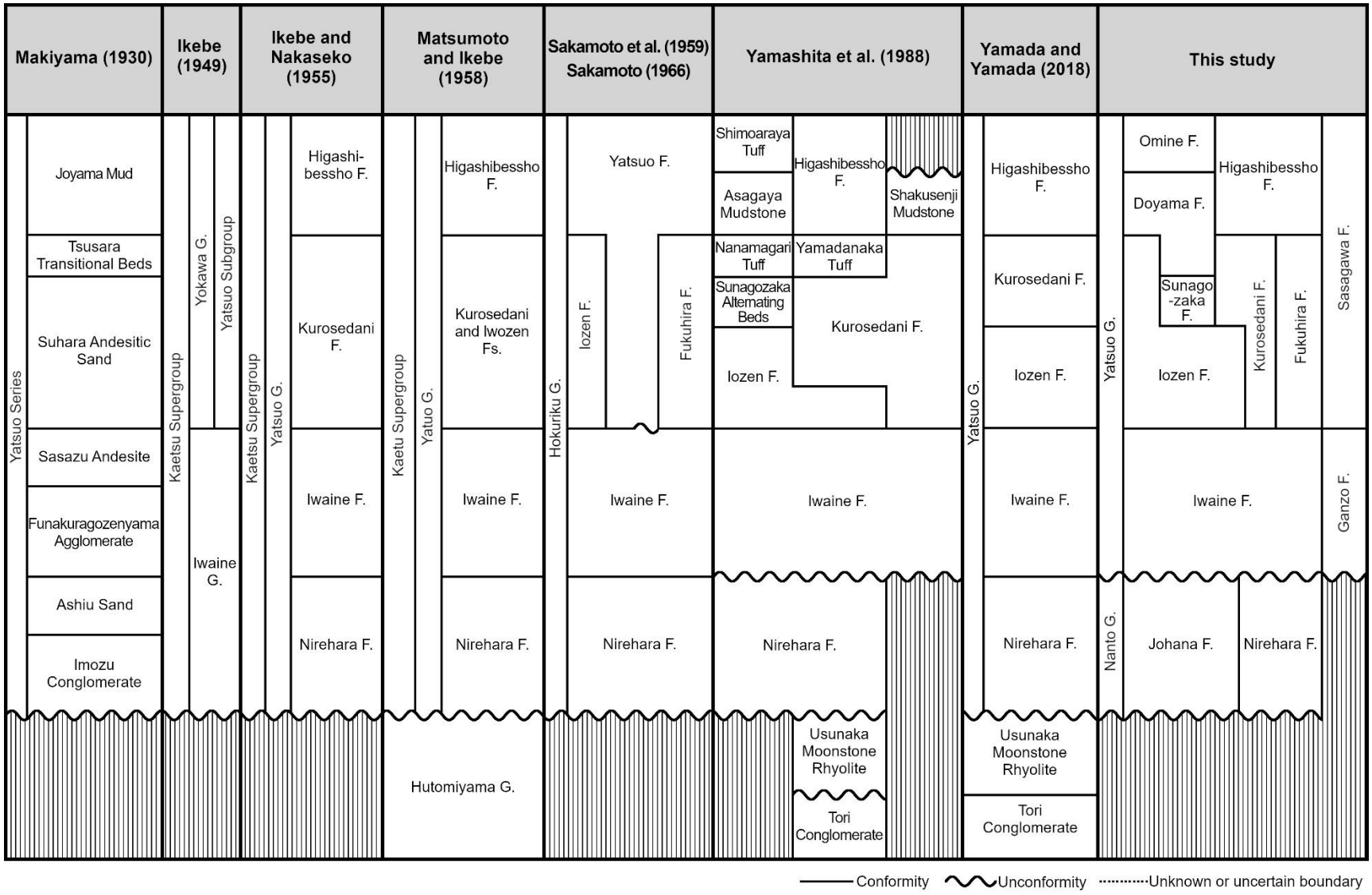
Makiyama (1930)
Ikebe (1949)
Ikebe and Nakaseko (1955)
Matsumoto and Ikebe (1958)
Sakamoto et al. (1959) Sakamoto (1966)
Yamashita et al. (1988)
Yamada and Yamada (2018)
This study
Yatsuo Series
Joyama Mud
Tsusara Transitional Beds
Suhara Andesitic Sand
Sasazu Andesite
Funakuragozenyama Agglomerate
Ashiu Sand
Imozu Conglomerate
Kaetsu Supergroup
Yokawa G.
Yatsuo Subgroup
Iwaine G.
Yatsuo G.
Higashi-bessho F.
Kurosedani F.
Iwaine F.
Nirehara F.
Kaetu Supergroup
Higashibessho F.
Kurosedani and Iwozen Fs.
Iwaine F.
Nirehara F.
Hutomiyama G.
Hokuriku G.
Yatsuo F.
Iozen F.
Fukuhira F.
Iwaine F.
Nirehara F.
Shimoaraya Tuff
Asagaya Mudstone
Higashibessho F.
Shakusenji Mudstone
Nanamagari Tuff
Yamadanaka Tuff
Sunagozaka Alternating Beds
Kurosedani F.
Iozen F.
Iwaine F.
Nirehara F.
Usunaka Moonstone Rhyolite
Tori Conglomerate
Yatsuo G.
Higashibessho F.
Kurosedani F.
Iozen F.
Iwaine F.
Nirehara F.
Usunaka Moonstone Rhyolite
Tori Conglomerate
Yatsuo G.
Omine F.
Doyama F.
Higashibessho F.
Sunago -zaka F.
Iozen F.
Kurosedani F.
Fukuhira F.
Sasagawa F.
Iwaine F.
Ganzo F.
Nanto G.
Johana F.
Nirehara F.
Conformity
Unconformity
Unknown or uncertain boundary

Figure 3.3 Regional comparison of main stratigraphic subdivisions of the Oligocene to Middle Miocene strata in Toyama Prefecture. G.: Group, F.: Formation.

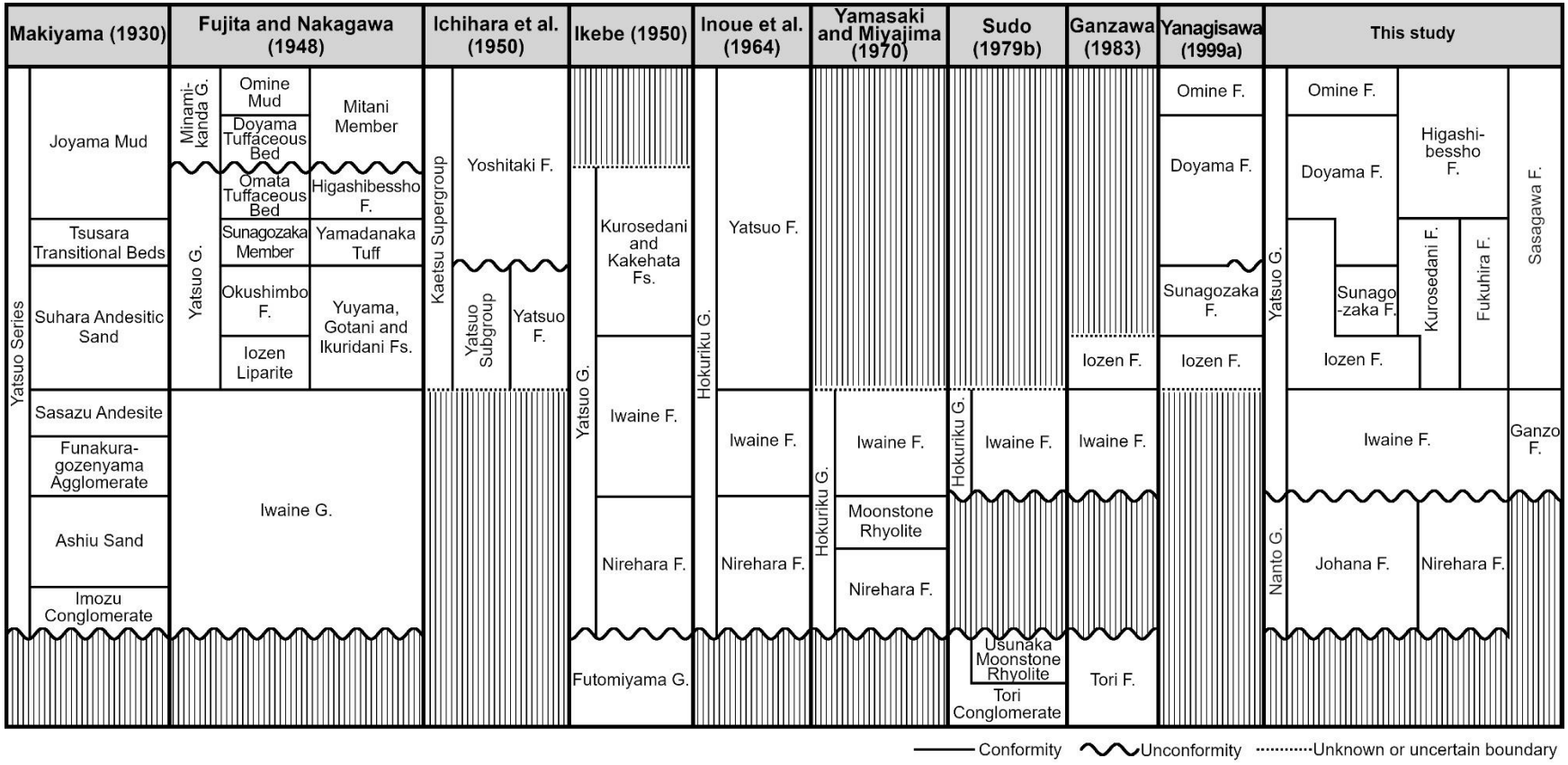
Makiyama (1930)
Fujita and Nakagawa (1948)
Ichihara et al. (1950)
Ikebe (1950)
Inoue et al. (1964)
Yamasaki and Miyajima (1970)
Sudo (1979b)
Ganzawa (1983)
Yanagisawa (1999a)
This study
Yatsuo Series
Joyama Mud
Tsusara Transitional Beds
Suhara Andesitic Sand
Sasazu Andesite
Funakura-gozenyama Agglomerate
Ashiu Sand
Imozu Conglomerate
Minami-kanda G.
Omine Mud
Doyama Tuffaceous Bed
Omata Tuffaceous Bed
Sunagozaka Member
Okushimbo F.
Iozen Liparite
Mitani Member
Higashibessho F.
Yamadanaka Tuff
Yuyama, Gotani and Ikuridani Fs.
Yatsuo G.
Iwaine G.
Kaetsu Supergroup
Yoshitaki F.
Yatsuo Subgroup
Yatsuo F.
Yatsuo G.
Kurosedani and Kakehata Fs.
Iwaine F.
Nirehara F.
Futomiyama G.
Hokuriku G.
Yatsuo F.
Iwaine F.
Nirehara F.
Hokuriku G.
Iwaine F.
Moonstone Rhyolite
Nirehara F.
Hokuriku G.
Iwaine F.
Usunaka Moonstone Rhyolite
Tori Conglomerate
Iozen F.
Iwaine F.
Tori F.
Omine F.
Doyama F.
Sunagozaka F.
Iozen F.
Iwaine F.
Yatsuo G.
Omine F.
Doyama F.
Sunago-zaka F.
Iozen F.
Higashi-bessho F.
Kurosedani F.
Fukuhira F.
Sasagawa F.
Iwaine F.
Ganzo F.
Nanto G.
Johana F.
Nirehara F.
Conformity
Unconformity
Unknown or uncertain boundary

Figure 3.4 Comparison of main stratigraphic subdivisions of Oligocene to Middle Miocene strata in the western part of Toyama Prefecture (See Fig. 3.1 for the location). G.: Group, F.: Formation.

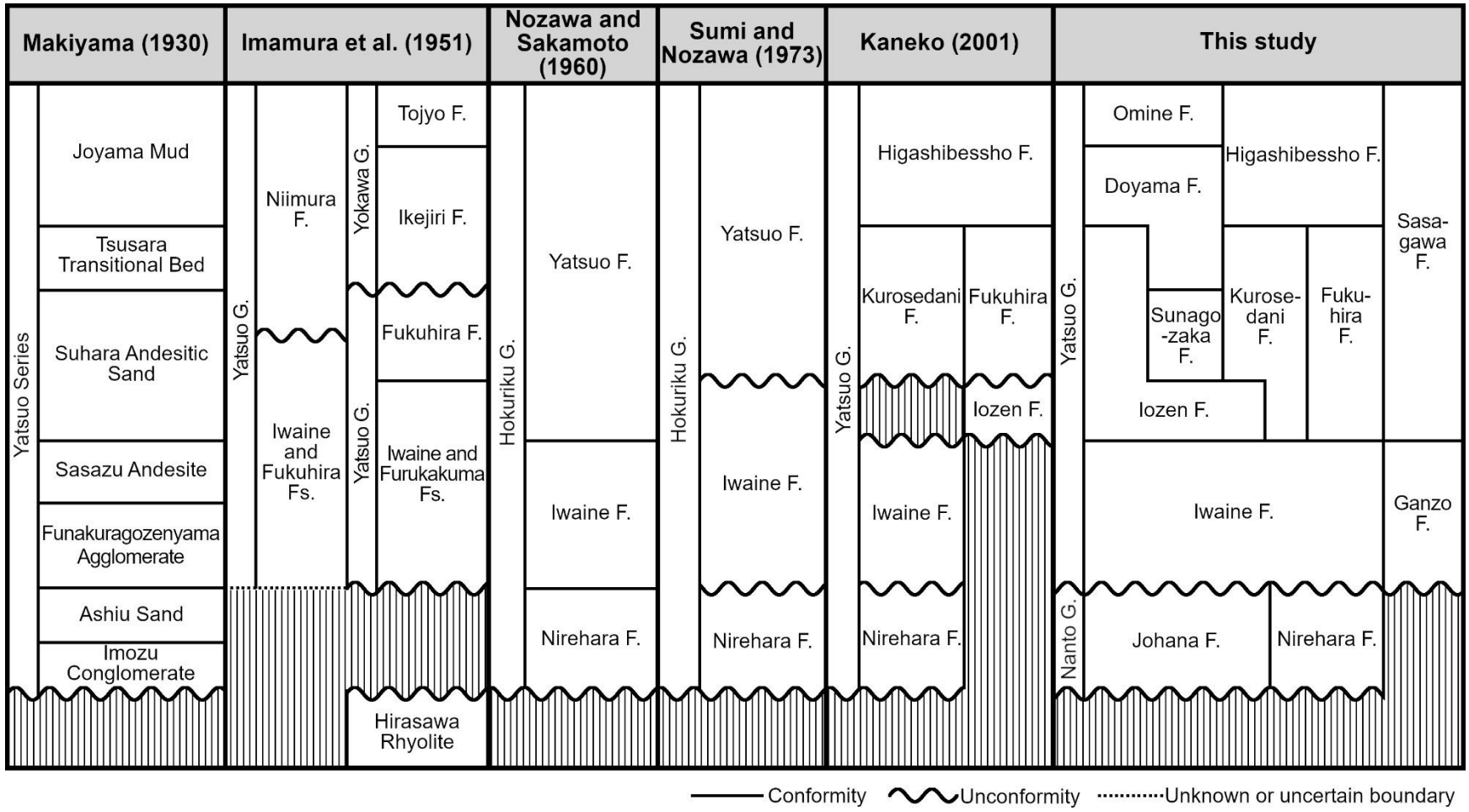
Makiyama (1930)
Imamura et al. (1951)
Nozawa and Sakamoto (1960)
Sumi and Nozawa (1973)
Kaneko (2001)
This study
Yatsuo Series
Joyama Mud
Tsusara Transitional Bed
Suhara Andesitic Sand
Sasazu Andesite
Funakuragozenyama Agglomerate
Ashiu Sand
Imozu Conglomerate
Yatsuo G.
Niimura F.
Iwaine and Fukuhira Fs.
Yokawa G.
Tojyo F.
Ikejiri F.
Fukuhira F.
Iwaine and Furukakuma Fs.
Hirasawa Rhyolite
Hokuriku G.
Yatsuo F.
Iwaine F.
Nirehara F.
Yatsuo F.
Iwaine F.
Nirehara F.
Yatsuo G.
Higashibessho F.
Kurosedani F.
Fukuhira F.
Iozen F.
Iwaine F.
Nirehara F.
Yatsuo G.
Omine F.
Doyama F.
Higashibessho F.
Sunago-zaka F.
Kurose-dani F.
Fuku-hira F.
Iozen F.
Sasa-gawa F.
Iwaine F.
Ganzo F.
Nanto G.
Johana F.
Nirehara F.
Conformity
Unconformity
Unknown or uncertain boundary

Figure 3.5 Comparison of main stratigraphic subdivisions of Oligocene to Middle Miocene strata in the eastern part of Toyama Prefecture (See Fig. 3.1 for the location). G.: Group, F.: Formation.

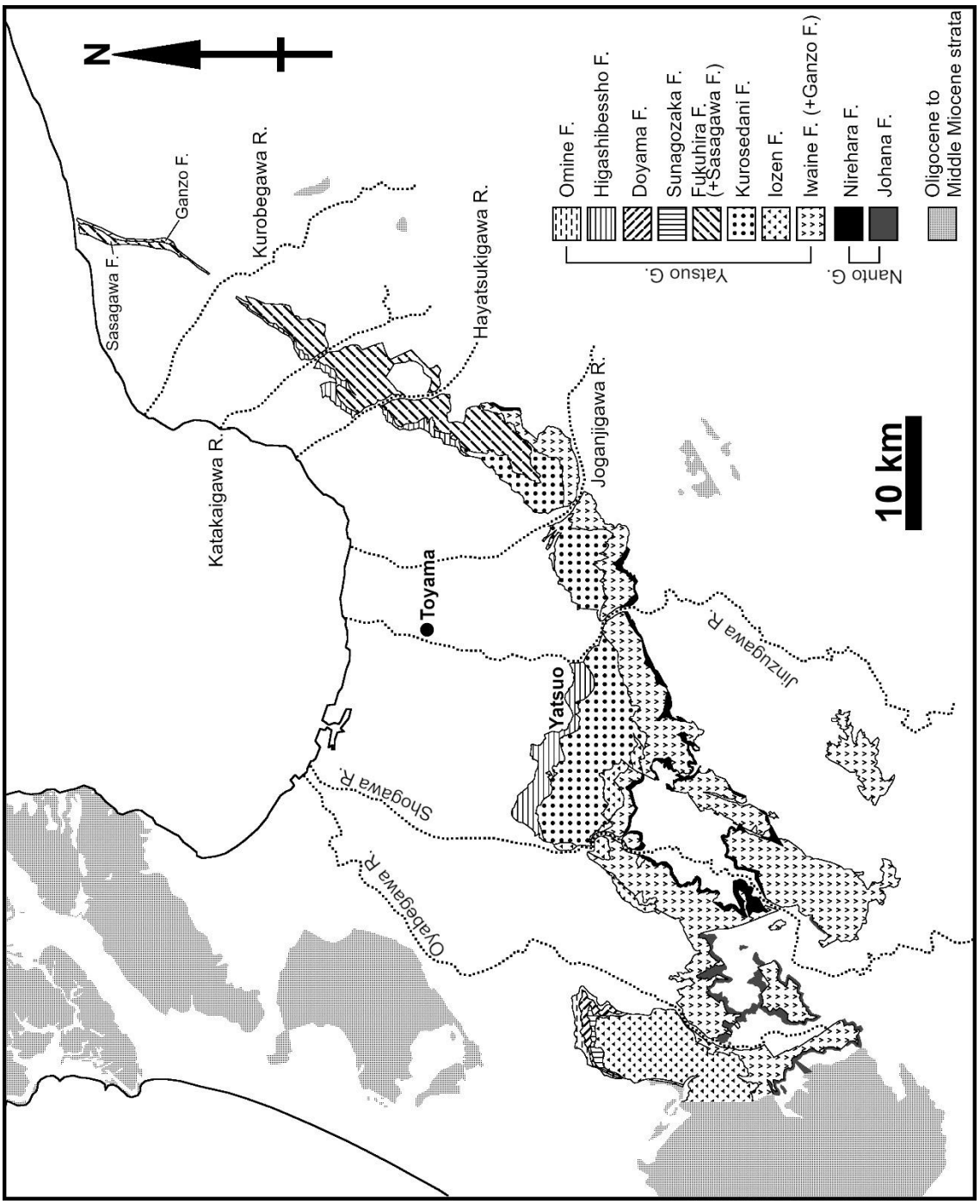

Figure 3.6 Geological map showing the distributions of the the Nanto and Yatsuo Groups, revised in this paper. Modified from Nozawa and Sakamoto (1960), Sakamoto and Nozawa (1960), Inoue et al. (1964), Sudo (1979b), Nozawa et al. (1981), Ganzawa (1983), Hayakawa and Takemura (1987), Kaneko (2001), Takeuchi et al. (2017), Yamada and Yamada (2018), and Geological Survey of Japan (2022). G.: Group,

F.: Formation.

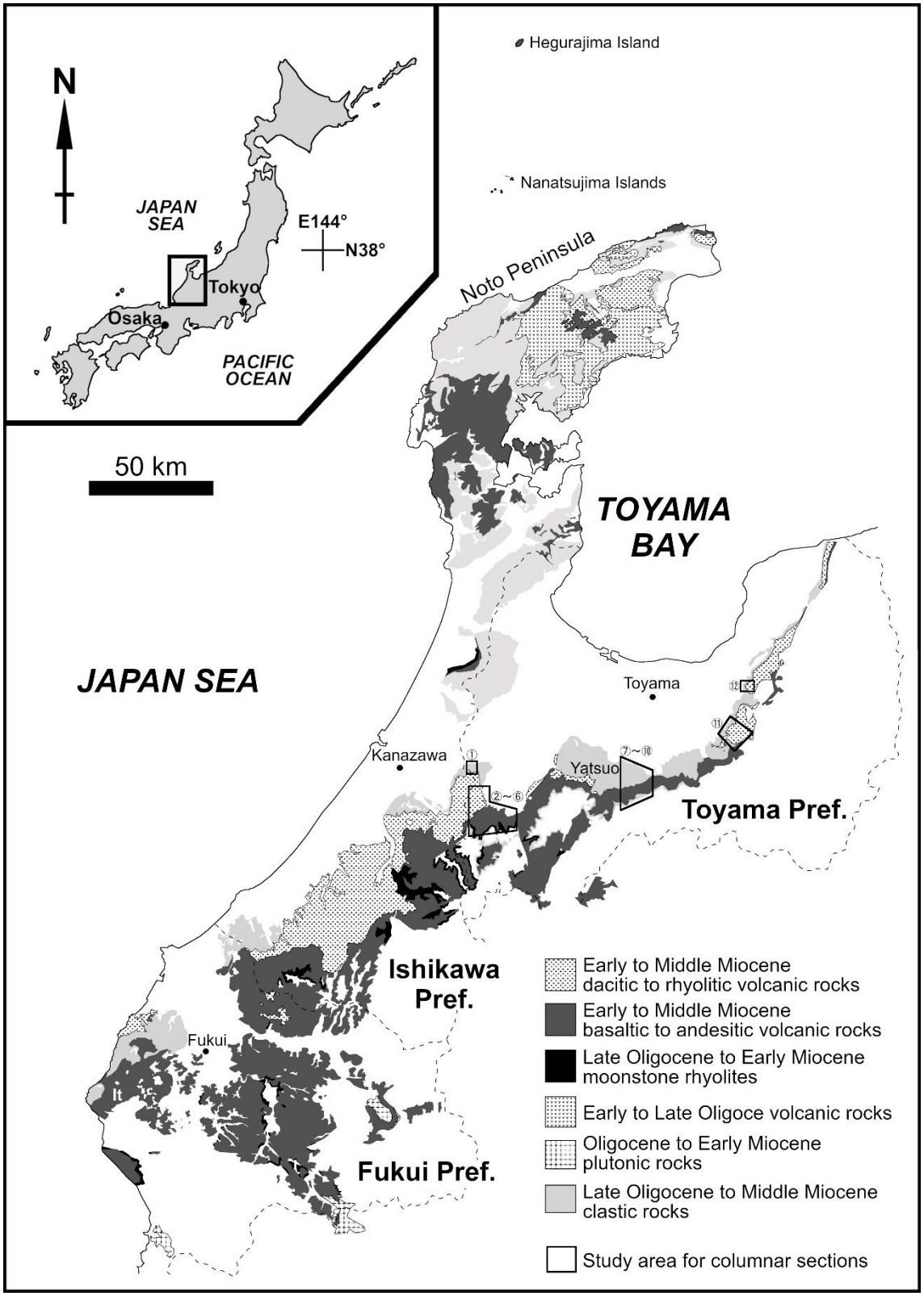

Figure 3.7 Index map showing the distributions of Oligocene to Miocene igneous rocks formed during and just after the Japan Sea

opening in the Hokuriku region (modified from Yamada and Takahashi, 2021). Numbers indicate routes for columnar sections. Pref.: prefecture.

Figure 3.8 Stratigraphic subdivision of the Oligocene to Middle Miocene strata in Toyama Prefecture. G.: Group, F.: Formation.

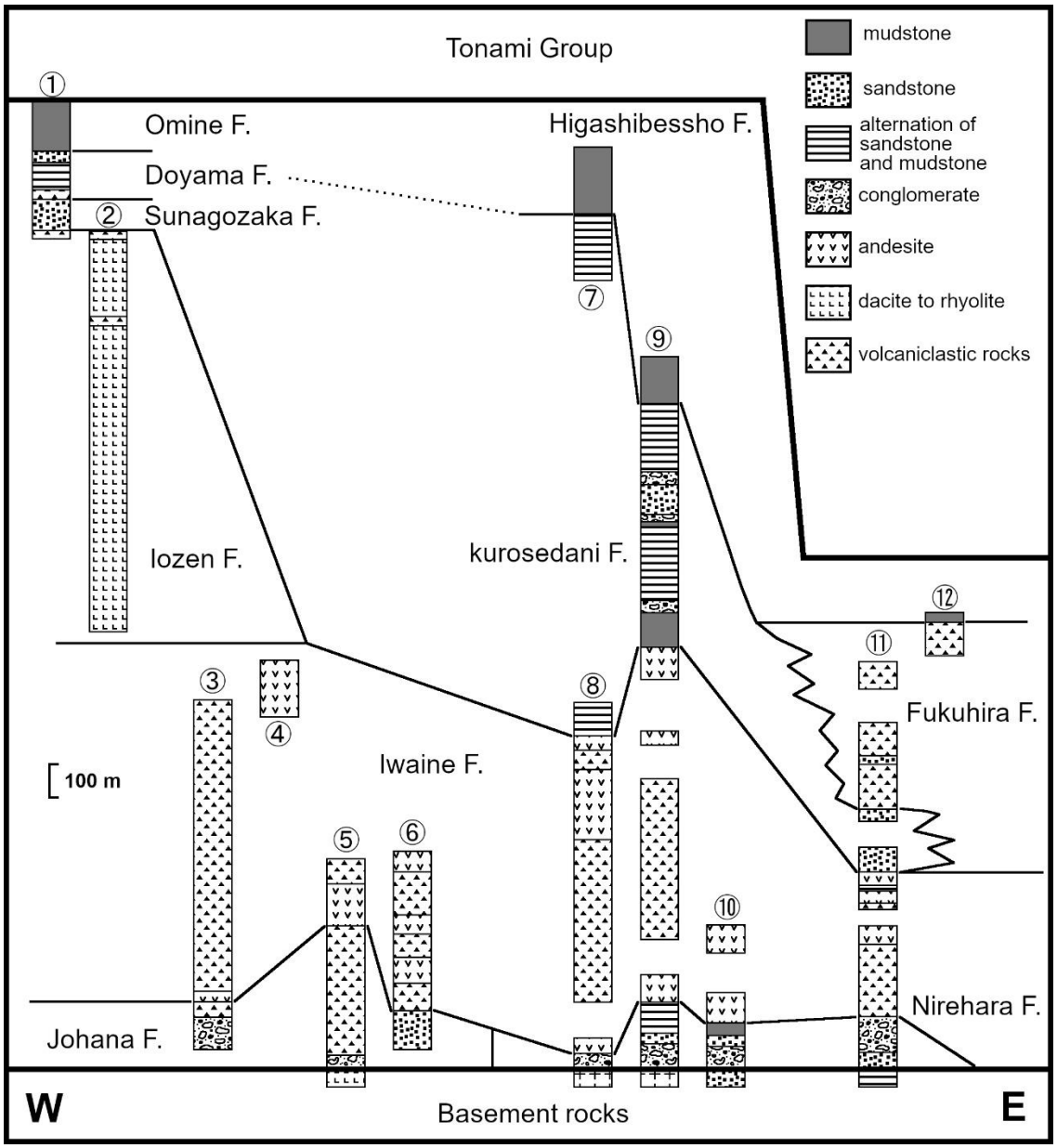

Figure 3.9 Columnar sections, obtained in this study, of Oligocene to Middle Miocene strata in Toyama Prefecture. See Figure 3.7 for the study area. F.: Formation.

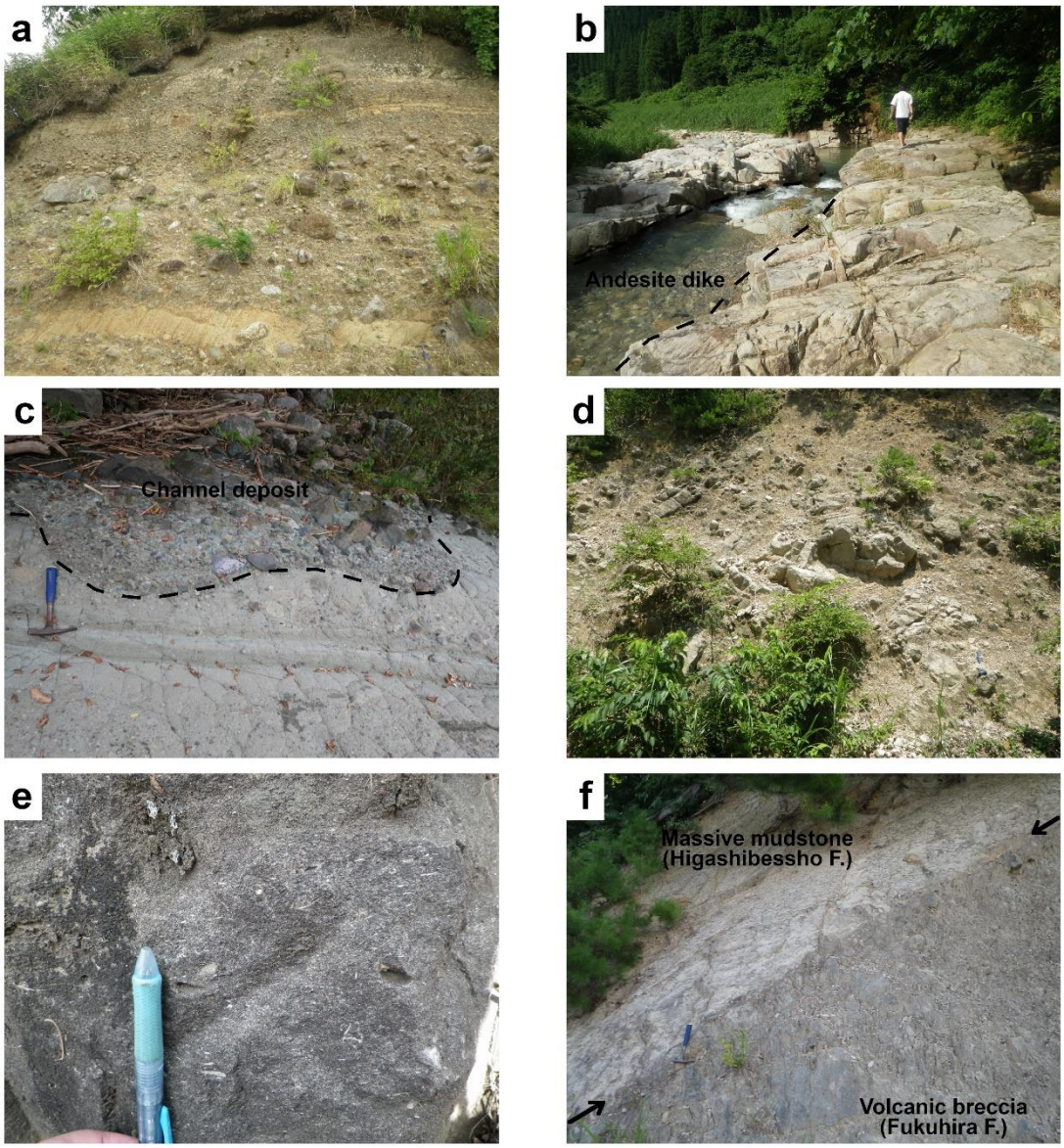

Figure 3.10 Field occurrences of the Oligocene to Middle Miocene strata in Toyama Prefecture. (a) alternation of conglomerate and sandstone of the Nirehara Formation in the Kamiichi area of eastern Toyama Prefecture. (b) densely welded tuff, intruded by an andesite dike, of the Usunaka Moonstone Rhyolite Member, the Johana Formation, in the Johana area of western Toyama Prefecture. (c) andesitic volcaniclastic rocks showing channel structure of the Iwaine Formation in the Yatsuo area of central Toyama Prefecture. (d) rhyolitic block lava of the Iozen Formation in the Iozen area of western

Toyama Prefecture. (e) fossiliferous massive sandstone, including fragments of fossils, of the Sunagozaka Formation in the Iozen area of western Toyama Prefecture. (f) a formation boundery between the Fukuhira and Higashibessho formations in the Uozu area of eastern Toyama Prefecture.

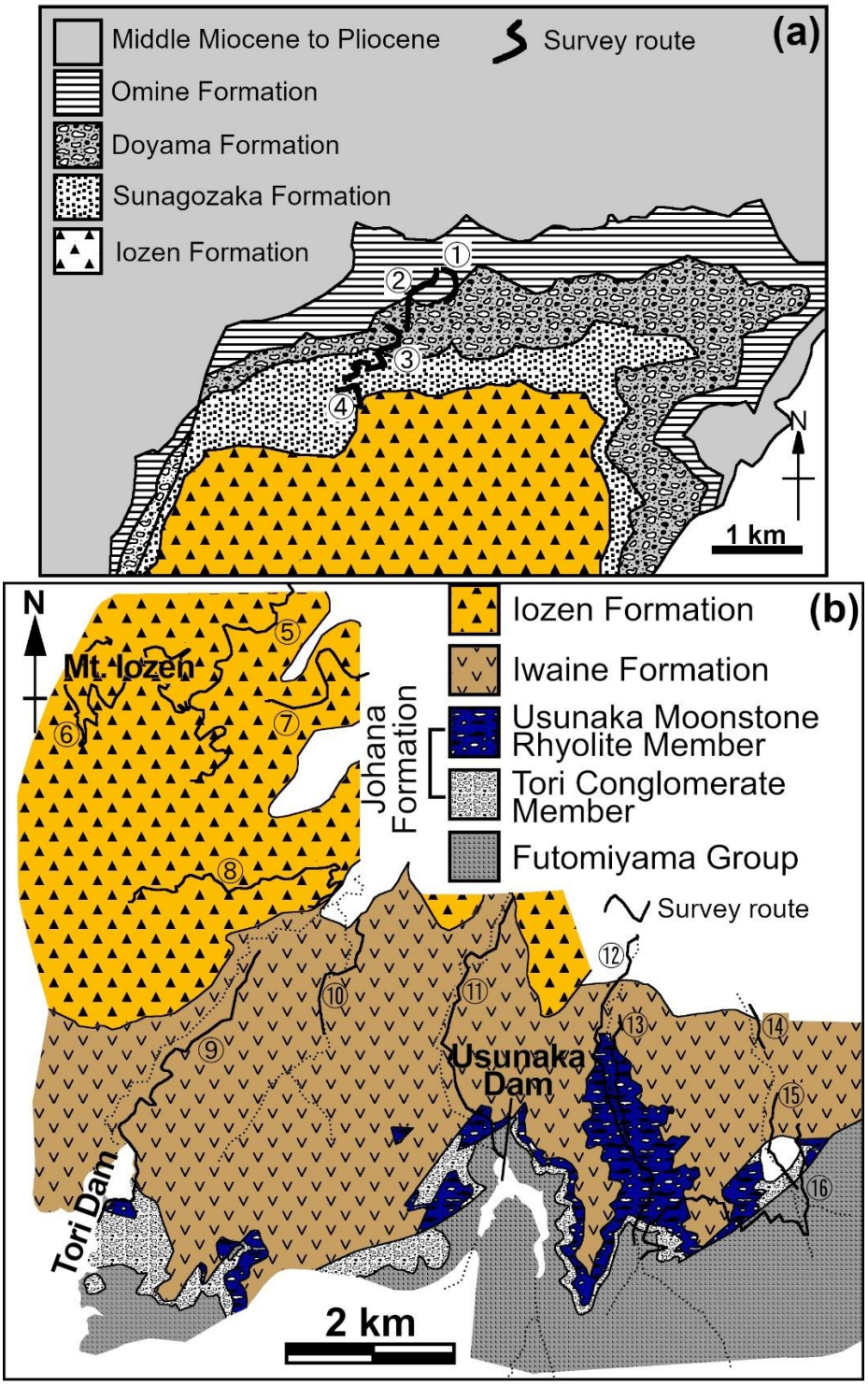

Figure 3.11 Geological map with survey route numbers in the Nanto area. (a) Northern study area modified from Yanagisawa (1999b). (b) Southern study area modified from Ganzawa (1983).

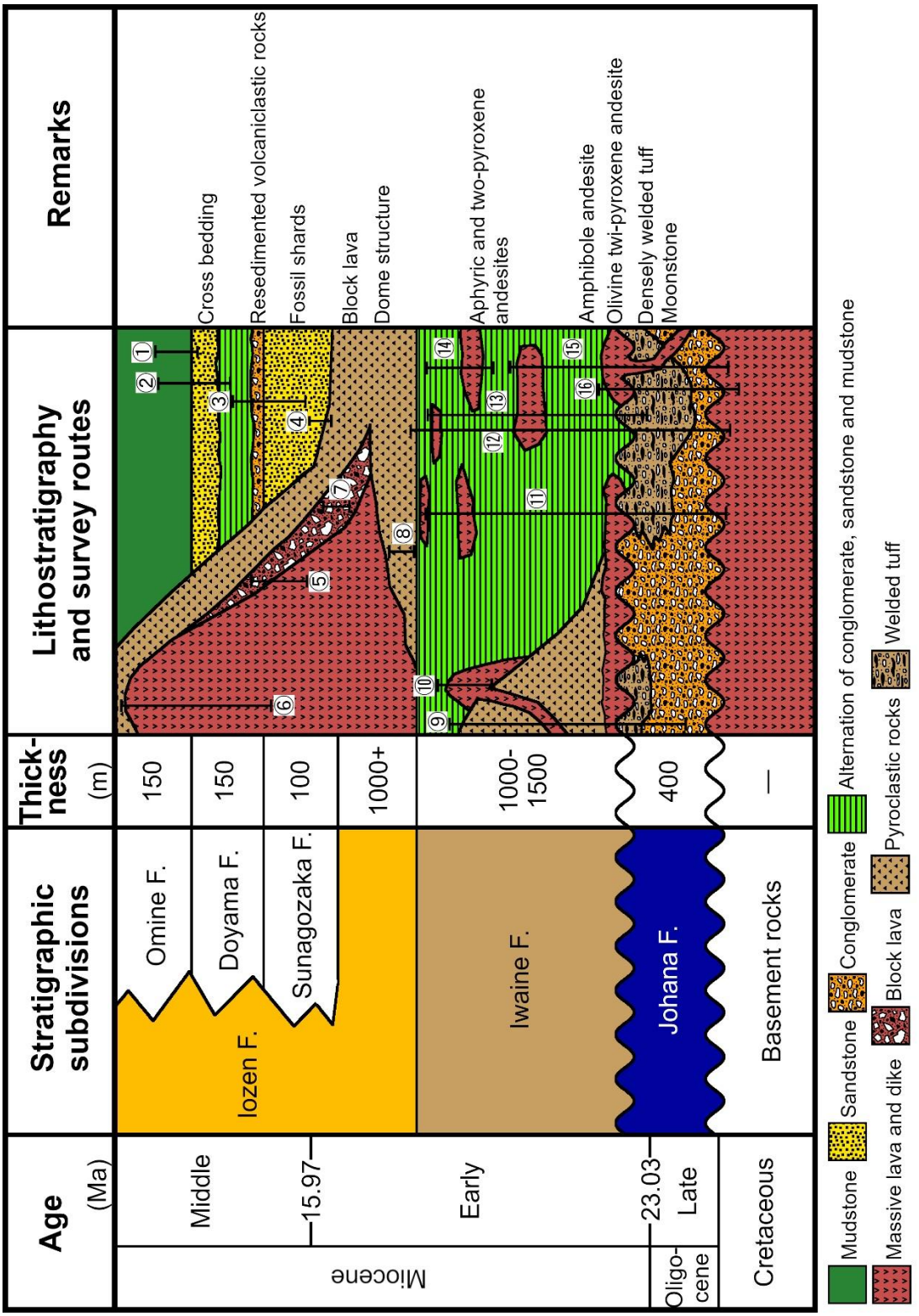

Figure 3.12 Stratigraphic subdivisions in this study and lithostratigraphy in the Nanto area. Survey routes are shown in Fig. 3.10.

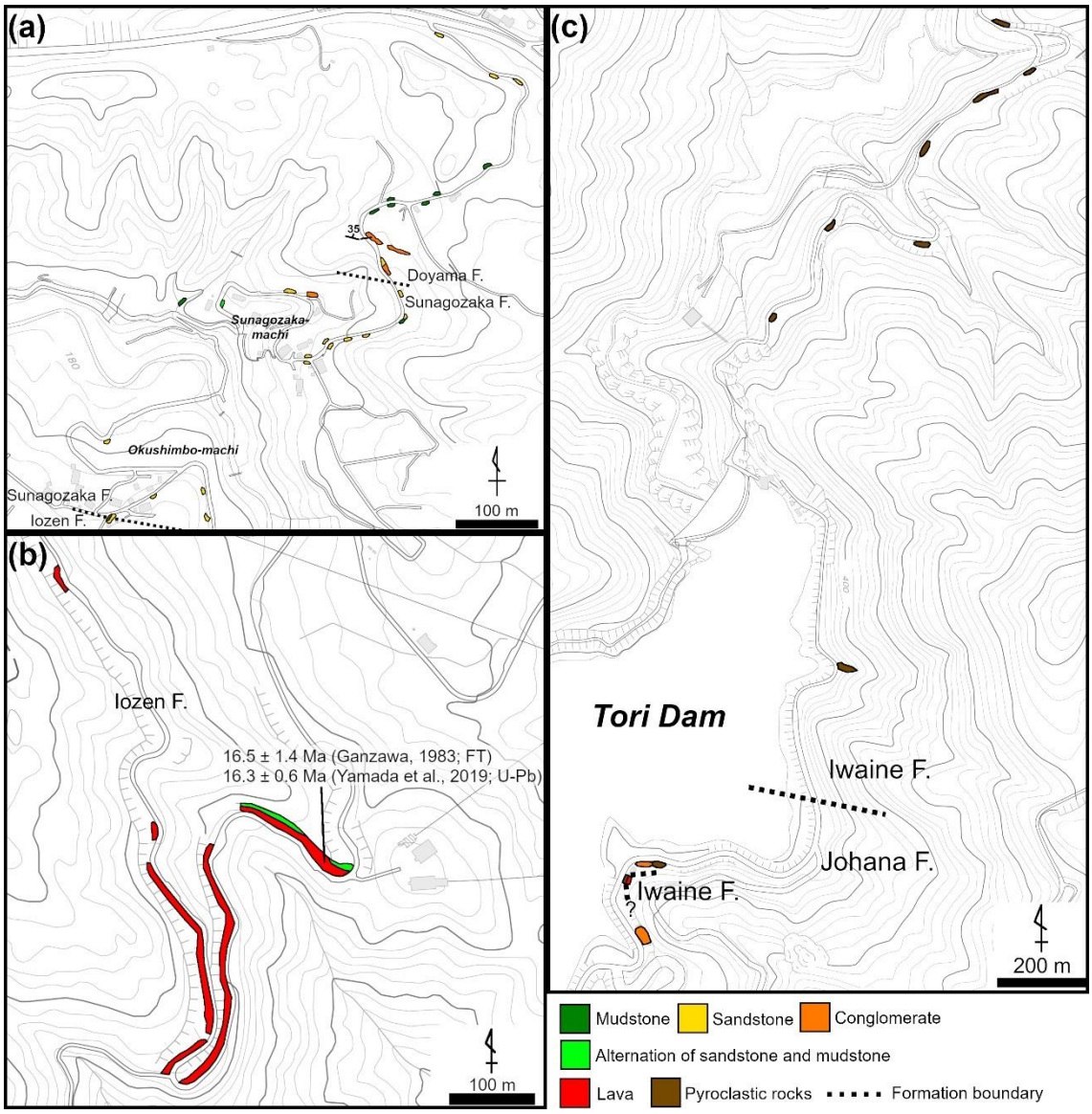

Figure 3.13 Route maps showing distribution of outcrops in the Nanto area. The locations of the survey routes are shown in Fig. 3.10. (a) Route 3 and 4. (b) Route 6. (c) Route 9.

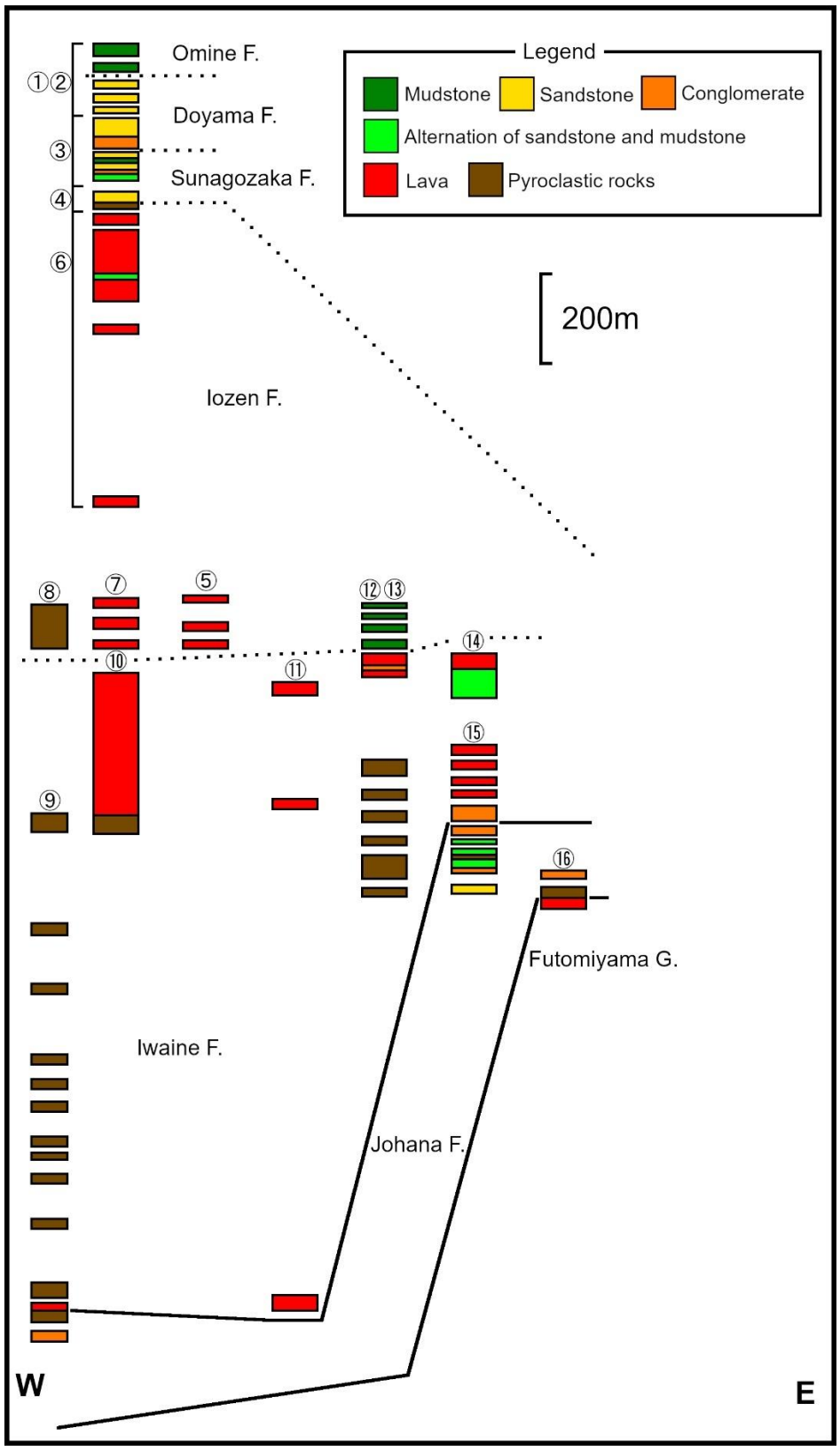

Figure 3.14 Columnar sections obtained in the Nanto area. The locations of the survey routes are shown in Fig. 3.10.

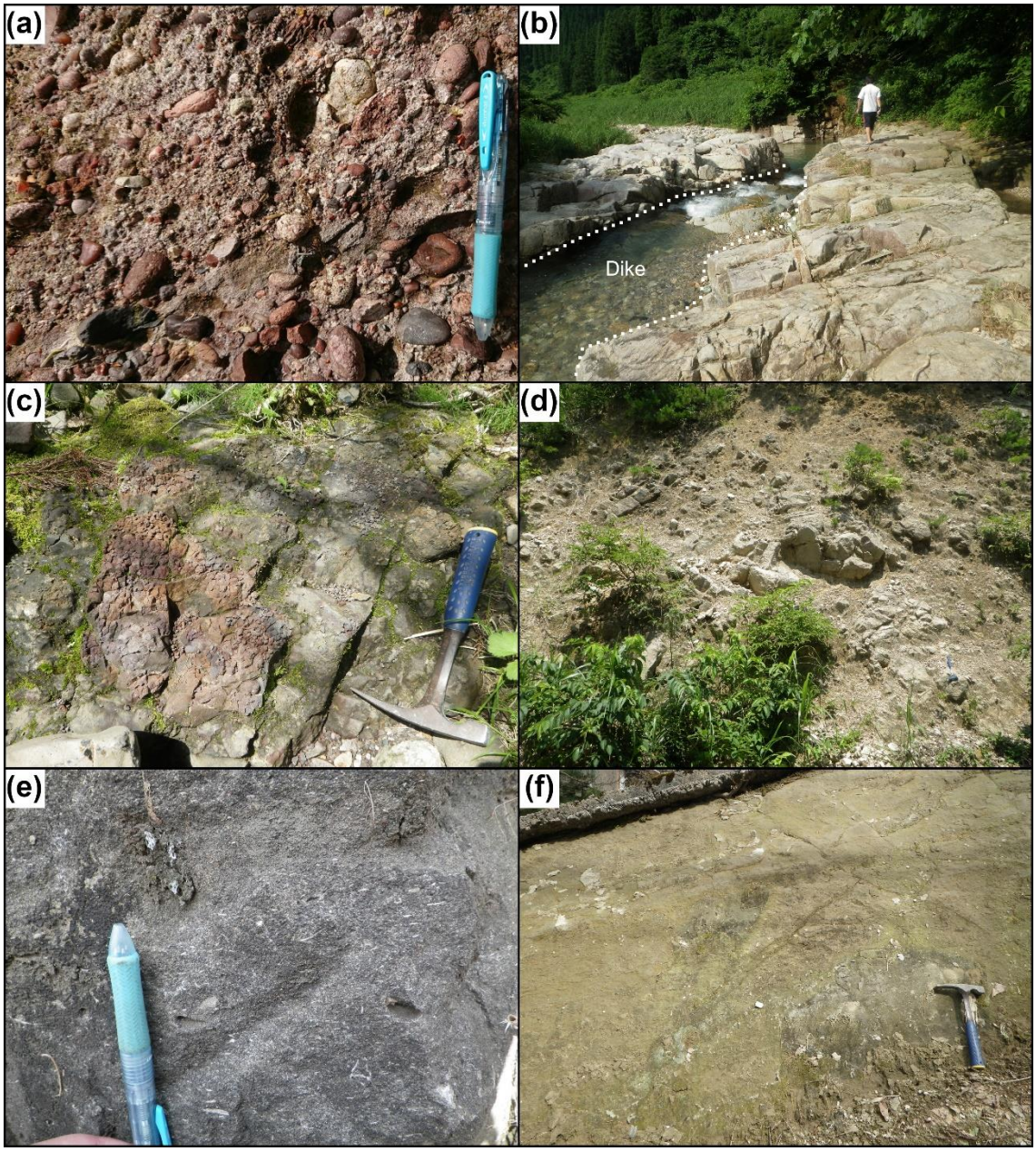

Figure 3.15 Photographs of outcrops showing typical occurrences in the Nanto area. (a) Alternating beds of conglomerate and sandstone in the Tori Conglomerate Member of the Johana Formation. (b) Jointed welded tuff in the Usunaka Moonstone Rhyolite Member of the Johana Formation, intruded by a andesitic dike. (c) Reddish brown colored massive mudstone due to high-temperature oxidization in the Iwaine Formation. (d) Block lava in the Iozen Formation. (e)

Massive sandstone containing fossil shards in the Sunagozaka Formation. (f) Massive mudstone in the Omine Formation.

4. Facies analysis

In this chapter, results of facies analysis for Oligocene to Middle Miocene strata in the Toyama basin are shown. I distinguished thirteen facies assemblages from the strata: subaerial lava (LF), in situ hyaloclastite (ISH), resedimented hyaloclastite (RSH), peperite (PR), dike (DK), subaerial pyroclastic flow deposit (PCF), pyroclastic fall deposit (TPH), debris flow deposit (DF), fluvial deposit (FD), inner bay deposit (IBD), shallow water deposit (SWD), turbidite (TDD), and deep water deposit (DWD) (**Table 1**). Facies geometry of each formation is as follows. The Johana Formation is composed of FD and PCF. The Nirehara Formation is composed of FD and SWD. The Iwaine Formation is composed of LF, ISH, RSH, PR, DK, PCF, TPH, DF, FD and IBD. The Iozen Formation is composed of LF, PCF, TPH, and FD. The Kurosedani Formation is composed of irregularly alternating beds of DF, FD, IBD, SWD. The Fukuhira Formation is composed mainly of LF, ISH, RSH, PR, DK, PCF, TPH, SWD. The Sunagozaka Formation is composed mainly of SWD. The Doyama Formation is composed of PCF, TPH, FD, SWD. The Higashibessho and Omine Formations are composed mainly of DWD with TDD.

4.1. Facies assemblages

4.1.1.Subaerial lava (LF)

[Facies] Mcvr: Massive volcanic rocks with platy or columnar joints (**Figure 4.1a**).

Mmvb: Monomictic massive volcanic breccia without cooling joints (**Figure 4.1b**). Most of the clasts are composed of angular to subangular cobble and boulder. This facies sometimes shows reddish

brown color.

[Characteristics] Three types of assemblages can be distinguished from LF: (1) only Mcvr, (2) only Mmvb, and (3) combination of Mcvr and Mmvb. Rock type of Mcvr and clasts of Mcvr in type 3 is the same, and facies changes gradually between Mcvr and Mcvr in type 3.

[Interpretation] This facies assemblage is interpreted as subaerial lava, based on lithological characteristics. Mmvb showing reddish brown color is considered as results of high-temperature oxidation under subaerial environment (McPhie et al., 1993). Type 2 and 3 are considered as block lava and massive lava with clinker, respectively.

4.1.2.In situ hyaloclastite (ISH)

[Facies] Jfmvb-g: Jigsaw-fitted monomictic volcanic breccia with cooling joints and glassy matrix. Clasts are poorly to moderately sorted and composed of angular to subangular granule to boulder.

[Characteristics] Facies assemblage ISH consists of only Jfmvb-g. This facies sometimes accompanies DK, RSH and/or PR (**Figure 4.1c**). Their rock type is the same, and lithofacies gradually changes between them.

[Interpretation] This facies assemblage is interpreted as in situ hyaloclastite (McPhie et al., 1993), based on lithological characteristics. Cooling joints are considered as results of quench by water.

4.1.3.Resedimented hyaloclastite (RSH)

[Facies] Mbvc: Monomictic bedded volcanogenic conglomerate. Clasts are moderately to well sorted and composed of subangular to subrounded granule to boulder, with cooling joints. This conglomerate shows stratified structure with parallel or cross laminae.

[Characteristics] Facies assemblage RSH consists of only Mbvc. This facies sometimes accompanies DK, ISH and/or PR (**Figure 4.1c** and **Figure 4.1d**). Their rock type is the same, and lithofacies

gradually changes between them.

[Interpretation] This facies assemblage is interpreted as resedimented hyaloclastite, based on lithological characteristics. Stratified stricture without jigsaw-fitting suggests that Mbvc was sedimented by gravity flow.

4.1.4.Peperite (PR)

[Facies] Jfmvb-s: Jigsaw-fitted monomictic breccia with sedimentary matrix. Clasts are poorly sorted and composed of subangular to rounded cobble and boulder. This facies does not show any sedimentary structure (**Figure 4.1d**).

[Characteristics] Facies assemblage PR consists of only Jfmvb-s. This facies sometimes accompanies DK, ISH and/or RSH. Their rock type is the same, and lithofacies gradually changes between them.

[Interpretation] This facies assemblage is interpreted as peperite (Cas and Wright, 1987; McPhie et al., 1993), based on lithological characteristics. The occurrence of PR suggests that lava or magma intruded not solidified sediments to mix each other (Cas and Wright, 1987; McPhie et al., 1993).

4.1.5.Dike (DK)

[Facies] Mdk: Intruded massive volcanic rocks (**Figure 4.1c**).

Pjvb: Volcanic breccia composed of platy- or columnar-jointed clasts. This facies sometimes show reddish brown color.

[Characteristics] Mdk is surrounded by Pjvb, and DK intrudes surrounding beds. In most of the cases, only Mdk is observed without Pjvb. This facies sometimes accompanies LF, ISH and/or RSH. Their rock type is the same, and lithofacies gradually changes between them.

[Interpretation] This facies assemblage is interpreted as feeder dike, based on lithological characteristics. Pjvb showing reddish brown color is considered as results of high-temperature oxidation under

subaerial environment (McPhie et al., 1993).

4.1.6.Subaerial pyroclastic flow deposit (PCF)

[Facies] Plt: Parallel bedded tuff containing fine grained pumice and volcanic glass.

Wdmt: Welded massive tuff containing flattened lenticular glass. Wdmt sometimes shows reddish brown color and columnar joints.

Mpt: Massive and pumiceous lappili tuff. Ratio of pumice and lithic clasts changes by stratigraphic horizons (**Figure 4.1e**).

[Characteristics] In typical case, combination of Plt→Wdmt→Mpt in stratigraphic ascending order can be observed. In most of the cases, only Mpt can be observed without Plt and Wdmt. Plt, Wdmt and Mpt are considered as 1, 2 and 3 of typical occurrences of subaerial pyroclastic flow deposit by Sparks et al. (1973).

[Interpretation] This facies assemblage is interpreted as subaerial pyroclastic flow deposit, based on lithological characteristics.

4.1.7.Pyroclastic fall deposit (TPH)

[Facies] Wst: Well-sorted tuff containing fine grained pumice and volcanic glass. In most of the cases, any sedimentary structures are not shown.

Wsls: Well-sorted lapilli stone with minor matrix composed of clay minerals (**Figure 4.1f**). Clasts are composed of subangular to subrounded monomictic lapilli and show reddish brown color.

Wpsvb: Well- to poor-sorted volcanic breccia composed of subangular to rounded monomictic cobble and boulder.

[Characteristics] In many cases, these three facies are not observed in the same outcrop. Combination Wst and Wpsvb sometimes occurs. Wst is intercalated in both of sedimentary and volcanic rocks.

[Interpretation] This facies assemblage is interpreted as pyroclastic fall deposit (tephra), based on lithological characteristics. Wst and Wsls are considered as distal pyroclastic fall deposits, because they

are composed of well sorted clasts (Ito, 2022). On the other hand, Wpsvb is considered as proximal pyroclastic fall deposit, because it is composed also of poor-sorted clasts (Ito, 2022).

4.1.8.Debris flow deposit (DF)

[Facies] Plmd: Parallel bedded or massive mudstone.

Mbc: Poor-sorted massive breccia composed of subangular to subrounded polymictic cobble and boulder.

Rgbc: Poor-sorted and reversely grading breccia composed of subangular to subrounded polymictic cobble and boulder (Figure 4.2a).

[Characteristics] Facies assemblage DF consists mainly of Mbc and Rgbc, and the thickness of a bed is up to more than 10 m. Mbc and Rgbc do not occur together in many cases, nevertheless, lithology of Mbc and Rgbc changes gradually in some cases. Plmd can be observed only in the base of DF, but Plmd is not observed in many cases.

[Interpretation] This facies assemblage is interpreted as debris flow deposit (debrite), based on lithological characteristics. DF is observed with FD in many cases.

4.1.9.Fluvial deposit (FD)

[Facies] Gcgl: massive or graded conglomerate (**Figure 4.2b** and **Figure 4.2c**). Gravels are moderately sorted and composed of subangular to rounded polymictic pebble to cobble.

Lsd: Lenticular sandstone.

Lmd: Lenticular mudstone.

Plsd: Parallel or cross bedded sandstone (**Figure 4.2b** and **Figure 4.2c**).

Mmd-f: Massive mudstone with plant fossils

[Characteristics] Each facies changes largely and laterally (one facies is not continuous laterally). Generally, Lsd and Lmd has

thickness of less than several meters and are intercalated in Gcgl. DF is sometimes intercalated in FD.

[Interpretation] This facies assemblage is interpreted as fluvial deposit, based on lithological characteristics. Lithological features suggest that FD was deposited in braided rivers.

4.1.10. Inner bay deposit (IBD)

[Facies] Msd-g: massive sandstone with minor rounded gravels (**Figure 4.2d**).

Mmd-g: massive mudstone with minor rounded gravels and plants and molluscan fossils (**Figure 4.2d**).

[Characteristics] IBD consists of irregularly alternating beds of Msd-g and Mmd-g whose thickness is up to several tens' centimeters.

[Interpretation] This facies assemblage is interpreted as inner bay deposit, based on lithological characteristics. Lithofacies of IBD suggests less effect of water flow. Molluscan fossils also suggest that IBD was formed in sea water.

4.1.11. Shallow water deposit (SWD)

[Facies] Mmd: massive mudstone.

Nssd: No sedimentary structured sandstone with fossils (**Figure 4.2e**).

Wclsd: wavy- and cross-laminated sandstone.

[Characteristics] SWD consists mainly of Wclsd and Nssd with minor Mmd. Thickness of each bed is up to less than several meters. Both of upward finning and coarsening are observed. Nevertheless, Mmd is observed rarely in finning-upward cycle.

[Interpretation] This facies assemblage is interpreted as shallow water deposit, based on lithological characteristics. Finning- and coarsening-upward cycles are considered to have been deposited in tide- and wave-dominated systems, respectively (Ito, 2022).

4.1.12. Turbidite (TDD)

[Facies] Ngcgl: Massive or normally graded conglomerate

Ngsd: Massive or normally graded sandstone
Ngmd: Massve or normally graded laminated mudstone
[Characteristics] TDD always shows upward finning or normally grading. In most of the cases, only one facies or combination of two facies (Ngsd-Ngmd and Ngcgl-Ngsd) are observed.
[Interpretation] This facies assemblage is interpreted as turbidite, based on lithological characteristics. These lithological features suggest Bouma-Sequence (Bouma, 1962).

4.1.13. Deep water deposit (DWD)

[Facies] Mmd-f: Massive mudstone with molluscan fossils (**Figure 4.2f**).
Nsmd: No sedimentary structured mudstone with fossils.
[Characteristics] Lithofacies of DWD does not change largely and laterally. Cross and wavy bedding suggesting wave effect are not observed.
[Interpretation] This facies assemblage is interpreted as deep water deposit, based on lithological characteristics. Nsmd is considered as result of bioactivity by, for instance, mollusks.

4.2. Facies geometry

4.2.1.Nanto Group

The Tori Conglomerate Member of the Johana Formation is composed mainly of FD (**Figure 4.3** and **4.4**). Any fossils were not found in this study. The Usunaka Moonstone Rhyolite Member of the Johana Formation is composed mainly of PCF with FD (**Figure 4.3** and **4.4**). The rock type is rhyolitic welded tuff. Some flow units of PCF were observed. Lithofacies between FD of the Tori Conglomerate Member and PCF of the Usunaka Moonstone Rhyolite Member changes gradually showing alternating beds of FD and PCF.

The Imozu Conglomerate Member of the Nirehara Formation is

composed mainly of FD (**Figure 4.3**). Especially, conglomerate were dominantly observed in this member. The Ashiu Sandstone Member is composed mainly of SWD (**Figure 4.3**). The Myogashima Alternation Member is composed mainly of SWD showing finning-upward cycles (**Figure 4.3**). Any fossils were not found in this study, except for fragments of plant fossils.

4.2.2. Yatsuo Group

The Iwaine Formation is composed of LF, ISH, RSH, PR, DK, PCF, TPH, DF, FD, SWD and IBD (**Figure 4.3**, **4.4** and **4.6**; Routes of **Figure 4.6** are shown in **Figure 4.5**). The volcanic and pyroclastic rocks are andesitic. Based on lithostratigraphy, the Iwaine Formation can be subdivided into four units: unit 1 (lowest part), unit 2 (lower part), unit 3 (middle part) and unit 4 (upper part). LF containing olivine or amphibole phenocrysts occupies unit 1 with PCF containing amphibole crystals. The unit 2 and 3 are observed only in the Yatsuo area. The unit 2 is composed of DF and FD, meanwhile the unit 3 is composed of PCF. The unit 4 is composed of irregular alternation of LF, ISH, RSH, PR, PCF, TPH, DF, FD and SWD. Aphyric or pyroxene-bearing LF, ISH, PR are observed in the unit 4. Some FD just under LF shows reddish brown color, suggesting high-temperature oxidation under the subaerial environment IBD is observed in the uppermost part of the unit 4 in the Yatsuo area, and DK is observed in the unit 1 and 4.

The Iozen Formation is composed of LF, PCF, TPH, and FD. The volcanic and pyroclastic rocks are rhyolitic (**Figure 4.3** and **4.4**). Massive lava flows (LF) are distributed in the proximal area of Mt. Iozen, forming lava domes, whereas block lava flows (LF) are observed in the distal area of Mt. Iozen. Although PCF, TPH and FD are intercalated in LF around the Mt. Iozen area, PCF, TPH and FD are dominantly distributed in the Yatsuo area.

The Kurosedani Formation is composed of irregularly alternating beds of DF, FD, IBD, SWD (**Figure 4.3**). Nevertheless, FD with DF, and SWD with IBD are abundant in the lower and upper part of the Kurosedani Formation, suggesting upward finning.

The Fukuhira Formation is composed mainly of LF, ISH, RSH, PR, DK, PCF, TPH, SWD (**Figure 4.3**). SWD is intercalated in andesitic to dacitic volcanic and pyroclastic rocks (LF, ISH, RSH, PR, DK, PCF, TPH).

The Sunagozaka Formation is composed mainly of SWD showing finning-upward cycle and IBD (**Figure 4.3**). TPH is intercalated in some stratigraphic horizons of the Sunagozaka Formation.

The Doyama Formation consists of three units: unit 1 (lower part), unit 2 (middle part), and unit 3 (upper part). The unit 1 is composed of PCF, TPH and FD. The unit 2 and 3 are composed of SWD. Alternating beds of sandstone and mudstone is abundant in the unit 2, whereas, cross-bedded sandstone is dominant in the unit 3 (**Figure 4.3** and **4.4**). Some beds of TPH are intercalated in some stratigraphic horizons.

The Higashibessho and Omine Formations are composed mainly of DWD with TDD (**Figure 4.3** and **4.4**).

Table 1 Summary of facies assemblages.

Facies assemblages	Lithofacies description	Interpretation
LF	Mcvr: massive volcanic rocks with platy or columnar joints Mmvb: monomictic massive volcanic breccia without cooling joints	Subaerial lava
ISH	Jfmvb-g: jigsaw-fitted monomictic volcanic breccia with cooling joints and glassy matrix	In situ hyaloclastite
RSH	Mbvc: monomictic bedded volcanogenic conglomerate	Resedimented hyaloclastite
PR	Jfmvb-s: jigsaw-fitted monomictic breccia with sedimentary matrix	Peperite
DK	Mdk: intruded massive volcanic rocks Pjvb: volcanic breccia composed of platy- or columnar-jointed clasts	Dike intruded near the surface
PCF	Plt: parallel bedded tuff Wdmt: welded massive tuff Mpt: massive and pumiceous lappili tuff	Subaerial pyroclastic flow deposit
TPH	Wst: well-sorted tuff Wsls: well-sorted lapilli stone Wpsvb: well- or poor-sorted volcanic breccia composed of rounded bomb	Subaerial or subaqueous pyroclastic fall deposit
DF	Plmd: parallel bedded or massive mudstone Mbc: poor-sorted massive breccia Rgbc: poor-sorted and reversely grading breccia	Debris flow deposit
FD	Gcgl: massive or graded conglomerate Lsd: lenticular sandstone Lmd: lenticular mudstone Plsd: parallel or cross bedded sandstone Mmd-f: massive mudstone with plant fossils	Fluvial deposit
IBD	Msd-g: massive sandstone with minor gravels Mmd-g: massive mudstone with minor gravels	Inner-bay deposit
SWD	Mmd: massive mudstone Nssd: no sedimentary structured sandstone with fossils Wclsd: wavy- and cross-laminated sandstone	Shallow water deposit above storm wave base
TDD	Ngcgl: massive or normally graded conglomerate Ngsd: massive or normally graded sandstone Ngmd: massve or normally graded laminated mudstone	Turbidite
DWD	Mmd-f: massive mudstone with molluscan fossils Nsmd: no sedimentary structured mudstone with fossils	Deep water deposit below storm wave base

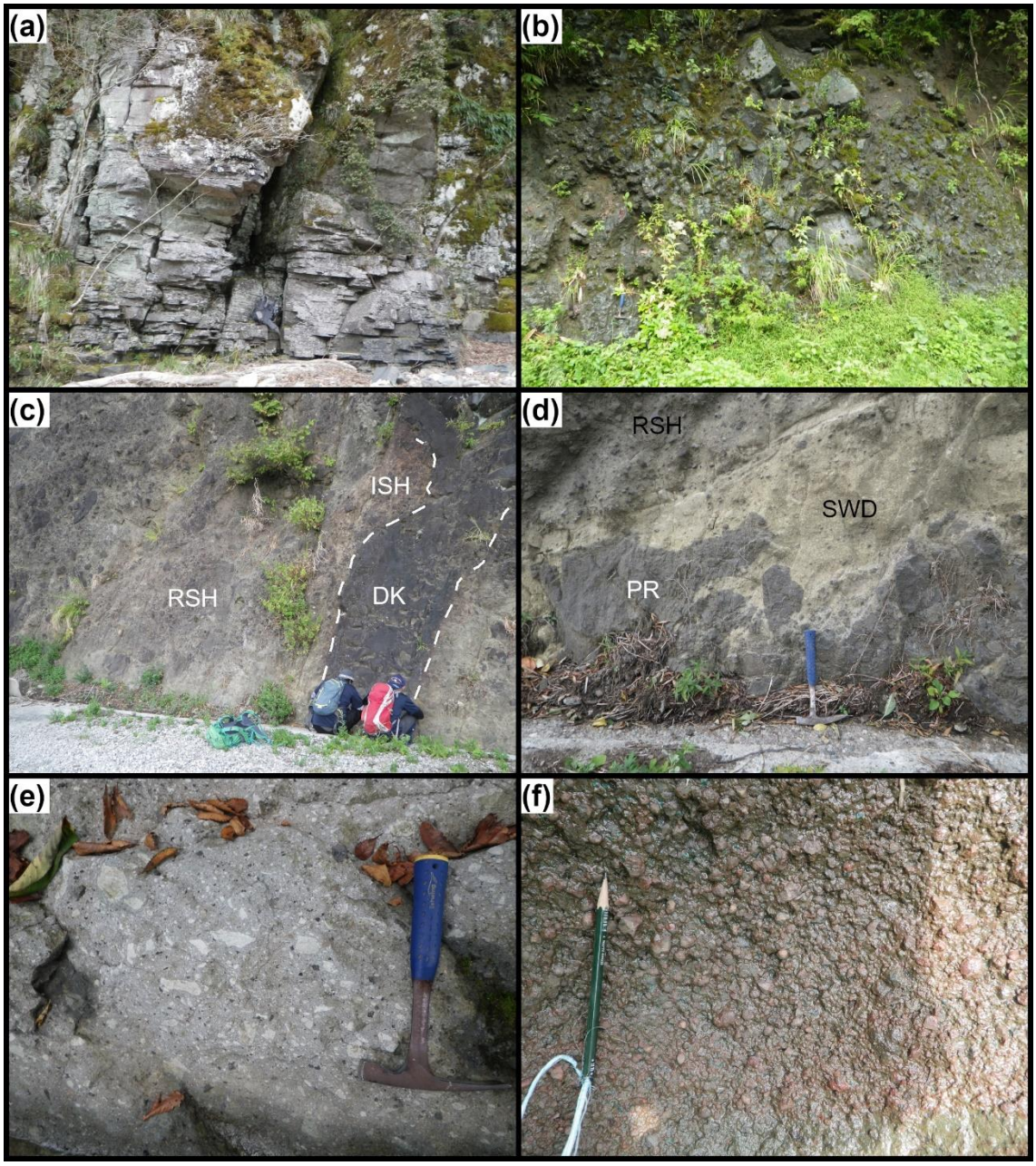

Figure 4.1 Field occurrences of volcanic and pyroclastic rocks in the Iwaine Formation. (a) Platy jointed lava (Mcvr of LF). (b) Monomictic massive volcanic breccia (Mmvb of LF). (c) Feeder dike (DK), in situ hyaloclastite (ISH) and resedimented hyaloclastite (RSH). (d) Peperite (PR) intruding to shallow water deposit (SWD) with resedimented hyaloclastite (RSH). (e) Massive and pumiceous lapilli tuff (Mpt) of PCF. (f) Well-sorted lapilli stone (Wsls) of TPH.

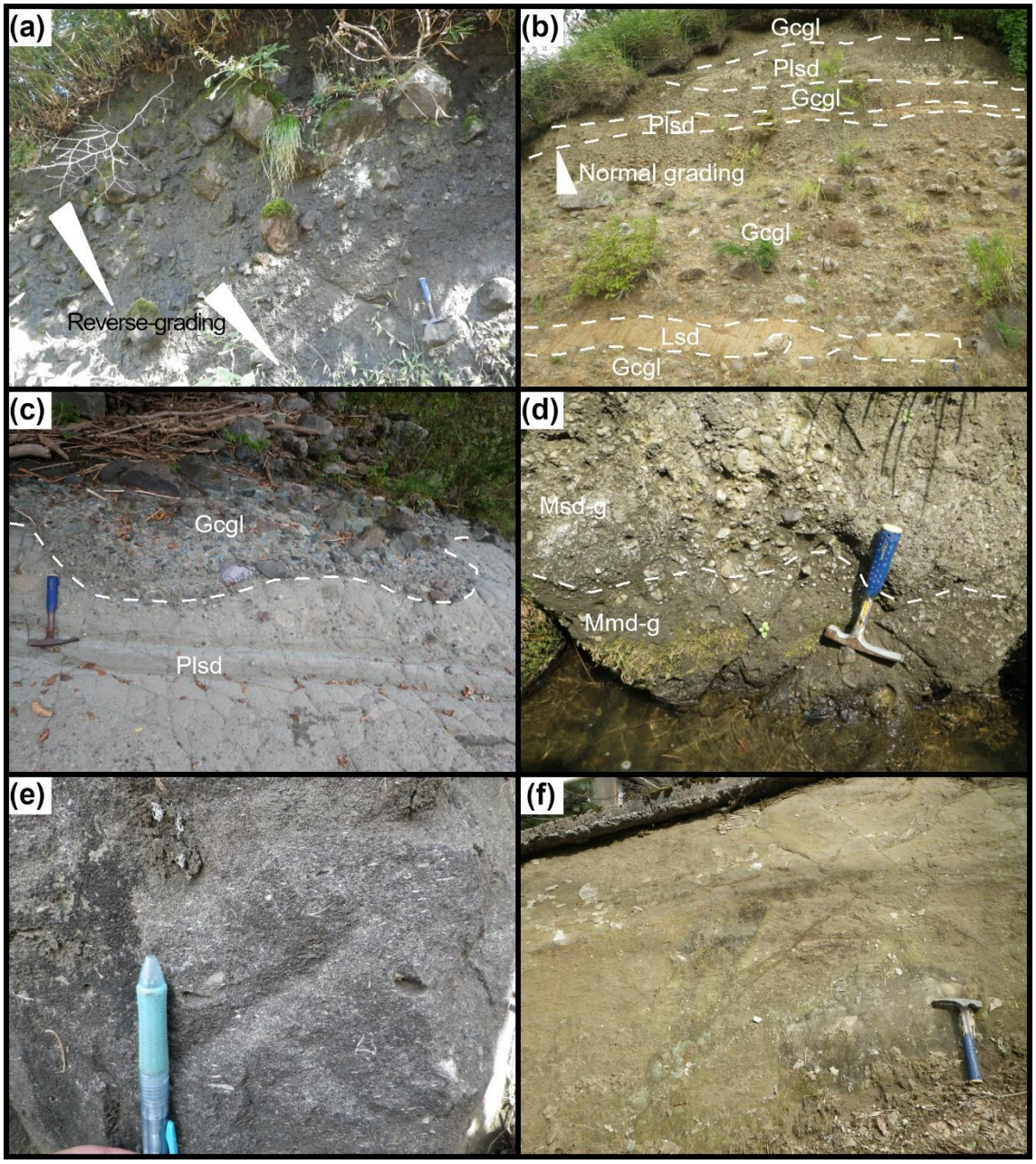

Figure 4.2 Field occurrences of clastic rocks. (a) Debris flow deposit (DF), showing reversely grading, in the Iwaine Formation. (b) Fluvial deposit (FD) of the Nirehara Formation. (c) Fluvial deposit (FD) of the Iwaine Formation. (d) Inner bay deposit (IBD) of the Iwaine Formation. (e) No sedimentary structured sandstone with fossils (Nssd), of SWD, in the Sunagozaka Formation (f) Massive mudstone of DWD in the Omine Formation.

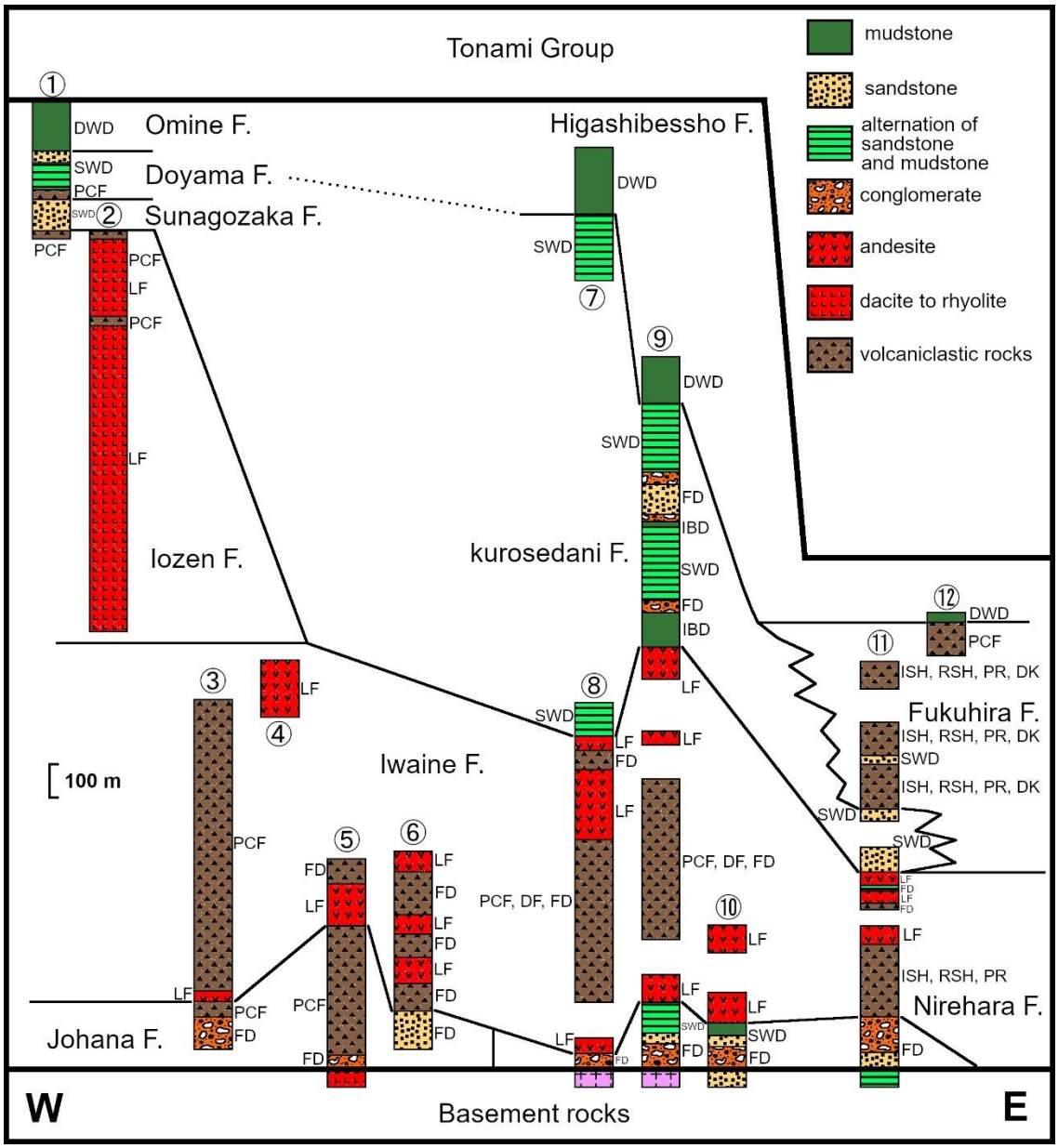

Figure 4.3 Correlated columnar sections with facies assemblage codes in the entire of the Toyama basin. Survey routes are shown in Fig. 3.7.

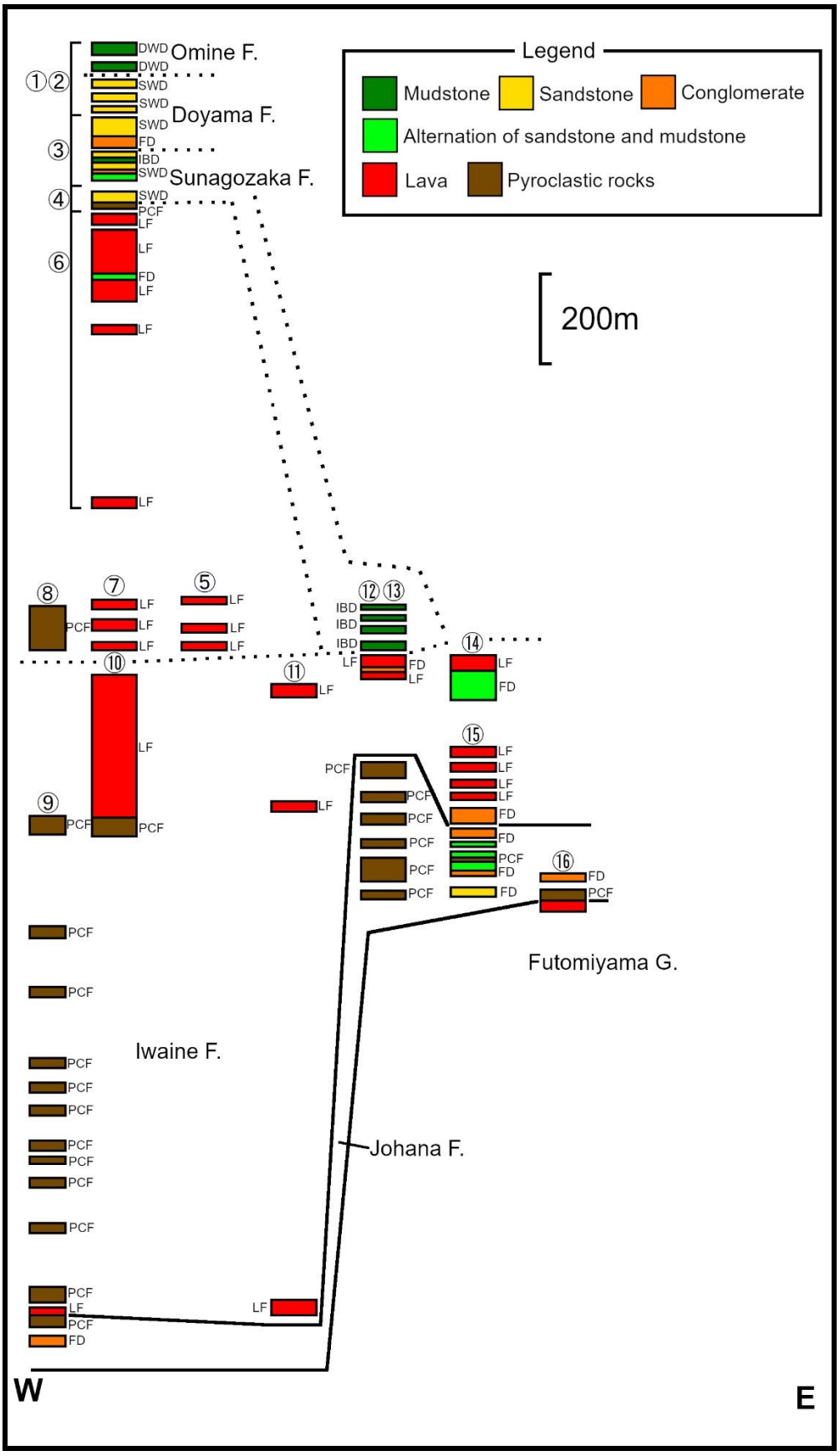
Legend
Mudstone
Sandstone
Conglomerate
Alternation of sandstone and mudstone
Lava
Pyroclastic rocks
200m
Omine F.
Doyama F.
Sunagozaka F.
Iwaine F.
Johana F.
Futomiyama G.
W
E

Figure 4.4 Correlated columnar sections with facies assemblage codes in the Nanto area. Survey routes are shown in Fig. 3.11.

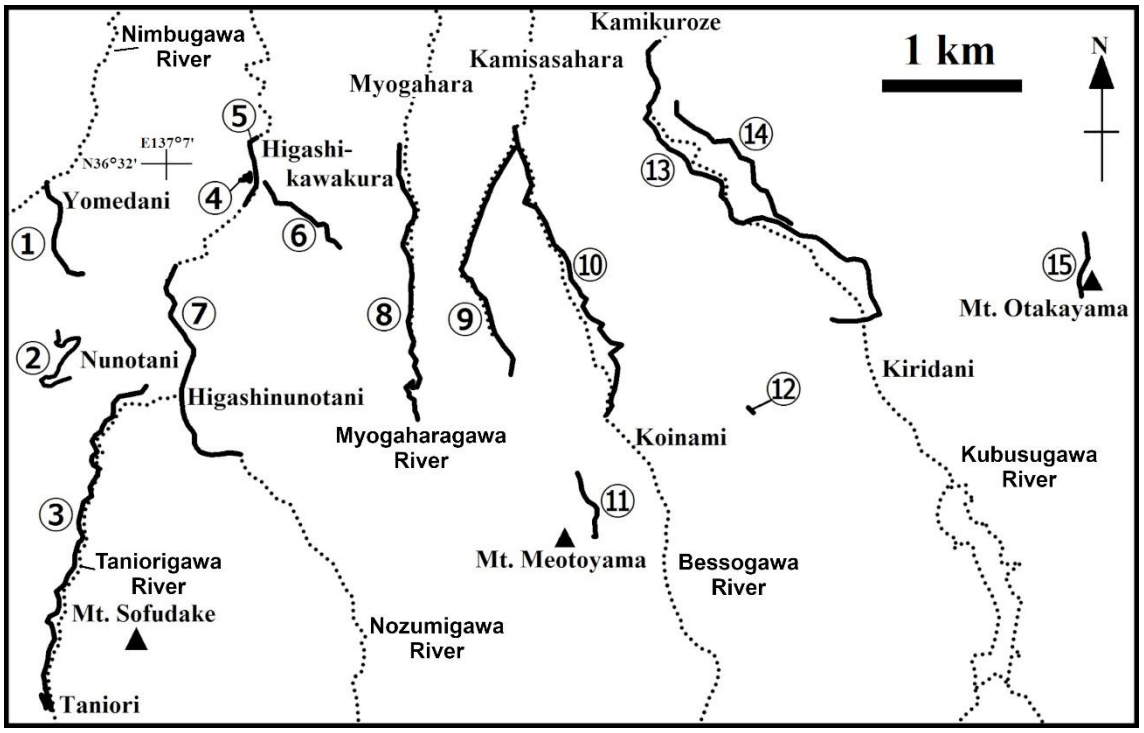

Figure 4.5 Route map which columnar sections of the Iwaine Formation in the Yatsuo area were obtained with place name, rivers, and mountains.

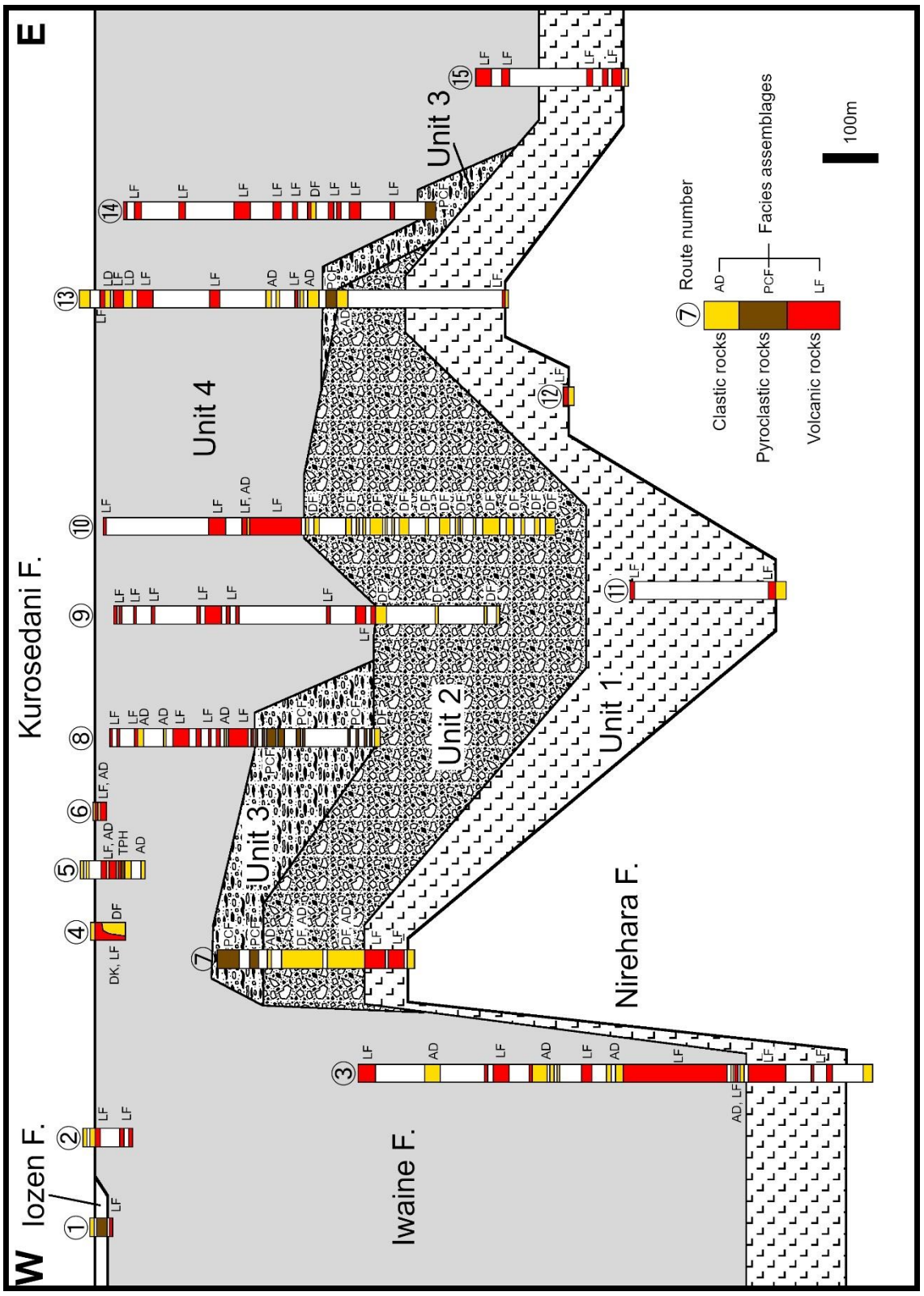

Figure 4.6 Correlated columnar sections of the Iwaine Formation with facies code. Survey routes are shown in Fig. 4.5. F.: formation.

5. Methods

In this chapter, analytical methods conducted in Ph.D. research is explained. I carried out zircon U–Pb dating, zircon trace element analysis, zircon Lu–Hf isotope analysis, Mineral chemical composition analysis for feldspar, whole-rock major and trace element analyses, and whole-rock Sr–Nd isotope analysis. Especially, zircon trace element analysis and zircon Lu–Hf isotope analysis have been rarely reported from the Japanese scientific community.

5.1. Zircon U–Pb dating

5.1.1.Sample description

In this study, four samples from the Johana, Nirehara, Iwaine and Iozen Formations were dated. Petrography of the dated samples are described in section.

The dated sample (rhyolitic welded tuff; NT63c) from the Usunaka Moonstone Rhyolite Member of Johana Formation was collected at 36°27’53.51”N, 136°52’30.75”E. NT63c contains euhedral to corroded phenocrysts of quartz and alkali feldspar, showing eutaxitic texture (**Figure 5.1a**).

A boulder-sized angular gravel of rhyolitic welded tuff (090705A; **Figure 5.1b**) was collected from massive conglomerate of the Nirehara Formation at 36°37’15.50”N, 137°25’41.37”E. 090705A contains euhedral to corroded phenocrysts of plagioclase, quartz, lenticular pumice (fiamme) and a small number of accessary clasts, showing eutaxitic texture.

The dated sample (andesitic pumice lapilli tuff; NT27) from the Iwaine Formation was collected at 36°28’19.72”N, 136°48’21.08”E.

NT27 contains plagioclase, pumice and shards of volcanic glass (**Figure 5.1c**)

The dated sample (massive lava; NT45) from the Iozen Formation was collected at 36°30’49.25”N, 136°48’12.35”E. NT45 is a sample of aphyric rhyolite lava containing small number of plagioclase phenocrysts (**Figure 5.1d**).

5.1.2.Methods

Zircon grains were extracted via a conventional method including panning, magnetic and heavy liquid separation, and finally hand-picked crystals were mounted in epoxy resin. Cathodoluminescence (CL) was imaged using Gatan Mini CL detector equipped on JEOL JSM5600 scanning electron microprobe at Niigata University.

U–Th–Pb mass ratios were determined using Agilent 7500a quadrupole ICP-MS coupled with 213 nm Nd-YAG laser ablation system of New Wave Research UP-213 at Niigata University. Procedures on measurement, data reduction, and calibration essentially follow Ueda et al. (2018) with modification adopting lower Pb signals in Neogene samples as follows. The laser diameter was set as 40 μm instead of 30 μm in samples with large zircons; pulse frequency was increased to be 10 Hz with energy density of 10 J/cm^2. Signals of ^{206}Pb, ^{207}Pb, ^{208}Pb, ^{232}Th and ^{238}U were measured with dwell times of 30, 60, 50, 3, and 3 ms respectively. Pb isotopes were measured in a pulse mode, whereas the detector was fixed in the analogue mode for ^{232}Th and ^{238}U in order to avoid automatic switching between pulse and analogue modes protecting electron multiplier from intense signals. Mass biases and their drifts were corrected by repetitive measurements of NIST SRM612 standard glass. OD-3 zircon (Iwano et al., 2013) was analyzed for the matrix matched standard calibrating down hole fractionation of ^{206}Pb/^{238}U. All uncertainties are given as double standard errors (2SE). In this study,

repetitive measurements of the Fish Canyon Tuff zircon resulted in a ^{238}U–^{206}Pb weighted mean age of 28.8 ± 0.5 Ma (n = 29), well compatible with the reference age (28.37 ± 0.05 Ma; Bachman et al., 2007). Excess dispersion (MSWD = 4.96; probability of fit = 0 %) for the weighted mean probably owes to non-simultaneous measurements by quadrupole ICP-MS as noted by Ueda et al. (2018).

Results with $^{206}Pb/^{238}U$ no greater than 10 % and $^{207}Pb/^{235}U$ no greater than 100% were accepted. After such screening, ^{238}U–^{206}Pb weighted mean age was calculated from concordant results with ($^{206}Pb/^{238}U$)/($^{207}Pb/^{235}Pb$) within 1 ± 2σ.

5.2. Zircon Trace element analysis

Trace element composition of the dated zircons were measured using the same LA-ICP-MS apparatus as for U–Pb dating, with a laser spot size of 40 μm, pulse frequency of 5Hz, energy density of ~7 J/cm^2, and ablation time of 50 sec. In the ICP-MS, time-resolved measurements were made for 70 sec., with varying dwell times by elements reflecting their general abundances in zircons (5 ms. for Si, P, Ca, Y, Zr, Hf, Th, and U; 8 ms. for Yb and Lu; 10 ms. for Ti, Er and Tm; 15 ms. for Dy and Ho; 30 ms. for Ce; 40 ms. for Nb; 50 ms. for Sm, Gd, Tb, and Ta; and 100 ms. for Pr, Nd, and Eu; and 200 ms. for La: totally 0.9352 sec/sweep). P, Ca, and Ti were monitored in order to detect microinclusions such as apatite and rutile, which significantly disturb (elevate) LREE concentrations. For analyses without inclusions, signals of 45 sec., except first 5 sec., during 50 sec. laser ablation were integrated. Mass biases and their drift were corrected by NIST SRM612 glass, and signal responses to concentration were internally calibrated by Zr approximating stoichiometry of pure $ZrSiO_4$. Accuracy of concentrations was checked by measurements of 91500 zircon.

5.3. Zircon Hf isotope analysis

Hf isotopes were determined using Neptune-Plus multiple-collecter ICP-MS coupled with 193 nm ArF eximer laser ablation system of Analyte G2 at JAEA (Japan Atomic Energy Agency). The laser diameter was set as 50 μm, pulse frequency of 15 Hz and energy density of 8.00 J/cm^2. The isotopes of ^{171}Yb, ^{173}Yb, ^{175}Lu, ^{176}(Hf + Yb + Lu), ^{177}Hf, ^{178}Hf, and ^{179}Hf were monitored using Faraday cups attached to the ICP-MS. The isobaric interference correction with a mass number of 176 was corrected using the isotopes of ^{173}Yb/^{171}Yb (1.12346; Thirlwall and Anczkiewicz, 2004), ^{176}Yb/^{173}Yb (0.78696; Thirlwall and Anczkiewicz, 2004) and ^{176}Lu/^{175}Lu (0.026549; Chu et al., 2002). The inter-laboratory bias correction of ^{176}Hf/^{177}Hf isotope was corrected by Mud Tank zircon (Gain et al., 2019). During the measurement of the unknown samples, the 91500 (^{176}Hf/^{177}Hf = 0.282308 ± 0.000006; Blichert-Toft, 2008) and TEMORA2 (^{176}Hf/^{177}Hf = 0.282686 ± 0.000009; Woodhead and Hergt, 2005) zircons were also measured to check the accuracy and precision of the Hf analysis. All uncertainties are given as double standard errors (2SE). The mean ^{176}Hf/^{177}Hf isotopes of 91500 and TEMORA2 were 0.282317 ± 0.000020 (2SD; n = 9; MSWD = 1.8; probability = 0.0080) and 0.282681 ± 0.000035 (2SD; n = 9; MSWD = 1.5; probability = 0.16), respectively.

5.4. Major element analysis for minerals

Major element compositions of feldspar in rhyolites from the Tori and Iozen Formations were determined by electron probe micro analyzer (EPMA) using the JEOL JXA-8530F at Japan Atomic Energy Agency (JAEA). Acceleration voltage, beam current and probe diameter were

set as 15 kV, 20 nA and 5 μm, respectively, during the analysis. Synthetic and natural minerals by Astimex Standards Ltd. were prepared and used as standard material.

5.5. Whole-rock major element analysis

Whole-rock major and trace element compositions were determined by X-ray fluorescence (XRF) spectrometry using the Rigaku RIX 3000 at Niigata University. The analysis was performed using the 1:2 glass bead method. We measured the compositions of 10 (SiO_2, TiO_2, Al_2O_3, FeO*, MnO, MgO, CaO, Na_2O, K_2O, and P_2O_5; FeO* is total iron) major and 11 trace elements (Ba, Ni, Pb, Th, Rb, Sr, Y, Zr, Nb, Cr, V) following the analytical procedures of Takahashi and Shuto (1997).

5.6. Whole-rock trace element analysis

Whole-rock concentrations of trace elements were determined using an Agilent 7500a quadrupole inductively coupled plasma mass spectrometry (ICP-MS) at Niigata University. Sample solution was prepared using two methods: acid digestion (AD) based on Neo et al. (2006) and alkali fusion after acid digestion (AFAD) following Senda et al. (2014). We measured the concentrations of 26 trace elements (Rb, Sr, Y, Zr, Nb, Cs, Ba, La, Ce, Pr, Nd, Sm, Eu, Gd, Tb, Dy, Ho, Er, Tm, Yb, Lu, Hf, Ta, Pb, Th, U) following the analytical procedures of Neo et al. (2006). The accuracy of the trace element concentrations was assessed using the concentrations of the United States Geological Survey reference material BHVO-2 (Eggins et al., 1997; Jochun et al., 2016). The averages of the trace element concentrations of BHVO-2 measured in this study are consistent with the reference values (**Table 4**; Eggins et al., 1997; Jochum et al., 2016). The nondissolution of zircon contained in the rhyolites in this

study for the AD method affects the whole-rock Zr and Hf concentrations (Senda et al., 2014). Hence, we use the Zr concentration measured by XRF, and Hf is not included in the discussion. Generally, the trace element concentrations measured by ICP-MS are used for the discussion.

5.7. Whole-rock Sr–Nd isotope analysis

Whole rock Sr–Nd isotopes were measured by thermal ionization mass spectrometer (TIMS) system of Finnigan MAT262 at Niigata University. Sr and Nd were extracted from sample powders following Takahashi et al. (2009) and Hamamoto et al. (2000), respectively. Procedures for measurement were following Takahashi et al. (2009; Sr isotope), and Miyazaki and Shuto (1998; Nd isotope). Obtained $^{87}Sr/^{86}Sr$ and $^{143}Nd/^{144}Nd$ ratios were normalized by $^{88}Sr/^{86}Sr = 0.1194$ and $^{146}Nd/^{144}Nd = 0.7219$, and then, calibrated by using NIST987 ($^{87}Sr/^{86}Sr = 0.710245$) and JNdi-1 ($^{143}Nd/^{144}Nd = 0.512106$), respectively. In this study, 0.710222 ± 0.000043 (2SD; n = 9) and 0.512118 ± 0.000156 (2SD; n = 9) were obtained as means of $^{87}Sr/^{86}Sr$ of NIST987 and $^{143}Nd/^{144}Nd$ of JNdi-1, respectively.

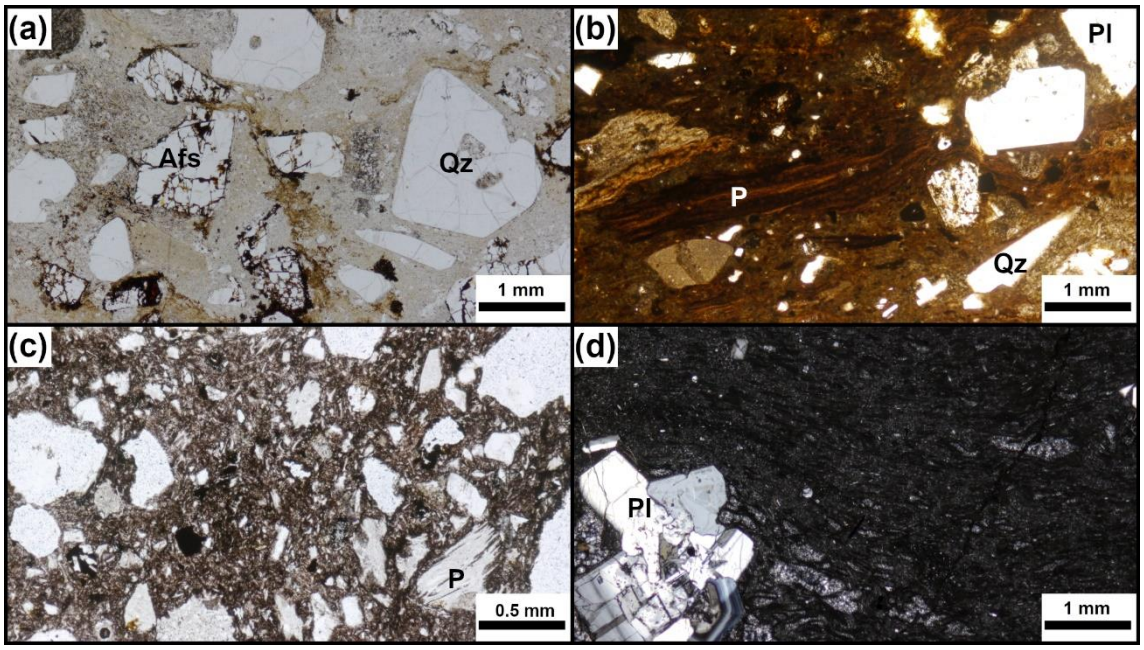

Figure 5.1 Microscope photographs of dated samples. (a) Rhyolitic welded tuff sample (NT63c) from the Johana Formation. (b) Rhyolitic welded tuff gravel sample (090705A) from the Nirehara Formation. (c) Pumiceous lapilli tuff sample (NT27) from the Iwaine Formation. (d) Rhyolite lava sample (NT45) from the Iozen Formation. Afs: alkali feldspar. P: pumice (welded or non-welded). Pl: plagioclase. Qz: quartz.

6. Petrography

In this chapter, petrography of the volcanic rocks collected from the Nanto area is described. Based on petrography, the volcanic rocks can be classified into five rock types: rhyolitic welded tuff (Jh-Pyr), olivine two-pyroxene andesite (Iw-OlPx), amphibole andesite (Iw-Amp), two-pyroxene andesite (Iw-Px), and aphyric rhyolite (Io-Aph). Jh-Pyr contains alkali feldspar and quartz. In contrast, Io-Aph contains plagioclase, amphibole and pyroxene. These differences in petrography reflect also whole-rock geochemistry.

6.1. Johana Formation (Jh-Pyr)

All samples from the Tori Formation are weakly to densely welded tuff without lithic clasts, described as Us-Pyr (**Figure 6.1a**). Although the welded tuff has partly vitric matrix showing eutaxitic texture, felsitic texture is observed in the most parts. As mineral grains, alkali feldspar, quartz and opaque minerals are contained with rare biotite grains (**Table 2**). Alkali feldspar (Or = 45–48 mol.%; **Table 3**) shows clear euhedral to subhedral shapes. Quartz exhibits corroded outline with complex embayment. Xenoliths of paragneiss containing alkali-feldspar, quartz and muscovite are rarely found (**Figure 6.1b**).

6.2. Iwaine Formation

6.2.1. Olivine two-pyroxene andesite (Iw-OlPx)

Olivine two-pyroxene andesite (Iw-OlPx; **Figure 6.1c**) contains phenocrysts of plagioclase, clinopyroxene, orthopyroxene, olivine and opaque minerals (**Table 2**), and the groundmass shows hyalopilitic to hyaloophitic texture. Plagioclase is found as euhedral to subhedral clear phenocrysts. Although all olivine phenocrysts are

altered to clay minerals, euhedral shape is well preserved. Clinopyroxene and orthopyroxene occur as euhedral to subhedral clear phenocrysts, and clinopyroxene often has rim composed of orthopyroxene and rarely shows oscillatory zoning.

6.2.2.Amphibole andesite (lw-Amp)

Typical amphibole andesite (lw-Amp; **Figure 6.1d**) is characterized by abundant amphibole phenocrysts in addition to clinopyroxene, orthopyroxene and opaque minerals (**Table 2**). However, some samples also contain plagioclase phenocryst. The groundmass shows hyalopilitic or hyaloophitic texture. Amphibole phenocrysts are strongly opacitized. Relatively large amphibole phenocrysts show subhedral or euhedral shapes, meanwhile small phenocrysts indicate corroded or subhedral shapes. Although amphibole phenocrysts are generally observed as monocrysts, glomerocrysts of amphibole with a clinopyroxene core are rarely found. Clinopyroxene and orthopyroxene are found as subhedral or euhedral phenocrysts. Dusty alkali feldspar occurs as anhedral xenocrysts, exhibit reaction rims brownish color and indicate wavy extinction. Quartz is observed as corroded xenocrysts. Xenolith of granitoid is commonly contained. Besides lava, lw-Amp includes pyroclastic rocks composed of andesitic pumiceous lapilli tuff whose mineral assemblage is the same as lava flows.

6.2.3.Two-pyroxene andesite (lw-Px)

Two-pyroxene andesite (lw-Px; **Figure 6.1e**) contains phenocrysts of plagioclase, clinopyroxene, orthopyroxene and opaque minerals. It includes a few glomerocrysts composed of plagioclase, clinopyroxene and orthopyroxene (**Table 2**). The groundmass shows intersertal to hyalopilitic or sometimes hyaloophitic textures. Plagioclase is generally found as euhedral to subhedral phenocryst with dusty zone. Clinopyroxene and orthopyroxene are found as subhedral or euhedral

phenocrysts.

6.3. Iozen Formation (Io-Aph)

All samples from the Iozen Formation are classified as aphyric rhyolite (Io-Aph; **Figure 6.1f**). This type contains a small number of phenocrysts mainly of plagioclase, amphibole, orthopyroxene, clinopyroxene, and opaque minerals (**Table 2**). The groundmass is composed almost of glass and shows flow texture, and some shows hyaloophitic texture. Plagioclase (An = 57–70 mol.%; **Table 3**) is found as subhedral or euhedral phenocrysts showing oscillatory zoning. Amphibole, orthopyroxene, and clinopyroxene are found as euhedral to subhedral phenocrysts. Amphibole phenocryst is sometimes opacitized.

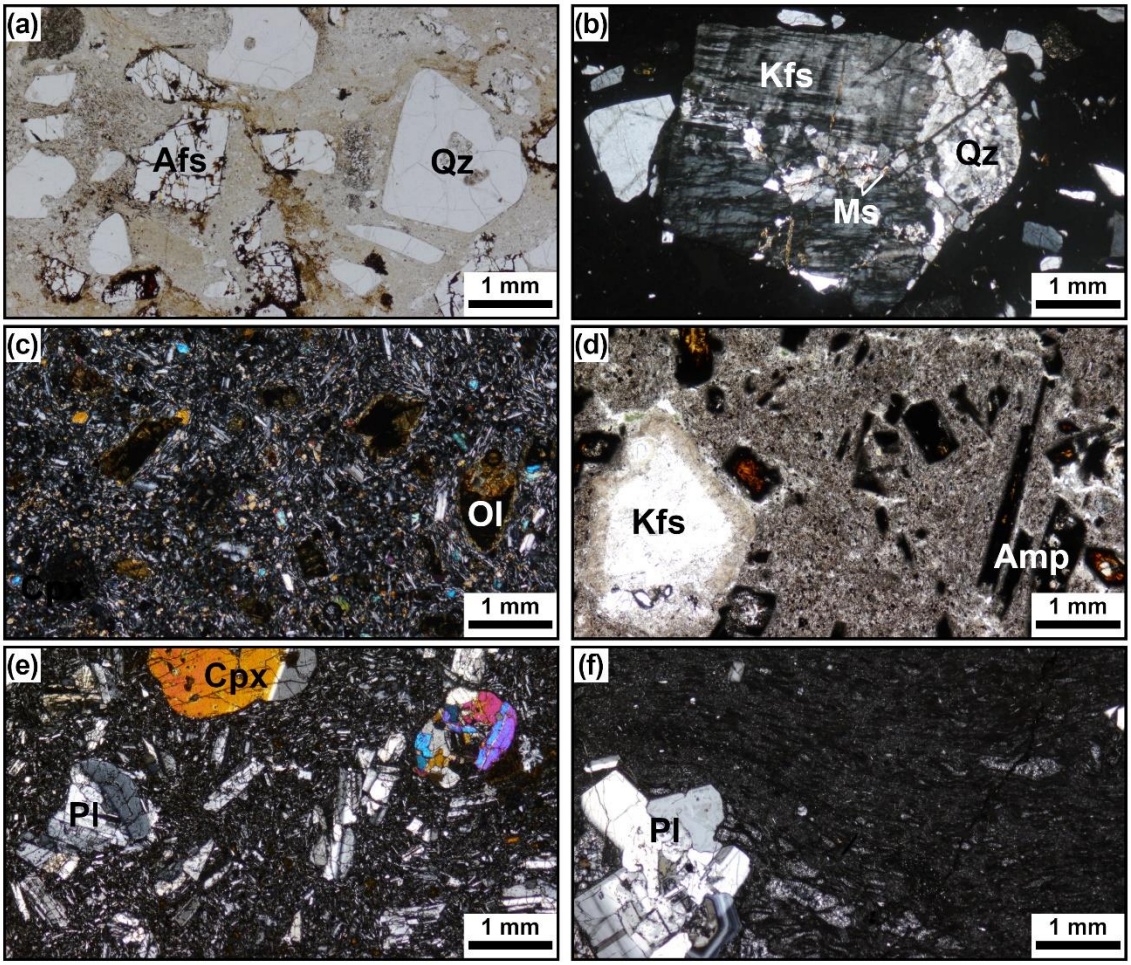

Figure 6.1 Thin section photomicrographs of the volcanic rocks. (a) Rhyolitic welded tuff from the Usunaka Moonstone Rhyolite Member of the Johana Formation (Jh-Pyr). (b) Paragneiss xenolith in Jh-Pyr from the Johana Formation. (c) Olivine two-pyroxene andesite from the Iwaine Formation (Iw-OlPx). (d) Amphibole andesite with xenocryst of K-feldspar from the Iwaine Formation (Iw-Amp). (e) Two-pyroxene andesite from the Iwaine Formation (Iw-Px). (f) Aphyric rhyolitic lava from the Iozen Formation (Io-Aph). Amp: amphibole. Cpx: clinopyroxene. Kfs: K-feldspar. Ms: muscovite. Ol: olivine. Pl: plagioclase. Qz: quartz.

Table 2 Mineral assemblages of volcanic rocks.

Formation	Rock type	Mineralogy								
		Olivine	Clino-pyroxene	Ortho-pyroxene	Amphibole	Biotite	Plagioclase	Alkali feldspar	Quartz	Ground mass (%)
Iozen	Io-Aph		++	++	++		++			~80-95
Iwaine	Iw-Px		++	++			+++			~55-75
	Iw-Amp		+		+++			++	+	~80
	Iw-OlPx	++	++	++			+++			~55-80
Johana	Jh-Pyr					+		+++	+++	~65-80

Notes: +++: >10%, ++: 0.1-10%, +: <0.1%

Table 3 Chemical compositions of feldspar from the rhyolites. Ab: albite. An: anorthite. Or: orthoclase.

Sample	NT74	NT74	NT74	NT74	NT63c	NT63c	NT63c	NT55	NT55	NT55	NT55
Spot	6_03	6_04	6_05	6_06	7_04	7_05	7_06	2_01	2_03	2_05	2_07
Mineral	Alkali feldspar	Alkali feldspar	Alkali feldspar	Alkali feldspar	Alkali feldspar	Alkali feldspar	Alkali feldspar	Plagioclase	Plagioclase	Plagioclase	Plagioclase
SiO_2	63.32	66.27	66.53	67.21	62.23	64.10	64.61	58.14	60.26	56.33	57.06
TiO_2	n.d.	n.d.	n.d.	n.d.	n.d.	n.d.	n.d.	n.d.	n.d.	n.d.	n.d.
Al_2O_3	17.73	18.31	18.50	18.77	17.30	17.99	17.95	28.01	26.64	28.76	28.52
FeO	0.16	0.17	0.15	0.18	0.09	0.15	0.12	0.37	0.36	0.40	0.29
MnO	0.05	0.04	0.01	0.02	n.d.	0.02	n.d.	n.d.	n.d.	n.d.	n.d.
MgO	0.01	n.d.	n.d.	n.d.	0.01	n.d.	n.d.	0.02	0.02	0.07	0.01
CaO	0.07	0.09	0.18	0.19	0.07	0.08	0.09	10.22	8.60	11.48	10.88
Na_2O	5.70	5.70	5.73	6.18	5.60	5.85	5.63	6.03	6.92	5.28	5.58
K_2O	7.82	8.07	7.86	7.90	7.19	7.55	7.78	0.27	0.35	0.22	0.24
P_2O_5	0.01	n.d.	n.d.	n.d.	n.d.	n.d.	n.d.	n.d.	n.d.	n.d.	n.d.
Total (wt.%)	94.87	98.64	98.96	100.45	92.48	95.73	96.18	103.06	103.15	102.53	102.58
An (mol.%)	0.70	0.86	1.80	1.76	0.79	0.78	0.88	64.54	57.07	70.07	67.73
Ab (mol.%)	52.17	51.34	51.60	53.36	53.80	53.63	51.94	34.44	41.55	29.15	31.40
Or (mol.%)	47.13	47.81	46.59	44.88	45.42	45.58	47.19	1.03	1.38	0.78	0.87

n.d.: not detected

7. Results

In this chapter, results of zircon U–Pb dating, zircon trace element analysis, zircon Lu–Hf isotope analysis, whole-rock major and trace element analysis, and whole-rock Sr–Nd isotope analysis are shown. The ^{238}U–^{206}Pb weighted mean ages of the Johana, Iwaine Iozen Formations are 22.8 ± 0.2 Ma, 17.1 ± 0.4 Ma, and 16.8 ± 0.2 Ma, respectively. Zircon grains from the volcanic rocks exhibit high U/Yb ratio and low εHf. The volcanic rocks from the Johana and Iozen Formations show rhyolitic chemical compositions, whereas the Iwaine Formation is composed of three types of andesites: high-Mg andesite (Iw-OlPx), high-Sr andesite (Iw-Amp), and tholeiitic andesite (Iw-Px). All volcanic rocks show negative anomalies of Nb and Ta. Iw-OlPx and Iw-Amp have relatively depleted Sr–Nd isotopic composition, whereas the others have more enriched isotopic composition than the bulk earth.

7.1. Zircon U–Pb ages

Results of CL images, Wetherill concordia diagrams and ^{238}U–^{206}Pb weighted mean age are shown in **Figure 7.1** and **7.2**, and zircon U–Pb dating data of each grain is available in **Supplementary Table A**.

Typical zircon grains from a rhyolitic welded tuff sample from the Tori Formation (NT63c) are euhedral or fragmented, commonly showing oscillatory zoning (Figure 7.1a). Concordant results provided a weighted mean age of 22.8 ± 0.2 Ma with MSWD = 1.4. Nine other grains showed older concordant ages ranging from ~1900–1850 and 200–100 Ma. Inner textures of some of these old grains are cut by thin growth rim, suggesting that these old grains are inherited zircon

derived from the basement rocks.

Zircon grains from a rhyolitic welded tuff sample of the Nirehara Formation (090705A) exhibit oscillatory zoning or no zoning in CL images (**Figure 7.2a**). 5 zircon grains of 11 grains were adopted, and the ^{238}U–^{206}Pb weighted mean age using the zircon grains was calculated to be 21.1 ± 2.2 Ma (MSWD = 20.35; probability of fit = 0 %; **Figure 7.2c**). Three grains of a coherent cluster provide 23.6 ± 0.3 Ma of the ^{238}U–^{206}Pb weighted mean age with MSWD = 0.15 and probability of fit = 0.858 (**Figure 7.2e**).

Typical zircon grains from the Iwaine Formation (NT27) are euhedral and show oscillatory zoning (**Figure 7.1b**). All but two grains comprise a single cluster around ~17 Ma. Among them, concordant results provided a weight mean age of 17.1 ± 0.4 Ma (MSWD = 6.0; **Figure 7.1b**). The two exceptions clustered around ~60 Ma. Rejected zircon grains in ^{238}U–^{206}Pb weighted mean age resulted probably from contamination from the Johana Formation during eruption, and its excess dispersion is considered as characteristics of the sample (NT27). One of these old grains exhibits diffusion zoning with a luminescent rim invading into a less luminescent core dated as 63.6 Ma (**Figure 7.1b**) suggesting inheritance. These two grains are considered as xenocrysts from the basement granites as this sample includes granite xenolith.

Typical zircon grains from an aphyric rhyolitic lava sample from the of the Iozen Formation (NT45) are euhedral showing oscillatory and sector zonings (**Figure 7.1c**). The ^{238}U–^{206}Pb weighted mean has excess dispersion (MSWD = 3.4). The concordant ^{238}U–^{206}Pb ages comprises a single cluster with a weighted mean of 16.8 ± 0.2 Ma (**Figure 7.1c**). This age is identical with zircon FT age (16.5 ± 1.4 Ma; Ganzawa, 1983) reported from the same outcrop.

7.2. Zircon Trace element compositions

Trace element data of zircon grains whose Ca and Ti concentrations are not greater than 400 and 3000 ppm, respectively, are adopted to avoid contamination by inclusions such as apatite, titanite and rutile. However, there is a possibility that some data may still include micro-inclusions. Zircon trace element composition on each grain is given in **Supplementary Table B**.

Rhyolitic welded tuff sample from the Usunaka Moonstone Rhyolite Member of the Tori Formation (NT63c) has the most enriched composition as the trace element pattern is shown in the **Figure 7.3**. Additionally, the Tori Formation shows clear negative spike of Eu and have relatively higher content of LREE to HREE, compared to the Iwaine (NT27) and Iozen Formations (NT45). Compared to the Tori Formation, the Iwaine and Iozen Formations have depleted compositions, and they exhibit clearer positive spike of Ce than that of the Johana Formation. In Hf–U/Yb diagram, most of all samples are plotted in the area of continental zircon (**Figure 7.3e**)

7.3. Zircon Lu–Hf isotopic compositions

Age–εHf diagrams are shown in **Figure 7.4b** and **7.4c**. Zircon Hf isotopic composition data on each grain is shown in **Supplementary Table C**.

Most of the grains from three volcanic rocks have homogenous composition (**Figure 7.4a**) ranging from 0.00075 to 0.01572 for $^{176}Lu/^{177}Hf$ and 0.28246–0.28282 for $^{176}Hf/^{177}Hf$, except for the Precambrian inherited grains from the Johana Formation. Trends of volcanic rocks cross with the 1000 Ma evolution line of the depleted mantle (DM; Griffin et al., 2000), plotted between the Hida metamorphic rocks (Cho et al., 2021a) and DM. The Precambrian grains have much lower $^{176}Hf/^{177}Hf$ ratio than those of young zircons.

In age–εHf diagram (**Figure 7.4b** and **7.4c**), young zircons except for the Precambrian grains from the Johana Formation are plotted densely ranging ~-10 to 0 in εHf.

7.4. Whole-rock geochemistry

Results of whole-rock major and trace element compositions and whole-rock Sr–Nd isotope are shown in **Table 4** and **Table 5,** respectively.

7.4.1.Johana Formation

Jh-Pyr is classified as rhyolite in SiO_2–Na_2O+K_2O diagram (**Figure 7.5a**). This type is characterized by low CaO (0.06–0.31 wt.%; **Figure 7.6**) and high K_2O (4.18–5.78 wt.%; **Figure 7.5b**) contents. Jh-Pyr shows decreasing (deplete) pattern from Cs to Lu, with flat pattern in MREE (middle rare earth element) to HREE (**Figure 7.7a**). This type has more enriched trace element compositions than those of the Io-Aph type from the Iozen Formation, showing strong negative anomalies of Ba, Nb, Ta, Sr and Eu and weak positive anomaly of Pb. The initial Sr and Nd isotopic ratios are calculated as 0.70769–0.70944 and 0.51203–0.51224, respectively. Jh-Pyr has the most enriched Sr–Nd isotopic compositions, showing much more enriched than the bulk earth, in all types of the volcanic rocks (**Figure 7.8a**).

7.4.2. Iwaine Formation

Iw-OlPx is classified as basaltic andesite in SiO_2–Na_2O+K_2O diagram (**Figure 7.5a**). Iw-OlPx type is characterized by higher MgO content (5.61–7.81 wt.%; **Figure 7.6**) than that of the other andesites from the Iwaine Formation and shows a calc-alkalic trend in FeO*/MgO–SiO_2 diagram (**Figure 7.5c**). Iw-OlPx type shows decreasing (deplete) pattern from Cs to Lu, exhibiting also decreasing pattern from MREE to HREE (**Figure 7.7b**). This type exhibits negative anomalies of Nb and Ta and positive anomalies of Pb and

Sr, but the degree of the negative anomalies of Nb and Ta is lower than the other andesites from the Iwaine Formation. The initial Sr and Nd isotopic ratios are calculated as 0.70482 and 0.51279, respectively. This type is more depleted in NdI than that of the bulk earth (**Figure 7.8a**).

Iw-Amp is classified as andesite, trachy-basaltic andesite, and trachy-andesite in SiO_2–Na_2O+K_2O diagram (**Figure 7.5a**). Iw-Amp is characterized by higher Na_2O+K_2O (4.46–6.96 wt.%; Fig. 4a), K_2O (1.80–4.02 wt.%; **Figure 7.5b**), P_2O_5 (0.19–0.57 wt.%; **Figure 7.6**) and Sr (866.9–2934.0; **Figure 7.6**) contents than those of the other andesites from the Iwaine Formation. In Y–Sr/Y, CaO+Na_2O–Sr, Sr–(SiO_2/MgO)×100–K/Rb, Rb–K diagrams (**Figure 7.9**), iw-Amp is plotted near low-SiO_2 adakite (LSA) of Martin et al. (2005).Iw-Amp shows decreasing (deplete) pattern from Cs to Lu, exhibiting also decreasing pattern from MREE to HREE (**Figure 7.7b**). This type has the most enriched trace element compositions in andesites from the Iwaine Formation. This type exhibits deep negative anomalies of Nb and Ta and positive anomalies of Pb and Sr. The initial Sr and Nd isotopic ratios are calculated as 0.70373–0.70432 and 0.51262–0.51284, respectively. This type is plotted near the bulk earth in SrI–NdI diagram (**Figure 7.8a**).

Iw-Px is classified as basaltic andesite to andesite in SiO_2–Na_2O+K_2O diagram (**Figure 7.5a**). Iw-Px shows tholeiitic trend in FeO*/MgO-SiO_2 diagram (**Figure 7.5c**). This type is characterized by high FeO* (5.78–11.36 wt.%) and CaO (7.43–9.04 wt.%) contents than those of the other andesites from the Iwaine Formation (**Figure 7.6**). Iw-Px shows decreasing (deplete) pattern from Cs to Lu, exhibiting also decreasing pattern from MREE to HREE (**Figure 7.7b**). This type exhibits negative anomalies of Nb and Ta and a positive anomaly of Pb. Compared to the basaltic andesites from continental

arc (North Sister volcano, USA) and island arc (Zao volcano, Japan), the trace element pattern of this type is similar to basaltic andesites from the continental arc (**Figure 7.7c**). The initial Sr and Nd isotopic ratios are calculated as 0.70713–0.70756 and 0.51237–0.51241, respectively. This type has most enriched Sr–Nd isotope in the andesites from the Iwaine Formation (**Figure 7.8a**).

7.4.3.Iozen Formation

Io-Aph is classified as dacite to rhyolite in SiO_2–Na_2O+K_2O diagram (**Figure 7.5a**). Io-Aph shows decreasing (deplete) pattern from Cs to Lu, with flat pattern in MREE to HREE (**Figure 7.7a**). Io-Aph exhibits negative anomalies of Nb, Ta, Sr and Eu and a positive anomaly of Pb, but the degree of the negative anomalies of Sr and Eu is much lower than those of Jh-Pyr. The initial Sr and Nd isotopic ratios are calculated as 0.70823–0.70750 and 0.51221–0.51236, respectively. This type has intermediate Sr–Nd isotopic compositions between the Tori and Iwaine Formations, and it has more enriched Sr–Nd compositions than the bulk earth (**Figure 7.8a**).

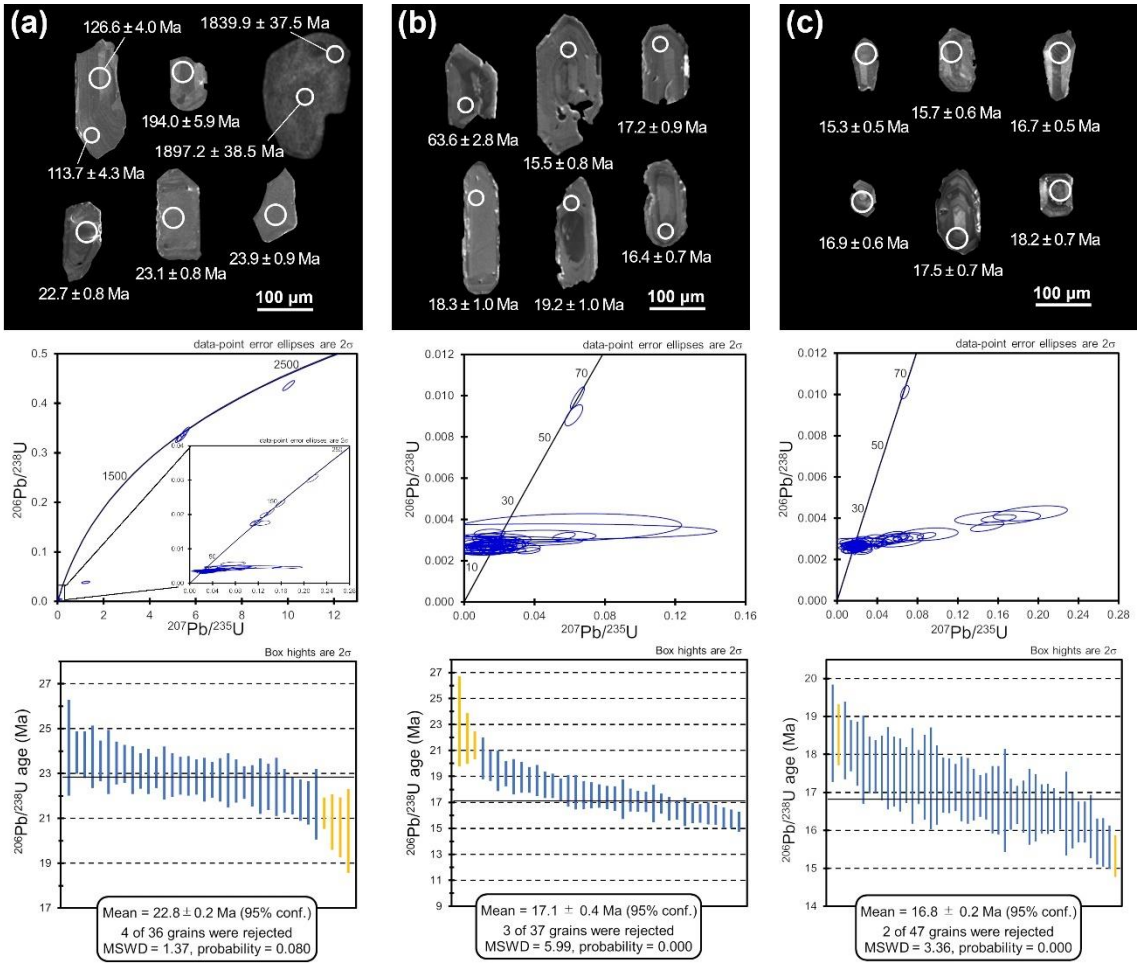

Figure 7.1 Cathodoluminescence (CL) images, Wetherill concordia diagrams, and weighted mean of ^{238}U–^{206}Pb ages of the Johana, Iwaine and Iozen Formations. (a) NT63c from the Tori Formation. (b) NT27 from the Iwaine Formation. (c) NT45 from the Iozen Formation.

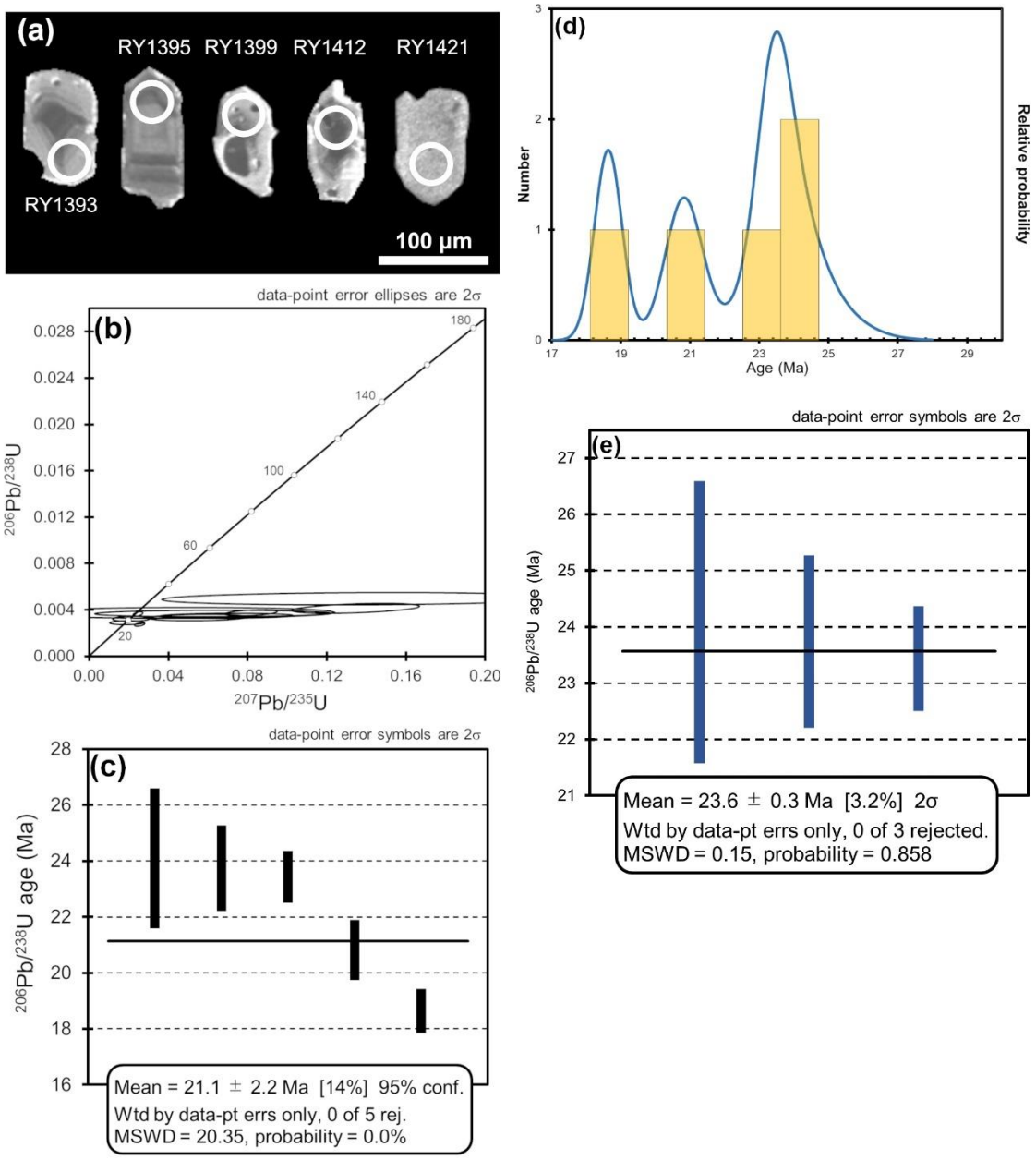

Figure 7.2 CL image and results of zircon U–Pb dating of the Nirehara Formation. (a) CL images of all adopted grains with sample number and $^{206}Pb/^{238}U$ age. (b) Wetherill concordia diagram. (c) Weighted mean of $^{206}Pb/^{238}U$ age of all adopted grains. (d) probability density plot. (e) Weighted mean of $^{206}Pb/^{238}U$ age of three grains forming coherent cluster.

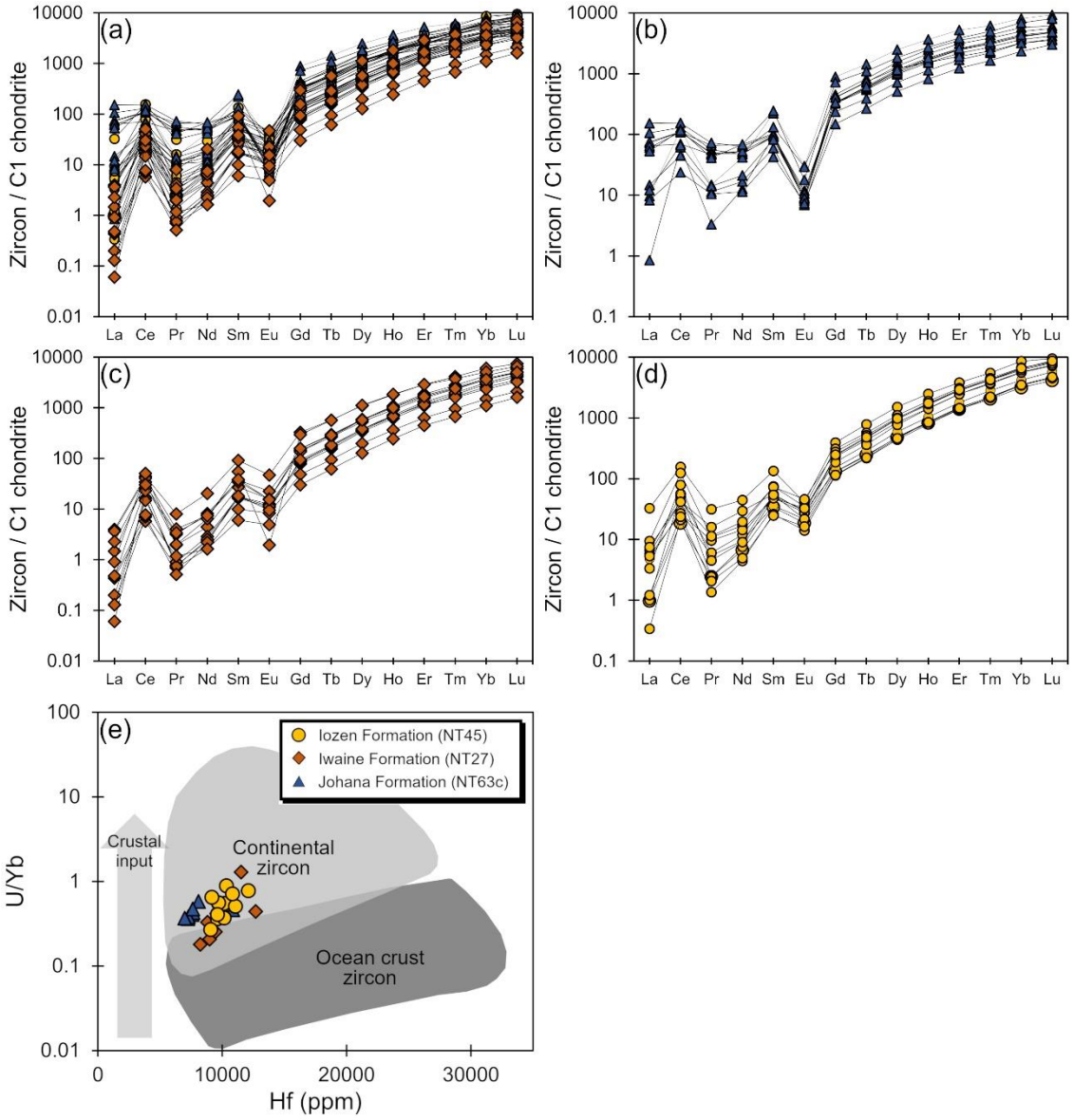

Figure 7.3 Zircon rare earth element patterns and Hf–U/Yb diagram. (a) all samples. (b) NT63c from the Tori Formation. (c) NT27 from the Iwaine Formation. (d) NT45 from the Iozen Formation. (e) Hf–U/Yb discrimination diagram of zircon for the volcanic rocks. Areas of oceanic crust and continental zircons are from Grimes et al. (2007).

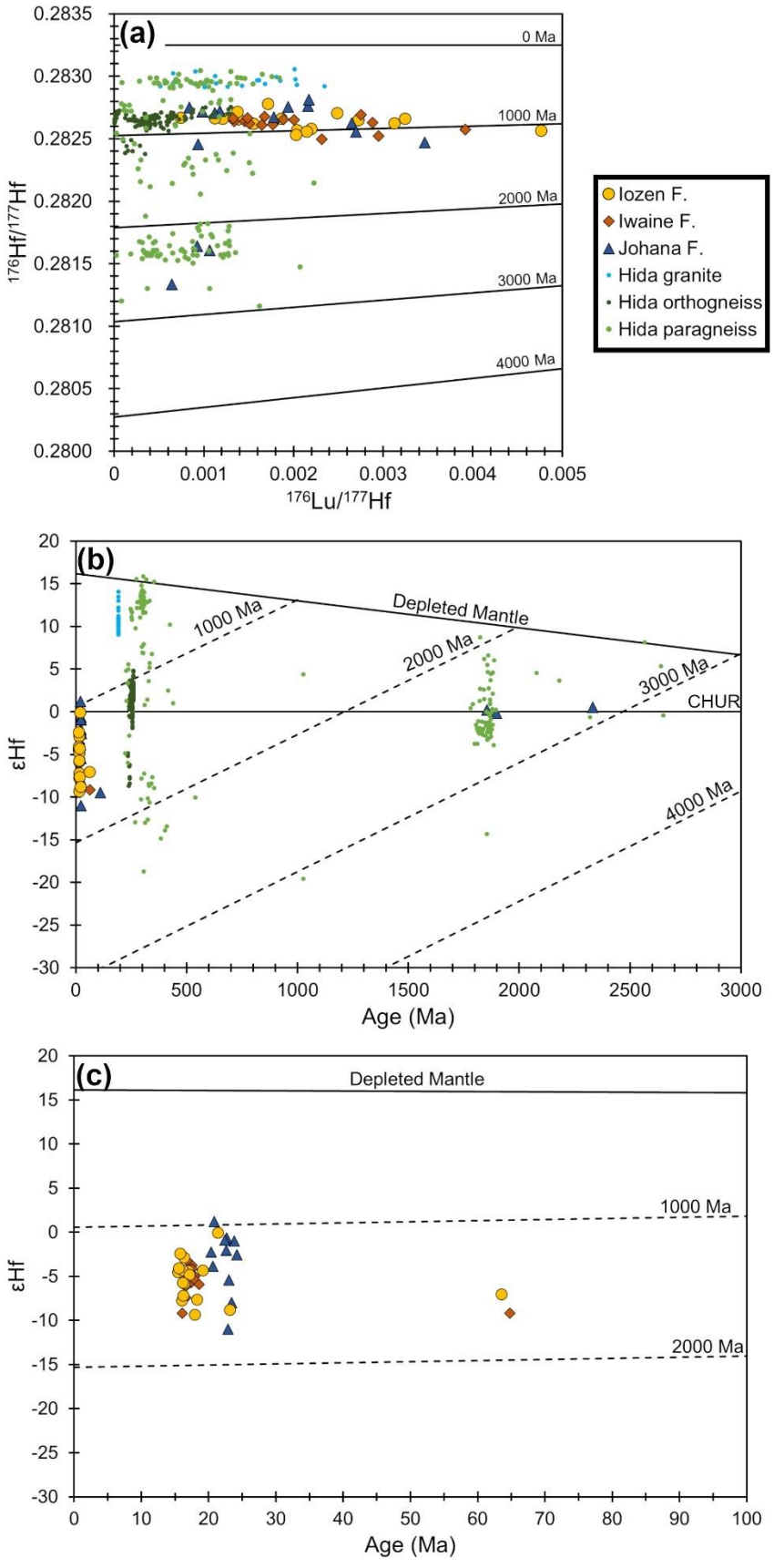
(a)
0 Ma
1000 Ma
2000 Ma
3000 Ma
4000 Ma
$^{176}Hf/^{177}Hf$
$^{176}Lu/^{177}Hf$
Iozen F.
Iwaine F.
Johana F.
Hida granite
Hida orthogneiss
Hida paragneiss
(b)
Depleted Mantle
1000 Ma
2000 Ma
3000 Ma
CHUR
4000 Ma
εHf
Age (Ma)
(c)
Depleted Mantle
1000 Ma
2000 Ma
εHf
Age (Ma)

Figure 7.4 Lu–Hf isotope variation diagrams. (a) $^{176}Lu/^{177}Hf$–$^{176}Hf/^{177}Hf$ isochron diagram with the model age lines based on Griffin et al. (2000; solid line). (b) Hf isotope evolution diagram with evolution line of depleted mantle (Griffin et al., 2000; $^{176}Lu/^{177}Hf = 0.015$). The CHUR is based on the evolution model by Iizuka et al. (2015). (c) Hf isotope evolution diagram showing only young ages. CHUR: Chondritic Uniform Reservoir.

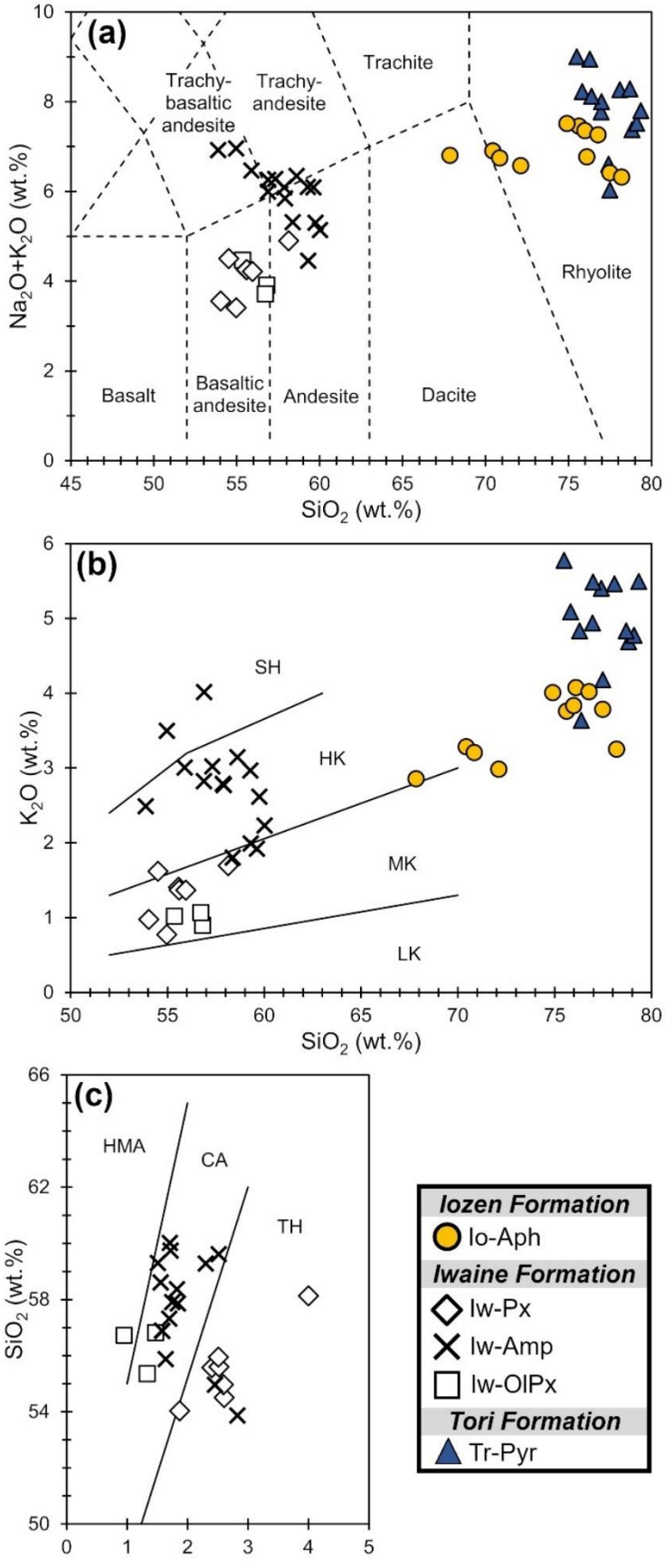
(a)
Trachy-basaltic andesite
Trachy-andesite
Trachite
Rhyolite
Basalt
Basaltic andesite
Andesite
Dacite
Na2O+K2O (wt.%)
SiO2 (wt.%)
(b)
SH
HK
MK
LK
K2O (wt.%)
SiO2 (wt.%)
(c)
HMA
CA
TH
SiO2 (wt.%)
Iozen Formation
Io-Aph
Iwaine Formation
Iw-Px
Iw-Amp
Iw-OlPx
Tori Formation
Tr-Pyr

Figure 7.5 Classification of the volcanic rocks. (a) SiO_2–Na_2O+K_2O diagram (LeMaitre et al., 2002). (b) SiO_2–K_2O diagram (Peccerollo and Taylor, 1976). (c) FeO*/MgO–SiO_2 diagram. Lines separating TH (tholeiite series), CA (calc-alkaline series), and HMA (high-magnesian andesite) are after Miyashiro (1974) and Sato (1989).

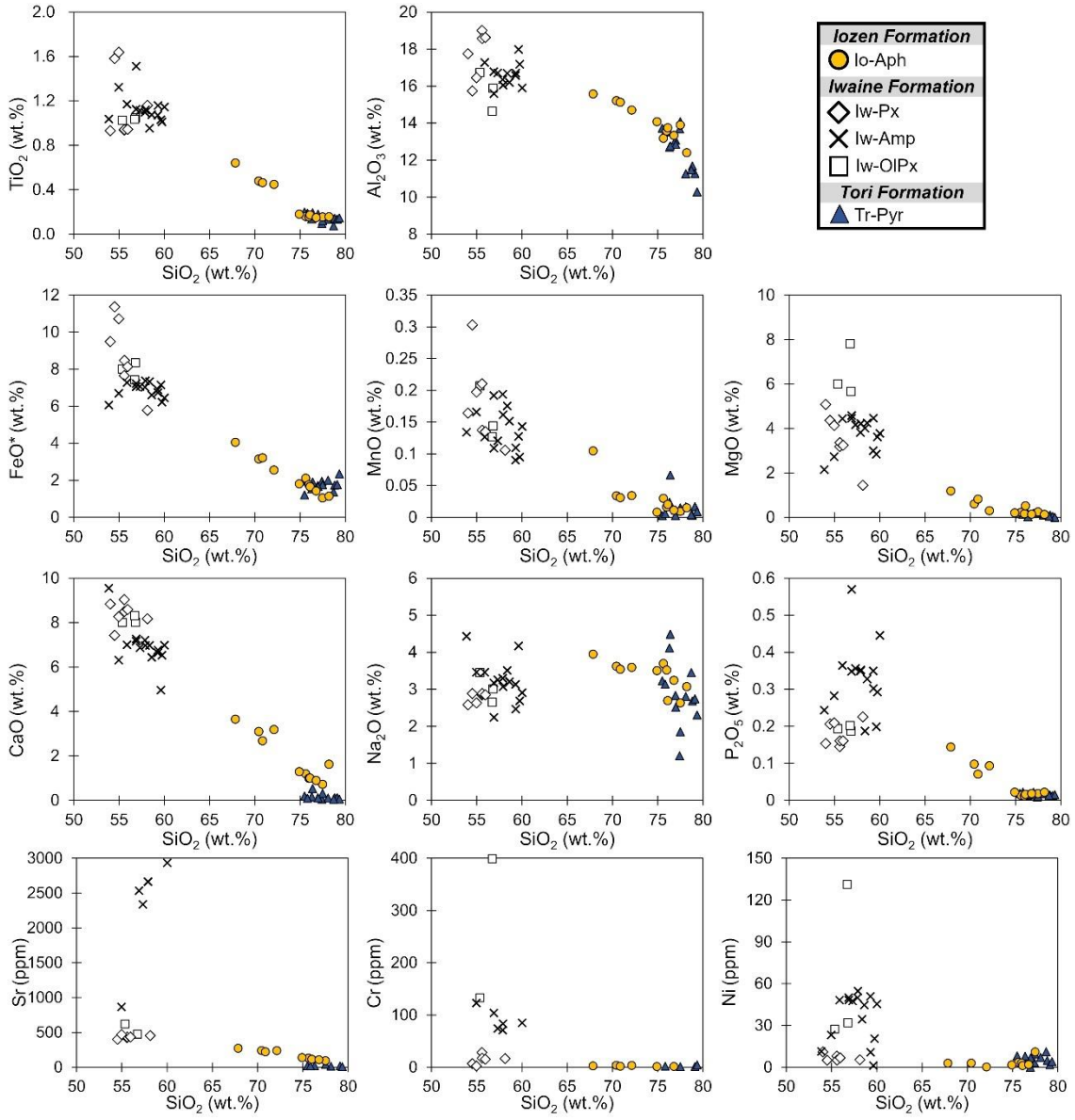

Figure 7.6 SiO_2 versus major and trace element variation diagrams of whole-rock chemical compositions.

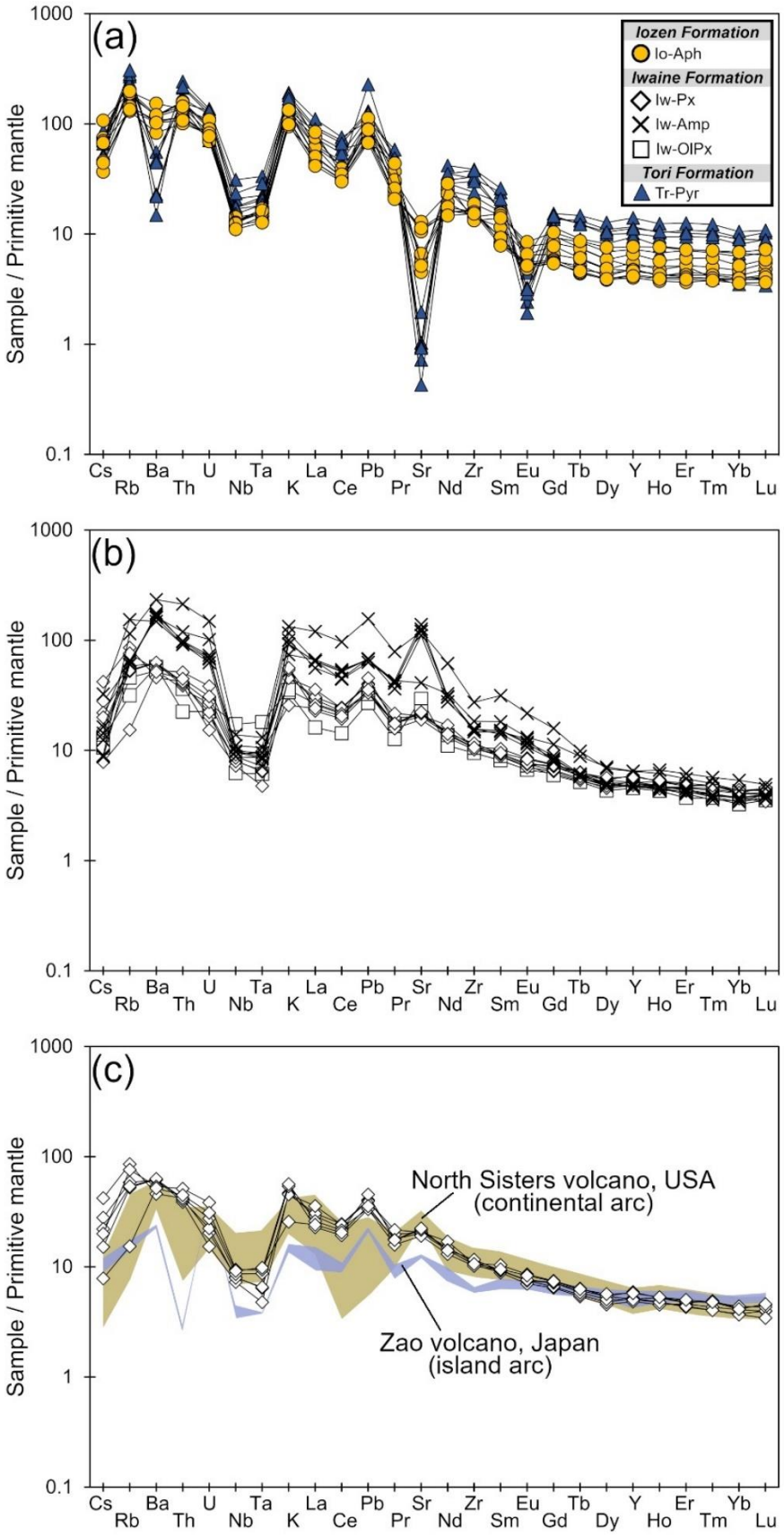
(a)
Iozen Formation
Io-Aph
Iwaine Formation
Iw-Px
Iw-Amp
Iw-OlPx
Tori Formation
Tr-Pyr
Sample / Primitive mantle
1000
100
10
1
0.1
Cs Rb Ba Th U Nb Ta K La Ce Pb Pr Sr Nd Zr Sm Eu Gd Tb Dy Y Ho Er Tm Yb Lu
(b)
Sample / Primitive mantle
(c)
North Sisters volcano, USA
(continental arc)
Zao volcano, Japan
(island arc)

Figure 7.7 Spider diagrams of incompatible elements. Trace element concentrations for normalization are from Sun and McDonough (1989; primitive mantle). (a) Rhyolites from the Johana (Jh-Pyr) and Iozen Formations (Io-Aph). (b) all types of the andesite from the Iwaine Formation. (c) Iw-Px compared with island arc type (Zao volcano, Japan; Tatsumi et al., 2008) and continental arc tholeiitic basaltic andesites (North Sisters volcano, USA; Schmidt and Grunder, 2011).

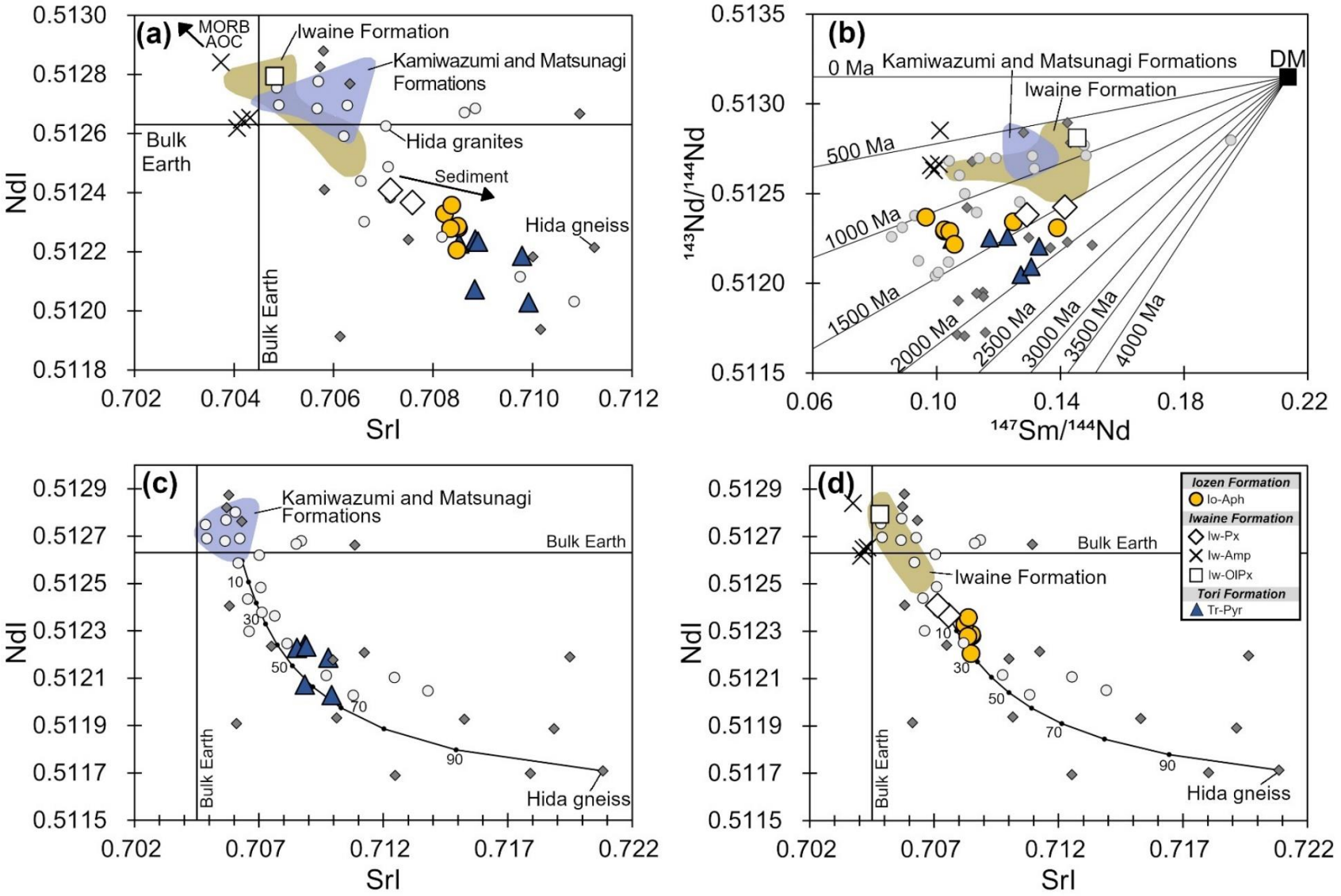
(a)
MORB
AOC
Iwaine Formation
Kamiwazumi and Matsunagi
Formations
Hida granites
Sediment
Hida gneiss
Bulk
Earth
Bulk Earth
Ndl
Srl
0.5130
0.5128
0.5126
0.5124
0.5122
0.5120
0.5118
0.702
0.704
0.706
0.708
0.710
0.712
(b)
0 Ma
Kamiwazumi and Matsunagi Formations
DM
Iwaine Formation
500 Ma
1000 Ma
1500 Ma
2000 Ma
2500 Ma
3000 Ma
3500 Ma
4000 Ma
143Nd/144Nd
147Sm/144Nd
0.5135
0.5130
0.5125
0.5120
0.5115
0.06
0.10
0.14
0.18
0.22
(c)
Kamiwazumi and Matsunagi
Formations
Bulk Earth
10
30
50
70
90
Hida gneiss
Bulk Earth
Ndl
Srl
0.5129
0.5127
0.5125
0.5123
0.5121
0.5119
0.5117
0.5115
0.702
0.707
0.712
0.717
0.722
(d)
Bulk Earth
Iwaine Formation
10
30
50
70
90
Hida gneiss
Bulk Earth
Iozen Formation
Io-Aph
Iwaine Formation
Iw-Px
Iw-Amp
Iw-OlPx
Tori Formation
Tr-Pyr
Ndl
Srl
0.5129
0.5127
0.5125
0.5123
0.5121
0.5119
0.5117
0.5115
0.702
0.707
0.712
0.717
0.722

Figure 7.8 Sr–Nd isotopic variation diagrams. (a) SrI–NdI diagram of the volcanic rocks with plots of the Iwaine, Kamiwazumi and Matsunagi Formations (Sato et al., 2013; Okamura et al., 2016) and the Hida Belt (Asano et al., 1990; Tanaka, 1992; Arakawa and Shinmura, 1995). Arrows showing MORB (Midocean Ridge Basalt), AOC (Altered Oceanic Crust) and sediment are based on Tatsumi (2006). (b) $^{147}Sm/^{144}Nd$–$^{143}Nd/^{144}Nd$ diagram of the volcanic rocks with plots of the Iwaine Formation, the Kamiwazumi and Matsunagi Formations, and Hida Belt. Sr and Nd isotopic values of the depleted mantle are from Goldstein et al. (1984). (c) Assimilation model of the rhyolite from the Johana Formation. (d) Assimilation model of the rhyolite from the Iozen Formation. Sr and Nd isotopic values of the bulk earth are from DePaolo and Wasserburg (1976) and Bouvier et al. (2008), respectively.

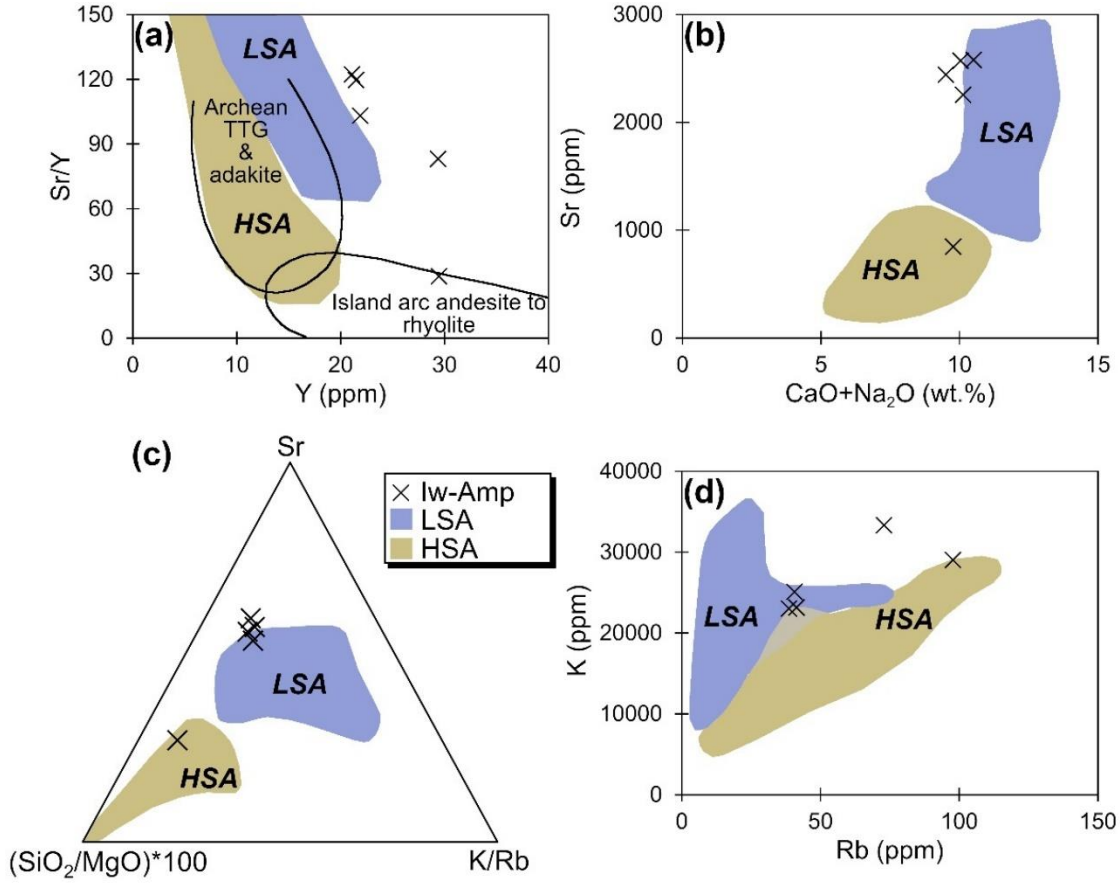

Figure 7.9 Comparison of Iw-Amp from the Iwaine Formation with HSA (high-SiO_2 adakite) and LSA (low-SiO_2 adakite) of Martin et al. (2005). (a) Y–Sr/Y variation diagram (Defant et al., 1991), (b) CaO+Na2O–Sr variation diagram, (c) Sr–SiO_2/MgO*100–K/Rb ternary graph, and (d) Rb–K variation diagram.

Table 4 Results of whole-rock major and trace element compositions.

Formation	Standard	Standard	Johana	Johana	Johana	Johana	Johana
Sample	BHVO-2	BHVO-2	NT01	NT05	NT07	NT09	NT16
Type			Jh-Pyr	Jh-Pyr	Jh-Pyr	Jh-Pyr	Jh-Pyr
Rock type	Basalt	Basalt	Welded tuff	Welded tuff	Welded tuff	Welded tuff	Welded tuff
Major elements by XRF (wt.%)							
SiO_2	-	-	76.72	76.41	77.93	76.23	75.01
TiO_2	-	-	0.09	0.17	0.14	0.14	0.20
Al_2O_3	-	-	13.57	13.00	11.25	12.69	13.64
FeO*	-	-	1.93	1.70	2.00	1.53	1.20
MnO	-	-	0.01	0.003	0.02	0.02	0.003
MgO	-	-	0.17	0.16	0.10	0.19	0.16
CaO	-	-	0.06	0.11	0.11	0.17	0.19
Na_2O	-	-	1.19	2.82	2.80	4.11	3.21
K_2O	-	-	5.36	4.90	5.45	4.83	5.74
P_2O_5	-	-	0.01	0.01	0.02	0.01	0.02
Total	-	-	99.11	99.29	99.80	99.93	99.37
Mg#			14	14	8	18	19
Trace elements by XRF (ppm)							
Ba	-	-	481	164	95	387	324
Ni	-	-	3	n.d.	7	4	8
Pb	-	-	10.5	12.0	16.5	13.4	14.4
Th	-	-	19.5	17.7	23.3	13.8	17.6
Rb	-	-	176	169	191	150	181
Sr	-	-	11	12	16	23	22
Y	-	-	38	22	53	35	43
Zr	-	-	271	409	356	246	432
Nb	-	-	15.5	13.7	20.2	11.2	13.4
Cr	-	-	5	3	5	5	5
V	-	-	11	7	10	13	5
Trace elements by ICP-MS (ppm)							
Method	ADAF	AD			ADAF	ADAF	ADAF
Rb	8.30	9.70	-	-	196	152	171
Sr	376	395	-	-	15.0	21.9	21.7
Y	28.0	28.2	-	-	53.0	33.0	46.0
Zr	173	183	-	-	343	236	444
Nb	19.2	19.6	-	-	22.2	12.0	14.9
Cs	0.064	0.092	-	-	1.69	2.77	2.12
Ba	133	134	-	-	104	389	323
La	15.4	15.5	-	-	64.5	43.8	76.0
Ce	37.3	38.0	-	-	125	81.4	134
Pr	5.37	5.44	-	-	14.2	9.47	16.1
Nd	23.8	25.0	-	-	48.0	33.4	56.8
Sm	6.24	5.99	-	-	10.6	7.03	11.6
Eu	2.12	2.00	-	-	0.407	0.549	0.750
Gd	5.89	6.28	-	-	8.14	5.55	8.49
Tb	0.969	0.912	-	-	1.43	0.915	1.34
Dy	4.88	5.16	-	-	8.09	5.07	7.33
Ho	0.988	1.04	-	-	1.68	1.11	1.55
Er	2.64	2.46	-	-	5.18	3.40	4.53
Tm	0.325	0.355	-	-	0.790	0.500	0.690
Yb	1.82	2.07	-	-	4.59	3.07	3.97
Lu	0.280	0.278	-	-	0.764	0.503	0.661
Hf	4.05	4.38	-	-	8.60	5.80	9.20
Ta	1.13	1.19	-	-	1.37	0.745	0.918
Pb	2.55	1.48	-	-	24.1	19.3	19.6
Th	1.35	1.23	-	-	20.6	13.2	18.0
U	0.411	0.382	-	-	2.87	2.74	2.57

n.d.: not detected

Table 4 (continued)

Formation	Johana	Johana	Johana	Johana	Johana	Johana	Johana
Sample	NT49	NT63a	NT63c	NT65	NT66	NT67	NT71
Type	Jh-Pyr	Jh-Pyr	Jh-Pyr	Jh-Pyr	Jh-Pyr	Jh-Pyr	Jh-Pyr
Rock type	welded tuff	welded tuff	welded tuff	welded tuff	welded tuff	welded tuff	welded tuff
Major elements by XRF (wt.%)							
SiO_2	77.65	79.20	79.51	79.32	75.77	76.56	78.45
TiO_2	0.12	0.14	0.14	0.15	0.19	0.18	0.07
Al_2O_3	14.11	11.75	11.34	10.28	13.53	12.78	11.43
FeO*	1.75	1.75	1.78	2.34	1.96	1.65	1.36
MnO	0.02	0.003	0.02	0.01	0.01	0.01	0.004
MgO	0.19	0.10	0.05	n.d.	0.14	0.18	0.04
CaO	0.31	0.12	0.12	0.05	0.10	0.11	0.05
Na_2O	1.86	2.70	2.76	2.31	3.13	2.50	3.44
K_2O	4.19	4.71	4.80	5.49	5.09	5.46	4.82
P_2O_5	0.01	0.01	0.01	0.02	0.02	0.02	0.01
Total	100.21	100.48	100.52	99.97	99.93	99.45	99.68
Mg#	16	9	4		11	16	5
Trace elements by XRF (ppm)							
Ba	345	133	159	161	323	237	56
Ni	10	5	2	4	4	7	11
Pb	42.2	17.2	14.6	20.1	21.5	17.2	15.5
Th	15.2	16.8	14.7	13.2	18.9	17.4	20.9
Rb	117	153	142	176	190	186	202
Sr	46	15	22	11	23	17	7
Y	64	32	25	44	51	51	57
Zr	266	393	370	336	424	426	266
Nb	13.7	13.3	11.8	12.4	17.6	15.6	16.5
Cr	5	3	3	7	5	3	3
V	12	3	8	9	4	8	4
Trace elements by ICP-MS (ppm)							
Method	AD		AD	AD	AD		
Rb	116	-	149	180	195	-	-
Sr	41.6	-	20.4	9.0	20.4	-	-
Y	63.8	-	23.0	42.8	51.1	-	-
Zr	192	-	136	179	286	-	-
Nb	12.6	-	12.4	10.8	16.7	-	-
Cs	2.38	-	1.60	2.26	2.30	-	-
Ba	331	-	160	154	312	-	-
La	42.6	-	54.3	51.0	61.5	-	-
Ce	73.9	-	104	95.4	118	-	-
Pr	11.2	-	12.0	11.1	13.4	-	-
Nd	39.2	-	41.8	38.9	47.7	-	-
Sm	8.47	-	7.26	7.35	9.25	-	-
Eu	1.03	-	0.322	0.481	0.533	-	-
Gd	9.14	-	5.75	6.85	8.71	-	-
Tb	1.59	-	0.806	0.977	1.32	-	-
Dy	9.38	-	4.35	6.01	7.71	-	-
Ho	2.03	-	0.840	1.27	1.73	-	-
Er	6.03	-	2.45	3.51	4.88	-	-
Tm	0.905	-	0.295	0.515	0.733	-	-
Yb	5.18	-	1.72	3.29	4.41	-	-
Lu	0.800	-	0.253	0.477	0.652	-	-
Hf	5.22	-	3.49	4.73	8.11	-	-
Ta	0.885	-	0.839	0.757	1.17	-	-
Pb	42.1	-	12.7	21.2	23.0	-	-
Th	14.4	-	14.1	12.6	18.5	-	-
U	2.55	-	1.49	2.10	2.73	-	-

n.d.: not detected

Table 4 (continued)

Formation	Johana	Iwaine	Iwaine	Iwaine	Iwaine	Iwaine	Iwaine
Sample	NT74	NT48b	NT51	NT69	NT26	NT03	NT20
Type	Jh-Pyr	Iw-OlPx	Iw-OlPx	Iw-OlPx	Iw-Amp	Iw-Amp	Iw-Amp
Rock type	welded tuff	lava	lava	lava	lava	lava	lava
Major elements by XRF (wt.%)							
SiO_2	75.83	56.78	55.63	55.89	56.77	56.92	58.26
TiO_2	0.19	1.05	1.03	1.02	0.93	1.10	1.05
Al_2O_3	12.67	15.87	16.82	14.43	16.23	15.78	16.29
FeO*	1.89	8.33	8.05	7.32	7.12	7.24	6.78
MnO	0.07	0.14	0.21	0.13	0.17	0.16	0.09
MgO	0.03	5.66	6.04	7.69	3.91	4.15	2.94
CaO	0.53	8.01	8.04	8.19	6.78	6.85	6.52
Na_2O	4.46	3.01	3.47	2.61	3.42	3.02	3.08
K_2O	3.61	0.90	1.02	1.05	1.75	2.73	2.92
P_2O_5	0.02	0.19	0.19	0.20	0.18	0.35	0.34
Total	99.28	99.94	100.49	98.53	97.27	98.29	98.27
Mg#	3	55	57	65	49	51	44
Trace elements by XRF (ppm)							
Ba	326	4	6	11	7	7	7
Ni	8	32	27	131	34	55	51
Pb	21.4	5.0	5.6	4.6	6.5	8.2	9.8
Th	17.5	2.0	2.6	1.5	5.1	7.2	6.8
Rb	198	17	19	26	36	33	37
Sr	39	615	634	476	791	2355	2311
Y	43	22	22	21	24	21	21
Zr	419	107	106	118	147	173	175
Nb	12.5	4.4	5.7	11.4	6.9	7.4	7.5
Cr	4	152	143	367	81	82	72
V	4	215	222	172	160	174	160
Trace elements by ICP-MS (ppm)							
Method			AD	AD		AD	
Rb	-	-	20.1	29.1	-	38.6	-
Sr	-	-	610	468	-	2571	-
Y	-	-	22.5	20.7	-	21.5	-
Zr	-	-	108	126	-	197	-
Nb	-	-	4.4	12.3	-	6.9	-
Cs	-	-	0.416	0.338	-	0.280	-
Ba	-	-	401	370	-	1181	-
La	-	-	11.1	18.3	-	44.2	-
Ce	-	-	25.3	39.2	-	93.0	-
Pr	-	-	3.49	4.84	-	11.3	-
Nd	-	-	15.0	18.7	-	41.6	-
Sm	-	-	3.60	3.95	-	6.75	-
Eu	-	-	1.12	1.22	-	2.00	-
Gd	-	-	3.68	3.55	-	5.32	-
Tb	-	-	0.567	0.559	-	0.658	-
Dy	-	-	3.46	3.19	-	3.74	-
Ho	-	-	0.768	0.704	-	0.768	-
Er	-	-	2.22	1.78	-	2.16	-
Tm	-	-	0.331	0.275	-	0.285	-
Yb	-	-	2.04	1.60	-	1.84	-
Lu	-	-	0.302	0.261	-	0.287	-
Hf	-	-	2.62	2.99	-	5.15	-
Ta	-	-	0.251	0.743	-	0.345	-
Pb	-	-	4.98	6.04	-	12.5	-
Th	-	-	1.92	3.06	-	8.36	-
U	-	-	0.472	0.561	-	1.53	-

n.d.: not detected

Table 4 (continued)

Formation	Iwaine	Iwaine	Iwaine	Iwaine	Iwaine	Iwaine	Iwaine
Sample	NT21	NT22	NT23	NT24	NT25	NT73	NT28
Type	Iw-Amp	Iw-Amp	Iw-Amp	Iw-Amp	Iw-Amp	Iw-Amp	Iw-Amp
Rock type	lava	lava	lava	lava	lava	lava	pumice tuff
Major elements by XRF (wt.%)							
SiO_2	54.42	56.03	57.38	55.97	56.34	57.90	59.35
TiO_2	1.14	1.09	1.05	1.11	1.07	1.11	1.03
Al_2O_3	16.83	16.34	15.86	16.52	15.93	15.34	17.90
FeO*	7.09	6.90	6.47	6.94	6.84	6.22	7.12
MnO	0.12	0.12	0.15	0.19	0.19	0.14	0.13
MgO	4.32	4.07	4.16	4.39	3.72	3.64	2.83
CaO	6.81	6.72	6.30	7.05	7.02	6.74	4.94
Na_2O	3.37	3.19	3.14	3.12	3.22	2.81	4.15
K_2O	2.93	2.96	3.08	2.78	2.72	2.15	1.91
P_2O_5	0.35	0.35	0.32	0.34	0.34	0.43	0.20
Total	97.38	97.76	97.91	98.41	97.37	96.48	99.55
Mg#	52	51	53	53	49	51	41
Trace elements by XRF (ppm)							
Ba	8	7	10	7	7	7	9
Ni	48	48	45	50	50	45	1
Pb	5.7	7.0	7.5	7.6	7.9	7.9	6.5
Th	7.1	10.8	8.3	9.4	9.5	7.7	6.2
Rb	37	44	51	33	36	30	55
Sr	2301	2244	2278	2372	2424	2388	438
Y	24	21	25	22	22	21	24
Zr	183	175	180	180	175	165	162
Nb	7.8	6.8	9.7	6.7	6.6	6.7	8.9
Cr	80	80	80	77	77	76	18
V	165	165	134	191	177	173	140
Trace elements by ICP-MS (ppm)							
Method		AD			AD	AD	
Rb	-	40.6	-	-	41.3	38.3	-
Sr	-	2256	-	-	2579	2893	-
Y	-	21.9	-	-	21.1	22.1	-
Zr	-	175	-	-	188	204	-
Nb	-	6.3	-	-	7.0	7.0	-
Cs	-	0.398	-	-	0.458	0.523	-
Ba	-	1117	-	-	1136	1230	-
La	-	38.4	-	-	44.2	45.7	-
Ce	-	80.3	-	-	91.8	96.0	-
Pr	-	10.0	-	-	11.2	11.9	-
Nd	-	37.4	-	-	41.0	41.8	-
Sm	-	6.24	-	-	6.73	6.58	-
Eu	-	1.79	-	-	1.93	2.13	-
Gd	-	4.89	-	-	5.03	4.68	-
Tb	-	0.659	-	-	0.646	0.623	-
Dy	-	3.50	-	-	3.61	3.52	-
Ho	-	0.716	-	-	0.745	0.739	-
Er	-	2.04	-	-	2.01	1.94	-
Tm	-	0.280	-	-	0.292	0.264	-
Yb	-	1.68	-	-	1.81	1.72	-
Lu	-	0.273	-	-	0.269	0.293	-
Hf	-	4.70	-	-	5.05	5.48	-
Ta	-	0.295	-	-	0.357	0.390	-
Pb	-	12.6	-	-	12.5	12.4	-
Th	-	7.81	-	-	10.2	8.21	-
U	-	1.32	-	-	2.13	1.45	-

n.d.: not detected

Table 4 (continued)

Formation	Iwaine	Iwaine	Iwaine	Iwaine	Iwaine	Iwaine	Iwaine
Sample	NT33b	NT34	NT35a	NT35b	NT36	NT10	NT11
Type	Iw-Amp	Iw-Amp	Iw-Amp	Iw-Amp	Iw-Amp	Iw-Px	Iw-Px
Rock type	pumice tuff	pumice tuff	pumice tuff	pumice tuff	pumice tuff	lava	lava
Major elements by XRF (wt.%)							
SiO_2	54.63	56.40	54.29	58.48	58.57	54.97	54.65
TiO_2	1.05	1.50	1.31	1.14	0.99	0.93	0.93
Al_2O_3	20.31	15.46	20.32	16.48	16.84	18.80	18.25
FeO*	6.15	7.16	6.61	6.64	6.10	7.57	8.33
MnO	0.14	0.11	0.16	0.11	0.09	0.21	0.13
MgO	2.18	4.54	2.70	4.40	3.55	3.15	3.31
CaO	9.68	7.21	6.23	6.67	6.41	8.94	8.35
Na_2O	4.50	2.22	3.42	2.43	2.64	2.82	2.84
K_2O	2.52	3.98	3.46	1.96	2.57	1.39	1.35
P_2O_5	0.25	0.57	0.28	0.30	0.29	0.14	0.16
Total	101.40	99.14	98.78	98.62	98.03	98.90	98.30
Mg#	39	53	42	54	51	43	41
Trace elements by XRF (ppm)							
Ba	9	10	9	6	8	6	6
Ni	11	48	23	11	21	8	5
Pb	6.8	19.3	8.6	7.4	10.2	3.7	3.8
Th	4.2	11.1	6.8	5.0	8.7	4.5	3.3
Rb	61	60	89	46	48	40	32
Sr	593	2222	875	1091	950	437	431
Y	21	29	30	25	21	22	22
Zr	188	307	206	166	205	117	122
Nb	8.7	10.0	8.5	6.5	7.7	6.0	6.4
Cr	79	104	126	36	51	35	19
V	188	209	235	199	142	233	226
Trace elements by ICP-MS (ppm)							
Method		AD	AD			AD	AD
Rb	-	72.9	97.7	-	-	37.1	33.3
Sr	-	2442	846	-	-	407	422
Y	-	29.4	29.5	-	-	22.0	23.6
Zr	-	399	223	-	-	119	129
Nb	-	9.9	7.9	-	-	5.2	5.7
Cs	-	0.289	1.04	-	-	0.895	0.485
Ba	-	1631	1036	-	-	430	437
La	-	82.4	44.5	-	-	19.9	21.0
Ce	-	171	78.8	-	-	40.2	43.5
Pr	-	21.8	11.9	-	-	4.92	5.43
Nd	-	83.4	44.3	-	-	19.2	20.3
Sm	-	14.0	8.09	-	-	3.94	4.09
Eu	-	3.65	2.20	-	-	1.18	1.26
Gd	-	9.46	6.77	-	-	3.85	3.94
Tb	-	1.06	0.955	-	-	0.581	0.601
Dy	-	5.03	5.22	-	-	3.35	3.52
Ho	-	1.01	1.09	-	-	0.742	0.785
Er	-	2.66	2.95	-	-	2.21	2.07
Tm	-	0.370	0.421	-	-	0.319	0.299
Yb	-	2.12	2.64	-	-	2.01	1.84
Lu	-	0.334	0.363	-	-	0.293	0.296
Hf	-	9.46	5.25	-	-	2.77	2.99
Ta	-	0.538	0.435	-	-	0.195	0.263
Pb	-	28.9	11.6	-	-	6.24	7.46
Th	-	18.1	7.77	-	-	3.29	3.55
U	-	3.13	1.42	-	-	0.322	0.426

n.d.: not detected

Table 4 (continued)

Formation	Iwaine	Iwaine	Iwaine	Iwaine	Iwaine	Iozen	Iozen
Sample	NT12	NT13	NT62	NT52	NT68	NT04	NT17
Type	Iw-Px	Iw-Px	Iw-Px	Iw-Px	Iw-Px	Io-Aph	Io-Aph
Rock type	lava	lava	lava	lava	lava	Lava	Lava
Major elements by XRF (wt.%)							
SiO_2	55.04	53.24	57.72	54.47	54.63	75.00	75.99
TiO_2	0.93	0.92	1.15	1.58	1.63	0.16	0.15
Al_2O_3	18.32	17.49	19.94	15.73	16.36	13.08	13.63
FeO*	8.00	9.35	5.74	11.36	10.66	2.09	1.02
MnO	0.13	0.16	0.11	0.30	0.20	0.03	0.01
MgO	3.19	5.01	1.44	4.36	4.11	0.23	0.24
CaO	8.45	8.71	8.12	7.42	8.22	1.19	0.71
Na_2O	2.81	2.54	3.19	2.88	2.62	3.67	2.58
K_2O	1.35	0.96	1.68	1.62	0.77	3.73	3.71
P_2O_5	0.16	0.15	0.22	0.21	0.21	0.01	0.02
Total	98.38	98.53	99.30	99.93	99.39	99.18	98.06
Mg#	42	49	31	41	41	16	30
Trace elements by XRF (ppm)							
Ba	6	6	8	7	6	833	1075
Ni	7	11	5	5	n.d.	4	11
Pb	4.2	3.2	6.2	4.6	3.8	11.9	16.9
Th	3.6	3.2	4.6	2.9	2.4	11.9	13.7
Rb	31	13	46	51	10	115	127
Sr	439	432	474	419	464	140	102
Y	27	30	23	25	26	21	26
Zr	120	119	130	114	119	168	159
Nb	5.7	6.1	8.0	7.0	6.4	8.3	8.9
Cr	18	49	22	11	7	4	4
V	219	227	227	404	414	9	11
Trace elements by ICP-MS (ppm)							
Method	AD		AD	AD	AD	ADAF	ADAF
Rb	34.1	-	48.3	54.4	9.76	114	124
Sr	423	-	440	393	460	132	94.6
Y	26.9	-	22.9	23.2	26.2	22.0	25.0
Zr	126	-	135	113	126	167	153
Nb	5.7	-	6.7	6.1	6.6	9.1	9.1
Cs	0.704	-	0.640	1.35	0.251	2.38	3.42
Ba	439	-	375	321	361	830	1069
La	24.5	-	17.9	15.7	16.6	35.0	42.3
Ce	42.8	-	38.1	34.3	36.2	59.1	60.4
Pr	5.96	-	4.85	4.37	4.83	6.77	8.03
Nd	23.0	-	19.2	17.7	19.1	22.2	26.1
Sm	4.60	-	4.11	4.14	4.22	4.17	5.13
Eu	1.43	-	1.28	1.26	1.40	0.877	1.08
Gd	4.46	-	4.28	4.27	4.40	3.39	3.91
Tb	0.686	-	0.631	0.659	0.677	0.555	0.638
Dy	3.99	-	3.74	3.98	4.17	3.06	3.52
Ho	0.854	-	0.782	0.860	0.870	0.681	0.776
Er	2.26	-	2.11	2.33	2.41	2.16	2.49
Tm	0.363	-	0.299	0.352	0.355	0.320	0.370
Yb	2.07	-	1.81	2.16	2.04	2.07	2.30
Lu	0.335	-	0.254	0.320	0.339	0.355	0.402
Hf	2.96	-	3.15	2.81	3.20	4.30	4.10
Ta	0.269	-	0.385	0.357	0.403	0.635	0.662
Pb	7.31	-	8.40	6.17	6.57	18.4	20.8
Th	3.44	-	4.36	3.57	3.80	13.6	11.6
U	0.469	-	0.806	0.577	0.649	1.97	2.28

n.d.: not detected

Table 4 (continued)

Formation	Iozen	Iozen	Iozen	Iozen	Iozen	Iozen	Iozen
Sample	NT18	NT41	NT43	NT53	NT55	NT56	NT57
Type	Io-Aph	Io-Aph	Io-Aph	Io-Aph	Io-Aph	Io-Aph	Io-Aph
Rock type	Lava	lava	lava	lava	lava	lava	lava
Major elements by XRF (wt.%)							
SiO_2	75.46	70.64	70.97	75.58	66.82	74.51	75.76
TiO_2	0.16	0.48	0.46	0.17	0.63	0.18	0.15
Al_2O_3	13.48	15.26	15.15	13.65	15.34	14.00	13.16
FeO*	1.74	3.15	3.21	1.64	3.99	1.80	1.40
MnO	0.02	0.03	0.03	0.02	0.10	0.01	0.01
MgO	0.16	0.60	0.82	0.51	1.17	0.20	0.14
CaO	0.99	3.11	2.69	1.00	3.60	1.29	0.88
Na_2O	3.50	3.63	3.55	2.68	3.89	3.49	3.20
K_2O	3.81	3.29	3.21	4.05	2.81	3.99	3.97
P_2O_5	0.01	0.10	0.07	0.02	0.14	0.02	0.02
Total	99.31	100.29	100.17	99.31	98.48	99.47	98.68
Mg#	14	25	31	36	34	16	15
Trace elements by XRF (ppm)							
Ba	821	747	756	923	628	829	874
Ni	3	3	n.d.	1	3	2	2
Pb	13.8	13.8	14.5	16.1	12.2	18.6	18.2
Th	12.7	9.3	10.0	13.2	9.7	11.6	13.5
Rb	116	91	93	119	81	119	124
Sr	123	259	240	131	291	151	120
Y	30	23	22	24	37	22	23
Zr	161	178	184	177	210	177	149
Nb	9.5	8.1	8.5	8.2	10.4	9.3	11.0
Cr	7	8	7	2	7	3	3
V	5	60	58	7	48	6	6
Trace elements by ICP-MS (ppm)							
Method	ADAF	AD	AD		AD	AD	AD
Rb	118	92.6	91.2	-	82.9	120	126
Sr	115	241	221	-	266	138	108
Y	30.0	21.5	19.5	-	34.8	18.3	21.0
Zr	161	136	134	-	219	94.6	92.6
Nb	9.3	8.2	8.5	-	10.1	9.0	8.9
Cs	2.23	1.18	1.43	-	2.15	1.47	2.15
Ba	818	722	746	-	579	813	840
La	51.7	30.7	30.7	-	34.4	34.6	57.9
Ce	70.0	55.8	54.9	-	58.9	58.5	61.7
Pr	10.2	6.14	6.26	-	8.51	7.12	12.1
Nd	34.1	21.8	21.5	-	31.4	23.8	38.9
Sm	6.79	3.70	3.66	-	6.49	4.10	6.20
Eu	1.30	0.929	0.893	-	1.42	0.814	1.10
Gd	4.95	3.49	3.39	-	6.17	3.28	4.62
Tb	0.800	0.514	0.473	-	0.931	0.483	0.654
Dy	4.32	3.23	2.87	-	5.55	2.83	3.57
Ho	0.933	0.701	0.658	-	1.25	0.614	0.704
Er	2.90	2.04	1.92	-	3.45	1.76	1.94
Tm	0.450	0.313	0.292	-	0.524	0.281	0.294
Yb	2.55	1.96	1.88	-	3.37	1.91	1.95
Lu	0.433	0.314	0.295	-	0.534	0.285	0.299
Hf	4.30	3.55	3.53	-	5.27	2.88	2.65
Ta	0.689	0.594	0.545	-	0.637	0.696	0.668
Pb	16.5	13.4	14.6	-	12.8	16.4	16.4
Th	13.3	9.89	9.80	-	8.57	11.6	12.2
U	1.88	1.66	1.59	-	1.68	1.46	1.72

n.d.: not detected

Table 4 (continued)

Formation	Iozen	Iozen
Sample	NT59	NT60
Type	Io-Aph	Io-Aph
Rock type	lava	lava
Major elements by XRF (wt.%)		
SiO_2	78.31	71.74
TiO_2	0.16	0.45
Al_2O_3	12.42	14.63
FeO*	1.14	2.53
MnO	0.02	0.03
MgO	0.13	0.29
CaO	1.62	3.17
Na_2O	3.08	3.57
K_2O	3.26	2.97
P_2O_5	0.02	0.09
Total	100.14	99.48
Mg#	17	17
Trace elements by XRF (ppm)		
Ba	876	714
Ni	n.d.	n.d.
Pb	13.7	14.0
Th	12.9	9.5
Rb	98	84
Sr	281	259
Y	20	20
Zr	147	171
Nb	8.5	8.2
Cr	3	8
V	7	53
Trace elements by ICP-MS (ppm)		
Method		AD
Rb	-	85.6
Sr	-	243
Y	-	18.9
Zr	-	131
Nb	-	7.9
Cs	-	1.42
Ba	-	714
La	-	28.5
Ce	-	53.1
Pr	-	5.74
Nd	-	19.9
Sm	-	3.48
Eu	-	0.868
Gd	-	3.23
Tb	-	0.498
Dy	-	2.88
Ho	-	0.642
Er	-	1.86
Tm	-	0.280
Yb	-	1.77
Lu	-	0.269
Hf	-	3.41
Ta	-	0.522
Pb	-	12.5
Th	-	9.14
U	-	1.62

n.d.: not detected

Table 5 Results of whole-rock Sr–Nd isotope.

Formation	Sample	Rock type	Age (Ma)	$^{87}Sr/^{86}Sr$	Error (2SE)	Rb/Sr	$^{87}Rb/^{86}Sr$	SrI	$^{143}Nd/^{144}Nd$	Error (2SE)	Sm/Nd	$^{147}Sm/^{144}Nd$	NdI
Johana	NT07	Welded tuff	22.8	0.720885	0.000013	13.03	37.76	0.70855	0.512207	0.000013	0.220	0.133	0.51219
Johana	NT09	Welded tuff	22.8	0.715993	0.000014	6.93	20.06	0.70944	0.512048	0.000012	0.210	0.127	0.51203
Johana	NT16	Welded tuff	22.8	0.716441	0.000014	7.89	22.86	0.70897	0.512260	0.000017	0.203	0.123	0.51224
Johana	NT49	Welded tuff	22.8	0.711244	0.000014	2.79	8.08	0.70860	0.512092	0.000018	0.216	0.131	0.51207
Johana	NT63c	Welded tuff	22.8	0.714648	0.000014	7.34	21.24	0.70771	0.512244	0.000014	0.174	0.105	0.51223
Johana	NT66	Welded tuff	22.8	0.716730	0.000014	9.55	27.67	0.70769	0.512252	0.000013	0.194	0.117	0.51223
Iwaine	NT51	lava	17.1	0.704836	0.000014	0.03	0.10	0.70481	0.512810	0.000014	0.241	0.145	0.51279
Iwaine	NT03	lava	17.1	0.704168	0.000014	0.02	0.04	0.70416	0.512658	0.000014	0.162	0.098	0.51265
Iwaine	NT22	lava	17.1	0.704334	0.000014	0.02	0.05	0.70432	0.512665	0.000014	0.167	0.101	0.51265
Iwaine	NT25	lava	17.1	0.704071	0.000014	0.02	0.05	0.70406	0.512630	0.000022	0.164	0.099	0.51262
Iwaine	NT34	Welded tuff	17.1	0.703755	0.000014	0.03	0.09	0.70373	0.512852	0.000021	0.167	0.101	0.51284
Iwaine	NT52	lava	17.1	0.707228	0.000014	0.14	0.40	0.70713	0.512425	0.000016	0.234	0.141	0.51241
Iwaine	NT62	lava	17.1	0.707651	0.000014	0.11	0.32	0.70757	0.512381	0.000020	0.214	0.129	0.51237
Iozen	NT41	lava	16.8	0.708750	0.000014	0.38	1.11	0.70848	0.512292	0.000013	0.170	0.103	0.51228
Iozen	NT43	lava	16.8	0.708761	0.000014	0.41	1.19	0.70847	0.512298	0.000014	0.170	0.103	0.51229
Iozen	NT55	lava	16.8	0.708420	0.000013	0.31	0.90	0.70820	0.512342	0.000014	0.206	0.125	0.51233
Iozen	NT56	lava	16.8	0.708887	0.000014	0.87	2.52	0.70828	0.512290	0.000014	0.172	0.104	0.51228
Iozen	NT57	lava	16.8	0.709084	0.000014	1.16	3.37	0.70827	0.512368	0.000014	0.160	0.096	0.51236
Iozen	NT60	lava	16.8	0.708701	0.000014	0.35	1.02	0.70846	0.512218	0.000014	0.175	0.106	0.51221

8. Discussion

In this chapter, temporal evolution and genesis of Cenozoic magmatism related to the Japan Sea opening in the Nanto area, the central part of the Toyama basin, are discussed. Whole-rock geochemistry and the petrogenesis further give implications for geotectonic history of the Japan Sea opening and evolution of arc crust during the back-arc spreading.

The Toyama basin was formed by deposition of terrestrial to shallow-water strata and rhyolitic pyroclastic flows at about 23 Ma, followed by andesitic volcanism (onshore to shallow water) at 18–17 Ma and dacite to rhyolitic volcanism (onshore to shallow water) at 17–16 Ma. The sedimentary environment is considered to have changed to deep water by around 15 Ma.

Among the strata that have been geologically examined above, the volcanic rocks collected from the Johana Iwaine and Iozen Formations in the Nanto area, where volcanic rocks are the most schematically exposed, were examined for their petrogenesis. Based on petrography, the volcanic rocks of each formation are classified into one type for the Johana Formation (rhyolitic tuff, Jh-Pyr), three types for the Iwaine Formation (olivine two-pyroxene andesite, Iw-OlPx; amphibole andesite, Iw-Amp; and two-pyroxene andesite, Iw-Px) and one type for the Iozen Formation (aphyric rhyolite, Io-Aph). Based on the major and trace element compositions, Sr–Nd isotopes, and zircon trace element compositions of the Jh-Pyr and Io-Aph Formations, Jh-Pyr and Io-Aph have different K_2O contents, but similar trace element trends. The involvement of crustal melting to produce this rhyolitic magma was inferred from enriched light rare

earth elements (LREE), Nb–Ta depletion, steeply positive trend in La–La/Yb diagram, low Cr and Ni concentrations, enriched Sr–Nd isotope, and enriched zircon trace element composition. The Iw-OlPx has a maximum Mg# of 65, suggesting that it was formed by the partial melting of mantle hydrous with slab-derived fluids. Iw-Amp is similar to the chemical composition of the LSA of Martin et al. (2005) and was formed by partial melting of mantle metasomatized by adakite melt. The Iw-Px is thought to be derived from non-alkaline basalts based on the trend of compositional variation diagrams, however it is thought to assimilate the crust because of its highly enriched Sr–Nd isotopic composition. Since the old, cold Pacific plate was subducted into the southwest Japan arc during the Japan Sea opening, phenomena that keep the mantle wedge hot, such as upwelling of the asthenospheric mantle into the mantle wedge, is required.

Because rhyolitic magmatism of the Johana and Iozen Formations accompanies basaltic to andesitic volcanism, the basaltic to andesitic volcanism is considered to have played a role as heat source. Jh-Pyr and Io-Aph have more enriched whole-rock Sr–Nd isotope and zircon Hf isotope than the Hida belt, suggesting that old continental crust such as the North and South China Craton involved the genesis of the rhyolites. Trace element compositions of rhyolites from the Johana and Iozen Formations are similar to those of the upper crust. Other rhyolites distributed in the rift zone in the subduction zone show similar trends. This indicates that siliciclastic igneous activity in the subduction zone associated with rifting in the subduction zone, such as back arc spreading, contributes to crustal recycling in the arc crust.

8.1. Development history of the Toyama basin

8.1.1. Depositional environment of the Toyama basin

The lower and upper parts of the Johana Formation are composed mainly of FD and PCF, respectively (**Figure 4.3**). Accordingly, it is considered that the Johana Formation was deposited on land. Since there are several flow units of PCF, eruption occurred several times to deposit it. Sudo (1979a, b) discussed that the Johana Formation was deposited in fluvial fan or fan delta. Nevertheless, shallow marine deposit was not found. Hence, it is difficult to judge whether the Johana Formation was deposited in fan delta or not.

The lower and upper parts of Nirehara Formation are composed mainly of FD and SWD, respectively (**Figure 4.3**). Especially, conglomerate was dominantly observed in the lower part. Therefore, the lower and upper parts of the Nirehara Formation are considered to have been deposited in braided river and shallow marine, respectively. This stratigraphy suggests transgression and/or fan delta system. This idea is not consistent with Ogasawara et al. (1990), Fujii et al. (1992a), and Kashiwagi (2012); they concluded that the Nirehara Formation was deposited only in river. Tsuda (1953, 1955), Nakajima et al. (2019) also considered that the Nirehara Formation was deposited in fan delta system. However, Nakajima et al. (2019) suggested also one more possibility that the Nirehara Formation was deposited in lake.

The Iwaine Formation can be subdivided into four units, based on lithostratigraphy (**Figure 4.6**). This result is consistent with Yamada and Yamada (2018) who examined lithostratigraphy of the Iwaine Formation in the Yatsuo area. LF containing olivine or amphibole phenocrysts occupies unit 1 of the Iwaine Formation with PCF containing amphibole crystals (**Figure 4.4** and **4.6**). These lithological features suggest that the unit 1 was formed in subaerial environment.

The unit 2 is composed of DF and FD, meanwhile the unit 3 is composed of PCF (**Figure 4.6**). These features also suggest that the unit 2 and 3 were deposited on land. The unit 2 is considered to have been deposited in braided river system. There is a possibility that the unit 3 was deposited to fill valleys. The unit 4 is composed of irregular alternation of LF, ISH, RSH, PR, PCF, TPH, DF, FD and SWD (**Figure 4.4 and 4.6**). These lithological features can be interpreted as eruption and eruptive hiatus. While eruptions occurred, LF, ISH, RSH, PR, PCF and TPH were emplaced or deposited. On the other hand, DF and FD were deposited while eruptions did not occur. These lithological features suggest that the unit 4 of the Iwaine Formation was deposited in shallow marine and on land. Inner bay system developed in the latest period of the formation of the Iwaine Formation.

Massive lava flows (LF) of the Iozen Formation are distributed in the proximal area of Mt. Iozen, forming lava domes, whereas block lava flows (LF) are observed in the distal area of Mt. Iozen (**Figure 4.4**). Although PCF, TPH and FD are intercalated in LF around the Mt. Iozen area, PCF, TPH and FD are dominantly distributed in the Yatsuo area. These lithological characteristics indicate that there were volcanic edifices around Mt. Iozen. Although Nakama et al. (2010) considered that the Iozen Formation was formed in marine environment, marine deposit was not observed in this study. Hence, the Iozen Formation is considered to have been formed in subaerial environment.

The Kurosedani Formation is composed of irregularly alternating beds of DF, FD, IBD, SWD (**Figure 4.3**). Nevertheless, FD with DF, and SWD with IBD are abundant in the lower and upper part of the Kurosedani Formation, suggesting upward finning. Based on these lithological characteristics, it is considered that the Kurosedani Formation was deposited mainly in delta environment. Tsuda (1953,

1955) also considered that the Kurosedani Formation was deposited mainly in delta. Yamanoi and Tsuda (1986) examined microfossils and concluded the Kurosedani Formation was deposited in an environment like mangrove. On the other hand, it is thought that the upper part of the Kurosedani Formation was deposited in inner bay and shelf.

The Fukuhira Formation is composed mainly of LF, ISH, RSH, PR, DK, PCF, TPH, SWD (**Figure 4.3**). SWD is intercalated in andesitic to dacitic volcanic and pyroclastic rocks (LF, ISH, RSH, PR, DK, PCF, TPH). Kaneko (2001) reported molluscan fossils living in shallow marine from clastic rocks in the Fukuhira Formation. These lithological features and reported fossils suggest that the Fukuhira Formation was deposited in an intermediate environment between shallow marine and land. Kaneko (2001) also concluded that the Fukuhira Formation was deposited in both of marine and land environments.

The Sunagozaka Formation is composed mainly of SWD showing finning-upward cycle and IBD (**Figure 4.4**). These lithological characteristics suggest that the Sunagozaka Formation was deposited in tide-dominated system and inner bay system.

The unit 1 of the Doyama Formation is composed of PCF, TPH and FD (**Figure 4.4**). This indicates that the unit 1 was deposited on land. The unit 2 and 3 of the Doyama Formation are composed of SWD (**Figure 4.4**). Alternating beds of sandstone and mudstone is abundant in the unit 2, whereas, cross-bedded sandstone is dominant in the unit 3. Some beds of TPH are intercalated in some stratigraphic horizons. Therefore, the unit 2 and 3 are considered to have been deposited in shallow marine. Based on the lithological characteristics of the unit 2 and 3, It is considered that the unit 2 and 3 was deposited in tide-dominated and wave-dominated systems. Lithological change

between the Sunagozaka Formation and the unit 1 indicates regression, whereas the lithological change of the unit 1, 2 and 3 indicates transgression.

The Higashibessho and Omine Formations are composed mainly of DWD with TDD (**Figure 4.3** and **4.4**). These lithological features suggest that the Higashibessho and Omine Formations were deposited in deep marine (probably on shelf).

8.1.2.Chrono-stratigraphy in the Nanto area

In this study, three new zircon ^{238}U–^{206}Pb weighted mean ages were obtained from the Johana (22.8 ± 0.2 Ma; n = 32; MSWD = 1.4), Iwaine (17.1 ± 0.4 Ma; n = 35; MSWD = 6.0), and Iozen Formations (16.8 ± 0.2 Ma; n = 45; MSWD = 3.4) (**Figure 7.1**). These zircon U–Pb ages and previous studies on radiometric ages, biostratigraphy, and magnetostratigraphy provide reliable formation ages of the Tori, Iwaine and Iozen Formations (**Figure 8.1**).

27.2–19.5 Ma of K–Ar (Ueda and Aoki, 1970), zircon FT (Ganzawa, 1983; Nakajima et al., 1983; Itoh et al., 2001; Kano et al., 2007b) and Rb–Sr (Ishida et al., 1998) ages have been reported from the Johana Formation and the equivalents. The zircon U–Pb age of this study (22.8 ± 0.2 Ma) constraints that the Johana Formation was deposited at ~ 23 Ma. Combination of zircon U–Pb age and reverse polarity (Itoh, 1988) suggests that the Tori Formation was deposited in C6Cn.1r (22.973–22.792 Ma; **Figure 8.1**) (Gradstein et al., 2020).

Obtained the zircon ^{238}U–^{206}Pb weighted mean age from the Iwaine Formation is consistent with 17.6 ± 0.3 Ma of zircon ^{238}U–^{206}Pb weighted mean age from the eastern part of the Toyama basin (Nakajima et al., 2019). Combination of these zircon U–Pb ages and normal polarity recorded in the Iwaine Formation (Itoh and Hayakawa, 1988; Itoh and Watanabe, 2000; Tamaki et al., 2006) suggests that the Iwaine Formation was formed in C5Dn (17.533–17.235 Ma;

Figure 8.1) (Gradstein et al., 2020). This suggests that there is no age gap in the Iwaine Formation between the eastern and central part of the Toyama basin.

Sample NT45 was collected from the same outcrop as FU06 where Ganzawa (1983) reported 16.5 ± 1.4 Ma of a zircon FT age. Since the zircon U–Pb age of this study and the zircon FT age by Ganzawa (1983) are consistent with each other, zircon U–Pb age of this study can be interpreted as reliable eruptive age of the Iozen Formation. Itoh and Hayakawa (1988, 1989), Itoh et al. (2000), Itoh and Watanabe (2000), Iwaki and Itoh (2000), Itoh and Kitada (2003), and Tamaki et al. (2006) reported paleomagnetic data from the Iozen Formation in the eastern and central part of the Toyama basin. Itoh and Watanabe (2000) and Tamaki et al. (2006) found the boundary from normal to reverse polarity from the Iozen Formation in the eastern part of the Toyama basin. Meanwhile, Yanagisawa (1999a) examined diatom biostratigraphy from Neogene sediments conformably covering the Iozen Formation in the Nanto area of the central part of the Toyama basin, suggesting formation of the Iozen Formation terminated by 16.3 Ma. Stratigraphic relationship with the lower Iwaine and upper Kurosedani Formations, zircon U–Pb age of this study, paleomagnetism and biostratigraphy suggest that the Iozen Formation was formed from late part of C5Dn (17.533–17.235 Ma) to early part of C5Cr (17.235–16.721 Ma) (Gradstein et al., 2020). The formative age of the Iozen Formation is probably 17.3–16.8 Ma (**Figure 8.1**).

8.1.3.Depositional age of the Nirehara Formation

5 zircon grains of 11 grains were adopted, and the ^{238}U–^{206}Pb weighted mean age using the zircon grains was calculated to be 21.1 ± 2.2 Ma (Age 1; MSWD = 20.35; probability of fit = 0 %; **Figure 7.2c**). Three grains of a coherent cluster provide 23.6 ± 0.3 Ma of the ^{238}U–

^{206}Pb weighted mean age (Age 2) with MSWD = 0.15 and probability of fit = 0.858 (**Figure 7.2e**). Because Age 1 has too high MSWD and probability of fit = 0%, it is not a geologically significant age. While, Age 2 has low MSWD (0.15) and high probability of fit (85.8%). Hence, Age 2 is considered as a geologically more reliable age rather than Age 1. There is a possibility that rejected two grains show young age due to Pb loss. However, the robust reason cannot be estimated here. Therefore, Age 2 (23.6 ± 0.3 Ma) is adopted as a formation age of welded tuff (090705A) in this study.

As shown in **Figure 5.1b**, dated sample in present study is rhyolitic welded tuff. According to the petrographic characteristics and zircon U–Pb age of present study, the dated gravel in this study is derived probably from the Usunaka Moonstone Rhyolite Member of the Johana Formation or related rhyolites in the Hokuriku region. These rhyolites are composed of mainly of rhyolitic welded tuff containing abundant quartz and alkali felspar (e.g., Sudo, 1979b; Ganzawa, 1983; Ishida et al., 1998; Kano et al., 2007b). K–Ar, zircon FT and zircon U–Pb ages reported from the rhyolitic welded tuff by Uyeda and Aoki (1970), Ganzawa (1983), Nakajima et al. (1983), Itoh et al. (2001), Kano et al. (2007b), Ota et al. (2019), and this study range from 27.2 Ma to 20.0 Ma, however, most of them indicates 23–22 Ma. The weighted mean age and petrography are consistent with those rhyolitic welded tuffs in the Hokuriku region. Moreover, characteristics of 090705A as boulder-sized angular gravel suggest that late Oligocene to early Miocene rhyolites such as the moonstone rhyolites in the Hokuriku region are/were distributed also in or around the Kamiichi area.

As Ota et al. (2018) and Nakajima et al. (2019) reported and discussed depositional age of the Nirehara Formation, some radiogenic and biostratigraphic ages could not constrain the

depositional age. Detrital zircon from sandstone of the Nirehara Formation suggests that the main provenance is the Nohi Rhyolites and the Hida granites (Ota et al., 2018; Nakajima et al., 2019). The ^{238}U–^{206}Pb weighted mean age of present study suggests that the Nirehara Formation in the eastern part of Toyama Prefecture was deposited after Late Oligocene (23.6 Ma).

The Nirehara Formation is unconformably covered by the Iwaine Formation, meanwhile it has been for long time discussed that the stratigraphic relationship with the Johana Formation (Ganzawa, 1983), which can be correlated to the Nirehara distributed in the western part of Toyama Prefecture. The Johana Formation consists of the lower Tori Conglomerate and the upper Usunaka Moonstone Rhyolite members (Sudo, 1979b; Ganzawa, 1983). 25–22 Ma of K–Ar, zircon FT and zircon U–Pb ages have been reported from the Usunaka Moonstone Rhyolite Member (Uyeda and Aoki, 1970; Ganzawa, 1983; Nakajima et al., 1983; Ota et al., 2019; this study). Generally, the Johana Formation is regarded as the stratigraphically lower formation than the Nirehara Formation (Nozawa et al., 1981; Yamashita et al., 1988; Fujii et al., 1992a, b; Yamada and Yamada, 2018). Meanwhile, some researchers considered that they are in the same stratigraphic horizon due to the similar lithology (conglomerate) and geological structures (Ikebe, 1950; Yamasaki and Miyajima, 1970; Ui and Kuroda, 1990; Yamada and Takahashi, 2021; this study). It has to be revealed that the stratigraphic relationship between the Tori and Nirehara formations, based on field geology. However, the depositional age of the Nirehara Formation can be discussed using previous stratigraphic studies and zircon U–Pb age of this study. Considered zircon U–Pb age of present result, the formation ages of the Usunaka Moonstone Rhyolite Member (23–22 Ma; Ota et al., 2019; this study), and the Iwaine Formation (17.5–17.2 Ma; Nakajima

et al., 2019), the depositional age of the Nirehara Formation can be estimated to be 23–19 Ma. Compared to paleomagnetic stratigraphy (Itoh and Hayakawa, 1988, 1989; Itoh et al., 1999; Itoh and Watanabe, 2000; Tamaki et al., 2006), the Nirehara Formation was deposited probably in C6Cn.1r (22.973–22.792 Ma; **Figure 8.1**).

8.1.4. Implications for the development history of the Toyama basin

The depositional environment and geochronology of the Toyama basin were discussed and revealed based on results of facies analysis, zircon U–Pb dating. In this section, the development history of the Toyama basin is discussed.

The formation of the Toyama basin initiated with deposition of the Nanto Group (the Johana and Nirehara Formations), because the Nanto Group is the stratigraphically lowest unit of the Toyama basin (Nakajima et al., 2019; Yamada and Takahashi, 2021; this study), unconformably covering the Paleozoic to Cretaceous basement rocks (the Hida belt, the Tetori Group, and the Futomiyama Group). Since zircon U–Pb age from the Johana Formation shows 22.8 ± 0.2 Ma, the timing of initiation of the formation is thought to be ~ 23 Ma. The Johana Formation and the lower part of the Nirehara Formation were deposited in braided river. Meanwhile, the upper part of the Nirehara Formation was deposited in shallow marine. This suggests transgression.

Information on the formation history of the Toyama basin is lack until the formation of the Iwaine Formation at 17.5 Ma due to regional unconformity between the Nanto Group and the Iwaine Formation. It is considered that this unconformity was formed between 19 Ma and 17.5 Ma, based on formation ages of the Nirehara and Iwaine Formations. This unconformity is found in entire of the Japan arc (Kano et al., 2007a).

After the formation of regional unconformity, the Iwaine Formation was formed in 17.5–17.3 Ma. The deposition and emplacement of the Iwaine Formation occurred mainly in subaerial environment with subaqueous environment. This suggests that uplift took place after the deposition of the Nanto Group. Volcanic edifices were not found from the Iwaine Formation. In addition, the Iwaine Formation and equivalent formations (including the Ganzo Formation) are distributed widely in the Hokuriku region, with huge volumes of andesites (Yamada and Takahashi, 2021; this study). Accordingly, the andesitic volcanism of the Iwaine Formation is considered as “flood andesite”.

Andesitic volcanism was followed by rhyolitic volcanism of the Iozen Formation. In the western part of the Toyama basin, voluminous rhyolitic lavas and pyroclastic flows were deposited and emplaced between 17.3 and 16.8 Ma, forming volcanic edifices in and around Mt. Iozen. This rhyolitic volcanism occurred on land. Matsumoto and Nakanishi (1967) also concluded that the rhyolitic volcanism of the Iozen Formation took place on land.

After formation of the Iozen Formation, the Kurosedani, Sasagawa, Fukuhira, Sunagozaka, Doyama Formations were deposited. The Kurosedani Formation was deposited mainly in delta, suggesting existence of large river. The Sunagozaka and Doyama Formations were deposited mainly in shallow marine. The Fukuhira Formation was deposited and emplaced in intermediate environment between subaerial and subaqueous environments. Pyroclastic rocks in the Doyama Formation might be derived from the rhyolitic volcanism of the Iozen Formation, because the thickness of pyroclastic rocks is very thick (~ 20 m; Inoue et al., 1964). These pyroclastic rocks can be correlated to the Yamadanaka Tuff (16.6 Ma; Nakajima et al., 2019). Assuming that the pyroclastic rocks of the Doyama Formation are derived from the Iozen Formation, there is a possibility that the

rhyolitic volcanism of the Iozen Formation lasted until the Doyama Formation was deposited (16.6 Ma). According to radiogenic ages (Nakajima et al., 2019), biostratigraphy (Yanagisawa, 1999a) and paleomagnetism (Tamaki et al., 2006), the depositional age of the Kurosedani Formation is considered as 16.8–16.6 Ma. Nevertheless, younger zircon U–Pb ages were reported from the contemporaneous formations of the Sasagawa (16.3–16.2 Ma; Itoh et al., 2016; Takeuchi et al., 2017) and Fukuhira Formations (15.9 ± 0.2 Ma; Takeuchi et al., 2017), which is distributed in the eastern part of the Toyama basin. This indicates that the depositional age of these formations becomes younger toward east in the Toyama basin, suggesting the not parallel opening of the Toyama basin and the Toyama trough.

Subsequently, the Higashibessho and Omine Formations were deposited in deep marine environment (probably shore) between 16.6 Ma and 15.3 Ma (Nakajima et al., 2019). The formation of the Toyama basin was terminated by the deposition of the Higashibessho and Omine Formations.

8.2. Petrogenesis of volcanic rocks from the Toyama basin

8.2.1. Petrogenesis of rhyolite from the Johana Formation

Jh-Pyr contains quartz, alkali feldspar and biotite. Fractional crystallization trends in Sr–Ba diagram are consistent with the predominance of alkali feldspar (**Figure 8.2e**). Trend in Nb–Th (**Figure 8.2b**) diagram does not suggest assimilation and magma mixing, and hence chemical variations can be explained by fractionation of phenocrystal minerals (**Figure 8.4**).

Highly-differentiated granitic and rhyolitic magma is thought to be formed by (a) continuous melt extraction from previously generated dikes, (b) crustal host rock melting, or (c) high-degree crystallization of basaltic sills, based on petrological and geodynamic calculations

(Rummel et al., 2020). Jh-Pyr shows enriched LREE, negative Nb and Ta anomalies (**Figure 7.7a**), low Cr and Ni concentrations (**Figure 7.6**), and enriched Sr–Nd isotopic composition (**Figure 7.8a**). These geochemical features suggest that the rhyolites were produced by partial melting of crustal material (e.g., Bickford et al., 2017; Zhu, 2022). Schiano et al. (2010) suggested that combination of REE or incompatible trace elements can distinguish fractional crystallization from partial melting, using H–H/M diagrams. H and M are different incompatible elements satisfying the condition of $(D^M - 1) \approx -1$ and $(D^H - 0.2) \approx 0.2$, where D is bulk solid/melt partition coefficient. Igneous rocks formed by partial melting (or magma mixing) display steep trends in H–H/M diagrams (Schiano et al., 2010). Whereas igneous rocks exhibit flat trends in H–H/M if fractional crystallization was dominant in their origin (Schiano et al., 2010). Trends of Jh-Pyr in La/Yb–La diagram (**Figure 8.2a**) indicate that partial melting was dominant in petrogenesis of the rhyolite. In addition to whole-rock geochemistry, zircon trace element composition (**Figure 7.3e**) also suggests crustal input. What kind of crustal material was melted is discussed later in section 8.3.2.

8.2.2.Petrogenesis of andesites from the Iwaine Formation

The whole-rock Mg# of Iw-OlPx reaches as high as 65 (NT69; **Table 4**). Assuming the Fe/Mg exchange partition coefficient of olivine/melt (0.3; Roeder and Emslie 1970), mantle olivine having Mg/(Mg+Fe) greater than 0.87, and an $Fe^{2+}/(Fe^{2+}+Fe^{3+})$ of 0.9 in the magma, then a mantle-derived andesitic magma should have Mg# greater than 64 (Tatsumi, 2006). Therefore, primary magma of Iw-OlPx is thought to be in equilibrium with the mantle peridotite. High Ni and Cr concentrations (131 and 367 ppm in the maximum, respectively; **Figure 7.6**) support this idea. Tatsumi (2006) and Hanyu et al. (2006) explained petrogenesis of high magnesian andesite

(HMA) from the Setouchi Volcanic Belt resulted from the interaction between slab melt [derived from AOC (altered oceanic crus) and sediments] and the mantle wedge. More enriched Sr–Nd isotope than MORB and AOC (**Figure 7.8a**) indicates that sediment-derived melt involved in the genesis of HMA from the Iwaine Formation. As discussed later, there is a possibility that Iw-Amp accompanied with Iw-OlPx was produced by melting of the mantle wedge metasomatized by slab melt. Nevertheless, Th/Yb and $(La/Sm)_N$ of Iw-OlPx, showing the degree of effect of slab melt (sediment-origin melt) (**Figure 8.2c** and **8.2d**), are not high compared to Iw-Amp and HMA from the Setouchi Volcanic Belt. This suggests that the mantle peridotite was hydrated by slab-derived fluid and melted to generate the HMA magma of Iw-OlPx (**Figure 8.4**). Otherwise, the contribution of slab melt was less than Iw-Amp.

Although petrography and some geochemical signatures (e.g., high Sr content) of Iw-Amp are similar to adakite (Defant and Drummond, 1990), Iw-Amp is plotted outside the field of adakite in Y–Sr/Y diagram (**Figure 7.9a**). Geochemical characteristics (e.g., low-SiO_2, high-MgO, high-K_2O, high-Sr; **Figure 7.9**) of Iw-Amp is similar to low-SiO_2 adakite (LSA) of Martin et al. (2005) rather than adakite of Defant and Drummond (1990). Martin et al. (2005) discussed that LSA magma is generated by partial melting of the mantle wedge metasomatized by slab-derived melt (**Figure 8.4**). High Th/Yb and high $(La/Sm)_N$ of Iw-Amp (**Figure 8.2c** and **8.2d**) suggest that sediment melt derived from the subducting slab involved the origin of Iw-Amp. On the other hand, Ba/Th of Iw-Amp is relatively small (**Figure 8.2d**). These geochemical features suggest that not only AOC but also sediments on the slab strongly contributed slab melt producing Iw-Amp. In SrI–NdI diagram (**Figure 7.8a**), Iw-Amp is plotted near the bulk earth. This suggest that the mantle was more enriched in Sr–Nd isotope than MORB and AOC

due to contamination of slab melt (and/or continental crust). Accordingly, the mantle wedge metasomatized by slab melt including sediment-derived melt was partially melted to produce lw-Amp. Therefore, lw-Amp is not pure adakite derived directly from slab melt (**Figure 8.4**). Adakites and volcanic rocks related to slab melt have been reported also from Oligocene to Miocene volcanic rocks in the eastern Toyama basin and the Noto peninsula (Uematsu et al., 1995; Takahashi and Shuto, 1999; Sato et al., 2013). Accordingly, the mantle wedge beneath the Toyama basin is thought to have been metasomatized intermittently since Oligocene epoch. On the other hand, Nb–Th diagram (**Figure 8.2b**) indicates that fractional crystallization was dominant in the high-Sr andesitic magma much more than crustal assimilation. Moreover, lw-Amp has enough depleted in Sr–Nd isotopes, compared to gneiss of the Hida belt including high Sr rocks such as limestone (**Figure 7.8a**). Therefore, the generation of high-Sr andesite by assimilation of mantle derived magma with the Sr rich crustal material seems to be difficult in this case.

As compared in **Figure 7.7b**, lw-Px (tholeiitic andesite) displays general geochemical features as andesites from subduction zone (e.g., Nb–Ta negative anomaly). Although lw-Px exhibits similar trends to lw-OlPx in many chemical variation diagrams (FeO*, CaO and P_2O_5; **Figure 7.6**), their trends in FeO*/MgO–SiO_2 diagram (**Figure 7.5c**) are clearly different with each other. In FeO*/MgO–SiO_2 (**Figure 7.5c**) and SiO_2–K_2O diagrams (**Figure 7.5b**), it seems that lw-Px was produced from relatively alkali-poor and tholeiitic basalt. Additionally, lw-Px has low Mg#, which cannot be in equilibrium with the mantle (**Table 4**). On the other hand, trace element pattern of lw-Px (**Figure 7.7b**) is coinciding with lw-OlPx, and hence their parental material is thought as similar peridotite. However, Sr–Nd isotope of

Iw-Px with more enriched isotope than the bulk earth is much enriched than that of Iw-OlPx (**Figure 7.8a**). Therefore, the crustal material involved the origin of the basaltic magma producing Iw-Px by, for instance, assimilation and fractional crystallization (AFC). Ishiwatari and Ohama (1997) also considered that the andesitic magma of the Iwaine Formation underwent assimilation of crustal material such as granitoids. From the above discussion, it is considered that mantle peridotite was melted to generate two magmas: HMA (Iw-OlPx) and basaltic magmas (original magma of Iw-Px). The difference in the degree of partial melting might have produced two different magmas, and the basaltic magma assimilated the continental crust to differentiate to form Iw-Px (**Figure 8.4**). Iw-Px shows enriched LILE and REE and has more similarities to continental-arc volcano than island-arc volcano in trace element pattern (**Figure 7.7c**). These geochemical characteristics suggest a possibility that the parental material of Iw-Px was enriched mantle such as continental lithosphere.

8.2.3.Petrogenesis of rhyolite from the Iozen Formation

Io-Aph contains plagioclase, amphibole and pyroxene. Fractional crystallization trend in Sr–Ba diagram is consistent with the observed mineral assemblages: plagioclase, amphibole and pyroxene affect differentiation of Io-Aph (**Figure 8.2f**). Trend of Io-Aph in Nb–Th diagram (**Figure 8.2b**) does not suggest assimilation and magma mixing, and hence chemical variation of Io-Aph also as Jh-Pyr can be explained by fractionation of phenocrysts.

Io-Aph also show enriched LREE, negative Nb–Ta anomalies (**Figure 7.7a**), low Cr–Ni concentrations (**Figure 7.6**) and enriched Sr–Nd isotopic composition (**Figure 7.8a**), suggesting that the rhyolites were produced by partial melting of crustal material. Trends of Io-Aph in La/Yb–La diagram (**Figure 8.2a**) indicate that partial melting was dominant in rhyolitic magma in the Iozen Formation. In

addition to whole-rock geochemistry, zircon trace element composition also suggests crustal input (**Figure 7.3e**). Since Io-Aph was formed just after active andesitic magma (Iwaine Formations), it is considered that the andesitic magmatism played a role as heat source to cause crustal melting. What kind of crustal material was melted is discussed later in section 8.3.2.

8.3. Mantle-crust dynamics during the Japan Sea opening

8.3.1. Temporal change of arc volcanism in the Toyama basin during the Japan Sea opening

Arc magmatism related to the Japan Sea opening in and around the Toyama basin initiated with formation of the Konosuyama Formation at 34 Ma (Yamada and Takahashi, 2021). Uematsu et al. (1995), López and Ishiwatari (2002), and Sato et al. (2013) reported tholeiitic basalt, calc-alkaline basaltic andesite, HMA, adakite from the Konosuyama Formation and concluded that injection of the asthenosphere into the mantle wedge caused basaltic to andesitic volcanism of the Konosuyama Formation. The Goroku Formation composed of dacitic pyroclastic flow deposits was formed at ~25 Ma after formation of the Konosuyama Formation (Yamada and Takahashi, 2021). Nevertheless, the petrogenesis of the dacite from the Goroku Formation has not been revealed by any researchers. Meanwhile, basaltic to dacitic volcanism occurred in Sikhote Alin of Russia during this period (e.g., Martynov and Khanchuk, 2013; Martynov et al., 2017). Martynov and Khanchuk (2013) and Martynov et al. (2017) also considered that the volcanism in Sikhote Alin was caused by injection of hot asthenosphere. Despite, they discussed that the injection of the hot asthenosphere was caused by slab window. Therefore, injection of the hot asthenosphere (more depleted Sr–Nd isotope) into the mantle wedge beneath the margin of the

eastern Asia already initiated in this period (**Figure 8.5a**).

Because the Johana and Nirehara Formations (Nanto Group) and equivalents are the stratigraphically lowest unit in the Toyama basin (Nakajima et al., 2019; Yamada and Takahashi, 2021; this study), the proto-Toyama basin is considered to have been formed at around 23 Ma (stage III) due to initiation of rifting with rhyolitic pyroclastic flows. Especially, these rhyolites are rift-type rhyolite such as the Great Rift Valley (Ishida et al., 1998; Ayalew and Ishiwatari, 2011). Contemporaneous formation of basaltic oceanic crust at ~ 24 Ma resulted in the extension of back arc basin (Kaneoka et al., 1992, 1996). It is considered that the heat flow caused rifting and crustal melting to generate the andesitic and rhyolitic magma of the Johana, Kamiwazumi, and Matsunagi Formations (**Figure 8.5b**). Rhyolites including moonstone rhyolite was deposited as pyroclastic flow deposits widely also in North Korea, Noto peninsula, Gifu Prefecture (Ayalew and Ishiwatari, 2011; Shinjoe et al., 2018; Yamada et al., unpublished data). These rhyolites might have formed by crustal melting.

The SW Japan arc was rapidly rotated clockwise in 18–16 Ma of stage IV (Hoshi et al., 2015; Hoshi, 2018), while the Iwaine and Iozen Formation were formed in 18–17 Ma. Contemporaneously, the second stage of spreading in the Yamato basin occurred near the Toyama basin in 18–15 Ma (Nohda, 2009; Nakajima, 2013). The Toyama basin has rifted rapidly in this period (Nakajima et al., 2021). Andesitic magmatism of the Iwaine Formation was followed by rhyolitic magmatism of the Iozen Formation (**Figure 8.5c** and **8.5d**). Since the old and cold Pacific plate was subducting to the SW Japan arc during the Japan Sea opening (Hall, 2002; Miller and Kennett, 2006; Kimura et al., 2014), additional heat source such as upwelling of the asthenospheric mantle into the mantle wedge (Tatsumi et al.,

1989; Okamura et al., 1998; Zadeh et al., 2013; Shuto et al., 2006, 2015) and/or slab tearing (slab window; Martynov et al., 2017) below the margin of the Eastern Asian continent is required to cause melting of the subducting slab. This slab melt generated HMA magma, and it metasomatized the mantle wedge to produce high-Sr andesite (**Figure 8.5c**). Contemporaneously, lithospheric mantle was partially molten to produce tholeiitic basaltic magma, and this basaltic magma assimilated the continental crust to generate tholeiitic andesite. The generated basaltic to andesitic magma formed a large batholith beneath the Toyama basin (Ishiyama et al., 2017), assimilating the continental crust to generate rhyolitic magma of the Iozen Formation (**Figure 8.5d**). The arc volcanism in the Toyama basin during the Japan Sea opening terminated with the basaltic (Kurokabe basalt; Sakayori et al., 1997) and rhyolitic magmatism of the Iozen Formation at ~ 16 Ma. Meanwhile, basaltic to dacitic volcanism caused by injection of hot asthenosphere occurred in the Fossa Magna province (e.g., Okamura et al., 2016).

8.3.2.What is the original material of the rhyolites?

As discussed in section 8.2, Jh-Pyr (Johana Formation) and Io-Aph (Iozen Formation) are considered to have been generated by melting of the crustal material. Because both of the rhyolites accompany andesitic rocks, the production processes of rhyolites are considered to be related to the andesitic volcanism. The production processes of rhyolites and the original material are inferred and discussed in this section.

As reviewed in chapter 2, Andesitic volcanism forming the Kamiwazumi and Matsunagi Formations contemporaneously occurred at the same timing of the formation of the Johana Formation and the equivalent rhyolites (23–22 Ma; Kano et al., 2007a; Yoshikawa et al., 2002; **Figure 8.5b**). Additionally, there is a possibility

that the related andesites are distributed widely also in north area of the Noto peninsula as the Hegurajima and Nanatsujima volcanic rocks (Yamada and Takahashi, 2021). On the other hand, rhyolitic magmatism of the Iozen Formation occurred in 17–16 Ma just after andesitic volcanism of the Iwiane Formation (18–17 Ma; **Figure 8.5c** and **8.5d**). In addition, low-K basalt effused as the Nanamagari Formation at the same timing of the rhyolitic magmatism of the Iozen Formation (e.g., Sakayori et al., 1997). Therefore, the rhyolitic magmatism is considered to have been caused by heat flow of andesitic magmatism. Because the rhyolites were produced by crustal melting as discussed in section 8.2, the andesitic magmatism caused melting of the crustal materials.

Although Jh-Pyr and Io-Aph have different Sr–Nd isotope (Jh-Pyr has more enriched Sr–Nd isotope), they have similar trend in SrI–NdI diagram (**Figure 7.8a**). This suggests two possibilities: (1) the original material of Jh-Pyr and Io-Aph is the same, and (2) the difference of enrichment of Sr–Nd isotope is because of different degree of melting of the crustal material.

Ishida et al. (1998) examined mineral chemical compositions of moonstone rhyolite, which is related to the Johana Formation, and discussed that not hydrous crustal material such as granulite, which is distributed in the Hida belt, is required to generate rhyolitic magma of the moonstone rhyolite. However, embayment of quartz grain in Jh-Pyr (**Figure 6.1a**) is considered to be formed in hydrous magma (Donaldson and Henderson, 1988). It should be reexamined in detail if rhyolitic magma of Jh-Pyr were hydrous or not hydrous. In addition, Jh-Pyr contains xenolith of gneiss, which may be derived from the Hida belt (**Figure 6.1b**). This suggests that the Hida belt involved the genesis of the rhyolites, however, texture suggesting that the xenolith was melted is not found.

Shuto et al. (2006) examined Sr–Nd isotope of 22–20 Ma and 14–11 Ma rhyolites from Niigata Prefecture, where the Hida belt is not distributed. Compared to them, Jh-Pyr and Io-Aph have more enriched Sr–Nd isotope (**Figure 8.3a**), suggesting that there is more enriched crustal material beneath the Toyama basin. Moreover, zircon Hf isotope of Jh-Pyr and Io-Aph also enriched composition, showing εHf = -10–0 (**Figure 8.3b**). Although the Hida belt shows enriched Sr–Nd–Hf isotopic composition, it has also depleted isotopic compositions, compared to Jh-Pyr and Io-Aph (**Figure 8.3a** and **8.3b**). Hence, it is considered that there is more enriched crustal material than the Hida belt beneath the Toyama basin and that the enriched crustal material (not the Hida belt) was melted to generate rhyolitic magmas of the Johana and Iozen Formations. This highly enriched crustal material might be derived from the old continental crust such as the North or South China Cratons.

Conclusions on the production processes of rhyolites from the (1) Johana and (2) Iozen Formations and the original material, based on the above discussions, are as follows. (1) The rhyolitic magmatism of the Johana Formation was caused by andesitic magmatism of the Kamiwazumi and Matsunagi Formations. The andesitic magma played a role as heat source and melted the more enriched crustal material than the Hida belt to generate rhyolitic magma. The percentage of mixing between the andesites and the crustal material is uncertain due to less geochemical information on andesites and crustal material. (2) The rhyolitic magmatism of the Iozen Formation was caused by basaltic to andesitic magmatism of the Iwaine and Nanamagari Formations. The basaltic to andesitic magma played a role as heat source and melted the more enriched crustal material than the Hida belt to generate rhyolitic magma. The percentage of mixing between the andesites and the crustal material is uncertain

due to less geochemical information on crustal material. The differences of Sr–Nd isotopic composition between Jh-Pyr and Io-Aph is considered because of difference of mixing ratio between the andesitic magma and the crustal material. Moreover, enriched Sr–Nd–Hf isotopic composition suggests that there is highly more enriched crustal material than the Hida belt beneath the Toyama basin. This highly enriched crustal material might be derived from the old continental crust such as the North or South China Cratons.

8.3.3.Comparison of Cenozoic rhyolites in the world

Ayalew and Ishiwatari (2011) compared the major and trace element compositions of rhyolites from three tectonic settings (continental rift, continental arc, and oceanic island). They found that the contents and concentrations of some major (CaO, Al_2O_3, and K_2O) and trace (e.g., Sr, Nb, Ta, Zr, and Y) elements vary depending on the tectonic setting. Accordingly, it is expected that the tectonic settings where rhyolites are produced can be discriminated geochemically. Here we compiled data on some major and trace elements (measured by XRF) of Cenozoic rhyolites from various tectonic settings (n = 462) to constrain in detail the tectonic settings where the rhyolites from the Johana and Iozen Formations were generated (**Figure 8.6**). Rhyolites can be classified into five types according to their tectonic settings: oceanic hotspot rhyolites, continental rift rhyolites, collisional zone rhyolites, island arc rhyolites, and continental arc rhyolites.

The K_2O composition appears to significantly change among rhyolites from different tectonic settings, as Ayalew and Ishiwatari suggested (**Figure 8.6a**). Cenozoic rhyolites from various settings can be distinguished in a Y+Nb–Rb diagram (**Figure 8.6b**), which is used to discriminate granites (Pearce et al., 1984). Moreover, rhyolites from various settings have different distributions in some diagrams (**Figure 8.6c** and **8.6d**). It is thus considered that these

results reflect some factors complicatedly. For instance, fH_2O, degree of partial melting, pressure and temperature during melting and differentiation, and original material are considered important factors. Compared with the Cenozoic rhyolites from around the world, the Usunaka Moonstone Rhyolite and Lower Miocene moonstone rhyolites in the Hokuriku region (Ishida et al., 1998; Ayalew and Ishiwatari, 2011) plot between the continental rift and continental arc types in many diagrams. Conversely, the Iozen Formation plots between the island arc and continental arc types. This suggests that the geochemical characteristics of the rhyolites changed from those of a continental arc rift type to those of continental or island arc types as the Japan Sea back-arc basin spread quickly.

8.3.4.Implications for evolution of arc crust

In the Toyama basin, Neogene sediments related to Stage III (18–15.3 Ma) of the Japan Sea opening occupy ~5 km of the upper crust, as revealed on the basis of seismic tomography (Ishiyama et al., 2017). Although the Johana Formation is only ~400 m thick, the thickness of the Iozen Formation reaches >1000 m. Furthermore, the rhyolite from the Iozen Formation is supplied as sediments to the Toyama basin composing the upper crust ~5 km in thickness (Ishiyama et al., 2017).

The trace element patterns of the Iozen Formation normalized by the upper continental crust indicate a parallel and similar enrichment (sample/upper continental crust ≈ 1) to that of the upper crust (**Figure 8.7**). Although the Usunaka Moonstone Rhyolite Member of the Johana Formation has a slightly more enriched composition than that of the upper crust, it also shows a similar compositional pattern to that of the upper continental crust. Furthermore, rhyolites from rifts along subduction zones show similar patterns to those of the rhyolites from the Johana and Iozen Formations. Rhyolites from continental rifts and

oceanic hot spots show a clear, positive Nb and Ta anomaly, whereas those from collisional zones and island arcs have depleted heavy rare earth element and light rare earth element compositions, respectively. The studied rhyolites have large volumes in the Toyama basin, suggesting large-scale volcanism. These imply that rhyolitic magmatism during the Japan Sea opening generated and supplied a large volume of new material similar in chemistry to the upper crust. Moreover, this indicates that felsic magmatism related to rifting in the subduction zone, such as back-arc spreading, contributes to recycling of crustal materials in the continental crust that the new upper crust is generated by crustal melting.

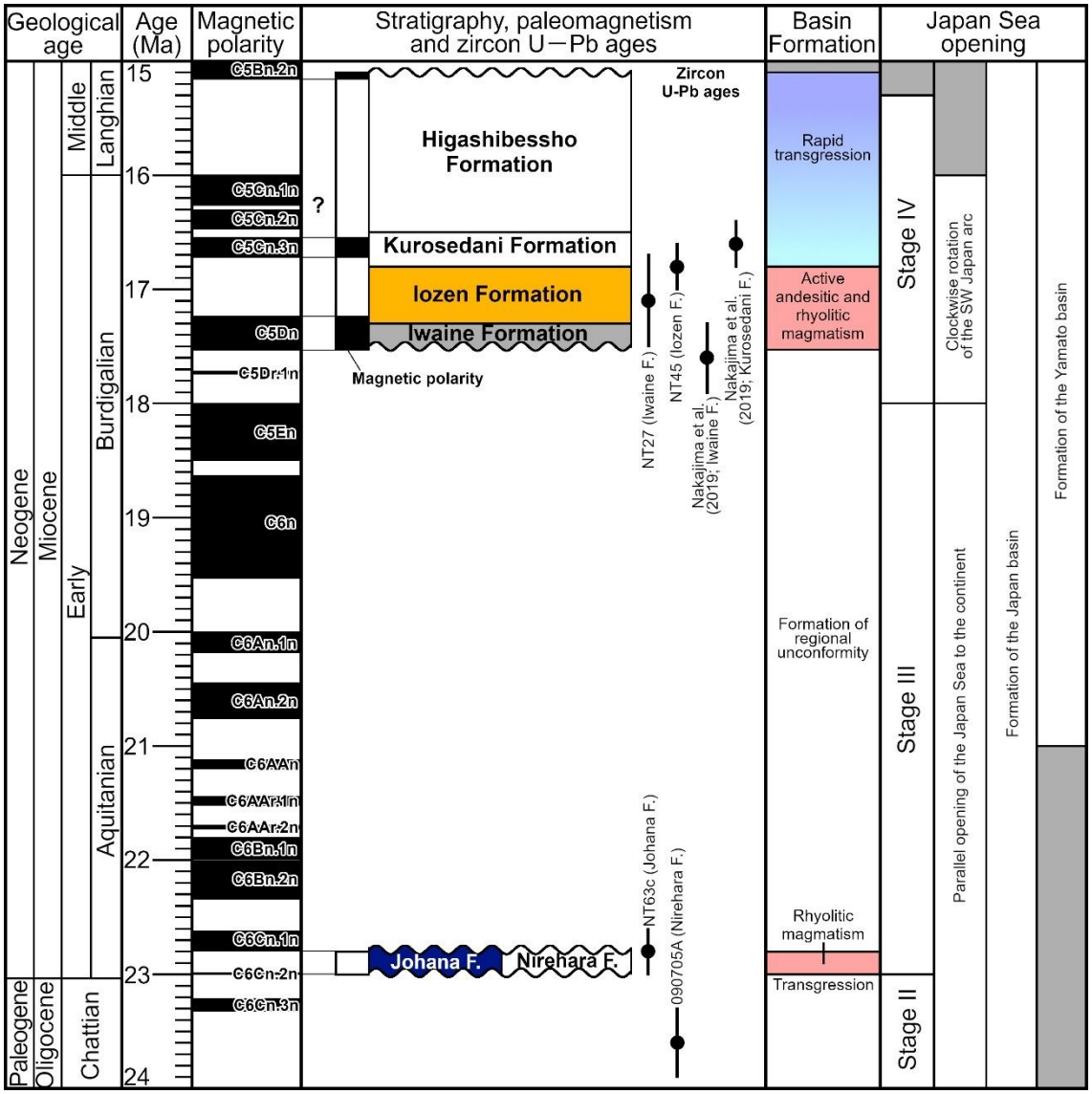

Figure 8.1 Chronostratigraphy of the Toyama basin with the geotectonic information of the Japan Sea opening. The geomagnetic polarity time scale is after Gradstein et al. (2020). Paleomagnetic data of sedimentary and volcanic rocks are from Itoh (1988), Itoh and Hayakawa (1988, 1989), Itoh et al. (1999), Itoh and Watanabe (2000), Iwaki and Itoh (2000), Itoh and Kitada (2003), and Tamaki et al. (2006).

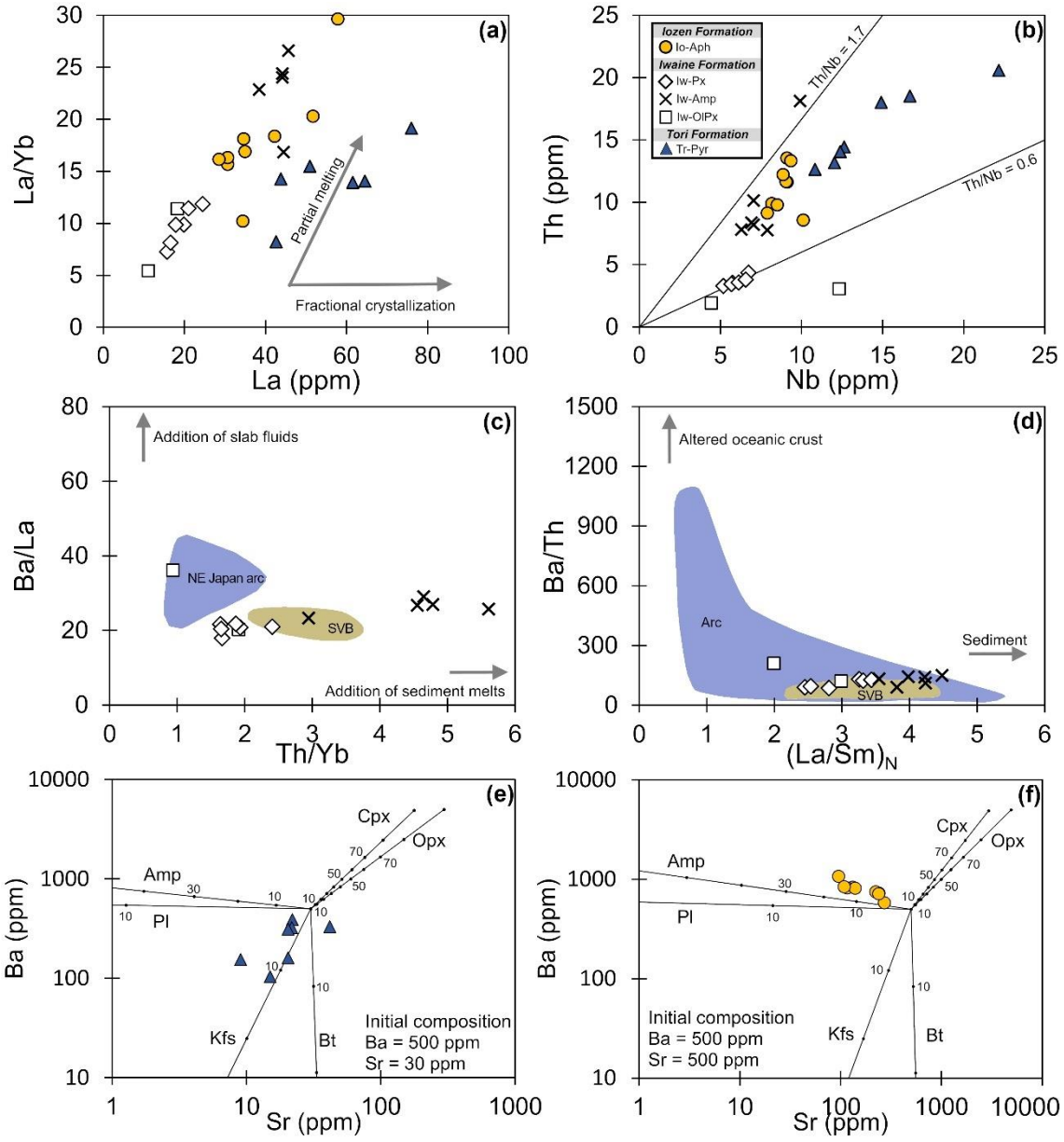

Figure 8.2 Plots of (a) La–La/Yb, (b) Nb–Th, (c) Th/Yb–Ba/La, and (d) $(La/Sm)_N$–Ba/Th diagrams, showing magma processes during petrogenesis, and vector diagrams for Sr vs. Ba, showing the effects of Rayleigh fractionation of rhyolitic melt for (g) the Tori Formation and (h) the Iozen Formation. Trends arrays of partial melting and fractional crystallization in (a) are from Li et al. (2020). Data on Setouch Volcanic Belt (SVB) and NE Japan are from Tatsumi (2006) and Hanyu et al. (2006), respectively. The partition coefficient values of

each mineral are from Rollinson and Pease (2021).

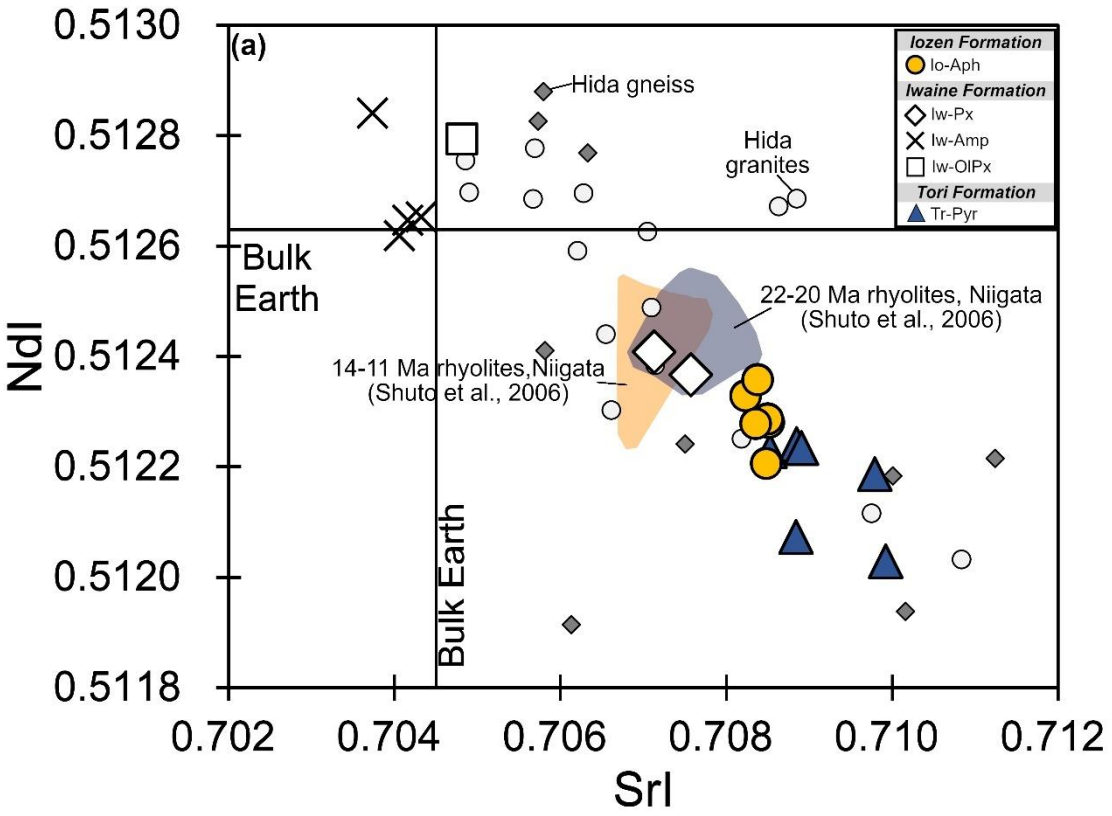

Figure 8.3 Isotopic comparison of rhyolites. (a) SrI–NdI isotopic variation diagrams compared with rhyolites from Niigata Prefecture (Shuto et al., 2006). Data of the Hida Belt is from Asano et al. (1990), Tanaka (1992), and Arakawa and Shinmura (1995). Sr and Nd isotopic values of the bulk earth are from DePaolo and Wasserburg (1976) and Bouvier et al. (2008), respectively. (b) Age vs. zircon εHf diagram of volcanic rocks from the Nanto area comparing with the data from the Japan arc. Data of the Japan arc, the Hida granites, the HIda metamorphic rocks are from Osozawa et al. (2019), Cho et al. (2021a, b) and Pastor-Galan et al. (2021). Evolution lines of depleted mantle and juvenile continental crust are based on Griffin et al. (2000) and Iizuka et al. (2017). The CHUR is based on the evolution model by Iizuka et al. (2015).

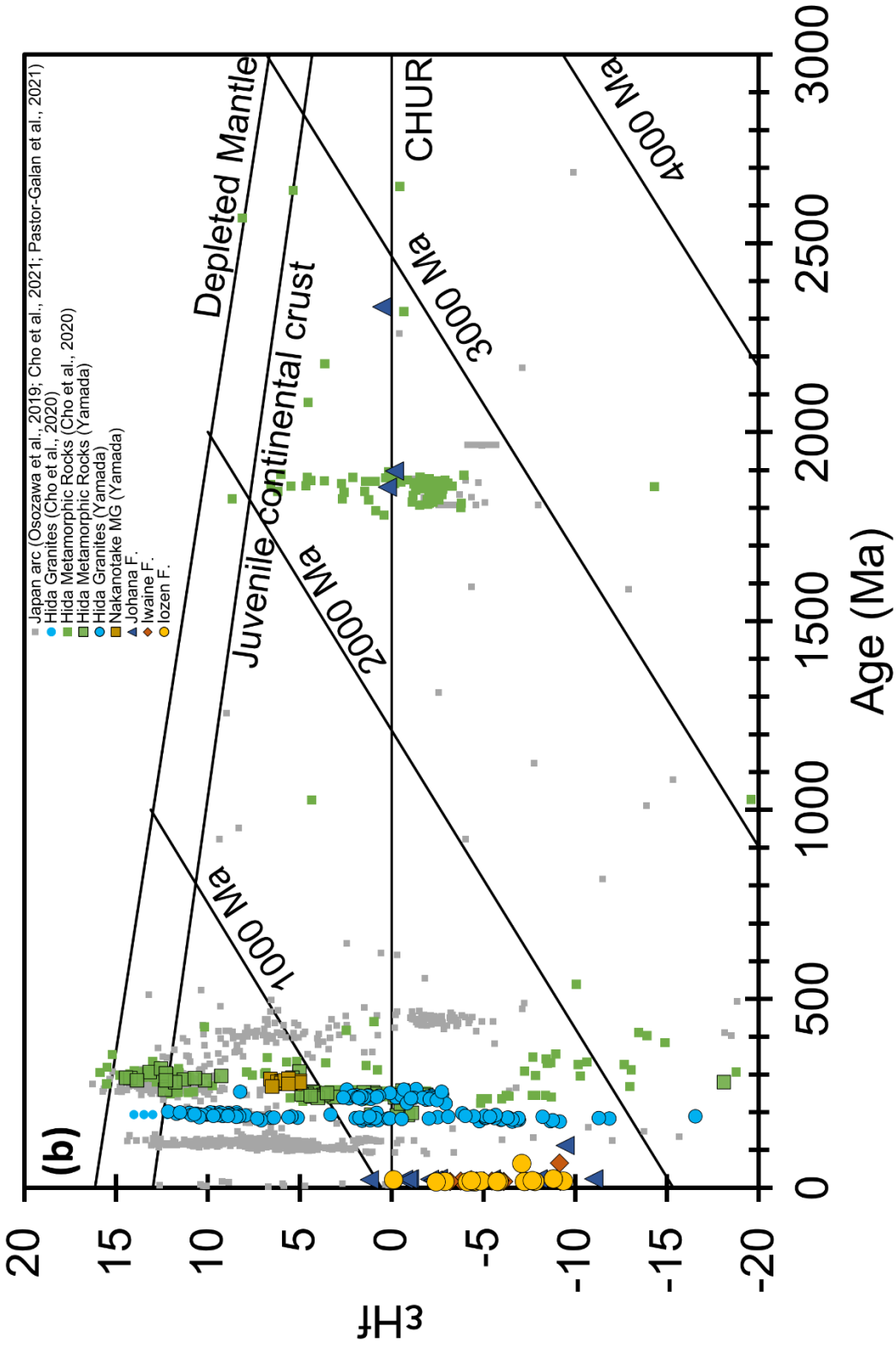

Figure 8.3 continued.

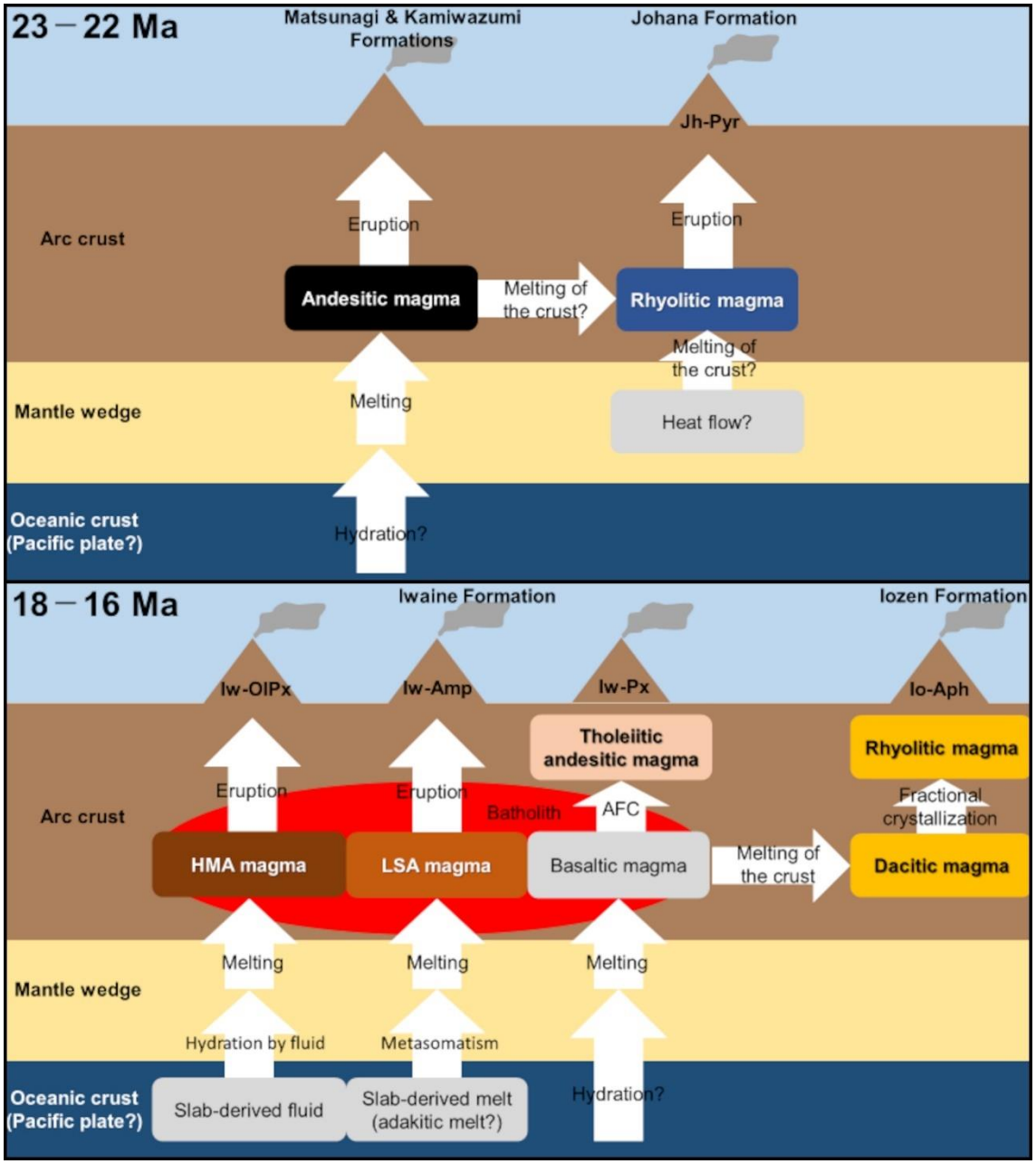

Figure 8.4 Schematic magmatic processes in the Toyama basin during the Japan Sea opening. See the text for details.

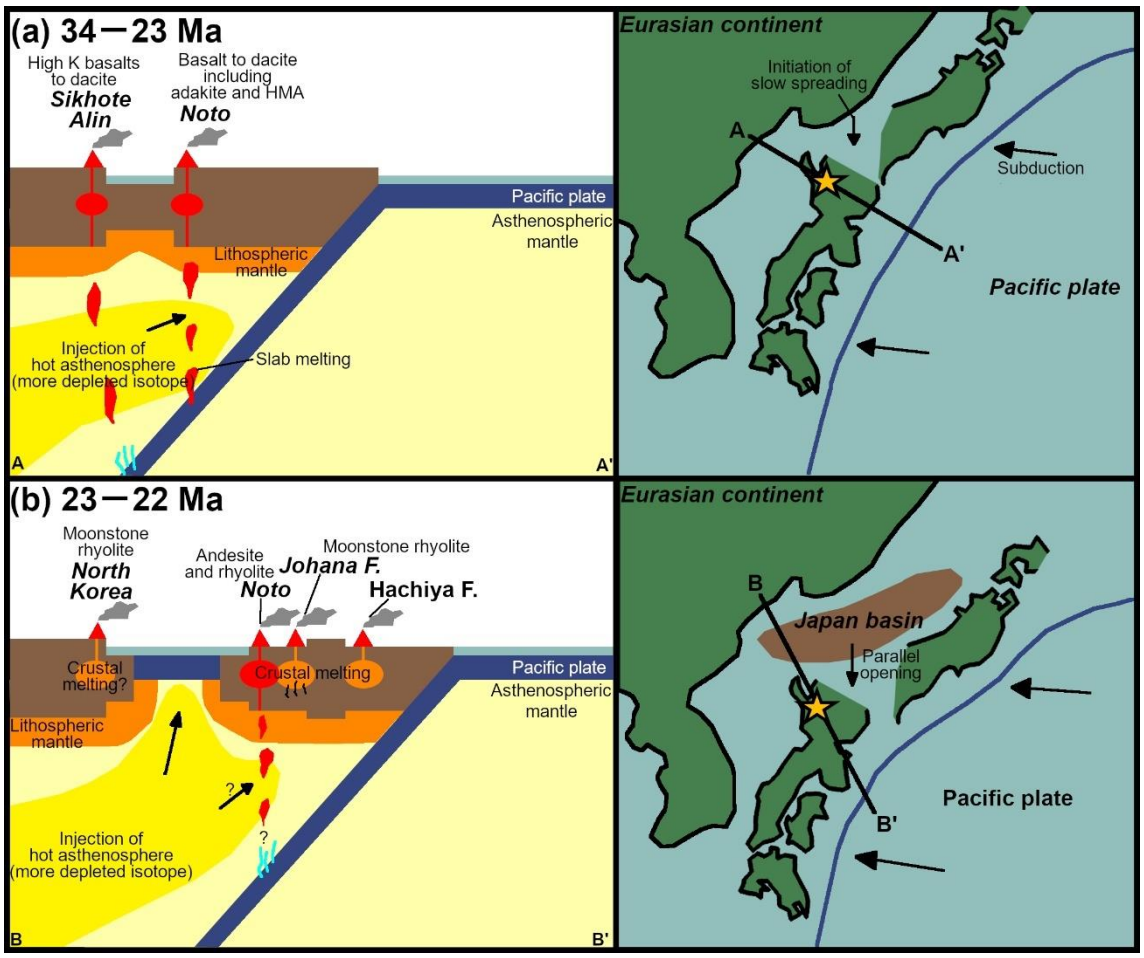

Figure 8.5 Schematic tectono-magmatic model of volcanism during the Japan Sea opening. See the text for details. (a) 34–23 Ma. (b) 23–22 Ma. (c) 22–17 Ma. (d) 17–16 Ma.

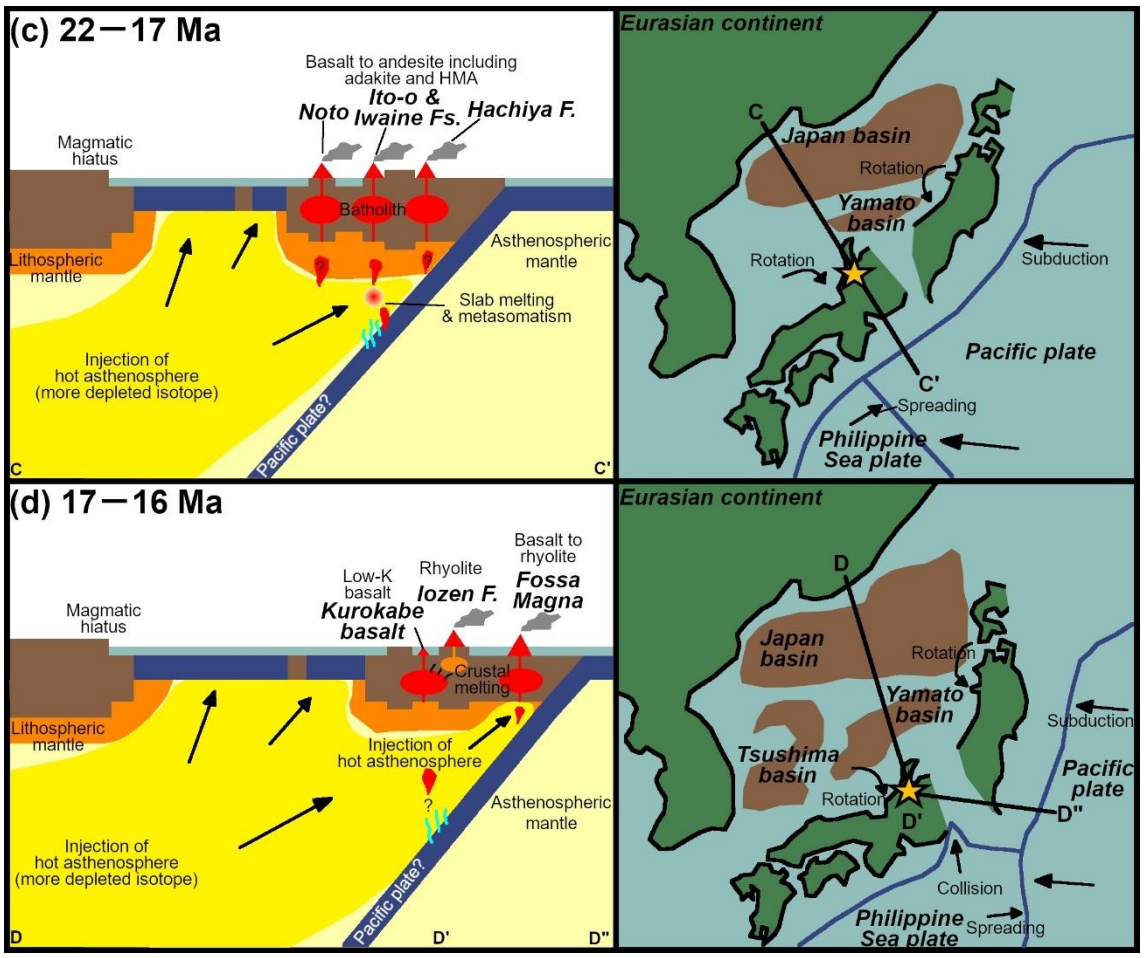

Figure 8.6 continued.

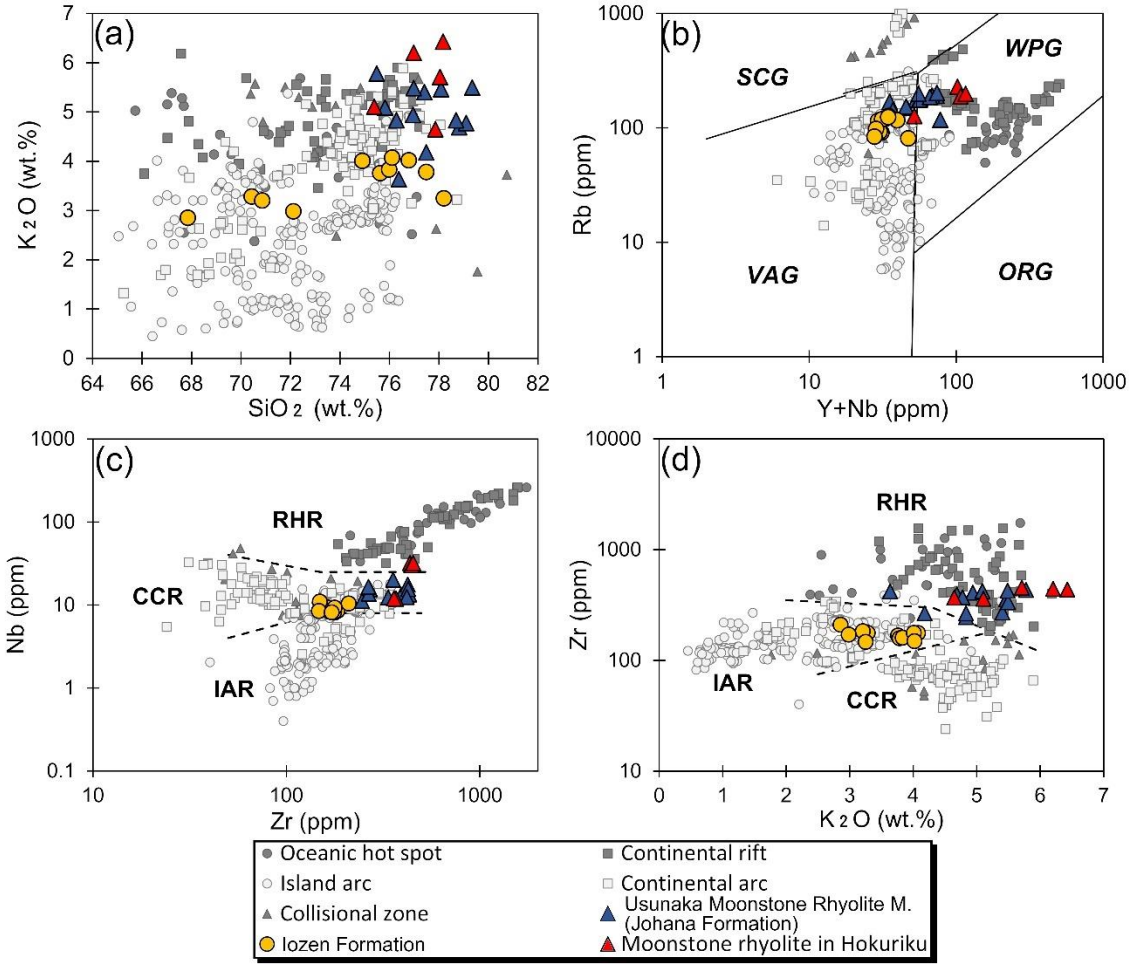

Figure 8.6 Comparison of Cenozoic rhyolites of the world. (a) SiO_2–K_2O variation diagram. (b) Y + Nb–Rb discrimination diagram for granites (Pearce et al., 1984). (c) Zr–Nb variation diagram. Boundary coordinates are (50, 4; 150, 8; 500, 8) and (50, 40; 150, 25; 550, 25). (d) K_2O–Zr variation diagram. Boundary coordinates are (2, 350; 4.3, 300; 5.2, 180; 6, 120) and (2.5, 75; 5.2, 180). SCG, Syn-collision granites; WPG, within plate granites; VAG, volcanic arc granites; ORG, ocean ridge granites; RHR, rift and hot spot rhyolites; CCR, continental arc and collisional zone rhyolites; IAR, island arc rhyolites. Lower Miocene moonstone rhyolites in the Hokuriku region are from Ishida et al. (1998) and Ayalew and Ishiwatari (2011). Oceanic hotspot rhyolites (n = 24) are from Ascension Island (Kar et al., 1998) and some volcanoes in Iceland (Jónnasson, 2007). Continental rift

rhyolites (n = 61) are from the Heise volcanic field (USA; Watts et al., 2011), Miocene to Quaternary Ethiopia (Peccerillo et al., 2003; Ayalew and Gibson, 2009), Western Pontine Archipelago (Italy; Conte et al., 2016), and Yellowstone caldera (USA; Girard and Stix, 2009). Collisional zone rhyolites (n = 17) are from Paleocene to Quaternary Tibet (China; Mo et al., 2008; Wang et al., 2012). Island arc rhyolites (n = 241) are from the Akagi volcano (Japan; Takahashi et al., 2012), Aniakchak caldera (Aleutian, USA; George et al., 2004), Aso volcano (Japan; Miyoshi et al., 2011), Batur caldera (Indonesia; Sutawidjaja et al., 2015), Bulusan volcano (Philippines; McDermott et al., 2005), some volcanoes in the Izu-Bonin arc (Japan; Tamura et al., 2009), some volcanoes in Kamchatka (Russia; Bindeman et al., 2010), Kutcharo volcano (Japan; Hoang et al., 2011), some volcanoes in Luzon Island (Philippines; Vogel et al., 2006), Narugo volcano (Japan; Ban et al., 2005), Okmok volcano (Aleutian, USA; Finny et al., 2008), Sakurajima volcano (Japan; Takahashi et al., 2011), South Sandwich Islands (UK; Leat et al., 2007), Taupo volcano (New Zealand; Sutton et al., 2000), and Toba caldera (Indonesia; Chesner and Luhr, 2010). Continental arc rhyolites (n = 119) are from Quaternary ignimbrites in Arequipa Province (Peru; Lebti et al., 2006), some volcanoes in Western USA (Reagan et al., 2003), Cerro de Vidrio volcano (Argentina; Bissig et al., 2002), Chaitén volcano (Chile; Lowenstern et al., 2012), Puyehue–Cordón Caulle Volcanic Complex (Chile; Naranjo et al., 2017), Jefferson volcano (USA; Conrey et al., 2001), Kos Plateau (Bachmann, 2010), La Pacana caldera (Chile; Lindsay et al., 2001), and Tlaloc volcano (Mexico; Ruenda et al., 2013).

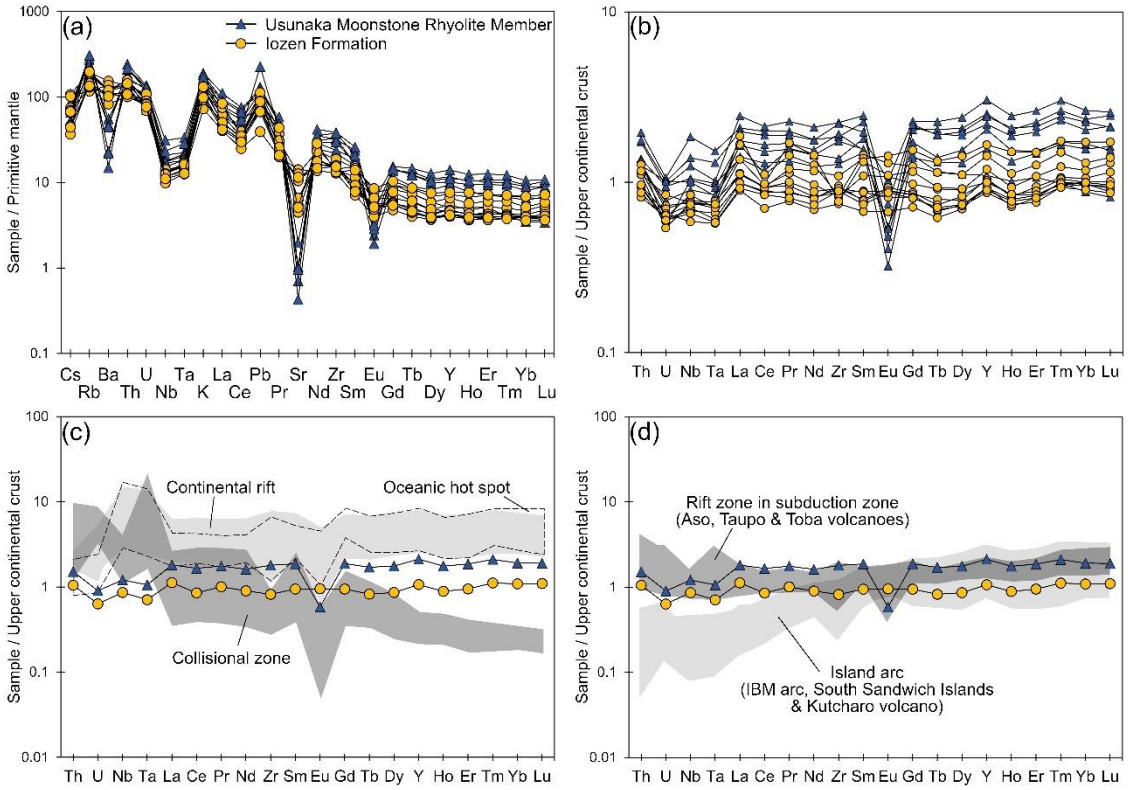

Figure 8.7 Spider diagrams of incompatible elements of rhyolites from the all over the world. Trace element concentrations for normalization are from Sun and McDonough (1989; primitive mantle) and Rundnik and Gao (2003, 2014; upper continental crust). (a) Primitive-mantle-normalized trace element patterns of rhyolites from the Johana and Iozen Formations. (b) Upper-continental-crust-normalized high-field strength element (HFSE) patterns of the rhyolites from the Johana and Iozen Formations. (c) Upper-continental-crust-normalized HFSE patterns of the averaged rhyolites compared with those of oceanic hot spot (Iceland; Jónasson, 2007), continental rift (Yellowstone volcano, Girard and Stix, 2009; Great Rift Valley in Ethiopia, Ayalew and Gibson, 2009), and collisional zone rhyolites (Wang et al., 2012). (d) Upper-continental-crust-normalized HFSE patterns of the averaged rhyolites compared with those of rhyolites from island arcs and rift zones in island arcs (Aso volcano, Japan, Miyoshi et al., 2011; Taupo volcano, New Zealand, Sutton et

al., 2000; Toba volcano, Indonesia, Chesner and Luhr, 2010).

9. Conclusions

In this study, geological and petrological survey and analyses (field mapping, facies analysis, zircon U–Pb dating, zircon trace element analysis, zircon Lu–Hf isotopic analysis, whole-rock major and trace element analysis, whole-rock Sr–Nd isotopic analysis) were conducted to reveal temporal change of arc volcanism in the Toyama basin during back-arc spreading in the Japan Sea and discuss recycling of arc crust during back-arc spreading. Conclusions based on results and discussion are as follows.

(1) Late Oligocene to Middle Miocene strata in the Toyama basin related to the Japan Sea opening are subdivided into the Nanto (the Johana and Nirehara Formations) and Yatsuo Groups (the Iwaine, Ganzo, Iozen, Kurosedani, Sasagawa, Fukuhira, Sunagozaka, Doyama, HIgashibessho, and Omine Formations).

(2) Thirteen facies assemblages are found from the Late Oligocene to Middle Miocene strata in the Toyama basin: subaerial lava, in situ hyaloclastite, resedimented hyaloclastite, peperite, dike, subaerial pyroclastic flow deposit, pyroclastic fall out deposit, debris flow deposit, fluvial deposit, inner bay deposit, shallow water deposit, turbidite, deep water deposit.

(3) 22.8 ± 0.2 Ma, 23.6 ± 0.3 Ma, 17.1 ± 0.4 Ma, and 16.8 ± 0.2 Ma of zircon ^{238}U–^{206}Pb weighted mean ages (errors are given as 2SE) were obtained from the Johana (welded tuff), Nirehara (rhyolite gravel), Iwaine (pumice tuff) and Iozen Formations (lava), respectively.

(4) The development history of the Toyama basin initiated at 23 Ma by deposition of non-marine to shallow marine deposits and pyroclastic flow deposits. After formation of regional

unconformity between 23 and 18 Ma, andesitic volcanism occurred in 18–17 Ma as flood andesite (non-marine to shallow marine). This andesitic volcanism was followed by dacitic to rhyolitic volcanism in 17–16 Ma (non-marine to shallow marine) with formation of delta. Subsequently, the Toyama basin was deepened to deposit deep marine deposits until 15 Ma.

(5) Both of the rhyolites from the Johana and Iozen Formations were generated by partial melting of the crustal material. The parent material is considered as old continental crust such as the North and South China Cratons. The Iwaine Formation is composed of three types of andesites; high-Mg andesite (HMA), high-Sr andesite, and tholeiitic andesite. HMA was generated by melting of the hydrous peridotite mantle source. High-Sr andesite was generated by melting of the mantle wedge metasomatized by slab-derived melt. Tholeiitic andesitic magma is considered to have been produced by melting of the lithospheric mantle and AFC.

(6) Upwelling of the asthenospheric mantle into the mantle wedge caused melting of the subducting Pacific plate, and andesitic magmatism caused crustal melting to generate rhyolitic magma.

(7) Petrogenesis of the rhyolites indicate that large heat flow related to the Japan Sea opening affected not only the mantle wedge but also the arc crust of the Toyama basin. Similar trace element pattern of the studied rhyolites to the upper continental crust indicates that felsic magmatism related to rifting in the subduction zone, such as back-arc spreading, contributes to recycling of crustal materials in the continental crust that the new upper crust is generated by crustal melting.

10. Achievement and future plan

10.1. Achievement of this study

- Thirteen facies assemblages were found from the Late Oligocene to Middle Miocene strata. The depositional environment and the development history of the Toyama basin were firstly and comprehensively discussed in this thesis.
- The chronostratigraphy of the Late Oligocene to Middle Miocene in the Toyama basin was reexamined in this thesis, based on results of zircon U–Pb dating and previous studies.
- Volcanic rocks from the Nanto area, related to the Japan Sea opening, were distinguished into five rock types, and the petrogenesis was discussed based mainly on whole-rock geochemistry.
- Temporal change of arc volcanism in the Toyama basin related to the Japan Sea opening was firstly and comprehensively discussed, based on geological history, chronostratigraphy, and petrogenesis.
- It was revealed that old continental crust involved the petrogenesis of rhyolites and that arc crust is recycled by arc volcanism during the back-arc spreading, based on petrography, whole-rock geochemistry and zircon Hf isotope

10.2. Remaining issues and future plan

In this thesis, the author considered that more enriched and older continental crust than the Hida belt involved the petrogenesis of the rhyolites. This hypothesis gives implications for the geotectonic history and crustal structure of the Hida belt. The author has been studying geology, chronology and petrology of igneous and metamorphic rocks from the Hida belt with some researchers since

the author was a master student. Accordingly, the geotectonic history of the Hida belt will be revealed in near future.

Acknowledgements

My sincere gratitude goes to Associate Professor Toshiro Takahashi (supervisor) of Niigata University. He accepted me to come to Niigata University and join his laboratory since master's course. The author has been taught many things by him. Words cannot describe how much I want to thank him.

I especially thank Dr. Nagata Mitsuhiro of the Tono Geoscience Center for helping me a lot. I have spent for long time with him, and he taught many things to me. In addition, he invited me to JAEA. Without him, I could not get the master and Ph.D. degrees. He is a best friend of mine and a research fellow forever.

I would like to appreciate Professor Eiichi Takazawa, Professor M. Satish-Kumar and Associate Professor Hayato Ueda of Niigata University. Professor Eiichi Takazawa (co-supervisor) helped and cheered me up a lot. Professor M. Satish-Kumar (co-supervisor) taught me how to write English papers and do research. In addition, he took us to India. This journey to India completely changes my life. Associate Professor Hayato Ueda taught me zircon U–Pb dating in detail and how to think logically.

I thank Ouchi Wataru of Suncoh Consultants Co., Ltd. for spending for long time with me and helping field survey. I and he used to go for lunch and dinner many times. He always makes me laugh. We are good friends forever.

Discussion with Syun Watanabe and Dr. Keisuke Suzuki is greatly appreciated. I and Syun Watanabe used to go for drink to discuss and talk many things. I cannot forget good memories with him. Discussion with Dr. Keisuke Suzuki is always interesting, and he gave me a lot of good ideas.

Great friendships with Dr. Silpa, Kiran, Dr. Sreehari, Dr. Sayantani and Dr. Anupam are thanked. They have mentally supported me. We used to go many places and drink together. I would like to be a good friend and a research fellow with them also in the future.

Members of the Tono Geoscience Center of the Japan Atomic Energy Agency are greatly thanked. They accepted me to come to the Tono Geoscience Center and helped me a lot during analysis and spending the dormitory. I also thank Takuya Harada of Mt. Kurikoma Area Geopark for doing zircon Lu–Hf isotopic analysis to me.

I thank Yasuhiro Ogita of the Tono Geoscience Center and Kazuya Shimooka of Ehime University for discussion on geology and petrology and geological trip with me. They are very good research fellows.

Naoki Takahashi and Akitaka Shibano of Niigata University are appreciated. They belong to the same lab. (Takahashi Lab.) with me and helped me a lot. They and I used to go to the field and drink much together. I hope they will do well their work from coming spring.

Professors and students in the department of geology, Niigata University are greatly appreciated. They accepted me who came from the University of Toyama to Niigata University very kindly and friendly. I am so happy to spend time in Niigata University owing to them.

My sincere gratitude goes to my family. They always have encouraged and helped me a lot. Especially, my mother understands my dream and always helped me. My father also financially helped me. Without them, I could not reach here. I thank them once again.

At the last, I would like to acknowledge Jaewon Ha and Yusin Ha. She, Jaewon Ha, passed away in last autumn. I never can forget your love to me. I hope she will rest in peace and love both of you forever.

References

Amano, K., Hamuro, T. and Hamuro, M. (2004) Latest early-earliest middle Miocene deep-sea molluscs in the Japan Sea borderland – the warm-water Higashibessho fauna in Toyama Prefecture, central Japan. Paleontological Research, 8, 29–42.

Arakawa, Y. and Shinmura, T. (1995) Nd-Sr isotopic and geochemical characteristics of two contrasting types of calc-alkaline plutons in the Hida belt, Japan. Chemical Geology, 124, 217–232.

Asano, M., Tanaka, T. and Suwa, K. (1990) Sm-Nd and Rb-Sr ages of the Hida metamorphic rocks in the Wada-gawa area, Toyama Prefecture. The Journal of the Geological Society of Japan, 96, 957–966 (in Japanese with English abstract).

Ayalew, D. and Gibson, S.A. (2009) Head-to-tail transition of the Afar mantle plume: Geochemical evidence from a Miocene bimodal basalt–rhyolite succession in the Ethiopian Large Igneous Province. Lithos, 112, 461–476.

Ayalew, D. and Ishiwatari, A. (2011) Comparison of rhyolites from continental rift, continental arc and oceanic island arc: Implication for the mechanism of silicic magma generation. Island Arc, 20, 78–93.

Bachman, O. (2010) The petrologic evolution and pre-eruptive conditions of the rhyolitic Kos Plateau Tuff (Aegean arc). Central European Journal of Geosciences, 2, 270–305.

Bachman, O., Oberli, F., Dungan, M. A., Meier, M., Mundil., R. and Fischer, H. (2007) $^{40}Ar/^{39}Ar$ and U–Pb dating of the Fish Canyon magmatic system, San Juan Volcanic Field, Colorado: evidence for an extended crystallization history. Chemical Geology, 236, 134–166.

Ban, M., Takahashi, K., Horie, T. and Toya, N. (2005) Petrogenesis of mafic inclusions in rhyolitic lavas from Narugo volcano, northeastern Japan. Journal of Petrology, 46, 1543–1563.

Bickford, M.E., Mishra, M, Mueller, P.A., Kamenov, G.D., Schieber, J. and Basu, A. (2017) U-Pb Age and Hf Isotopic Compositions of Magmatic Zircons from a Rhyolite Flow in the Porcellanite Formation in the Vindhyan Supergroup, Son Valley (India): Implications for Its Tectonic Significance. The Journal of Geology, 125, 367–379.

Bindeman, I.N., Leonov, V.L., Izbekov, P.E., Ponomareva, V.V., Watts, K.E., Shipley, N.K., Perepelov, A.B., Bazanova, L.I., Jicha, B.R., Singer, B.S., Schmitt, A.K., Portnyagin, M.V. and Chen, C.H. (2010) Large-volume silicic volcanism in Kamchatka: Ar–Ar and U–Pb ages, isotopic, and geochemical characteristic of major pre-Holocene caldera-forming eruptions. Journal of Volcanology and Geothermal Research, 189, 57–80.

Bissig, T., Clark, A.H. and Lee, J.K.W. (2002) Cerro de Vidrio rhyolitic dome: evidence for Late Pliocene volcanism in the central Andean flat-slab region, Lama-Veladero district, 29°20’S, San Juan Province, Argentina. Journal of South American Earth Sciences, 15, 571–576.

Bito, A., Hayakawa, T., Kaseno, Y., Ogasawara, K. and Takayama, T. (1980) The Neogene stratigraphy around Kaga City, Ishikawa Prefecture, Japan. Annals of Science, Kanazawa University, 17, 45–70 (in Japanese with Emglish abstract).

Blichert-Toft, J. (2008) The Hf isotopic composition of zircon reference material 91500. Chemical Geology, 253, 252–257.

Bouma, A.H. (1962) Sedimentology of some flysch deposits: A graphic approach to facies interpretation. Elsevier, Amsterdam, 168 p.

Bourvier, A., Vervoort, J.D. and Patchett, P.J. (2008) The Lu–Hf and Sm–Nd isotopic composition of CHUR: Constraints from unequilibrated chondrites and implications for the bulk composition of terrestrial planets. Earth and Planetary Science Letters, 273, 48–57.

Brown, M. and Johnson, T. (2018) Secular change in metamorphism and the onset of global plate tectonics. American Mineralogist, 103, 181–196.

Cas, R.A.F. and Wright, J.V. (1987) Volcanic successions: Modern and ancient. Chapman and Hall, London, 528 p.

Chesner, C.A. and Luhr, J.F. (2010) A melt inclusion study of the Toba Tuffs, Sumatra, Indonesia. Journal of Volcanology and Geothermal Research, 197, 259–278.

Chiji, M. (1961) Neogene biostratigraphy of the Toyama sedimentary basin, Japan Sea coast. Bulletin of Osaka Museum of Natural History, 14, 1–88 (in Japanese with English abstract).

Chinzei, K. (1986) Faunal succession and geographic distribution of Neogene molluscan faunas in Japan. The Palaeontologic Society of Japan, Special Papers, 29, 17– 32.

Cho, D.L., Lee, T.H., Takahashi, Y., Kato, T., Yi, L., Lee, S. and Cheong, A.C. (2021a) Zircon U–Pb geochronology and Hf isotope geochemistry of magmatic and metamorphic rocks from the Hida Belt, southwest Japan. Geoscience frontiers, 12, 101145.

Cho, D.L., Takahashi, Y., Kim, S.W., Yi, K. and Lee, B.C. (2021b) Zircon U-Pb-Hf and geochemical analyses of paragneiss and granitic gneiss from Oki-Dogo Island, Southwest Japan and its tectonic implications. Lithos, 396–397, 106217.

Chu, N. C., Taylor, R. N., Chavagnac, V., Nesbitt, R. W., Boella, R. M., Milton, J. A., German, C.R., Bayon, G. and Burton, K. (2002) Hf isotope ratio analysis using multi-collector inductively coupled plasma mass spectrometry: An evaluation of isobaric interference corrections. Journal of Analytical Atomic Spectrometry, 17, 1567–1574.

Conrey, R.M., Hooper, P.R., Larson, P.B., Chesley, J. and Ruiz, J. (2001) Trace element and isotopic evidence for two types of crustal melting beneath a High Cascade volcanic center, Mt. Jefferson, Oregon. Contribution to Mineralogy and Petrology, 141, 710–732.

Conte, A.M., Perinelli, C., Bianchini, G., Natali, C., Martorelli, E. and Chiocci, F.L. (2016) New insights on the petrology of submarine volcanics from the Western Pontine Archipelago (Tyrrhenian Sea, Italy). Journal of Volcanology and Geothermal Research, 327, 223–239.

Defant, M.J. and Drummond, M.S. (1990) Derivation of some modern arc magmas by melting of young subducted lithosphere. Nature, 347, 662–665.

Defant, M.J., Richerson, P.M., Boer, J.Z.D., Stewart, R.H., Maury, R.C., Bellon, H., Drummond, M.S., Feigenson, M. D. and Jackson, T.E. (1991) Dacite genesis via both slab melting and differentiation: petrogenesis of La Yeguada volcanic complex, Panama. Journal of Petrology, 32, 1101–1142.

DePaolo, D.J. and Wasserburg, G.J. (1976) Inferences about magma sources and mantle structure from variations of $^{143}Nd/^{144}Nd$. Geophysical Research Letters, 3, 743–746.

Doglioni, C. (1993) Geological evidence for a global tectonic polarity. Journal of Geological Society, London, 150, 991–1002.

Donaldson, C.H. and Henderson, C.M.B. (1988) A new interpretation of round embayments in quartz crystals. Mineralogical Magazine, 52, 27–33.

Eggins, S.M., Woodhead, J.D., Kinsley, L.P.J., Mortimer, G.E., Sylvester, P., McCulloch, M.T., Hergt, J.M. and Handler, M.R. (1997) A simple method for the precise determination of ≥ 40 trace elements in geological samples by ICPMS using enriched isotope internal standardization. Chemical Geology, 134, 311–326.

Elsasser, W.M. (1971) Sea-floor spreading as thermal convection. Journal of Geophysical Research, 76, 1101–1112.

Finney, B., Turner, S., Hawkesworth, C., Larsen, J., Nye, C., George, R., Bindeman, I. and Eichelberger, J. (2008) Magmatic differentiation at an island-arc Caldera: Okmok volcano, Aleutian Islands, Alaska. Journal of Petrology, 49, 857–884.

Flower, M.F.J., Russo, R.M., Tamaki, K. and Hoang, N. (2001) Mantle contamination and the Izu-Bonin-Mariana (IBM) 'high-tide mark': Evidence for mantle extrusion caused by Tethyan closure. Tectonophysics, 333, 9–34.

Fujii, S. (1959) The Cenozoic in the eastern part of Asahi Town, Toyama Prefecture, Geographic Study of Toyama Prefecture, 3, 121–126 (in Japanese)*.

Fujii, S., Kaseno, Y. and Nakagawa, T. (1992a) Neogene paleogeography in the Hokuriku region, Central Japan, based on the revised stratigraphic correlation. Memoir of the Geological Society of Japan, 37, 85–95 (in Japanese with English abstract).

Fujii, S., Sohma, T., Goto, M., Kamishima, T., Shimizu, M., Kaneko, K, et al. (1992) 1:100,000 scale geological map. Naigai Map Production Co., 201 p (in Japanese)*.

Fujita, K. and Nakagawa, C. (1948) Tertiary in the Tonami area, Toyama Prefecture. The Journal of the Geological Society of Japan, 54, 125–125 (in Japanese).

Fukui Prefecture (2010) Geological Map of Fukui Prefecture and Its Explanatory Note. Fukui Pref. Public Co. Construct. Tech., 173 p.

Gain, S. E., Gréau, Y., Henry, H., Belousova, E., Dainis, I., Griffin, W. L. and O'reilly, S. Y. (2019) Mud Tank Zircon: Long-term evaluation of a reference material for U–Pb dating, Hf-isotope analysis and trace element analysis. Geostandards and Geoanalytical Research, 43, 339–354.

Ganzawa, Y. (1983) "Green Tuff" Movement defined by fission track ages of igneous rocks Part 2: Futomiyama area of Toyama Prefecture, central Japan. The Journal of the Geological Society of Japan, 89, 271–286 (in Japanese with English abstract).

Garfunkel, Z., Anderson, C.A. and Schubert, G. (1986) Mantle circulation and the lateral migration of subducted slabs. Journal of Geophysical Research, 91, 7205–7223.

Geological Survey of Japan, AIST (2022) Seamless digital geological map of Japan V2 1: 200,000. https://gbank.gsj.jp/seamless [Accessed: Jun. 17th, 2022]

George, R., Turner, S., Hawkesworth, C., Bacon, C.R., Nye, C., Stelling, P. and Dreher, S. (2004) Chemical versus temporal controls on the evolution of tholeiitic and calc-alkaline magmas at two volcanoes in the Alaska–Aleutian arc. Journal of Petrology, 45, 203–219.

Gill, J.B., Stork, A.L. and Whelan, P.M. (1984) Volcanism accompanying back-arc basin development in the southwest Pacific. Tectonophysics, 102, 207–224.

Girard, G. and Stix, J. (2009) Magma recharge and crystal mush rejuvenation associated with early post-collapse upper basin member rhyolites, Yellowstone Caldera, Wyoming. Journal of Petrology, 50, 2095–2125.

Goldstein, S.L., O'Nions, R.K. and Hamilton, P.J. (1984) A Sm-Nd isotopic study of atmospheric dusts and particulates from major river systems. Earth and Planetary Science Letters, 70, 221–236.

Gradstein, F.M., Ogg, J.G., Schmitz, M.D. and Ogg, G.M., 2020. Geologic time scale 2020, Elsevier, Amsterdam, 1357 p., https://doi.org/10.1016/C2020-1-02369-3.

Griffin, W.L., Pearson, N.J., Belousova, E., Jackson, S.E., Achterbergh, E.V., O'Reilly, S.Y. and Shee, S.R. (2000) The Hf isotope composition of cratonic mantle: LAM-MC-ICPMS analysis of zircon megacrysts in kimberlites. Geochimica et Cosmochimica Acta, 64, 133–147.

Grimes, C.B., John, B.E., Kelemen, P.B., Mazdab, F.K., Wooden, J.L., Cheadle, M.J., Hanghøj, K. and Schwartz, J.J. (2007) Trace element chemistry of zircons from oceanic crust: A method for distinguishing detrital zircon provenance. Geology, 35, 643–646.

Hall, R. (2002) Cenozoic geological and plate tectonic evolution of SE Asia and SW Pacific: computer-based reconstructions, model and animations. Journal of Asian Earth Sciences, 20, 353–431.

Hamamoto, T., Yuhara, M., Miyazaki, T., Fukase, M., Kondo, H., Ikawa, T., Ishioka, J., Kagami, H. and Shuto, K. (2000) Rb, Sr, Sm and Nd separation from rocks, minerals and natural water using ion-exchange resin. Science Reports of Niigata University, Series E (Geology), 15, 49–58.

Hanyu, T., Tatsumi, Y., Nakai, S., Chang, Q., Miyazaki, T., Sato, K., Tani, K., Shibata, T. and Yoshida, T. (2006) Contribution of slab melting and slab dehydration to magmatism in the NE Japan arc for the last 25 Myr: Constraints from geochemistry. Geochemistry Geophysics Geosystems, 7, Q08002, doi:10.1029/2005GC001220.

Hayakawa, H. (1983) Stratigraphy and geochronology of the Neogene in the west part of the Yatsuo area, Toyama Prefecture, Central Japan. News Osaka Micropaleontologist, 10, 1–13 (in Japanese with English abstract).

Hayakawa, H. and Danhara, T. (1986) Fission-track age of a tuff layer intercalated in the Kurosedani Formation, Yatsuo area, central Japan. News of Osaka Micropaleontologist, 14, 63–69 (in Japanese with English abstract).

Hayakawa, H. and Takemura, A. (1987) The Neogene System in the Yatsuo area, Toyama Prefecture, central Japan. The Journal of the Geological Society of Japan, 93, 717–732 (in Japanese with English abstract).

Hayashida, A., Fukui, T. and Torii, M. (1991) Paleomagnetism of the Early Miocene Kani Group in southwest Japan and its implication for the opening of the Japan Sea. Geophysical Research Letters, 18, 1095–1098.

Herzberg, C., Condie, K. and Korenaga, J. (2010) Thermal history of the Earth and its petrological expression. Earth and Planetary Science Letters, 292, 79–88.

Heuret, A. and Lallemand, S. (2005) Plate motions, slab dynamics and back-arc deformation. Physics of the Earth and Planetary Interiors, 149, 31–51.

Hiroi, Y. (1978) Geology of the Unazuki District in the Hida Metamorphic Terrain, central Japan. The Journal of the Geological Society of Japan, 84, 521–530 (in Japanese with English abstract).

Hiroi, Y. (1983) Progressive metamorphism of the Unazuki Pelitic Schists in the Hida Terrane, central Japan. Contribution to Mineralogy and Petrology, 82, 334–350.

Hoang, N., Itoh, J. and Miyagi, I. (2011) Subduction components in Pleistocene to recent Kurile arc magmas in NE Hokkaido, Japan. Journal of Volcanology and Geothermal Research, 200, 255–266.

Horie, K., Tsutsumi, Y., Takehara, M. and Hidaka, H. (2018) Timing and duration of regional metamorphism in the Kagasawa and Unazuki areas, Hida metamorphic complex, southwest Japan. Chemical Geology, 484, 148–167.

Horne, A. V., Sato, H. and Ishiyama, T. (2017) Evolution of the Sea of Japan back-arc and some unsolved issues. Tectonophysics, 710–711, 6–20.

Hoshi, H. (2018) Miocene clockwise rotation of Southwest Japan. The Journal of the Geological Society of Japan, 124, 675–691 (in Japanese with English abstract).

Hoshi, H., Kato, D., Ando, Y. and Nakashima, K. (2015) Timing of clockwise rotation of Southwest Japan: constraints from new middle Miocene paleomagnetic results. Earth, Planets and Space, 67, 92, doi: 10.1186/s40623-015-0266-3.

Hoshina, H. (1984) Neogene volcanic rocks in the northern part of the Noto Peninsula, with special reference to aphyric andesites. Memoir of the Geological Society of Japan, 24, 45–58 (in Japanese with English abstract).

Ichihara, M., Ishio, H., Morishita, A., Nakagawa, C. and Tsuda K. (1950) Tertiary in the western Toyama Prefecture and the eastern Ishikawa Prefecture: geological studies in Toyama and Ishikawa prefectures 2. Science of the Earth (Chigaku), 1, 14–26 (in Japanese)*.

Ichimura, K (1935) Fossils from the Tertiary in the southeast part of Tomari Town, Shimoniikawa District, Toyama Prefecture. The Journal of the Geological Society of Japan, 42, 59–73 (in Japanese)*.

Iizuka, T., Yamaguchi, T., Hibiya, Y. and Amelin, Y. (2015) Meteorite zircon constraints on the bulk Lu–Hf isotope composition and early differentiation of the Earth. PNAS, 112, 5331–5336.

Iizuka, T., Yamaguchi, T., Itano, K., Hibiya, Y. and Suzuki, K. (2017) What Hf isotopes in zircon tell us about crust–mantle evolution. Lithos, 274–275, 304–327.

Ikebe, N. (1949) Tertiary in the western Toyama Prefecture and the eastern Ishikawa Prefecture: geological studies in Toyama and Ishikawa prefectures 1. Sci. Earth (Chigaku), 1, 14–26 (in Japanese)*.

Ikebe, N. (1950) Geology of Mt. Takashouzu, Toyama Prefecture: Special reference to the Johana fault and the Kaminashi fault. Nature and Society, 5–6, 12–16 (in Japanese).

Ikebe, N. and Nakaseko, Y. (1955) Re-examination of the Neogene stratigraphy of the Toyama productive basin. The Journal of the Geological Society of Japan, 61, 360–360 (in Japanese).

Imamura, S. (1931) Occurrence of Operculina around Yatsuo area, Toyama Prefecture and its relation with *Vicarya verueuili* (*D'Archiac*) var. The Journal of the Geological Society of Japan, 38, 541–542 (in Japanese).

Imamura, S. (1932) New locality of moonstone rhyolite in Toyama Prefecture. The Journal of the Geological Society of Japan, 39, 669–670 (in Japanese)*.

Imamura, S. (1936) Geology Geology of the Jinzu-gawa River Region. Journal of Toyama High School Natural History Club, a, 1–25 (in Japanese)*.

Imamura, S. (1936) Geology Geology of the Jinzu-gawa River Region. Journal of Toyama High School Natural History Club, 3, 1–11 (in Japanese)*.

Imamura, S., Hase, A., Murata, S., Yoshida, H., Tai, Y. and Nakajima, H. (1951) On the Neogene Tertiary formation in the Uozu-Kamiichi district, in the eastern part of Toyama Prefecture. Geological Report of Hiroshima University, 1, 15–36 (in Japanese with English abstract).

Imaoka, T., Kiminami, K., Nishida, K., Takemoto, M., Ikawa, K., Itaya, T., Kagami, H. and Iizumi, S. (2011) K–Ar age and geochemistry of the SW Japan

Paleogene cauldron cluster: Implications for Eocene–Oligocene thermo-tectonic reactivation. Journal of Asian Earth Sciences, 40, 509–533.

Inoue, M., Sakamoto, T. and Nozawa, T. (1964) Geological Map of the Johana District. Quadrangle Series, 1: 50,000, Geological Survey of Japan, 32p (in Japanese with English abstract).

Ishida, H., Ishiwatari, A., Kagami, H. (1998) The Mt. Wasso moonstone rhyolitic welded tuff in the Neogene Hokuriku Group, central Japan. The Journal of the Geological Society of Japan, 104, 281–295 (in Japanese with English abstract).

Ishiwatari, A. and Ohama, H. (1997) Clinopyroxene basalt dikes in the Miocene Iwaine Formation, Hokuriku Province, Japan: Various continental arc magmas including shoshonite and origin of the clinopyroxene phenocrysts. The Journal of the Geological Society of Japan, 103, 565–578 (in Japanese with English abstract).

Ishiwatari, A., Tsuchihashi, N., Shuto, K. and Sato, M. (2007) Sr–Nd isotopic ratio of the Miocene adakite in western Toyama Prefecture, central Japan and Sr content of its plagioclase. 114th Annual Meeting of the Geological Society of Japan, Abstract, 357–357 (in Japanese).

Ishiwatari, A. and Tsujimori, T. (2001) Rocks of the Japan Sea and Surrounding Areas. Japan Sea Study Series, Toyama Prefecture, 59 p (in Japanese).

Ishiyama, T., Sato, H., Kato, N., Koshiya, S., Abe, S., Shiraishi, K. and Matsubara, M. (2017) Structures and active tectonics of compressionally reactivated back-arc failed rift across the Toyama trough in the Sea of Japan, revealed by multiscale seismic profiling. Tectonophysics, 710–711, 21–36.

Ito, M. (2022) Field manual: The world of sedimentary structures. Asakura Publishing Co., Ltd., 210 p (in Japanese).

Ito, Y. (1986) Diatom biostratigraphy of the Neogene system in the Hokuriku orivince, central Japan. News of Osaka Micropaleontologist, 14, 1–27 (in Japanese with English abstract).

Itoh, Y. (1985) Stratigraphy and geochronology of the Neogene in the Tomari area, Toyama Prefecture, Central Japan. News of Osaka Micropaleontologist, 13, 1–12 (in Japanese with English abstract).

Itoh, Y. (1988) Differential rotation of the eastern part of southwest Japan inferred from paleomagnetism of Cretaceous and Neogene rocks. Journal of Geophysical Research, 93, 3401–3411.

Itoh, Y., Doshida, S., Kitada, K. and Danhara, T. (2001) Paleomagnetism and fission-track ages of the Mt. Wasso moonstone rhyolitic welded tuff in the Ishikawa Prefecture, central Japan. Bulletin of the Geological Survey of Japan, 52, 573–579 (in Japanese with English abstract).

Itoh, Y. and Hayakawa, H. (1988) Magnetostratigraphy of Neogene rocks around the Yatsuo area in Toyama Prefecture, Japan. The Journal of the Geological Society of Japan, 94, 515–525 (in Japanese with English abstract).

Itoh, Y. and Hayakawa, H. (1989) On the boundary of polarity chron C5B/C5C in the Neogene section of the Yatsuo area in Toyama Prefecture, Japan. The Journal of the Geological Society of Japan, 95, 133–136 (in Japanese with English abstract).

Itoh, Y and Kitada, K. (2003) Early Miocene rotational process in the eastern part of south-west Japan inferred from paleomagnetic studies. Island Arc, 12, 348–356.

Itoh, Y., Kusumoto, S. and Uda, T. (2016) Tanayama Terrace, A Multidisciplinary Study of an Arc-Arc Collision Front. LAP LAMBERT Academic Publ., Saarbrücken, 103 p.

Itoh, Y., Nakajima, T. and Takemura, A. (1997) Neogene deformation of the back-arc shelf of Southwest Japan and its impact on the paleoenvironments of the Japan Sea. Tectonophysics, 281, 71–82.

Itoh, Y. and Watanabe, M. (2000) Refined magnetostratigraphy of the Early Miocene sequence in the Yatsuo area, central Japan. Bulletin of the Geological Survey of Japan, 51, 37–45 (in Japanese with English abstract).

Itoh, Y. and Watanabe, M. (2005) Fission-track dating and paleomagnetic polarity of the Lower Miocene in the Yatsuo area, central Japan. Bulletin of the Geological Survey of Japan, 56, 425–429 (in Japanese with English abstract).

Itoh, Y. and Watanabe, M. (2006) Fission-track dating of the Lower to Middle Miocene in the Uozu area, central Japan. Bulletin of the Geological Survey of Japan, 57, 57–59 (in Japanese with English abstract).

Itoh, Y., Yamamoto, A., Iwano, H., Danhara., T. and Watanabe, M. (2000) Paleomagnetism and fission-track ages of the Miocene sequence in the Kanazawa and Iozen areas, central Japan. Bulletin of the Geological Survey of Japan, 51, 495–504 (in Japanese with English abstract).

Itoh, Y., Yanagisawa, Y. and Watanabe, M. (1999) Magnetostratigraphy and diatom biostratigraphy of Neogene rocks distributed in the Yatsuo area, central Japan. Bulletin of the Geological Survey of Japan, 50, 215–223 (in Japanese with English abstract).

Iwaki, H. and Itoh, Y. (2000) Paleomagnetic Study of Neogene Rocks Around the Uozu Area, Eastern Part of Toyama Prefecture. Bulletin of the Geological Survey of Japan, 51, 229–236 (in Japanese with English abstract).

Iwano, H., Orihashi, Y., Hirata, T., Ogasawara, M., Danhara, T., Horie, K., Hasebe, N., Sueoka, S., Tamura, A., Hayasaka, Y., Katsube, A., Ito, H., Tani, K., Kimura, J., Chang, Q., Kouch, Y., Haruta, Y. and Yamamoto, K. (2013) An inter-laboratory evaluation of OD-3 zircon for use as a secondary U–Pb dating standard. Island Arc, 22, 382–394.

Japan National Oil Corporation (1985) Survey Report of MITI “Toyama” Well. Japan National Oil Corporation, 60 p (in Japanese)*.

Jochum, K.P., Weis, U., Schwager, B., Stoll, B., Wilson, S.A., Haug, G.H., Andreae, M.O. and Enzweiler, J. (2016) Reference Values Following ISO Guidelines for Frequently Requested Rock Reference Materials. Geostandards and Geoanalytical Research, 40, 333–350.

Jolivet, L., Tamaki, K. and Fournier, M. (1994) Japan Sea, opening history and mechanism: A synthesis. Journal of Geophysical Research, 99, 22237–22259.

Jónasson, K. (2007) Silicic volcanism in Iceland: Composition and distribution within the active volcanic zones. Journal of Geodynamics, 43, 101–117.

Kaneko, K. (2001) Stratigraphy and geotectonic history of Miocene volcanic–volcaniclastic rocks in the eastern part of Toyama Prefecture, central Japan. The Journal of the Geological Society of Japan, 107, 729–748 (in Japanese with English abstract).

Kaneko, K., Nagata, M., Kouchi, Y., Yamamoto, K. and Otoh, S. (2019) Zircon U–Pb zircon ages of the Futomiyama Group in Toyama Prefecture, contral Japan. The Journal of the Geological Society of Japan, 125, 781–792 (in Japanese with English abstract).

Kaneoka, I., Matsuda, J., Lelikov, E. P. and S'edin, V. T. (1996) Isotope geochemistry of igneous rocks in the Japan Sea. In Isezaki, N., Bersenev, I. I., Tamaki, K., Karp, B. Y. and Lelikov, E. P. (eds.) Geology and Geophysics of the Japan Sea (Japan-USSR Monograph Series, Vol. 1), TERRAPUB, Tokyo, 369–383.

Kaneoka, I., Takigami, Y., Takaoka, N., Yamashita, S. and Tamaki, K. (1992) ^{40}Ar–^{39}Ar analysis of volcanic rocks recovered from the Japan Sea floor: constraints on the age of formation of the Japan Sea. In Tamaki, K., Suehiro, H., Allan, J., McWiliams, M. et al. (eds.) Proceedings of the Ocean Drilling Program, Scientific Results, 127/128, Pt. 2, Ocean Drilling Program, College Station, 819–836.

Kano, K. (2018) Stratigraphic framework of the Green Tuff successions in Japan with reference to the associated geologic events. The Journal of the Geological Society of Japan, 124, 781–803 (in Japanese with English abstract).

Kano, K., Harayama, S., Yamamoto, H., Takeuchi, M., Uto, K., Komazawa, M., Hiroshima, T. and Sudo, S. (1999) Geological Map of Japan 1:200,000, Kanazawa. Geological Survey of Japan (in Japanese).

Kano, K., Kato, H., Yanagisawa, Y. and Yoshida, F. (1991) Stratigraphy and Geologic History of the Cenozoic of Japan. Report of the Geological Survey of Japan, 274, Geological Survey of Japan, 114p.

Kano, K., Uto, K. and Ohguchi, T. (2007a) Stratigraphic review of Eocene to Oligocene successions along the eastern Japan Sea: Implication for early opening of the Japan Sea. Journal of Asian Earth Sciences, 30, 20–32.

Kano, K., Yamamoto, H. and Nakagawa, T. (2007b) Geology of the Fukui District. Quadrangle Series, 1:50,000, Geological Survey of Japan, AIST, 68 p (in Japanese with English abstract).

Kano, K., Yoshikawa, T., Yanagisawa, Y., Ogasawara, K. and Danhara, T. (2002) An unconformity in the early Miocene syn-rifting succession, northern Noto Peninsula, Japan: Evidence for short-term uplifting precedent to the rapid opening of the Japan Sea. Island Arc, 11, 170–184.

Kar, A., Weaver, B., Davidson, J. and Colucci, M. (1998) Origin of differentiated volcanic and plutonic rocks from Ascension Island, South Atlantic Ocean. Journal of Petrology, 39, 1009–1024.

Kaseno, Y. (1964) Biostratigraphic problems of the Neogene strata in Hokuriku region, central Japan. Fossils, 7, 27–35 (in Japanese with English abstract).

Kaseno, Y. (1993) Geology of Ishikawa-ken, Japan (with Geological Maps). Ishikawa Prefecture and the Geological Institute of Hokuriku, 321 p (in Japanese).

Kaseno, Y. and Shimokawa, H. (1989) Stratigraphy of the Neogene strata in Ishikawa and Toyama Prefectures. Kobayashi, I. and Tateishi, M. (eds.) Paleo-Japan Sea, 2, 56–64 (in Japanese)*.

Kaseno, Y., Sakamoto, T. and Ishida, S. (1961) A contribution to the Neogene history of the eastern Hokuriku district, central Japan. Professor Jiro Makiyama Memorial Volume, 83–95 (in Japanese with English abstract).

Kashiwagi, K. (2012) Sedimentary environment of the Nirehara Formation (Lower Miocene) in the Yatsuo area, Toyama Prefecture of central Japan and Paleozoic and Mesozoic radiolarian fossils from chert pebbles and cobbles. Memoir of the Fukui Prefectural Dinosaur Museum, 11, 27–47 (in Japanese with English abstract).

Katsuragi, T. and Ishiwatari, A. (2001) Petrological study about alkali rich Miocene basalt in north part of Fukui prefecture. 108th Annual Meeting of the Geological Society of Japan, Abstract, 297–297 (in Japanese).

Katsuragi, T. and Ishiwatari, A. (2002) Miocene volcanic rocks of the Ito Formation, Echizen Central Mountains, Fukui prefecture: primitive calc-alkaline magmas. 109th Annual Meeting of the Geological Society of Japan, Abstract, 318–318 (in Japanese).

Kimura, G., Hashimoto, Y., Kitamura, Y., Yamaguchi, A. and Koge, H. (2014) Middle Miocene swift migration of the TTT triple junction and rapid crustal growth in southwest Japan: A review. Tectonics, 33, 1219–1238.

Kimura, G. and Tamaki, K. (1986) Collision, rotation, and back-arc spreading in the region of the Okhotsk and Japan seas. Tectonics, 5, 389–401.

Kimura, J.I., Kunikiyo, T., Osaka, I., Nagao, T., Yamauchi, S., Kakubuchi, S., Okada, S., Fujibayashi, N., Okada, R., Murakami, H., Kusano, T., Umeda, K., Hayashi, S., Ishimaru, T., Ninomiya, A. and Tanase, A. (2003) Late Cenozoic volcanic activity in the Chugoku area, southwest Japan arc during back-arc basin opening and reinitiation of subduction. The Island Arc, 12, 22–45.

Kimura, J.I., Stern, R. J. and Yoshida, T. (2005) Reinitiation of subduction and magmatic responses in SW Japan during Neogene time. Geological Society of America Bulletin, 117, 969–986.

Kobayashi, H., Yamaji, A. and Masuda, F. (2005) Miocene stratigraphy, sedimentary environments and tectonics in the Wajima area, Noto Peninsula, southern margin of the Japan Sea. The Journal of the Geological Society of Japan, 111, 286–299 (in Japanese with English abstract).

Komiya, T. (2004) Material circulation model including chemical differentiation within the mantle and secular variation of temperature and composition of the mantle. Physics of the Earth and Planetary Interiors, 146, 333–367.

Lallemand, S. and Jolivet, L. (1986) Japan Sea: a pull-apart basin? Earth and Planetary Science Letters, 76, 375–389.

Leat, P.T., Larter, R.D. and Millar, I.L. (2007) Silicic magmas of Protector Shoal, South Sandwich arc: indicators of generation of primitive continental crust in an island arc. Geological Magazine, 144, 179–190.

Lebti, P.P., Thouret, J.C., Wörner, G. and Fornari, M. (2006) Neogene and Quaternary ignimbrites in the area of Arequipa, Southern Peru: Stratigraphical and petrological correlations. Journal of Volcanology and Geothermal Research, 154, 251–275.

LeMaitre, R.W., Streckeisen, A., Zanettin, B., Le Bas, M.J., Bonin, B. (2002) A classification of igneous rocks and glossary of terms, second edition. Blackwell, Oxford, 236 p, https://doi.org/10.1017/CBO9780511535581.

Li, B., Wang, X., Du, L., Xiang, Z., Tang, G. and Huang, Z. (2020) Zircon U–Pb ages and geochemistry of granite porphyries in the Yangla Cu deposit, SW China: Constraints on petrogenesis and tectonic evolution of the Jinshajiang Suture Belt. Geofluids, 9, 1–35.

Lindsay, J.M., Schmitt, A.K., Trumbull, R.B., Silva, S.L.D., Siebel, W. and Emmermann, R. (2001) Magmatic evolution of the La Pacana Caldera system, central Andes, Chile: Compositional variation of two cogenetic, large-volume felsic ignimbrites. Journal of Petrology, 42, 459–486.

López, J. C. and Ishiwatari, A. (2002) Petrogenesis of the tholeiitic basalt, calc-alkaline basaltic andesite and high magnesian andesite lava succession of the Oligo-Miocene Anamizu Formation in northeastern Noto Peninsula, central Japan. Journal of Mineralogical and Petrological Sciences, 97, 85–113.

Lowenstern, J.B., Bleick, H., Vazquez, J.A., Castro, J.M. and Larson, P.B. (2012) Degassing of Cl, F, Li, and Be during extrusion and crystallization of the

rhyolite dome at Volcán Chaitén, Chile during 2008 and 2009. Bulletin of Volcanology, 74, 2303–2319.

Makiyama, J. (1930) Outline of Tertiary in Ishikawa and Toyama Prefecture. Chikyu (Earth), 14, 161–174 (in Japanese)*.

Martin, A.K. (2011) Double saloon door tectonics in the Japan Sea, Fossa Magna, and the Japan Island Arc. Tectonophysics, 498, 45–65.

Martin, H., Smithies, R.H., Rapp, R., Moyen, J.-F. and Champion, D. (2005) An over view of adakite, tonalite–trondhjemite–granodiorite (TTG), and sanukitoid: relationships and some implications for crustal evolution. Lithos, 79, 1–24.

Martynov, Y.A. and Khanchuk, A.I. (2013) Cenozoic volcanism of the eastern Sikhote Alin: Petrological studies and outlooks. Petrology, 21, 85–99.

Martynov, Y.A., Khanchuk, A.I., Grebennikov, A.V., Chashchin, A.A. and Popov, V.K. (2017) Late Mesozoic and Cenozoic volcanism of the East Sikhote-Alin area (Russian Far East): A new synthesis of geological and petrological data. Gondwana Research, 47, 358–371.

Maruyama, S. and Ebisuzaki, T. (2017) Origin of the Earth: A proposal of new model called ABEL. Geoscience Frontiers, 8, 253–274.

Matsumoto, T. and Ikebe, N. (1958) Volcano stratigrafical studies on the Neogene Hokuriku province, North Central Japan, with special reference to the volcanic rocks in Toyama basin. Journal of the Institute of Polytechnic, Osaka City University, Series G., 3, 79–112.

Matsuo, H. and Nakanishi, N. (1967) The Iozen Formation and the Iozen Flora in the northern foot area of Mt. Iozen, Kanazawa City. Professor Ichiro Hayasaka's 77th Birthday Memorial Volume, Professor Ichiro Hayasaka's 77th Birthday Memorial committee, 287–296 (in Japanese)*.

McDermott, F., Delfin Jr., F.G., Defant, M.J. Turner, S. and Maury, R. (2005) The petrogenesis of volcanics from Mt. Bulusan and Mt. Mayon in the Bicol arc, the Philippines. Contribution to Mineralogy and Petrology, 150, 652–670.

McPhie, J., Doyle, M. and Allen, R. (1993) Volcanic Textures: a guide to the interpretation of textures in volcanic rocks. University of Tasmania, Hobart, 196 p.

Miller, M.S. and Kennett, B.L.N. (2006) Evolution of mantle structure beneath the northwest Pacific: Evidence from seismic tomography and paleogeographic reconstructions. Tectonics, 25, TC4002, doi:10.1029/2005TC001909.

Miura, S. (1979) On the volcanostratigraphy of the Lower Neogene Tertiary in Hokuriku district, central Japan. Memoir of the Geological Society of Japan, 16, 149–155 (in Japanese with English abstract).

Miura, S. and Azuma, Y. (1974) On some problems relating to the Early Miocene formations in the Hokuriku sedimentary basin, central Japan. Memoir of the Faculty of Education, Fukui University, Series II, Natural Science, 24, 15–25 (in Japanese with English abstract).

Miyashiro, A. (1974) Volcanic rock series in island arcs and active continental margins. American Journal of Science, 274, 321–355.

Miyazaki, T., Shuto, K. (1998) Sr and Nd isotope ratios of twelve GSJ rock reference samples. Geochemical Journal, 32, 345–350.

Miyoshi, M, Shibata, T., Yoshikawa, M., Sano, T., Shinmura, T. and Hasenaka, T. (2011) Genetic relationship between post-caldera and caldera-forming magmas from Aso volcano, SW Japan: Constraints from Sr isotopic and trace element compositions. Journal of Mineralogical and Petrological Sciences, 106, 114–119.

Mo, X., Niu, Y., Dong, G., Zhao, Z., Hou, Z., Zhou, S. and Ke, S. (2008) Contribution of syncollisional felsic magmatism to continental crust growth: A case study of Paleogene Lizizong volcanic Succession in southern Tibet. Chemical Geology, 250, 49–67.

Molnar, P. and Atwater, T. (1978) Interarc spreading and Cordilleran tectonics as alternates related to the age of subducted oceanic lithosphere. Earth and Planetary Science Letters, 41, 330–340

Momma, K., Tsutsumi, Y., Sano, T., Miyawaki, R., Shigeoka, M. and Yokokawa, K. (2016) Chevkinite-bearing tuffs from the Boso and Noto peninsulas in central Japan and from Primorye, Far East Russia. Memoirs of the National Museum of Nature and Science, Tokyo, 51, 89–98.

Moresi, L.N. and Solomatov, V.S. (1995) Numerical investigation of 2D convection with extremely large viscosity variations. Physics of Fluids, 7, 2154–2162.

Morishita, A. (1950) Neogene Echinoids from Ishikawa and Toyama Prefecture. The Journal of the Geological Society of Japan, 55, 254–259 (in Japanese with English abstract).

Morishita, T., Arai, S., Wakimoto, R., Mizuta, T., Ishiyama, D., Sato, H., Umeka, M., Fujisawa, A., Moriichi, S., Ohzeko, M., Mori, T., Yamazaki, M. and Yamamoto, S. (2006) Petrological characteristics of dark-colored silica veins in Tertiary rhyolite (the Iozen Formation) from the southern part of Ishikawa Prefecture, Japan. The Journal of the Geological Society of Japan, 112, 273–283 (in Japanese with English abstract).

Murphy, M.A. and Salvador, A. (1999) International stratigraphic guide: An abridged version. Episodes, 22, 255–271.

Nakagawa, T. and Tahara, N. (1991) The Miocene lithostratigraphy in the northern part of the Niu mountains, Fukui Prefecture, central Japan. Professor Sizuka Miura Memorial Volume, Professor Shizuka Miura Memorial Committee, 11–27 (in Japanese with English abstract).

Nakajima, M. and Mizushima, S. (1984) Fission-track ages of Miogypsina-Operculina horizons in Hokuriku District, central Japan. The Journal of the Geological Society of Japan, 90, 667–670 (in Japanese with English abstract).

Nakajima, M., Morimoto, Y., Suzuki, Y., Watanabe, I. and Miura, S. (1983) Fission Track Ages of the Tertiary Rocks Distributed in Fukui Prefecture. Memoir of the Faculty of Education, Fukui University, Series II, Natural Science, 33, 53–65 (in Japanese with English abstract).

Nakajima, T. (2013) Late Cenozoic tectonic events and intra-arc basin development in Northeast Japan. In Itoh, Y. (ed.) Mechanism of Sedimentary basin formation–Multidisciplinary approach on active plate margins. InTech, Rijeka, 153–189.

Nakajima, T. (2018) Tectonics of sedimentary basins in and around Japan since the opening of the Sea of Japan. The Journal of the Geological Society of Japan, 124, 693–722 (in Japanese with English abstract).

Nakajima, T., Iwano, H., Danhara, T., Yamashita, T., Yanagisawa, Y., Tanimura, Y., Watanabe, M., Sawaki, T., Nakanishi, S., Mitsuishi, H., Yamashina, O., Imahori, S. (2019) Revised Cenozoic chronostratigraphy and tectonics in the Yatsuo Area, Toyama Prefecture, central Japan. The Journal of the Geological Society of Japan, 125, 483–516 (in Japanese with English abstract).

Nakajima, T., Yoshikawa, K. and Okitsu, O. (2021) Geologic structures and basin formation tectonics in and around Toyama Trough, the Sea of Japan. The Journal of the Geological Society of Japan, 127, 165–188 (in Japanese with English abstract).

Nakakuni, T. and Mura, E. (2013) Dynamics of slab rollback and induced back-arc basin formation. Earth and Planetary Science Letters, 361, 287–297.

Nakama, T., Hirata, T., Otoh, S., Aoki, K., Yanai, S. and Maruyama, S. (2010) Paleogeography of the Japanese Islands: Age spectra of detrital zircon and provenance history of the orogen. Journal of Geography (Chigaku Zasshi), 119, 1161–1172 (in Japanese with English abstract).

Nakaseko, Y. (1953) On the stratigraphy of the upper Neogene Formation in the southern part of Toyama Prefecture. Southern and Northern Colleges of Osaka University, Science Report, 2, 87–100 (in Japanese)*.

Nakaseko, Y. (1954) Correction of the stratigraphy of the upper Neogene Formation in the southern Toyama Southern and Northern Colleges of Osaka University, Science Report, 3, 97–105 (in Japanese)*.

Naranjo, J.A., Singer, B.S., Jicha, B.R., Moreno, H. and Lara, L.E. (2017) Holocene tephra succession of Puyehue-Cordón Caulle and Antillanca/Casablanca volcanic complexes, southern Andes (40–41°S). Journal of Volcanology and Geothermal Research, 332, 109–128.

Neo, N., Takazawa, E. and Shuto, K. (2006) Quantitative analysis of trace elements in basaltic and peridotitic rocks by quadruple inductively-coupled plasma mass spectrometry. Report of Grant-in-Aid for Scientific Research (C), no.16540413, 79–94 (in Japanese).

Nohda, S. (2009) Formation of the Japan Sea basin: Reassessment from Ar–Ar ages and Nd–Sr isotopic data of basement basalts of the Japan Sea and adjacent regions. Journal of Asian Earth Sciences, 34, 599–609.

Nomura, T., Yonemichi, H. and Fujita, Y. (1978) Mutual Relations Between Collapse, Subsidence and Volcanism at the Initial Stage of the Green Tuff Geosyncline: Geologic Structure of the Tertiary Formations in the Upper Reaches of the River Fuse, Toyama Prefecture. Chikyukagaku (Earth Science), 32, 185–193 (in Japanese with English abstract).

Nozawa, T. and Sakamoto, T. (1960) Geological Map of the Gohyakkoku District. Quadrangle Series, 1: 50,000, Geological Survey of Japan, 68p (in Japanese with English abstract).

Nozawa, T., Sakamoto, T. Kano, T. and Inazuki, T. (1981) Geological Map of the Shirakimine District. Quadrangle Series, 1: 50,000, Geological Survey of Japan, 85p (in Japanese with English abstract).

Ogasawara, K., Kaneko, K., Shimizu, M. and Hirooka, K. (1990) Neogene of the Yatsuo area. 97th Annu. Meeting of the Geological Society of Japan, Excursion Guide Book, 1–23 (in Japanese).

Ogasawara, K., Takano, M., Nagato, H. and Nakano, T. (2008) Cenozoic molluscan faunas and climatic changes in the northern Pacific related to Pacific gateways: review and perspective. Bulletin of the Geological Survey of Japan, 59, 355–364.

Okamura, S., Arculus, R. J., Martynov, Y. A., Kagami, H., Yoshida, T. and Kawano, Y. (1998) Multiple magma sources involved in marginal-sea formation: Pb, Sr, and Nd isotopic evidence from the Japan Sea region. Geology, 26, 619–622.

Okamura, S., Inaba, M., Adachi, Y., Shinjo, R. (2016) Miocene-Pliocene mantle depletion event in the northern Fossa Magna, western NE Japan. Journal of Geodynamics, 97, 42–61.

Osozawa, S., Usuki, T., Usuki, M., Wakabayashi, J. and Jahn, B. (2019) Trace elemental and Sr-Nd-Hf isotopic compositions, and U-Pb ages for the Kitakami adakitic plutons: Insights into interactions with the early Cretaceous TRT triple junction offshore Japan. Journal of Asian Earth Sciences, 184, 103968.

Ota, H., Kaneko, K., Yamamoto, K. and Otoh, S. (2018) Detrital-zircon ages from the Yatsuo Group in Toyama Prefecture and its provenance. 125th Annual Meeting of the Geological Society of Japan, Abstract, 236–236 (in Japanese).

Ota, H., Kaneko, K., Yamamoto, K. and Otoh, S. (2019) The Tori Formation in western Toyama Prefecture: Zircon ages and provenance. 126th Annual Meeting of the Geological Society of Japan, Abstract, 215–215 (in Japanese).

Otofuji, Y., Matsuda, T. and Nohda, S. (1985) Opening mode of the Japan Sea inferred from the paleomagnetism of the Japan Arc. Nature, 317, 603–604.

Oyama, K. (1950) Studies on fossil molluscan biocoenosis, no. 1. Biocoenological studies of the mangrove swamps, with description of new species from Yatsuo Group. Reports of the Geological Survey of Japan, 132, 16 p.

Ozaki, M. (2010) 1:200,000 Geological Map of the Northern Part of Noto Peninsula. S-1. Seamless Geoinformation of Coastal Zone "Northern Coastal Zone of Noto Peninsula", Geological Survey of Japan, AIST, 15p (in Japanese with English abstract).

Pastor-Galán, D., Spencer, C.J., Furukawa, T. And Tsujimori, T. (2021) Evidence for crustal removal, tectonic erosion and flare-ups from the Japanese

evolving forearc sediment provenance. Earth and Planetary Science Letters, 564, 116893.

Pearce, J.A., Harris, N.B.W. and Tindle, A.G. (1984) Trace element discrimination diagrams for the tectonic interpretation of granitic rocks. Journal of Petrology, 25, 956–983.

Peccerillo, A., Barberio, M.R., Yirgu, G., Ayalew, D., Barbieri, M. and Wu, T.W. (2003) Relationships between mafic and peralkaline silicic magmatism in continental rift settings: a petrological, geochemical and isotopic study of the Gedemsa volcano, central Ethiopian Rift. Journal of Petrology, 44, 2003–2032.

Peccerillo, A., Taylor, S.R. (1976) Geochemistry of Eocene calc-alkaline volcanic rocks from the Kastamonu area, Northern Turkey. Contribution to Mineralogy and Petrology, 58, 63–81.

Pearce, J.A. and Stern, R.J. (2006) Origin of Back-Arc Basin Magmas: Trace Element and Isotope Perspectives. Back-Arc Spreading Systems: Geological, Biological, Chemical, and Physical Interactions, Geophysical Monograph Series 166, 63–86, 10.1029/166GM06.

Potter, P.E. and Szatmari, P. (2015) The global and Late Miocene and the deep earth: Model for earlier orogenies. Marine and Petroleum Geology, 68, 178–191.

Putirka, K.D., Dorn, C., Hinkel, N.R. and Unterborn, C.T. (2021) Compositional diversity of rocky exoplanets. Elements, 17, 235–240.

Reagan, M.K., Sims, K.W.W., Erich, J., Thomas, R.B., Cheng, H., Edwards, R.L., Layne, G. and Ball, L. (2003) Time-scales of differentiation from mafic parents to rhyolite in North American continental arcs. Journal of Petrology, 44, 1703–1726.

Ren, R., Tamaki, K., Li., S. and Junxia, Z. (2002) Late Mesozoic and Cenozoic rifting and its dynamic setting in Eastern China and adjacent areas. Tectonophysics, 344, 175–205.

Ricard, Y., Doglioni, C. and Sabadini, R. (1991) Differential rotation between lithosphere and mantle: A consequence of lateral mantle viscosity variations. Journal of Geophysical Research, 96, 8407–8416.

Roeder, P.L. and Emslie, R.F. (1970) Olivine-liquid equilibrium. Contribution to Petrology and Mineralogy, 29, 275–289.

Rollinson, H. and Pease, V. (2021) Using geochemical data, to understand geological processes. Cambridge University Press, Cambridge, 346 p..

Rundnick, R.L. and Gao, S. (2003) Composition of the continental crust. In Rundnick, R.L. (Ed.) The crust, Treatise on geochemistry. Elsevier Oxford, 1–64.

Rundcnick, R.L. and Gao, S. (2014) Composition of the continental crust. In Holland, H.D. and Holland, K.K. (Eds.) Treatise in Geochemistry, Second Edition. Elsevier, Oxford, 1–51.

Rueda, H., Macías, J.L., Arce, J.L., Gardner, J.E. and Layer, P.W. (2013) The ~31 ka rhyolitic Plinian to sub-Plinian eruption of Tlaloc volcano, Sierra Nevada, central Mexico. Journal of Volcanology and Geothermal Research, 252, 73–91.

Rummel, L., Kaus, B.J.P., Baumann, T.S., White, R.W., et al. (2020) Insights into the compositional evolution of crustal magmatic systems from coupled petrological-geodynamical model. Journal of Petrology, 61, egaa029.

Sakamoto, T. (1966) Cenozic strata and structural development in the southern half of the Toyama basin, central Japan. Reports of the Geological Survey of Japan, 213, 28 p (in Japanese with English abstract).

Sakamoto, T., Imai, I., Mizuno, A., Sumi, Y. and Inoue, M. (1959) Cenozoic strata in the southern part of the Toyama sedimentary basin. Bulletin of the Geological Survey of Japan, 10, 1–8 (in Japanese with English abstract).

Sakamoto, T. and Nozawa, T. (1960) Geological Map of the Yatsuo District. Quadrangle Series, 1: 50,000, Geological Survey of Japan, 69p (in Japanese).

Sakayori, A., Kawamura, J., Yamagishi, T., Sugimoto, M. and Yoshida, T. (1997) Petrological characteristics of basalts from the Miocene Nanamagari Formation in Ishikawa Prefecture: Low-K basalts from the back-arc side of central Japan. Journal of Mineralogy, Petrology and Economic Geology, 92, 410–424 (in Japanese with English abstract).

Sano, S. (2015) New view of the stratigraphy of the Tetori Group in central Japan. Memoir of the Fukui Prefectural Dinosaur Museum, 14, 25–61.

Sasaki, O. and Ogasawara, K. (1986) Intertidal Molluscan Assemblage from the Miocene Sunakozaka Formation, Ishikawa-Toyama Area, Hokuriku District, Japan. Memoirs of the National Museum of Nature and Science, Tokyo, 19, 79–89 (in Japanese with English abstract).

Sato, H. (1989) Genetic Environments of High-Magnesian Andesite and Related Rocks. pp. 99, Report of Grant-in-Aid for Scientific Research (C), no. 61540593 (in Japanese).

Sato, M., Shuto, K., Nohara-Imanaka, R., Takazawa, E., Osanai, Y. and Nakano, N. (2014) Repeated magmatism at 34 Ma and 23-20 Ma producing high magnesian adakitic andesites and transitional basalts on southern Okushiri Island, NE Japan arc. Lithos, 205, 60–83.

Sato, M., Shuto, K., Uematsu, M., Takahashi, T., Ayabe, M., Takanashi, K., Ishimoto, H. and Kawabata, H. (2013) Origin of late Oligocene to middle Miocene adakitic andesites, high magnesian andesites and basalts from the back-arc margin of the SW and NE Japan arcs. Journal of Petrology, 54, 481–524.

Sawada, H., Isozaki, Y. and Maruyama, S. (2018a) Pattern of continental growth and its secular change. Journal of Geography (Chigaku Zasshi), 127, 705–721 (in Japanese with English abstract).

Sawada, H., Isozaki, Y., Sakata, S., Hirata, T. and Maruyama, S. (2018b) Secular change in lifetime of granitic crust and the continental growth: A new view from detrital zircon ages of sandstones. Geoscience Frontiers, 9, 1099–1115.

Sawada, H., Maruyama, S., Sakata, S. and Hirata, T. (2016) Detrital zircon geochronology by LA-ICP-MS of the Neoarchean Manjeri Formation in the Archean Zimbabwe craton– the disappearance of Eoarchean crust by 2.7 Ga? Journal of African Earth Sciences, 113, 1–11.

Schiano, P., Monzier, M., Eissen, J.P., Martin, H. and Koga, K.T. (2010) Simple mixing as the major control of the evolution of volcanic suites in the Ecuadorian Andes. Contribution to Petrology and Mineralogy, 160, 297–312.

Schmidt, M.E. and Grunder, A.L. (2011) Deep mafic roots to arc volcanoes: mafic recharge and differentiation of basaltic andesite at North Sister volcano, Oregon Cascades. Journal of Petrology, 52, 603–641.

Schmincke, H.U. (2004) Volcanism. Springer, 324 p., https://doi.org/10.1007/978-3-642-18952-4.

Scholz, C.H. and Campos, J. (1995) On the mechanism of seismic decoupling and back arc spreading at subduction zones. Journal of Geophysical Research, Solid Earth, 100, 22103–22115.

Sdrolias, M. and Müller, R.D. (2006) Controls on back-arc basin formation. Geochemistry Geophysics Geosystems, 7, Q04016.

Senda, R., Kimura, J. and Chang, Q. (2014) Evaluation of a rapid, effective sample digestion method for trace element analysis of granitoid samples containing acid-resistant minerals: Alkali fusion after acid digestion. Geochemical Journal, 48, 99–103.

Shibata, K. (1973) K–Ar ages of volcanic rocks from the Hokuriku group. Memoir of the Geological Society of Japan, 8, 143–149 (in Japanese with English abstract).

Shimazu, M., Kagami, H., Kawano, Y. and Yamamoto, G. (1993) Geochemistry of Early-Middle Miocene volcanic rocks in the back-arc regions of Japan: Sado, Noto and Tadami areas. The Journal of the Geological Society of Japan, 99, 799–811.

Shimizu, M., Fujii, S. and Hamuro, T. (2000) Newly found Aturia and molluscan fossil assemblages from Higashibessho Formation, Hokuriku Group, Toyama

Prefecture, Central Japan. Chikyukagaku (Earth Science), 54, 43–48 (in Japanese with English abstract).

Shinjoe, H., Furukawa, K., Orihashi, Y., Hokanishi, N. and Wada, Y. (2018) Zircon U-Pb ages of Tochibora welded tuff Member at the lowest part of the Hachiya Formation, in Kani Basin, Gifu Prefecture. The Journal of the Geological Society of Japan, 124, 533–538 (in Japanese with English abstract).

Shinmura, T., Arakawa, Y. (2008) K–Ar age of andesite lava in Miocene Iwaine Formation, western part of Toyama Prefecture, central Japan. The Kumamoto Gakuen University journal of liberal arts and sciences, 15, 19–27 (in Japanese with English abstract).

Shinmura, T., Kobayashi, Y., Arakawa, Y. and Itaya, T. (1994) K–Ar ages of andesite dykes in the Hida region. Journal of Mineralogy, Petrology and Economic Geology, 89, 285–293 (in Japanese with English abstract).

Shuto, K. (2009) The Northeast Japan Arc, Opening of the Japan Sea and Magma Genesis. Kyoritsu Publ. Co., 236p (in Japanese).

Shuto, K., Ishimoto, H., Hirahara, Y., Sato, M., Matsui, K., Fujibayashi, N., Takazawa, E., Yabuki, K., Sekine, M., Kato, M. and Rezanov, A.I. (2006) Geochemical secular variation of magma source during Early to Middle Miocene time in the Niigata area, NE Japan: Asthenospheric mantle upwelling during back-arc basin opening. Lithos, 86, 1–33.

Shuto, K., Imanaka, R. N., Sato, M., Takahashi, T., Takazawa, E., Kawabata, H., Takanashi, K., Ban, M., Watanabe, N. and Fujibayashi, N. (2015) Across-arc variations in geochemistry of Oligocene to Quaternary basalts from the NE Japan arc: Constraints on source composition, mantle melting and slab input composition. Journal of Petrology, 56, 2257–2294.

Sigurdsson, H., Houghton, B., McNutt, S., Rymer, H. and Stix, J. (2015) The encyclopedia of volcanoes, 2nd edition. Elsevier, 1456 p., https://doi.org/10.1016/C2015-0-00175-7.

Solomatov, V.S. (1995) Scaling of temperature- and stress-dependent viscosity convection. Physics of Fluids, 7, 266–274.

Solomatov, V.S. and Moresi, L.N. (1996) Stagnant lid convection on Venus. Journal of Geophysical Research: Planets, 101, 4737–4753.

Solomatov, V.S., Zharkov, V.N., 1990. The thermal regime of Venus. Icarus, 84, 280–295.

Sohma, T. and Kunugiza, K. (1993) The formation of the Hida nappe and the tectonics of Mesozoic sediments: The tectonic evolution of the Hida region, Central Japan. Memoir of the Geological Society of Japan, 42, 1–20 (in Japanese with English abstract).

Sohma, T. and Maruyama, S. (1989) Formation of the Japan Sea and the origin of Fossa Magna. Chikyu Monthly, 11, 526–531 (in Japanese)*.

Sparks, R.S.J., Self, S. and Walker, G.P.L. (1973) Products of Ignimbrite Eruptions. Geology, 1, 115–118.

Stern, R.J. (2005) Evidence from ophiolites, blueschists, and ultrahigh-pressure metamorphic terranes that the modern episode of subduction tectonics began in Neoproterozoic time. Geology, 33, 557–560.

Sudo, S. (1979a) On the formation of the Japan Sea from the suggestion of the Tori Conglomerate Formation. Circular Nihonkai (Japan Sea), 10, 183–185 (in Japanese).

Sudo, S. (1979b) On the geology of the Futomiyama Mountains, Toyama Prefecture, central Japan (preliminary report). Memoir of the Geological Society of Japan, 17, 187–194 (in Japanese with English abstract).

Sugimoto, M. (1979) Geologic Structure of the Southwestern Part of the Mt. Iozen - Geological Studies of the Sunagozaka Formation, Neogene Tertiary, Hokuriku, Central Japan (I) -. Bulletin of the Faculty of Education, Kanazawa University, 27, 27–35 (in Japanese with English abstract).

Sugimoto, M. (1981) The Sunagozaka Formation in the Drainage Basin of the River Sai, Kanazawa City, Central Japan - Geological Studies of the Sunagozaka Formation, Neogene Tertiary, in Hokuriku, Central Japan (III) -, Bulletin of the Faculty of Education, Kanazawa University, 29, 15–29 (in Japanese with English abstract).

Sugimoto, M. (1988) Geological Structure in the Northern Part of the Steep Dip Belt of the Western Margin of Mt. Iozen - Geological Studies of the Nanamagari Formation, Neogene Tertiary, in Hokuriku, Central Japan (VIII), Bulletin of the Faculty of Education, Kanazawa University, 37, 37–58 (in Japanese with English abstract).

Sugimoto, M. (1996) Rock-stratigraphy of the Sunagozaka Formation in the “type locality”–geological studies of the Sunagozaka Formation, Neogene Tertiary, in Hokuriku, central Japan [V]. Japan Sea Research, 27, 1–15 (in Japanese with English abstract).

Sugimoto, M. (1999) Geological Structure of the Sunagozaka Formation in the "Type locality" - Geological Studies of the Sunagozaka Formation, Neogene Tertiary, in Hokuriku, central Japan (VI) -. Bulletin of the Faculty of Education, Kanazawa University, 48, 31–45 (in Japanese with English abstract).

Sugimoto, M., Nakanishi, N. and Yasukawa, J. (1980) The Sunagozaka Formation in the Drainage Basin of the River Asano, Kanazawa City, Central Japan - Geological Studies of the Sunagozaka Formation, Neogene Tertiary, in Hokuriku, Central Japan (II) -, Bulletin of the Faculty of Education, Kanazawa University, 28, 51–67 (in Japanese with English abstract).

Sugimoto, M. and Sakaguchi, H. (1984) The Sunagozaka Formation in the Southern Hills of the Kanazawa City - Geological Studies of the Sunagozaka Formation, Neogene Tertiary, in Hokuriku, Central Japan (IV) -, Bulletin of the Faculty of Education, Kanazawa University, 33, 53–67 (in Japanese with English abstract).

Sugimoto, M. and Toyoshima, S. (1984) The Rock-stratigraphic Correlation between the Doyama Tuffceous Member and the Nanamagari Formation - Geological Studies of the Nanamagari Formation, Neogene Tertiary, in Hokuriku, Centarl Japan (IV) -Bulletin of Japan Sea Research Institute, Kanazawa University, 16, 29–43 (in Japanese with English abstract).

Sumi, Y. and Nozawa, T. (1973) Geology of the Uozu District. With Geological Sheet Map at 1 : 50,000, Geological Survey of Japan, 104p (in Japanese with English abstract).

Sun, S.S. and McDonough, W.F. (1989) Chemical and isotopic systematics of oceanic basalts: implications for mantle composition and processes. Geological Society, London, Special Publication, 42, 313–345.

Sutawidjaja, I.S., Rosana, M.F. and Watanabe, K. (2015) Magma chamber model of Batur Caldera, Bali, Indonesia: Compositional variation of two facies, large-volume dacitic ignimbrites. Indonesian Journal of Geosciences, 2, 111–124.

Sutton, A.N., Blake, S., Wilson, C.J.N. and Charlier, B.L.A. (2000) Late Quaternary evolution of a hyperactive rhyolite magmatic system: Taupo volcanic centre, New Zealand. Journal of Geological Society, London, 157, 537–552.

Takahashi, M., Seki, S., Suzuki, H., Takemoto, H., Nagai, M. and kanamaru, T. (2012) Whore-rock chemistry for eruptive products of Akagi volcano, central Japan: Summary of 381 analytical data. Proceedings of the Institute of Natural Sciences, Nihon University, 47, 341–400 (in Japanese with English abstract).

Takahashi, M., Otsuka, T., Kawamata, H., Sako, H., Yasui, M., Kanamaru, T., Otsuki, M., Shimada, J., Atsuchi, T., Shiroishi, T., Ichiki, Y., Satake, S., Kobayashi, T., Ishihara, K. and Miki, D. (2011) Whole-rock chemistry for eruptive products of the Sakurajima volcano and Aira caldera, southern Kyushu: summary of 583 analytical data. Proceedings of the Institute of Natural Sciences, Nihon University, 46, 133–200 (in Japanese with English abstract).

Takahashi, T., Hirahara, Y., Miyazaki, T., Vaglarov, B.S., Chang, Q., Kimura, J. and Tatsumi, Y. (2009) Precise determination of Sr isotope ratios in igneous rock samples and application to micro-analysis of plagioclase phenocrysts. JAMSTEC-R IFREE Special Issue, 59–64.

Takahashi, T. and Shuto, K. (1997) Major and trace element analyses of silicate rocks using fluorescence spectrometer RIX3000. Rigaku-Denki Journal, 28, 25–37 (in Japanese).

Takahashi, T. and Shuto, K. (1999) Genesis of adakitic andesite, high-magnesian andesite, calk-alkaline andesite and tholeiitic andesite in the Miocene Iwaine Formation, southern part of Toyama Prefecture, Japan. The Journal of the Geological Society of Japan, 105, 789–809 (in Japanese with English abstract).

Takahashi, Y., Cho, D.L. and Kee, W.S. (2010) Timing of mylonitization in the Funatsu Shear Zone within Hida Belt of southwest Japan: Implications for correlation with the shear zones around the Ogcheon Belt in the Korean Peninsula. Gondwana Research, 17, 102–115.

Takahashi, Y., Cho, D.L., Mao, J., Zhao, X. and Yi, K. (2018) SHRIMP U–Pb zircon ages of the Hida metamorphic and plutonic rocks, Japan: Implications for late P aleozoic to Mesozoic tectonics around the Korean Peninsula. Island Arc, DOI: 10.1111/iar. 12220.

Takeuchi, M., Furukawa, R., Nagamori, H. and Oikawa, T. (2017) Geology of the Tomari District. With Geological Sheet Map at 1 : 50,000. Geological Survey of Japan, AIST, 121p (in Japanese with English abstract).

Tamaki, M., Itoh, Y. and Watanabe, M. (2006) Paleomagnetism of the Lower to Middle Miocene Series in the Yatsuo area, eastern part of southwest Japan: clockwise rotation and marine transgression during a short period. Bulletin of the Geological Survey of Japan, 57, 73–88.

Tamura, Y., Gill, J.B., Tollstrup, D., Kawabata, H., Shukuno, H., Chang, Q., Miyazaki, T., Takahashi, T., Hirahara, Y., Kodaira, S., Ishizuka, O., Suzuki, T., Kido, Y., Fiske, R.S. and Tatsumi, Y. (2009) Silicic magmas in the Izu–Bonin Oceanic arc and implications for crustal evolution. Journal of Petrology, 50, 685–723.

Tamura, Y., Sato, T., Fujiwara, T., Kodaira, S. and Nichols, A. (2016) Advent of continents: A new hypothesis. Scientific Reports, 6, 33517.

Tanaka, G., Tsukawaki, S. and Ooji, A. (2004) Preliminary report on Ostracods from the Miocene Sunagozaka Formation, southern part of Kanazawa City, Ishikawa Prefecture, central Japan. Japan Sea Report, 35, 53–63 (in Japanese with English abstract).

Tanaka, S. (1992) Origin of the early Mesozoic granitic rocks in the Hida terrane, Japan, and its implication for evolution of the continental crust. Journal of Science of Hiroshima University, Series C, 9, 435–493.

Tatsumi, Y. (2006) High-Mg andesites in the Setouchi Volcanic Belt, southwestern Japan: analogy to Archean magmatism and continental crust formation? Annual Review of Earth and Planetary Sciences, 34, 467–499.

Tatsumi, Y., Maruyama, S. and Nohda, S. (1990) Mechanism of backarc opening in the Japan Sea: Role of asthenospheric injection. Tectonophysics, 181, 299–306.

Tatsumi, Y., Otofuji, Y., Matsuda, T. and Honda, S. (1989) Opening of the Sea of Japan back-arc basin by asthenospheric injection. Tectonophysics, 166, 317–329.

Tatsumi, Y., Takahashi, T., Hirahara, Y., Chang, Q., Miyazaki, T., Kimura, J.I., Ban, M. and Sakayori, A. (2008) New insights into andesite genesis: the role of mantle-derived calc-alkalic and crust-derived tholeiitic melts in magma differentiation beneath Zao volcano, NE Japan. Journal of Petrology, 49, 1971–2008.

Taylor, B. (1995) Backarc basins: Tectonics and magmatism. Springer, 524 p, https://doi.org/10.1007/978-1-4615-1843-3.

Taylor, B. and Martinez, F. (2003) Back-arc basin basalt systematics. Earth and Planetary Science Letters, 210, 481–497.

Thirlwall, M. F. and Anczkiewicz, R. (2004) Multidynamic isotope ratio analysis using MC–ICP–MS and the causes of secular drift in Hf, Nd and Pb isotope ratios. International Journal of Mass Spectrometry, 235, 59–81.

Tomioka, N., Ishiwatari, A., Tanase, A., Shimizu, S. and Kagami, H. (2000) Geology and petrology of the Early Miocene Arashimadake cauldron in Ono

City, Fukui Prefecture, central Japan. The Journal of the Geological Society of Japan, 106, 313–329 (in Japanese with English abstract).

Tsuchihashi, H. and Ishiwatari, A. (2006) Adakitic hornblende-andesite and xenoliths in the Miocene volcanic rocks, western part of Toyama Prefecture, central Japan. 113th Annual Meeting of the Geological Society of Japan, Abstract, 243–243 (in Japanese).

Tsuda, K. (1953) Geology around Yatsuo Town, Toyama Prefecture with special reference to geohistrical study on the Yatsuo Group. Journal of the Faculty of Science, Niigata University, Series II, 2, 1–35 (in Japanese with English abstract).

Tsuda, K. (1955) On the Sedimentary Environment of the Yatuo Group: A Study of the Sedimentary Environment of the Miocene Deposits in the so-called "Green Tuff" Region-(Part I). The Journal of the Geological Society of Japan, 61, 532–542 (in Japanese with English abstract).

Tsuda, K. (1959) New Miocene molluscs from the Kurosedani Formation in Toyama Prefecture, Japan. Journal of the Faculty of Science, Niigata University, Series II, 3, 67–110.

Tsuda, K. (1960) Paleo-ecology of the Kurosedani fauna. Journal of the Faculty of Science, Niigata University, Series 2, 3, 171–203.

Tsuda, K. and Chiji, M. (1950) Some problems in geology around Yatsuo area. The Journal of the Geological Society of Japan, 56, 303–304 (in Japanese).

Tsukamoto, I. (1988) K–Ar ages of volcanic rocks from the Noto Peninsula. In Kaseno, Y. (ed.) Geology of Ishikawa-ken, Japan (with Geological Maps). Ishikawa Prefecture and the Geological Institute of Hokuriku, 225–226 (in Japanese).

Tsukawaki, S. and Ooji, A. (2008) Upper Cenozoic stratigraphy of Kanazawa City and its environs, central Japan. Japan Sea Research, 39, 17–30 (in Japanese with English abstract).

Ueda, H., Takazawa, E., Kato, R. and Adachi, Y. (2018) Evaluation of time-resolved mean-of-ratios reduction for laser ablation zircon U-Pb dating using quadrupole ICPMS. Geochemical Journal, 52, 241–254.

Uematsu, M., Shuto, K. and Kagami, H. (1995) Genesis of tholeiitic basalt, high magnesian andesite, bronzite andesite and adakite-like andesite of the Late Oligocene Anamizu Formation, northern Noto Peninsula, Japan. Memoir of the Geological Society of Japan, 44, 101–124 (in Japanese with English abstract).

Ui, H. and Kuroda, H. (1990) Geology of National Tateyama Children's Center area: particularly on the Jozen Toge Formation. 97th Annual Meeting of the Geological Society of Japan, Abstract, 194–194 (in Japanese).

Umeda, M. (1997) Petrography of orthoquarzite clasts and radiolarian fossils in chert clasts in the Late Oligocene conglomerate on the Mesozoic complex of the Nanjo Massif in the Mino Terrane, Central Japan. Earth Science (Chikyu Kagaku), 51, 199–211 (in Japanese with English abstract).

Uyeda, S. and Kanamori, H. (1979) Back arc opening and the mode of subduction. Journal of Geophysical Research, Solid Earth, 84, 1049–1061.

Uyeda, Y. and Aoki, K. (1970) K-Ar dating on moonstone rhyolite in Toyama Prefecture, central Honshu. Journal of Japanese Association of Mineralogists, Petrologists and Economic Geologists, 63, 28–29 (in Japanese with English abstract).

Vogel, T.A., Flood, T.P., Patino, L.C., Wilmot, M.S., Maximo, R.P.R., Arpa, C.B. Arcilla, C.A. and Stimac, J.A. (2006) Geochemistry of silicic magmas in the Macolod Corridor, SW Luzon, Philippines: evidence of distinct, mantle-derived, crustal sources for silicic magmas. Contribution to Mineralogy and Petrology, 151, 267–281.

Wadatsumi, K., Ikebe, N., Fujii, S., Akamine, H., Ichihara, M., Tsuda, K. and Matsumoto, T. (1955) The Cenozoic strata in eastern part of the Toyama basin. The Journal of the Geological Society of Japan, 61, 360–360 (in Japanese).

Wallis, S.R., Yamaoka, K., Mori, H., Ishiwatari, A., Miyazaki, K. and Ueda, H. (2020) The basement geology of Japan from A to Z. Island Arc, DOI: 10.1111/iar.12339.

Wang, Q., Chung, S.L., Li, X.H., Wyman, D., Li, Z.X., Sun, W.D., Qiu, H.N., Liu, Y.S. and Zhu, Y.T. (2012) Crustal melting and flow beneath Northern Tibet: Evidence from Mid-Miocene to Quaternary strongly peraluminous rhyolites in the Southern Kunlun Range. Journal of Petrology, 53, 2523–2566.

Watanabe, S. and Takahashi, T. (2019) Petrological and geochemical features of Miocene adakitic volcanic rocks in eastern part of Hokuriku region, SW Japan. Japan Geoscience Union Annual Meeting 2019, SGC41-P05.

Watanabe, S., Yamada, R. and Takahashi, T. (2020) Miocene adakitic volcanism in Toyama prefecture in the Hokuriku region, northern end of the SW Japan arc. JpGU-AGU Joint Meeting 2020, SGC49-01.

Watts, K.E., Bindeman, I.N. and Schmitt, A.K. (2011) Large-volume rhyolite genesis in caldera complexes of the Snake River Plain: insights from the Kilgore Tuff of the Heise Volcanic Field, Idaho, with comparison to Yellowstone and Bruneau–Jarbidge Rhyolites. Journal of Petrology, 52, 857–890.

Wiens, D.A., Kelley, K.A. and Plank, T. (2006) Mantle temperature variations beneath back-arc spreading centers inferred from seismology, petrology, and bathymetry. Earth and Planetary Science Letters, 248, 30–42.

Wolfram, L.C., Weinberg, R.F., Nebel, O., Hamza, K., Hasalová, P., Míkova, J. and Becchio, R. (2019) A 60-Myr record of continental back-arc differentiation through cyclic melting. Nature Geoscience, 12, 215–219.

Woodhead, J. D. and Hergt, J. M. (2005) A preliminary appraisal of seven natural zircon reference materials for in situ Hf isotope determination. Geostandards and Geoanalytical Research, 29, 183–195.

Yabe, A. (2008) Plant megafossil assemblage from the Lower Miocene Ito-o Formation, Fukui Prefecture, central Japan. Memoir of the Fukui Prefectural Dinosaur Museum, 7, 1–24.

Yamada, N., Sakamoto, T. and Kaneko, K. (1998) K–Ar ages of “the Takamineyama Volcanic Rocks”, Toyama Prefecture, central Japan. Earth Science (Chikyu Kagaku), 52, 235–239 (in Japanese with English abstract).

Yamada, R., Sawada, H., Aoyama, S., Ouchi, W., Niki, S., Nagata, M., Takahashi, T. and Hirata., T. (2021) Zircon U-Pb ages and whole-rock geochemistry from the Hida granites: implications for the geotectonic history and the origin of Mesozoic granites in the Hida belt, Japan. Journal of Mineralogical and Petrological Sciences, 116, 61–66.

Yamada, R. and Takahashi, T. (2021) Temporal and spatial changes of magmatism related to the Japan Sea opening in the Hokuriku region, central Japan: stratigraphy, chronology and petrology of Oligocene to middle Miocene volcanic rocks. The Journal of the Geological Society of Japan, 127, 507–525 (in Japanese with English abstract).

Yamada, R. and Yamada, N. (2018) Lithostratigraphy of the Miocene Iwaine Formation in the Yatsuo area, central Japan. Science Reports of Niigata University (Geology), 33, 25–40.

Yamada, T., Teduka, S., Kamiya, T. and Yanagisawa, Y. (2017) Stratigraphic revision of the Miocene “Saikawa Formation” distributed in the southern Kanazawa area, Ishikawa Prefecture, central Japan. Bulletin of the Geological Survey of Japan, 68, 183–221 (in Japanese with English abstract).

Yamanoi, T. and Tsuda, K. (1986) On the conditions of paleo-mangrove forest in the Kurosedani Formation (Middle Miocene), central Japan. Memoir of the Natural Science Museum, 19, 55–68 (in Japanese with English abstract).

Yamasaki, M. and Miyajima, Y. (1970) Eruption age of moonstone rhyolite in Toyama Prefecture, central Honshu. The Journal of the Japanese Association of Mineralogists, Petrologists and Economic Geologists, 63, 22–27 (in Japanese with English abstract).

Yamashita, N., Kaseno, Y. and Itoigawa, J. (1988) Regional geology of Japan, Part 5, Chubu II. Kyoritu Publ. Co., 310 p (in Japanese).

Yamazaki, R. and Ishiwatari, A. (2007) Petrologic study of volcanic rocks from the Miocene Itoo Formation in the Niu Mountains, Fukui Prefecture, central Japan: with notes on low-Ni basalt. 114th Annual Meeting of the Geological Society of Japan, Abstract, 305–305 (in Japanese).

Yanagisawa, Y. (1999a) Diatom biostratigraphy of the Miocene sequence in the Iozen area, Hokuriku Province, central Japan. Bulletin of the Geological Survey of Japan, 50, 67–81 (in Japanese with English abstract).

Yanai, S., Aoki, K. and Akahori, Y. (2010) Opening of Japan Sea and major tectonic lines of Japan: MTL, TTL and Fossa Magna. Journal of Geography (Chigaku Zasshi), 119, 1079–1124 (in Japanese with English abstract).

Yin, A. (2010) Cenozoic tectonic evolution of Asia: A preliminary synthesis. Tectonophysics, 488, 293–325.

Yoshikawa, T., Kano, K., Yanagisawa, Y., Komazawa, M., Joshima, M. and Kikawa, E. (2002) Geology of the Suzimisaki, Noto-iida and Horyuzan District. Quadrangle Series, 1:50,000, Geological Survey of Japan, AIST, 76 p (in Japanese with English abstract).

Zadeh, A. I., Honda, S. and Tsepelev, I. (2013) Linking mantle upwelling with the lithosphere descent and the Japan Sea evolution: a hypothesis. Scientific Reports, 3, https://doi.org/10.1038/srep01137.

Zhu, J. (2022) Episodic bimodal magmatism in Central Inner Mongolia, China: Insights from geochronological, geochemical, and Sr-Nd isotopic evidence. Lithos, 424–425, 106765.

*English translation from the original written in Japanese

Supplementary table A: Data on zircon U–Pb age

Sample	Spot no.	206Pb/238U		207Pb/206Pb		206Pb/238U age (Ma)		207Pb/235U age (Ma)	
		ratio	error (2SE)	ratio	error (2SE)				
OD-3	RY0025	0.005200	0.000301	0.044505	0.002626	33.4 ±	1.9	31.9 ±	2.6
OD-3	RY0043	0.005024	0.000184	0.045695	0.003090	32.3 ±	1.2	31.6 ±	2.4
OD-3	RY0061	0.005141	0.000177	0.044393	0.003440	33.1 ±	1.1	31.5 ±	2.6
OD-3	RY0079	0.005311	0.000240	0.042954	0.003104	34.1 ±	1.5	31.4 ±	2.6
OD-3	RY0102	0.005265	0.000244	0.038634	0.016614	33.9 ±	1.6	28.1 ±	12.0
OD-3	RY0120	0.005250	0.000202	0.040664	0.009993	33.8 ±	1.3	29.5 ±	7.2
OD-3	RY0174	0.005141	0.000217	0.047483	0.003920	33.1 ±	1.4	33.6 ±	3.1
OD-3	RY0198	0.005005	0.000218	0.046055	0.002546	32.2 ±	1.4	31.8 ±	2.2
OD-3	RY0220	0.005068	0.000196	0.046617	0.002677	32.6 ±	1.3	32.5 ±	2.2
OD-3	RY0242	0.005313	0.000230	0.047376	0.002084	34.2 ±	1.5	34.6 ±	2.1
OD-3	RY0286	0.005001	0.000213	0.052695	0.005150	32.2 ±	1.4	36.2 ±	3.8
OD-3	RY0332	0.005227	0.000236	0.047878	0.002880	33.6 ±	1.5	34.4 ±	2.5
OD-3	RY0354	0.005528	0.000217	0.045010	0.002051	35.5 ±	1.4	34.3 ±	2.0
OD-3	RY0596	0.005192	0.000317	0.050839	0.011287	33.4 ±	2.0	36.3 ±	8.2
OD-3	RY0618	0.005074	0.000312	0.050962	0.010836	32.6 ±	2.0	35.6 ±	7.7
OD-3	RY0640	0.005325	0.000286	0.049912	0.008333	34.2 ±	1.8	36.5 ±	6.3
OD-3	RY0662	0.005026	0.000263	0.053614	0.008836	32.3 ±	1.7	37.0 ±	6.3
OD-3	RY0684	0.005367	0.000264	0.049514	0.008263	34.5 ±	1.7	36.5 ±	6.2
OD-3	RY0706	0.005167	0.000238	0.050209	0.007027	33.2 ±	1.5	35.7 ±	5.2
FCT	RY0008	0.004334	0.000139	0.044624	0.002280	27.9 ±	0.9	26.7 ±	1.6
FCT	RY0026	0.004422	0.000137	0.046455	0.002508	28.4 ±	0.9	28.4 ±	1.7
FCT	RY0044	0.004342	0.000153	0.043416	0.003396	27.9 ±	1.0	26.1 ±	2.2
FCT	RY0062	0.004305	0.000137	0.046478	0.002257	27.7 ±	0.9	27.6 ±	1.6
FCT	RY0080	0.004436	0.000186	0.042923	0.003824	28.5 ±	1.2	26.3 ±	2.6
FCT	RY0121	0.004633	0.000164	0.046514	0.021736	29.8 ±	1.1	29.7 ±	13.7
FCT	RY0139	0.004553	0.000161	0.043154	0.002725	29.3 ±	1.0	27.1 ±	1.9
FCT	RY0157	0.004615	0.000171	0.045750	0.003671	29.7 ±	1.1	29.1 ±	2.5
FCT	RY0175	0.004594	0.000159	0.049797	0.005282	29.5 ±	1.0	31.5 ±	3.5
FCT	RY0199	0.004214	0.000189	0.041760	0.004785	27.1 ±	1.2	24.3 ±	3.0
FCT	RY0221	0.004294	0.000165	0.043648	0.002861	27.6 ±	1.1	25.9 ±	1.9
FCT	RY0265	0.004629	0.000196	0.041511	0.004617	29.8 ±	1.3	26.6 ±	3.1
FCT	RY0287	0.004398	0.000200	0.043986	0.005285	28.3 ±	1.3	26.7 ±	3.4
FCT	RY0311	0.004534	0.000233	0.042683	0.007943	29.2 ±	1.5	26.7 ±	5.1
FCT	RY0333	0.004512	0.000193	0.043860	0.002469	29.0 ±	1.2	27.3 ±	1.9
FCT	RY0355	0.004610	0.000191	0.043585	0.004134	29.6 ±	1.2	27.7 ±	2.8
FCT	RY0553	0.004390	0.000488	0.058625	0.029340	28.2 ±	3.1	35.4 ±	17.8
FCT	RY0575	0.004551	0.000411	0.043822	0.022522	29.3 ±	2.6	27.5 ±	14.2
FCT	RY0597	0.005003	0.000330	0.055964	0.014331	32.2 ±	2.1	38.5 ±	10.0
FCT	RY0663	0.004696	0.000223	0.045660	0.006176	30.2 ±	1.4	29.6 ±	4.2
FCT	RY0685	0.004737	0.000226	0.045406	0.007486	30.5 ±	1.4	29.7 ±	5.0
FCT	RY0707	0.004826	0.000324	0.053434	0.010489	31.0 ±	2.1	35.5 ±	7.2
FCT	RY0729	0.004937	0.000280	0.051588	0.009650	31.7 ±	1.8	35.0 ±	6.7
FCT	RY0751	0.004806	0.000219	0.048017	0.004520	30.9 ±	1.4	31.8 ±	3.3
FCT	RY0773	0.004744	0.000298	0.048479	0.012408	30.5 ±	1.9	31.7 ±	8.2

NT63c (Tori Formation)

Spot no.	206Pb/238U		207Pb/206Pb		206Pb/238U age (Ma)			207Pb/235U age (Ma)			Discordant (D) or discordant (C)
	ratio	error (2SE)	ratio	error (2SE)							
RY0009	0.003797	0.000152	0.082025	0.021526	24.4	±	1.0	42.7	±	11.1	D
RY0010	0.017513	0.000599	0.046350	0.001548	111.9	±	3.8	107.7	±	4.9	C
RY0011	0.023199	0.000801	0.049642	0.001207	147.8	±	5.0	149.6	±	5.9	C
RY0012	0.003647	0.000149	0.042905	0.019012	23.5	±	1.0	21.7	±	9.5	C
RY0013	0.003999	0.000175	0.074315	0.021261	25.7	±	1.1	40.8	±	11.6	D
RY0014	0.019831	0.000635	0.047585	0.001563	126.6	±	4.0	124.2	±	5.4	C
RY0015	0.003719	0.000147	0.039299	0.007992	23.9	±	0.9	20.3	±	4.2	C
RY0016	0.004743	0.000275	0.102377	0.051576	30.5	±	1.8	65.8	±	32.3	D
RY0017	0.003588	0.000157	0.050358	0.003596	23.1	±	1.0	25.0	±	2.1	C
RY0018	0.003708	0.000174	0.055707	0.006138	23.9	±	1.1	28.5	±	3.4	D
RY0027	0.003599	0.000115	0.050428	0.002172	23.2	±	0.7	25.1	±	1.3	D
RY0028	0.003592	0.000124	0.042903	0.004877	23.1	±	0.8	21.3	±	2.5	C
RY0029	0.003531	0.000123	0.043627	0.004070	22.7	±	0.8	21.3	±	2.1	C
RY0030	0.003930	0.000136	0.082334	0.020031	25.3	±	0.9	44.3	±	10.7	D
RY0031	0.003642	0.000119	0.051816	0.003768	23.4	±	0.8	26.1	±	2.1	D
RY0032	0.004465	0.000263	0.150213	0.029877	28.7	±	1.7	89.8	±	17.8	D
RY0033	0.003581	0.000109	0.047499	0.003356	23.0	±	0.7	23.5	±	1.8	C
RY0034	0.038205	0.002069	0.232055	0.024202	241.7	±	12.8	810.9	±	65.6	D
RY0035	0.003704	0.000161	0.062944	0.022905	23.8	±	1.0	32.1	±	11.6	C
RY0036	0.003299	0.000109	0.041601	0.005021	21.2	±	0.7	19.0	±	2.4	C
RY0045	0.003549	0.000122	0.047070	0.003318	22.8	±	0.8	23.1	±	1.8	C
RY0046	0.004155	0.000208	0.121312	0.030364	26.7	±	1.3	68.2	±	16.8	D
RY0047	0.003587	0.000138	0.053503	0.003272	23.1	±	0.9	26.5	±	1.9	D
RY0048	0.003841	0.000155	0.089504	0.010932	24.7	±	1.0	47.0	±	5.9	D
RY0049	0.003686	0.000142	0.059170	0.007023	23.7	±	0.9	30.1	±	3.7	D
RY0050	0.003661	0.000142	0.051117	0.004274	23.6	±	0.9	25.9	±	2.4	C
RY0051	0.003743	0.000148	0.071646	0.018991	24.1	±	0.9	36.9	±	9.7	D
RY0052	0.003522	0.000151	0.037479	0.017792	22.7	±	1.0	18.3	±	8.7	C
RY0053	0.003614	0.000123	0.055505	0.004843	23.3	±	0.8	27.7	±	2.6	D
RY0054	0.003558	0.000131	0.046525	0.006120	22.9	±	0.8	22.9	±	3.1	C
RY0063	0.003418	0.000127	0.051039	0.005574	22.0	±	0.8	24.1	±	2.8	C
RY0064	0.003846	0.000207	0.087815	0.037336	24.7	±	1.3	46.2	±	19.4	D
RY0065	0.003505	0.000151	0.067950	0.010012	22.6	±	1.0	32.8	±	5.0	D
RY0066	0.003784	0.000160	0.101088	0.009242	24.3	±	1.0	52.2	±	5.1	D
RY0067	0.003930	0.000165	0.111334	0.011888	25.3	±	1.1	59.5	±	6.6	D
RY0068	0.003512	0.000114	0.044422	0.004015	22.6	±	0.7	21.6	±	2.1	C
RY0069	0.003762	0.000159	0.056008	0.007438	24.2	±	1.0	29.1	±	4.0	D
RY0070	0.030546	0.000938	0.051151	0.001162	194.0	±	5.9	198.1	±	6.9	C
RY0071	0.003389	0.000145	0.043253	0.006282	21.8	±	0.9	20.3	±	3.0	C
RY0072	0.003489	0.000143	0.054010	0.009612	22.5	±	0.9	26.0	±	4.7	C
RY0081	0.003295	0.000136	0.051127	0.003072	21.2	±	0.9	23.3	±	1.7	D
RY0082	0.003456	0.000152	0.036529	0.016154	22.2	±	1.0	17.5	±	7.7	C
RY0083	0.003518	0.000156	0.064197	0.006458	22.6	±	1.0	31.1	±	3.4	D
RY0084	0.003690	0.000216	0.056709	0.038129	23.7	±	1.4	28.9	±	19.2	C
RY0085	0.004088	0.000190	0.081176	0.006344	26.3	±	1.2	45.4	±	4.0	D
RY0086	0.003563	0.000152	0.048951	0.007237	22.9	±	1.0	24.1	±	3.7	C
RY0087	0.003494	0.000160	0.073458	0.011045	22.5	±	1.0	35.3	±	5.5	D
RY0088	0.003486	0.000193	0.048878	0.017953	22.4	±	1.2	23.6	±	8.7	C
RY0089	0.004722	0.000306	0.163233	0.069797	30.4	±	2.0	102.5	±	42.2	D
RY0090	0.003531	0.000151	0.045245	0.005499	22.7	±	1.0	22.1	±	2.8	C
RY0357	0.017477	0.000693	0.047460	0.002158	111.7	±	4.4	110.0	±	6.3	C
RY0358	0.020638	0.000801	0.049266	0.001082	131.7	±	5.1	133.2	±	5.6	C
RY0360	0.017802	0.000677	0.048390	0.001488	113.7	±	4.3	114.0	±	5.3	C
RY0361	0.003598	0.000166	0.038781	0.015966	23.2	±	1.1	19.4	±	7.9	C
RY0363	0.003531	0.000152	0.036857	0.025239	22.7	±	1.0	18.1	±	12.3	C
RY0364	0.003482	0.000160	0.044290	0.016606	22.4	±	1.0	21.4	±	8.0	C
RY0366	0.003370	0.000151	0.047526	0.004720	21.7	±	1.0	22.2	±	2.4	C

RY0367	0.003654	0.000223	0.064168	0.037917	23.5	±	1.4	32.3	±	18.9	C
RY0369	0.003575	0.000191	0.080209	0.019252	23.0	±	1.2	39.4	±	9.5	D
RY0370	0.003485	0.000170	0.077895	0.021522	22.4	±	1.1	37.3	±	10.3	D
RY0622	0.003633	0.000211	0.060403	0.012656	23.4	±	1.4	30.3	±	6.5	D
RY0624	0.003526	0.000190	0.056830	0.011807	22.7	±	1.2	27.7	±	5.9	C
RY0625	0.003557	0.000137	0.053178	0.006078	22.9	±	0.9	26.1	±	3.1	C
RY0628	0.003632	0.000163	0.056075	0.007142	23.4	±	1.1	28.1	±	3.7	D
RY0630	0.004576	0.000260	0.270231	0.031021	29.4	±	1.7	159.8	±	18.9	D
RY0631	0.003236	0.000192	0.056026	0.013414	20.8	±	1.2	25.1	±	6.1	C
RY0633	0.003362	0.000246	0.053349	0.015405	21.6	±	1.6	24.8	±	7.3	C
RY0634	0.435825	0.008287	0.166853	0.001618	2331.9	±	37.2	2437.2	±	19.7	D
RY0643	0.003200	0.000209	0.040725	0.010447	20.6	±	1.3	18.1	±	4.7	C
RY0644	0.330304	0.007734	0.116355	0.001638	1839.9	±	37.5	1868.7	±	23.3	C
RY0646	0.342185	0.008024	0.117352	0.001631	1897.2	±	38.5	1906.3	±	23.4	C
RY0647	0.003754	0.000333	0.066463	0.027766	24.2	±	2.1	34.3	±	14.4	C
RY0649	0.003577	0.000184	0.052282	0.010386	23.0	±	1.2	25.9	±	5.2	C
RY0650	0.017494	0.000557	0.052961	0.004216	111.8	±	3.5	122.1	±	9.9	C
RY0652	0.333333	0.008445	0.117530	0.002270	1854.5	±	40.8	1885.1	±	27.3	C
RY0653	0.003902	0.000172	0.068331	0.006488	25.1	±	1.1	36.7	±	3.8	D
RY0655	0.004449	0.000321	0.065414	0.014177	28.6	±	2.1	39.9	±	8.9	D
RY0656	0.005693	0.000429	0.096914	0.021257	36.6	±	2.7	74.4	±	16.6	D
RY0665	0.003334	0.000202	0.076958	0.016549	21.5	±	1.3	35.3	±	7.8	D
RY0666	0.003392	0.000141	0.058665	0.006876	21.8	±	0.9	27.5	±	3.4	D
RY0668	0.003641	0.000132	0.051129	0.006134	23.4	±	0.9	25.7	±	3.2	C
RY0669	0.004432	0.000256	0.066686	0.010078	28.5	±	1.6	40.6	±	6.4	D
RY0671	0.003702	0.000200	0.106694	0.017254	23.8	±	1.3	53.8	±	8.9	D
RY0672	0.003481	0.000202	0.054538	0.007923	22.4	±	1.3	26.2	±	4.1	C
RY0674	0.003223	0.000205	0.077282	0.018078	20.7	±	1.3	34.3	±	8.2	D
RY0675	0.003175	0.000291	0.059048	0.022141	20.4	±	1.9	25.9	±	9.9	C
RY0677	0.004002	0.000211	0.142172	0.024844	25.7	±	1.4	76.7	±	13.5	D
RY0678	0.003365	0.000204	0.067692	0.014496	21.7	±	1.3	31.4	±	6.9	D

NT27 (Iwaine Formation)

Spot no.	206Pb/238U ratio	206Pb/238U error (2SE)	207Pb/206Pb ratio	207Pb/206Pb error (2SE)	206Pb/238U age (Ma)			207Pb/235U age (Ma)			Discordant (D) or discordant (C)
RY0211	0.009048	0.000421	0.049945	0.002448	58.1	±	2.7	61.4	±	4.0	C
RY0213	0.002754	0.000203	0.069035	0.017892	17.7	±	1.3	26.3	±	7.0	D
RY0214	0.002507	0.000132	0.037290	0.009791	16.1	±	0.8	13.0	±	3.5	C
RY0223	0.002441	0.000113	0.045814	0.012077	15.7	±	0.7	15.5	±	4.1	C
RY0227	0.002644	0.000121	0.044484	0.010752	17.0	±	0.8	16.3	±	4.0	C
RY0229	0.002655	0.000127	0.058295	0.015186	17.1	±	0.8	21.4	±	5.6	C
RY0233	0.002406	0.000119	0.032813	0.031258	15.5	±	0.8	11.0	±	10.4	C
RY0236	0.002686	0.000147	0.040529	0.030291	17.3	±	0.9	15.1	±	11.3	C
RY0248	0.002699	0.000140	0.041599	0.007294	17.4	±	0.9	15.6	±	2.8	C
RY0249	0.002716	0.000141	0.032319	0.030203	17.5	±	0.9	12.2	±	11.4	C
RY0252	0.002528	0.000171	0.023882	0.035378	16.3	±	1.1	8.4	±	12.4	C
RY0255	0.002984	0.000152	0.046304	0.005355	19.2	±	1.0	19.2	±	2.4	C
RY0257	0.002485	0.000121	0.106110	0.015231	16.0	±	0.8	36.3	±	5.4	D
RY0258	0.003192	0.000154	0.128611	0.010398	20.5	±	1.0	55.9	±	5.1	D
RY0267	0.002775	0.000189	0.051547	0.035779	17.9	±	1.2	19.8	±	13.7	C
RY0268	0.002849	0.000158	0.028282	0.025406	18.3	±	1.0	11.2	±	10.0	C
RY0273	0.002669	0.000137	0.035810	0.015154	17.2	±	0.9	13.3	±	5.6	C
RY0274	0.002861	0.000152	0.058759	0.010435	18.4	±	1.0	23.3	±	4.3	D
RY0276	0.003169	0.000252	0.093175	0.063590	20.4	±	1.6	40.5	±	27.3	C
RY0279	0.002838	0.000148	0.053948	0.018078	18.3	±	1.0	21.2	±	7.1	C
RY0280	0.002545	0.000114	0.046575	0.003811	16.4	±	0.7	16.5	±	1.5	C
RY0289	0.002456	0.000127	0.050229	0.008015	15.8	±	0.8	17.1	±	2.8	C
RY0290	0.009908	0.000434	0.047096	0.001222	63.6	±	2.8	63.3	±	3.1	C
RY0292	0.003081	0.000181	0.032562	0.018066	19.8	±	1.2	13.9	±	7.7	C
RY0293	0.002724	0.000157	0.032505	0.021561	17.5	±	1.0	12.3	±	8.2	C
RY0295	0.002509	0.000111	0.045535	0.003144	16.2	±	0.7	15.9	±	1.3	C
RY0296	0.002727	0.000168	0.053433	0.032600	17.6	±	1.1	20.2	±	12.3	C
RY0298	0.003325	0.000169	0.031510	0.015533	21.4	±	1.1	14.6	±	7.2	C
RY0299	0.002678	0.000239	0.031276	0.023636	17.2	±	1.5	11.7	±	8.8	C
RY0301	0.002795	0.000132	0.045183	0.003854	18.0	±	0.8	17.5	±	1.7	C
RY0313	0.002909	0.000155	0.039847	0.016847	18.7	±	1.0	16.1	±	6.8	C
RY0314	0.002902	0.000186	0.055882	0.016548	18.7	±	1.2	22.5	±	6.7	C
RY0316	0.002763	0.000207	0.041475	0.030016	17.8	±	1.3	15.9	±	11.5	C
RY0320	0.002564	0.000141	0.054015	0.024631	16.5	±	0.9	19.2	±	8.7	C
RY0323	0.002672	0.000152	0.073878	0.012565	17.2	±	1.0	27.3	±	4.8	D
RY0326	0.002563	0.000134	0.071804	0.010621	16.5	±	0.9	25.4	±	3.9	D

NT45 (Iozen Formation)

Spot no.	206Pb/238U ratio	206Pb/238U error (2SE)	207Pb/206Pb ratio	207Pb/206Pb error (2SE)	206Pb/238U age (Ma)			207Pb/235U age (Ma)			Discordant (D) or discordant (C)
RY0104	0.004014	0.000279	0.288578	0.059963	25.8	±	1.8	150.4	±	30.6	D
RY0105	0.002641	0.000102	0.066713	0.009457	17.0	±	0.7	24.4	±	3.5	D
RY0106	0.002703	0.000111	0.063417	0.017978	17.4	±	0.7	23.7	±	6.7	C
RY0107	0.002539	0.000079	0.057113	0.007387	16.3	±	0.5	20.1	±	2.6	D
RY0108	0.002748	0.000108	0.039173	0.016303	17.7	±	0.7	15.0	±	6.2	C
RY0110	0.002753	0.000117	0.068442	0.049200	17.7	±	0.8	26.0	±	18.5	C
RY0111	0.002660	0.000096	0.062984	0.024575	17.1	±	0.6	23.2	±	9.0	C
RY0112	0.002571	0.000084	0.088137	0.007994	16.6	±	0.5	31.2	±	3.0	D
RY0113	0.002519	0.000084	0.040789	0.005379	16.2	±	0.5	14.3	±	1.9	C
RY0122	0.002520	0.000084	0.046164	0.007150	16.2	±	0.5	16.2	±	2.5	C
RY0123	0.002589	0.000079	0.047860	0.005026	16.7	±	0.5	17.2	±	1.9	C
RY0124	0.002557	0.000067	0.047896	0.002425	16.5	±	0.4	17.0	±	1.0	C
RY0125	0.002627	0.000086	0.037260	0.014024	16.9	±	0.6	13.6	±	5.1	C
RY0126	0.003994	0.000155	0.291813	0.023230	25.7	±	1.0	151.3	±	12.5	D
RY0127	0.003114	0.000117	0.154250	0.010037	20.0	±	0.8	65.1	±	4.7	D
RY0129	0.002592	0.000105	0.061325	0.017582	16.7	±	0.7	22.0	±	6.3	C
RY0130	0.002436	0.000099	0.034200	0.018814	15.7	±	0.6	11.6	±	6.4	C
RY0131	0.003021	0.000096	0.157893	0.018636	19.4	±	0.6	64.7	±	7.7	D
RY0141	0.002999	0.000132	0.123731	0.023976	19.3	±	0.8	50.7	±	9.8	D
RY0142	0.002712	0.000116	0.035078	0.017515	17.5	±	0.7	13.2	±	6.6	C
RY0143	0.002668	0.000112	0.036091	0.018584	17.2	±	0.7	13.4	±	6.9	C
RY0145	0.002853	0.000158	0.072970	0.054447	18.4	±	1.0	28.7	±	21.2	C
RY0146	0.002741	0.000132	0.038425	0.020096	17.6	±	0.8	14.6	±	7.6	C
RY0147	0.002671	0.000114	0.052810	0.034362	17.2	±	0.7	19.6	±	12.6	C
RY0148	0.002566	0.000091	0.048931	0.007548	16.5	±	0.6	17.4	±	2.7	C
RY0149	0.002833	0.000105	0.049824	0.004682	18.2	±	0.7	19.6	±	2.0	C
RY0158	0.002502	0.000085	0.054169	0.002546	16.1	±	0.5	18.8	±	1.1	D
RY0159	0.002651	0.000106	0.072672	0.013045	17.1	±	0.7	26.6	±	4.8	D
RY0160	0.002469	0.000087	0.056242	0.003242	15.9	±	0.6	19.3	±	1.3	D
RY0161	0.002573	0.000101	0.048539	0.005858	16.6	±	0.6	17.3	±	2.2	C
RY0162	0.002496	0.000088	0.054514	0.003563	16.1	±	0.6	18.9	±	1.4	D
RY0163	0.002524	0.000113	0.054307	0.015974	16.3	±	0.7	19.0	±	5.6	C
RY0164	0.002572	0.000103	0.035703	0.025455	16.6	±	0.7	12.8	±	9.1	C
RY0165	0.002667	0.000113	0.110910	0.006956	17.2	±	0.7	40.6	±	3.0	D
RY0166	0.002416	0.000090	0.044913	0.003179	15.6	±	0.6	15.1	±	1.2	C
RY0167	0.002632	0.000106	0.055477	0.010905	16.9	±	0.7	20.2	±	4.0	C
RY0176	0.002566	0.000084	0.063384	0.005806	16.5	±	0.5	22.5	±	2.2	D
RY0177	0.002534	0.000074	0.065468	0.002943	16.3	±	0.5	23.0	±	1.2	D
RY0178	0.002688	0.000085	0.112384	0.004326	17.3	±	0.5	41.4	±	2.0	D
RY0179	0.002625	0.000095	0.049251	0.005237	16.9	±	0.6	17.9	±	2.0	C
RY0180	0.002316	0.000069	0.055326	0.002938	14.9	±	0.4	17.8	±	1.1	D
RY0182	0.003160	0.000127	0.203589	0.015933	20.3	±	0.8	86.3	±	7.3	D
RY0183	0.002440	0.000095	0.044157	0.011045	15.7	±	0.6	15.0	±	3.8	C
RY0184	0.002754	0.000119	0.114113	0.016056	17.7	±	0.8	43.1	±	6.2	D
RY0185	0.002380	0.000085	0.038489	0.018083	15.3	±	0.5	12.7	±	6.0	C
RY0336	0.003605	0.000194	0.300407	0.021842	23.2	±	1.2	141.3	±	11.9	D
RY0338	0.002419	0.000117	0.031674	0.010341	15.6	±	0.8	10.7	±	3.5	D
RY0341	0.002656	0.000132	0.035267	0.021034	17.1	±	0.9	13.0	±	7.7	C
RY0342	0.002578	0.000137	0.039065	0.009609	16.6	±	0.9	14.0	±	3.5	C
RY0344	0.002591	0.000137	0.065845	0.012918	16.7	±	0.9	23.6	±	4.7	D
RY0345	0.002998	0.000198	0.140887	0.022915	19.3	±	1.3	57.5	±	9.8	D
RY0348	0.002608	0.000141	0.042281	0.020476	16.8	±	0.9	15.3	±	7.4	C
RY0555	0.002544	0.000094	0.054677	0.005218	16.4	±	0.6	19.3	±	2.0	D
RY0556	0.002726	0.000143	0.059108	0.014086	17.5	±	0.9	22.3	±	5.4	C
RY0558	0.002554	0.000172	0.051205	0.013253	16.4	±	1.1	18.1	±	4.8	C
RY0559	0.002698	0.000209	0.048275	0.017236	17.4	±	1.3	18.1	±	6.5	C
RY0561	0.002438	0.000156	0.077043	0.022006	15.7	±	1.0	26.0	±	7.5	D
RY0562	0.002708	0.000196	0.044149	0.015202	17.4	±	1.3	16.6	±	5.8	C

RY0564	0.003070	0.000188	0.166978	0.027444	19.8	±	1.2	69.4	±	11.8	D
RY0565	0.002611	0.000138	0.052769	0.009655	16.8	±	0.9	19.1	±	3.6	C
RY0567	0.010109	0.000264	0.048334	0.002037	64.8	±	1.7	66.2	±	3.2	C
RY0568	0.002775	0.000181	0.059103	0.021055	17.9	±	1.2	22.7	±	8.1	C
RY0577	0.003221	0.000252	0.203136	0.053468	20.7	±	1.6	87.7	±	23.1	D
RY0578	0.002703	0.000174	0.048190	0.013592	17.4	±	1.1	18.1	±	5.2	C
RY0580	0.002647	0.000135	0.047305	0.008324	17.0	±	0.9	17.4	±	3.2	C
RY0581	0.003069	0.000231	0.130353	0.026359	19.8	±	1.5	54.5	±	11.4	D
RY0583	0.002712	0.000150	0.042506	0.010230	17.5	±	1.0	16.0	±	3.9	C
RY0584	0.002945	0.000210	0.087586	0.022786	19.0	±	1.4	35.5	±	9.4	D
RY0586	0.002608	0.000212	0.060254	0.020867	16.8	±	1.4	21.8	±	7.7	C
RY0587	0.007850	0.000561	0.565464	0.052290	50.4	±	3.6	484.8	±	45.1	D
RY0589	0.004237	0.000295	0.328991	0.046325	27.3	±	1.9	178.5	±	25.7	D
RY0599	0.002799	0.000131	0.047370	0.008583	18.0	±	0.8	18.4	±	3.4	C
RY0600	0.002940	0.000271	0.146807	0.051162	18.9	±	1.7	58.7	±	20.6	D
RY0602	0.002671	0.000163	0.040290	0.012329	17.2	±	1.0	15.0	±	4.6	C
RY0603	0.002582	0.000156	0.047610	0.010422	16.6	±	1.0	17.1	±	3.8	C
RY0605	0.002883	0.000200	0.061788	0.022470	18.6	±	1.3	24.6	±	9.0	C
RY0606	0.002927	0.000158	0.134228	0.019431	18.8	±	1.0	53.6	±	8.1	D
RY0608	0.002739	0.000169	0.057854	0.015678	17.6	±	1.1	21.9	±	6.0	C
RY0609	0.002501	0.000130	0.056455	0.012167	16.1	±	0.8	19.6	±	4.3	C
RY0611	0.002582	0.000107	0.054033	0.007022	16.6	±	0.7	19.3	±	2.6	C
RY0612	0.002505	0.000136	0.081370	0.015321	16.1	±	0.9	28.1	±	5.4	D

Supplementary table B: Data on zircon trace element

Formation	Standard	Standard	Standard	Standard	Standard	Standard	Standard	Standard	Standard	Standard	Standard	Standard	Standard	Standard	Standard	Standard	Standard
Sample	91500	91500	91500	91500	91500	91500	91500	91500	91500	91500	91500	91500	91500	91500	91500	91500	91500
Spot no.	RY0377	RY0387	RY0397	RY0407	RY0417	RY0427	RY0437	RY0447	RY0457	RY0467	RY0477	RY0487	RY0497	RY0507	RY0517	RY0527	RY0537
(ppm)																	
P	19	13	8	20	25	18	14	19	22	19	15	19	23	18	12	16	23
Ca	0	0	0	0	166	0	0	0	156	115	0	138	26	0	98	202	109
Ti	5.3	6.2	6.8	6.6	6.5	4.6	6.2	7.1	5.3	5.6	6.1	5.8	6.0	5.4	6.7	4.7	6.2
Y	141.4	139.3	145.9	143.2	139.6	135.7	138.5	135.2	141.1	132.0	136.3	137.0	142.1	141.1	135.8	130.9	143.3
Nb	0.87	0.84	0.87	0.79	0.82	0.78	0.79	0.82	0.82	0.80	0.80	0.80	0.84	0.80	0.84	0.77	0.92
La	0.008	0.000	0	0.002	0	0.0003	0.002	0.001	0.002	0.0003	0.002	0.002	0.001	0.019	0.000	0	0.147
Ce	2.52	2.29	2.55	2.46	2.40	2.32	2.43	2.47	2.57	2.26	2.46	2.43	2.46	2.36	2.47	2.45	2.62
Pr	0.016	0.009	0.012	0.011	0.011	0.010	0.011	0.011	0.010	0.012	0.012	0.009	0.012	0.016	0.014	0.012	0.036
Nd	0.17	0.18	0.21	0.21	0.21	0.18	0.22	0.19	0.18	0.19	0.19	0.20	0.19	0.22	0.20	0.18	0.29
Sm	0.48	0.41	0.46	0.43	0.41	0.39	0.41	0.46	0.40	0.40	0.44	0.39	0.41	0.41	0.41	0.40	0.40
Eu	0.216	0.217	0.241	0.212	0.220	0.200	0.222	0.217	0.221	0.212	0.214	0.217	0.231	0.213	0.220	0.218	0.219
Gd	2.40	2.15	2.56	2.32	2.19	2.15	2.27	2.36	2.25	2.18	2.17	2.20	2.17	2.27	2.21	2.16	2.25
Tb	0.83	0.80	0.88	0.84	0.85	0.77	0.81	0.82	0.83	0.79	0.82	0.82	0.82	0.82	0.79	0.78	0.79
Dy	12.0	11.7	13.1	12.0	11.9	11.2	11.1	11.4	11.5	11.2	11.9	11.2	11.8	11.7	11.3	11.5	11.7
Ho	4.81	4.56	5.00	4.88	4.79	4.61	4.60	4.66	4.81	4.65	4.69	4.64	4.62	4.76	4.69	4.63	4.80
Er	25.8	25.2	27.8	26.3	25.3	24.6	25.7	25.0	26.4	24.9	24.8	24.8	24.9	25.1	24.4	24.8	26.2
Tm	7.07	6.63	7.27	6.92	6.81	6.53	6.71	6.63	6.95	6.58	6.50	6.60	6.86	6.67	6.62	6.63	7.14
Yb	72.8	71.4	78.3	73.7	75.3	69.6	73.0	71.2	72.5	71.8	73.6	73.6	73.3	73.3	73.2	74.4	75.7
Lu	13.5	12.7	13.9	13.4	13.2	13.0	13.2	12.6	12.9	12.7	13.2	13.0	13.2	12.7	12.8	12.6	13.4
Hf	6028	5945	6432	6149	5995	5806	6034	5983	6022	5845	6006	5987	5981	5968	5770	5818	5900
Ta	0.57	0.54	0.59	0.55	0.56	0.520	0.55	0.54	0.54	0.54	0.54	0.54	0.54	0.55	0.55	0.55	0.53
Th	27.9	27.9	29.3	28.5	28.2	27.0	27.2	26.3	26.4	27.1	27.6	27.1	28.1	26.6	26.8	26.5	29.2
U	74.9	71.8	81.8	81.4	71.5	70.4	74.3	69.1	73.4	68.5	72.1	71.0	72.2	70.3	71.0	70.2	80.8

Formation	Tori	Tori	Tori	Tori	Tori	Tori	Tori	Tori
Sample	NT63c	NT63c	NT63c	NT63c	NT63c	NT63c	NT63c	NT63c
Spot no.	RY0440	RY0443	RY0449	RY0452	RY0471	RY0479	RY0482	RY0483
(ppm)								
P	361	227	304	196	145	447	194	195
Ca	164	39	372	109	0	155	84	44
Ti	17.6	4.8	19.9	52.4	11.0	14.1	6.9	24.2
Y	2714.0	3696.4	2522.9	3205.0	1733.0	2632.3	2718.2	1358.5
Nb	7.83	6.38	4.38	6.01	3.10	2.16	6.34	2.45
La	14.248	0.200	17.069	35.928	3.456	15.210	2.842	1.938
Ce	65.57	36.92	65.77	92.88	27.00	41.97	40.11	14.31
Pr	4.399	0.302	6.000	6.618	1.038	4.242	1.282	0.952
Nd	22.55	5.89	31.68	29.59	7.81	24.47	9.85	5.29
Sm	13.91	14.12	15.76	15.17	9.09	20.19	12.65	6.55
Eu	0.476	0.514	0.550	0.511	0.405	1.720	0.528	0.430
Gd	66.80	93.17	69.67	83.00	48.42	84.21	68.81	30.47
Tb	21.77	31.08	21.22	26.98	14.58	27.45	23.03	9.97
Dy	276.7	396.5	257.8	339.1	183.5	309.5	294.7	129.0
Ho	99.83	140.55	93.78	120.36	64.38	86.83	103.16	46.11
Er	423.2	587.8	407.5	516.2	280.6	320.3	432.7	203.9
Tm	83.52	113.89	80.79	101.16	57.94	61.59	86.27	42.93
Yb	706.9	965.6	681.5	836.3	533.9	534.4	735.2	393.0
Lu	116.4	150.2	116.9	136.5	91.0	87.6	119.4	73.9
Hf	8092	7575	7235	7649	7265	10845	7622	6980
Ta	2.01	1.63	1.12	1.54	0.93	0.73	1.74	0.69
Th	321.4	318.6	179.0	252.5	160.6	287.0	336.1	109.2
U	409.8	391.1	247.3	358.0	204.5	246.6	346.9	144.8

Formation	Iwaine	Iwaine	Iwaine	Iwaine	Iwaine	Iwaine	Iwaine	Iwaine	Iwaine	Iwaine	Iwaine
Sample	NT27	NT27	NT27	NT27	NT27	NT27	NT27	NT27	NT27	NT27	NT27
Spot no.	RY0492	RY0503	RY0509	RY0510	RY0521	RY0522	RY0523	RY0531	RY0533	RY0542	RY0543
(ppm)											
P	235	179	286	131	271	262	236	156	128	320	323
Ca	272	193	172	0	189	0	76	7	168	115	168
Ti	92.9	7.2	8.2	12.6	94.2	163.1	36.9	125.5	14.8	5.9	9.3
Y	1647.9	1076.3	1875.0	632.2	1824.5	1211.4	1300.3	1105.5	441.8	3044.2	1732.0
Nb	2.30	1.77	4.54	0.72	4.85	1.83	2.60	2.14	0.72	17.44	2.43
La	0.111	0.030	0.347	0.102	0.862	0.047	0.014	0.031	0.113	0.214	0.538
Ce	15.62	9.88	20.57	3.46	24.55	8.91	13.92	4.22	4.63	30.37	18.19
Pr	0.289	0.070	0.178	0.063	0.369	0.082	0.068	0.047	0.107	0.183	0.309
Nd	3.80	1.08	2.06	0.77	3.47	1.33	1.17	1.03	0.76	2.99	3.45
Sm	5.74	2.52	4.17	1.52	5.29	2.68	2.68	2.77	0.92	8.40	5.89
Eu	1.320	0.639	0.932	0.488	0.926	0.737	0.674	0.561	0.290	0.114	0.906
Gd	30.20	16.11	28.27	10.04	32.38	17.50	17.95	19.45	6.20	60.79	32.38
Tb	10.02	5.83	10.19	3.56	11.18	6.40	6.76	6.89	2.31	21.38	10.81
Dy	135.2	86.6	148.8	50.2	150.7	91.8	97.3	96.9	32.6	285.4	146.6
Ho	51.98	35.18	61.46	20.80	59.21	38.43	40.81	38.62	13.80	105.13	56.64
Er	261.3	183.5	312.6	106.1	294.4	200.8	217.6	193.1	74.6	479.8	279.0
Tm	61.53	44.24	73.08	25.31	65.90	48.06	51.88	42.18	17.70	97.75	63.08
Yb	607.2	433.9	728.3	253.5	641.9	492.7	531.5	394.2	184.9	859.7	610.6
Lu	121.9	87.4	145.5	51.8	126.0	102.1	110.8	80.6	39.9	162.4	123.6
Hf	9786	9552	9831	8225	9741	8809	9485	8976	9446	11509	12686
Ta	0.72	0.68	1.38	0.30	1.21	0.58	0.96	0.64	0.30	4.83	0.88
Th	370.7	158.0	469.7	30.0	480.3	129.3	286.8	41.8	30.8	890.5	305.2
U	263.0	180.9	398.0	45.6	323.6	161.8	300.7	81.7	46.9	1106.8	269.0

Formation	Iozen	Iozen	Iozen	Iozen	Iozen	Iozen	Iozen	Iozen	Iozen	Iozen	Iozen	Iozen	Iozen
Sample	NT45	NT45	NT45	NT45	NT45	NT45	NT45	NT45	NT45	NT45	NT45	NT45	NT45
Spot no.	RY0379	RY0383	RY0389	RY0390	RY0401	RY0402	RY0403	RY0409	RY0410	RY0411	RY0421	RY0431	RY0432
(ppm)													
P	449	283	1745	492	378	286	561	600	645	1122	543	520	295
Ca	64	0	0	284	327	0	0	379	348	192	221	0	0
Ti	9.5	7.0	268.5	27.8	21.6	10.8	7.9	8.2	25.5	113.7	64.2	10.0	9.2
Y	1493.8	1440.0	4186.3	1889.5	2559.9	1361.3	2821.4	3251.7	3050.0	4776.6	2818.1	2918.8	1406.7
Nb	4.50	1.29	13.71	2.26	4.13	1.84	5.67	10.72	3.42	9.26	4.44	7.61	2.32
La	1.358	0.229	7.690	1.133	1.574	0.080	0.236	2.224	1.260	62.354	1.760	0.790	0.286
Ce	25.61	11.18	93.80	17.35	30.42	12.68	33.90	74.55	16.18	157.71	25.02	47.57	14.31
Pr	1.461	0.221	2.867	0.493	0.553	0.124	0.223	0.988	0.878	13.985	1.037	0.412	0.190
Nd	13.72	3.09	20.76	4.42	5.55	2.06	3.52	7.85	6.68	54.42	9.09	4.20	2.30
Sm	8.54	5.22	20.65	5.53	8.10	4.01	7.44	11.47	7.35	24.26	11.19	8.33	3.80
Eu	1.674	1.096	2.391	1.267	1.778	0.828	1.618	2.042	1.909	4.558	2.694	1.274	0.959
Gd	26.77	26.98	81.01	31.64	47.83	23.46	49.89	64.20	38.63	91.64	56.88	51.20	23.83
Tb	8.98	9.20	29.58	10.85	16.14	8.18	17.64	21.32	13.68	28.91	19.43	18.16	8.38
Dy	123.2	122.2	386.0	150.4	215.8	111.9	243.0	282.7	196.9	378.8	254.9	248.9	118.1
Ho	48.81	47.03	141.27	58.80	81.40	44.79	94.50	107.08	80.73	141.44	96.38	99.45	48.23
Er	246.4	231.9	636.3	297.6	411.9	230.8	468.2	512.5	410.7	662.2	473.8	488.9	241.7
Tm	57.96	54.05	144.48	74.23	95.37	56.48	110.19	118.15	99.09	150.18	110.41	112.60	58.31
Yb	588.4	531.8	1444.3	702.2	943.4	579.9	1081.5	1130.7	950.0	1388.8	1032.4	1112.3	590.2
Lu	116.4	101.8	234.1	141.6	178.2	111.9	204.2	208.0	184.2	263.0	198.4	214.9	116.6
Hf	10013	9614	12106	9615	10148	11068	9708	10344	9077	9161	10151	10826	9618
Ta	1.83	0.54	2.70	0.62	1.26	0.67	1.73	2.90	1.01	1.92	1.02	2.05	0.81
Th	228.4	172.1	1709.5	315.0	679.8	221.8	875.1	2286.0	227.3	1737.3	449.7	1149.1	210.8
U	233.1	191.7	1120.1	287.5	515.6	294.5	602.7	1003.1	255.7	900.6	381.7	791.7	239.3

Supplementary table C: Data on zircon Hf isotope

Formation	Sample	Spot no.	Age (Ma)	$^{176}Hf/^{177}Hf$	2SE	$^{176}Lu/^{177}Hf$	2SE	$^{176}Yb/^{177}Hf$	2SE	$\varepsilon_{Hf}(t)$	2SE
Standard	91500	91500-01	1065.4	0.282300	0.000015	0.0002302	0.0000032	0.008394	0.000100	6.6	0.4
Standard	91500	91500-02	1065.4	0.282308	0.000019	0.0003596	0.0000014	0.012936	0.000038	6.9	0.6
Standard	91500	91500-03	1065.4	0.282329	0.000016	0.0003314	0.0000001	0.012372	0.000033	7.6	0.5
Standard	91500	91500-04	1065.4	0.282309	0.000018	0.0003326	0.0000002	0.012666	0.000049	6.9	0.5
Standard	91500	91500-05	1065.4	0.282316	0.000019	0.0003275	0.0000005	0.012230	0.000017	7.2	0.6
Standard	91500	91500-06	1065.4	0.282303	0.000017	0.0003243	0.0000005	0.012228	0.000037	6.5	0.5
Standard	91500	91500-07	1065.4	0.282320	0.000016	0.0003267	0.0000002	0.011920	0.000010	7.1	0.5
Standard	91500	91500-08	1065.4	0.282316	0.000017	0.0003513	0.0000002	0.013248	0.000021	6.9	0.5
Standard	91500	91500-09	1065.4	0.282322	0.000016	0.0001714	0.0000012	0.006262	0.000040	7.2	0.5
Standard	Mud Tank	Mudtank_01	731.0	0.282488	0.000016	0.0000294	0.0000001	0.001152	0.000003	5.6	0.3
Standard	Mud Tank	Mudtank_02	731.0	0.282479	0.000017	0.0000619	0.0000001	0.002473	0.000005	5.3	0.4
Standard	Mud Tank	Mudtank_03	731.0	0.282499	0.000016	0.0000462	0.0000003	0.001814	0.000009	6.0	0.3
Standard	Mud Tank	Mudtank_04	731.0	0.282462	0.000017	0.0000635	0.0000001	0.002566	0.000004	4.7	0.4
Standard	Mud Tank	Mudtank_05	731.0	0.282475	0.000016	0.0000380	0.0000002	0.001506	0.000014	5.2	0.4
Standard	Mud Tank	Mudtank_01	731.0	0.282482	0.000012	0.0000413	0.0000002	0.001638	0.000006	5.4	0.4
Standard	Mud Tank	Mudtank_02	731.0	0.282483	0.000012	0.0000444	0.0000001	0.001744	0.000005	5.4	0.4
Standard	Mud Tank	Mudtank_03	731.0	0.282469	0.000011	0.0000443	0.0000001	0.001746	0.000003	5.0	0.3
Standard	Mud Tank	Mudtank_04	731.0	0.282473	0.000011	0.0000513	0.0000000	0.002051	0.000007	5.1	0.3
Standard	Mud Tank	Mudtank_05	731.0	0.282456	0.000013	0.0000567	0.0000001	0.002308	0.000004	4.5	0.4
Standard	Mud Tank	Mudtank_06	731.0	0.282486	0.000011	0.0000559	0.0000001	0.002331	0.000020	5.5	0.4
Standard	Mud Tank	Mudtank_07	731.0	0.282488	0.000012	0.0000581	0.0000001	0.002390	0.000009	5.6	0.4
Standard	Mud Tank	Mudtank_08	731.0	0.282471	0.000012	0.0000560	0.0000001	0.002329	0.000013	5.0	0.4
Standard	Mud Tank	Mudtank_09	731.0	0.282489	0.000010	0.0000514	0.0000001	0.002129	0.000012	5.7	0.3
Standard	Mud Tank	Mudtank_10	731.0	0.282479	0.000010	0.0000458	0.0000002	0.001913	0.000006	5.3	0.3
Standard	Mud Tank	Mudtank_11	731.0	0.282475	0.000014	0.0000437	0.0000001	0.001796	0.000007	5.2	0.5
Standard	Mud Tank	Mudtank_12	731.0	0.282490	0.000011	0.0000446	0.0000001	0.001802	0.000007	5.7	0.4
Standard	Mud Tank	Mudtank_13	731.0	0.282488	0.000013	0.0000350	0.0000002	0.001437	0.000003	5.6	0.4
Standard	Mud Tank	Mudtank_14	731.0	0.282483	0.000013	0.0000394	0.0000003	0.001609	0.000020	5.4	0.4
Standard	Mud Tank	Mudtank_15	731.0	0.282478	0.000015	0.0000617	0.0000002	0.002537	0.000005	5.2	0.5
Standard	Mud Tank	Mudtank_16	731.0	0.282491	0.000012	0.0000383	0.0000002	0.001548	0.000004	5.7	0.4
Standard	TEMORA 2	Temora2_01	416.8	0.282699	0.000016	0.0004791	0.0000044	0.017136	0.000333	5.9	0.4
Standard	TEMORA 2	Temora2_02	416.8	0.282676	0.000016	0.0005404	0.0000031	0.019754	0.000177	5.1	0.4
Standard	TEMORA 2	Temora2_03	416.8	0.282697	0.000017	0.0014102	0.0000178	0.054320	0.000712	5.5	0.5
Standard	TEMORA 2	Temora2_04	416.8	0.282690	0.000017	0.0006965	0.0000038	0.024140	0.000157	5.5	0.5
Standard	TEMORA 2	Temora2_05	416.8	0.282674	0.000015	0.0010459	0.0000112	0.035134	0.000821	4.8	0.4
Standard	TEMORA 2	Temora2_06	416.8	0.282642	0.000025	0.0011928	0.0000113	0.047585	0.000356	3.7	0.4
Standard	TEMORA 2	Temora2_07	416.8	0.282686	0.000025	0.0009585	0.0000181	0.036428	0.000738	5.3	0.4
Standard	TEMORA 2	Temora2_08	416.8	0.282692	0.000025	0.0005401	0.0000095	0.019293	0.000548	5.6	0.4
Standard	TEMORA 2	Temora2_09	416.8	0.282672	0.000026	0.0012932	0.0000264	0.043713	0.001073	4.7	0.5

Formation	Sample	Spot no.	Spot no. of U-Pb dating	Age (Ma)	$^{176}Hf/^{177}Hf$	2SE	$^{176}Lu/^{177}Hf$	2SE	$^{176}Yb/^{177}Hf$	2SE	$\varepsilon_{Hf}(t)$	2SE
Tori	NT63c	Unk2_01	RY0621	23.8	0.282751	0.000252	0.0008353	0.0000143	0.029038	0.000259	-1.0	0.4
Tori	NT63c	Unk2_02	RY0624	22.7	0.282761	0.000252	0.0021611	0.0000548	0.087265	0.001805	-0.7	0.4
Tori	NT63c	Unk2_03	RY0625	22.9	0.282469	0.000252	0.0034623	0.0001440	0.131869	0.006159	-11.0	0.7
Tori	NT63c	Unk2_04	RY0627	22.6	0.282721	0.000252	0.0011790	0.0000031	0.045511	0.000356	-2.1	0.5
Tori	NT63c	Unk2_05	RY0631	20.8	0.282815	0.000253	0.0021726	0.0000435	0.086912	0.001392	1.2	0.9
Tori	NT63c	Unk2_06	RY0634	2331.9	0.281333	0.000251	0.0006403	0.0000378	0.027356	0.002030	0.6	0.4
Tori	NT63c	Unk2_07	RY0643	20.6	0.282672	0.000252	0.0017814	0.0000943	0.064161	0.004146	-3.9	0.5
Tori	NT63c	Unk2_08	RY0646	1897.2	0.281606	0.000251	0.0010632	0.0000168	0.038583	0.000503	-0.1	0.4
Tori	NT63c	Unk2_09	RY0647	24.2	0.282706	0.000252	0.0011199	0.0000155	0.038824	0.000335	-2.5	0.5
Tori	NT63c	Unk2_10	RY0649	23	0.282626	0.000252	0.0026487	0.0000577	0.096187	0.002241	-5.4	0.5
Tori	NT63c	Unk2_11	RY0650	111.8	0.282457	0.000252	0.0009341	0.0000080	0.034608	0.000162	-9.4	0.5
Tori	NT63c	Unk2_12	RY0652	1854.5	0.281641	0.000251	0.0009262	0.0000120	0.033728	0.000620	0.2	0.5
Tori	NT63c	Unk2_13	RY0668	23.4	0.282554	0.000252	0.0026968	0.0000154	0.111591	0.001141	-8.0	0.6
Tori	NT63c	Unk2_14	RY0672	22.4	0.282755	0.000252	0.0019398	0.0000331	0.079615	0.001517	-0.9	0.5
Tori	NT63c	Unk2_15	RY0675	20.4	0.282717	0.000252	0.0009823	0.0000508	0.038685	0.001520	-2.2	0.5
Iwaine	NT27	Unk3_01	RY0214	16.1	0.282564	0.000046	0.0047633	0.0000816	0.143375	0.002057	-7.8	1.2
Iwaine	NT27	Unk3_02	RY0227	17	0.282658	0.000034	0.0012150	0.0000473	0.038450	0.001179	-4.4	0.4
Iwaine	NT27	Unk3_03	RY0230	16	0.282661	0.000039	0.0011244	0.0000282	0.032771	0.000702	-4.3	0.8
Iwaine	NT27	Unk3_04	RY0233	15.5	0.282655	0.000034	0.0013876	0.0000288	0.048392	0.001275	-4.5	0.5
Iwaine	NT27	Unk3_05	RY0235	16.2	0.282660	0.000036	0.0018660	0.0000952	0.062382	0.002993	-4.4	0.6
Iwaine	NT27	Unk3_06	RY0252	16.3	0.282579	0.000034	0.0022037	0.0002492	0.074866	0.008893	-7.2	0.4
Iwaine	NT27	Unk3_07	RY0268	18.3	0.282565	0.000036	0.0020436	0.0000899	0.077858	0.005039	-7.7	0.5
Iwaine	NT27	Unk3_08	RY0273	17.2	0.282646	0.000042	0.0027261	0.0000962	0.078192	0.002064	-4.9	0.9
Iwaine	NT27	Unk3_09	RY0280	16.4	0.282701	0.000040	0.0024910	0.0000970	0.074300	0.001672	-2.9	0.9
Iwaine	NT27	Unk3_10	RY0289	15.8	0.282715	0.000034	0.0013763	0.0001238	0.047177	0.003981	-2.4	0.4
Iwaine	NT27	Unk3_11	RY0290	63.6	0.282555	0.000033	0.0021484	0.0000182	0.082347	0.000781	-7.1	0.4
Iwaine	NT27	Unk3_12	RY0298	21.4	0.282777	0.000037	0.0017201	0.0000427	0.055447	0.001340	-0.1	0.6
Iwaine	NT27	Unk3_13	RY0301	18	0.282522	0.000061	0.0157194	0.0004640	0.500057	0.008818	-9.4	1.8
Iwaine	NT27	Unk3_14	RY0317	23.2	0.282530	0.000040	0.0020330	0.0001457	0.066472	0.004903	-8.8	0.9
Iwaine	NT27	Unk3_15	RY0320	16.5	0.282618	0.000034	0.0015582	0.0001228	0.056939	0.003686	-5.8	0.4
Iwaine	NT27	Unk3_16	RY0270	15.6	0.282667	0.000034	0.0007469	0.0000023	0.025365	0.000203	-4.1	0.4
Iwaine	NT27	Unk3_17	RY0255	19.2	0.282659	0.000041	0.0032490	0.0000174	0.101018	0.000639	-4.3	0.9
Iwaine	NT27	Unk3_18	RY0295	16.2	0.282621	0.000038	0.0031267	0.0001412	0.095289	0.002314	-5.7	0.7
Iozen	NT45	Unk1_01	RY0556	17.5	0.282676	0.000030	0.0016746	0.0000536	0.055867	0.001555	-3.8	0.3
Iozen	NT45	Unk1_02	RY0558	16.4	0.282654	0.000033	0.0018879	0.0000368	0.063365	0.000644	-4.6	0.6
Iozen	NT45	Unk1_03	RY0562	17.4	0.282642	0.000030	0.0013382	0.0000106	0.043735	0.000682	-5.0	0.3
Iozen	NT45	Unk1_04	RY0565	16.8	0.282693	0.000033	0.0027550	0.0001843	0.092064	0.005965	-3.2	0.6
Iozen	NT45	Unk1_05	RY0567	64.8	0.282496	0.000031	0.0023173	0.0001670	0.086496	0.006625	-9.1	0.4
Iozen	NT45	Unk1_06	RY0568	17.9	0.282640	0.000031	0.0014541	0.0000245	0.051579	0.001053	-5.0	0.4
Iozen	NT45	Unk1_07	RY0578	17.4	0.282620	0.000031	0.0015072	0.0000089	0.051213	0.000643	-5.7	0.4
Iozen	NT45	Unk1_08	RY0580	17	0.282664	0.000033	0.0013285	0.0000185	0.046333	0.001091	-4.2	0.6
Iozen	NT45	Unk1_09	RY0583	17.5	0.282665	0.000030	0.0014847	0.0000737	0.050282	0.002470	-4.1	0.4
Iozen	NT45	Unk1_10	RY0599	18	0.282628	0.000036	0.0028825	0.0000589	0.099251	0.002513	-5.5	0.8
Iozen	NT45	Unk1_11	RY0602	17.2	0.282652	0.000032	0.0020068	0.0000149	0.069766	0.000844	-4.6	0.5
Iozen	NT45	Unk1_12	RY0603	16.6	0.282611	0.000030	0.0016436	0.0000173	0.056914	0.000367	-6.1	0.4
Iozen	NT45	Unk1_13	RY0605	18.6	0.282615	0.000033	0.0017701	0.0000367	0.062410	0.001848	-5.9	0.6
Iozen	NT45	Unk1_14	RY0609	16.1	0.282524	0.000037	0.0029505	0.0003124	0.113578	0.012816	-9.2	0.9
Iozen	NT45	Unk1_15	RY0611	16.6	0.282575	0.000034	0.0039146	0.0000918	0.140392	0.003145	-7.4	0.7